BEHAVIOUR
OF
AXIALLY LOADED PILES

A thesis

submitted in partial fulfilment

of the requirements for the Degree

of

Doctor of Philosophy in Civil Engineering

at the

University of Canterbury

by

CHEUNG Ka-Ching

University of Canterbury,

Christchurch, New Zealand

1988

吃的苦中苦

方为人上人

ABSTRACT

This project may be described in three parts. The first part mainly involves the evaluation of existing soil models under undrained conditions. The second part of the project is to evaluate the currently used methods for representation of the pile installation process. The third part of the work involves the study of the axially loaded pile problem, and particular interest is paid to the investigation of pile load displacement, shear transfer and load diffusion along the pile. Three different soil model have been used to represent the soil for this problem. Theoretical solutions have been compared with field test results.

The modified Cam-clay model and the more advanced bounding surface model developed from classical plasticity theories, and the rate-type model founded upon hypoelasticity theory have been studied. Model predictions of these three models were compared and evaluated base on results of triaxial tests and direct simple shear tests under undrained conditions. Both the modified Cam-clay model and the rate-type model are closely related by the similarity of their yield surfaces, but the rate type model requires only three soil parameters and provided reasonable agreement with test results on normally to heavily overconsolidated clay. The modified Cam-clay model is relatively restricted to the lightly overconsolidated clay. The sophisticated bounding surface model provides remarkable model prediction power to fit the test results, but numerous model parameters are required.

The cylindrical cavity expansion approach and the simple pile method, both of which may be used to simulate the pile installation process have been investigated. The rate-type model has been choosen to represent the soil. The simple pile method attempts to include the tip effect due to pile advancement which has been ignored in the cylindrical cavity expansion approach. The simple pile method approximates the strain field around the pile by an ideal fluid, but it is found that this method results in unrealistic pile-soil interaction. The predicted excess pore pressures from both methods were compared with field test results. This indicated that the simple pile method provided better agreement with test results than did the cylindrical cavity expansion approach.

An idealized one-dimensional pile model has been proposed. The modified Cam-clay model, bounding surface model and the rate-type model have all been used to simulated the soil response due to axial pile loading. Theoretical solutions were compared with three well documented pile test results. The pile tests were carried out in lightly to heavily overconsolidated clay deposits. The pile model predicted good agreement with test results, especially in regard to the pile load displacement response, shear transfer and load diffusion along the pile at low stress level.

ACKNOWLEDGEMENTS

This project was carried out in the Civil Engineering Department of the University of Canterbury under the overall guidance of Professor R.Park.

I wish to express my special gratitude to Dr. R. O. Davis, the main supervisor for this research project, for his invaluable advice, helpful guidance and particularly for a great deal of encouragement throughout the project. I am also most grateful for his support which extended well beyond my academic involvement. His constant care of my personal financial situation and the welfare of my family will be well remembered by all its members.

My special gratitude is also due to Dr. G. Mullenger, the co-supervisor for this project, for his invaluable discussions.

I would like to thank Mr. G. Evan for his in-depth discussions on the pile foundation problems during his visit to this department for three months.

The financial support provided by the National Road Board is also gratefully acknowledged.

Thanks are due also to the academic staff and graduate students of the Civil Engineering Department for their advice and assistance throughout the project. Mrs. V. Grey deserves special thanks for her draughting.

The role played by my wife, Ka-Min, during the research period should not be neglected. She sacrifices her career wholehearthedly to look after our little daughter and my home so that I could concentrate on my work and that is very much appreciated.

I also express my deepest gratitude to my parents overseas for their precious support and encouragement. Special thanks are given to my sister and brother for they took and still take good care of my parents; it is my duty but I was unable to perform it during the period of my study.

Finally, I give thanks to our God, Jesus Christ, who gave me guidance in every field of my life and strength to cope with every difficult situation; this project would not have been completed without Him.

TABLE OF CONTENTS

LIST OF TABLES

LIST OF FIGURES

PAGE

PAGE

PAGE

LIST OF NOTATION

A_c = bounding surface model parameter.

A_p = cross sectional area of a pile.

B = bulk modulus.

B_{cf} = bearing capacity factor..

Cu = undrained shear strength in triaxial conditions.

Cus = undrained shear strength in plane strain conditions .

D_{ij} = the components of the rate of deformation tensor.

E_p = Young's modulus of pile material.

F = yield surface or bounding surface.

G = elastic shear modulus.

H = plastic modulus associated with σ_{ij} .

H = plastic modulus associated with σ_{ij} .

J_0 = hardening parameter, $J_0 = J_0 (\varepsilon^p_{kk})$.

J_1 = first invariant of σ_{ij} , $J_1 = \sigma_{kk}$.

J_2 = second invariant of σ^*_{ij} , $J_2 = \sigma^*_{ij} \sigma^*_{ij}$

$\tilde{J}_2$ = dimensionless stress invariant, $\sqrt{\tilde{J}_2} = \sqrt{J_2} / 2Cus$.

J_3 = third invariant of σ^*_{ij} , $J_3 = \sigma^*_{im}\sigma^*_{mn}\sigma^*_{nj} /3$.

K = coefficient of lateral earth pressure at rest.

L = loading function.

L_p = pile length.

$\bar{M}$ = strength parameter of the rate-type model which is equal to $\sqrt{2}$ Cus.

M_c = the slope of the critical state line in the q - p plane determined from triaxial compression tests.

M_e = the slope of the critical state line in the q - p plane determined from triaxial extension tests.

N = the slope of the critical state line in $J_1 - \sqrt{J_2}$.

N_c = value of N determined from triaxial compression tests.

N_e = value of N determined from triaxial extension tests.

OCR = overconsolidation ratio (isotropically consolidated soil).

$\overline{OCR}$ = over consolidation ratio (one-dimensionally consolidated soil).

$\tilde{P}$ = dimensionless effective pressure.

P_a = atmospheric pressure, $101 kN/m^2$.

$\tilde{P}_i$ = dimensionless initial pressure.

Q_o = applied pile loading at the ground surface.

Q_p = axial load in the pile at depth z.

Q_{sp} = penetration resistance of a simple pile.

$\tilde{S}_1$ = deviatoric stress measure.

$\tilde{S}_2$ = deviatoric stress measure.

$\tilde{S}_3$ = deviatoric stress measure.

S_{ij} = the components of the dimensionless effective stress tensor.

S^*_{ij} = the components of the dimensionless deviatoric effective stress tensor.

T_{ij} = the components of the dimensionless total stress tensor.

U = dimensionless pore pressure.

U_i = dimensionless initial pore pressure.

ΔU = dimensionless excess pore pressure.

V_z = uniform flow velocity.

W_{ij} = the components of the spin tensor.

a = pile shaft radius.

a_i = inside radius of hollow pile.

e = void ratio.

e_i = initial void ratio.

n = ratio of N_e to N_c .

n_{ij} = unit normal vector to the yield or bounding surface .

p = effective pressure.

p_0 = virgin isotropic consolidation pressure.

p_c = effective pressure at critical state.

p_e = the equivalent pressure at void ratio e.

p_i = initial effective pressure.

q = deviatoric stress in triaxial conditions.

r_m = radius of influence.

t_c = hardening shape parameter determined from triaxial compression test.

t_e = hardening shape parameter determined from triaxial extension test.

u = pore pressure.

u_i = initial pore pressure.

Δu = excess pore pressure.

Δus = shear induced pore pressure.

u_z = vertical soil displacement.

v_r = soil velocity in r direction.

v_z = soil velocity in z direction.

x = bounding surface model parameter.

$(\sigma_{rz})_a$ = induced shear traction at the pile shaft .

α = distance factor.

β = rigidity index.

γ_{oct} = octahedral shear strain.

χ = shear stress and strain response function.

δ = distance between σ_{ij} and σ_{ij} in stress space.

δ_{ij} = Kronecker delta.

Δ_a = pile shaft displacement.

Δ_b = pile tip displacement.

Δ_p = elastic shortening of the pile at depth z.

$\dot{\varepsilon}_{ij}$ = strain rate.

$\overset{e}{\varepsilon}_{ij}$ = the components of the elastic strain tensor

$\overset{p}{\varepsilon}_{ij}$ = the components of the plastic strain tensor

ε_{kk} = volumetic strain.

$\overset{p}{\varepsilon}_{kk}$ = plastic volumetic strain.

Φ = stress power.

ϕ = the effective angle of friction of soil at critical state .

Γ_{ij} = isotropic tensor function.

η = dimensionless stress ratio, $\eta = \sqrt{J_2} / J_1$.

κ = the slope of swelling line in the e - ln p plane.

λ = the slope of normal consolidation line in the e - ln p plane.

$\overset{\circ}{\sigma}_{ij}$ = co-rotational stress rate.

σ_{ij} = the components of the effective stress tensor.

$\bar{\sigma}_{ij}$ = image stress state of σ_{ij} on the bounding surface.

$\overset{t}{\sigma}_{ij}$ = the components of the total stress tensor.

σ_{nv} = normal traction due to effective stresses at the simple pile.

τ_{nv} = shear traction at the simple pile .

υ' = Poisson's ratio.

Ω = t - z curve.

ω = Lode angle.

ξ_{ij} = the components of the natural strain tensor.

CHAPTER ONE

INTRODUCTION

Within the last two decades, development of large digital computers and a wide range of numerical techniques such as the finite element, finite difference, and boundary element methods, together with constitutive laws for soils have rendered possible solution of many complex problems in the various fields of geomechanics.

It may be possible to employ realistic soil models with the use of the finite element method to approach close approximation to general geotechnical engineering problems. However, most of the recently developed soil models require numerous model parameters which need extensive test results to be identified, and are verified only under quite limited stress or strain paths such as triaxial or plane strain conditions etc. It may be notable from existing engineering literature that no constitutive law developed at this time would be capable of predicting all stress paths with an equal degree of agreement with soil test results. In addition, use of the finite element method for most problems requires large scale efforts in data preparation and complicated solution techniques, especially when dealing with non-linear material such as hardening or softening soils. Therefore, the primary aim of this work is to investigate the effectiveness and efficiency of currently available soil models and to make use of three selected isotropic hardening soil models to predict or reproduce actual field measurement, particularly the pile penetration problem and the axially loaded pile problem. Realistic loading configurations are employed without the need of sophisticated or time consuming numerical methods.

The theory of plasticity is not a recently developed theory. The study of metal plasticity was first originated by Tresca, Saint Venant and Levy in the 1870's but the first historical plasticity theory may be attributed to Coulomb(1773). He proposed a yield criterion for soils. Prior to about 1940, the theory was mostly applied to metal and very few studies had been made in the area of soil mechanics. The rheological behaviour of soils differs from that of metals in that, in general, soil is a pressure sensitive material but metal is a pressure insensitive material. By 1950, the problems of soil mechanics were still analyzed on the basis of elasticity theory. Drucker et al. (1957) proposed the first soil model using plasticity theory. Roscoe et al.(1958) of Cambridge University interpreted a series of experimental test results on both drained and undrained (remoulded) Weald clay. The well known critical state theory and the Cam-clay model, which considered soil as an isotropic hardening material, were then proposed. Furthermore, the fast growth of computer techniques in the past two decades enabled the use of numerical methods to study the behaviour of soils. A wide variety of soil models based upon the theory of plasticity have since been proposed. A review of the basic concept and formulations of many plasticity models can be found in Desai and Sirivardane (1984).

In 1955, Truesdell introduced the hypoelasticity theory which offers an alternative material description to the plasticity theories. The general hypoelastic material model describes

the material behaviour in terms of a mathematical series expansion and requires 12 response functions. Green (1956) proposed a special hypoelastic constitutive equation which corresponds to an isotropic hardening model, following associative flow rule, of classical plasticity theory during loading conditions. Davis and Mullenger (1978,1979) followed the basic assumptions given by Romano (1974). They proposed two soil models which incorporate the concept of critical state theory. Their models are classified by Truesdell and Noll (1965) as the rate-type fluid models, or simply rate-type models. Independently, Gudehus and Kolymbas (1979) also proposed a rate-type model for sand.

Davis and Mullenger(1979) employed some basic ideas from the critical state theory and selected a certain choice of material parameters, the yield surface implied in the rate-type model reduces to the elliptical yield surface proposed in the well known modified Cam-clay model of Roscoe and Burland (1968). Inside the yield surface, it is assumed that loading and unloading processes may involve inelastic deformations and a linear elastic domain may not exist. This rate-type model is applicable to both normally consolidated and overconsolidated clay and requires few soil parameters (i.e., three for undrained conditions). Another advantage of this model is that, in the sense of plasticity theory, soil yielding and plastic flow are incorporated within the model without an additional flow rule or hardening rule and thus it greatly simplified the model formulation and application. However, the model violated the condition of continuity in such a way that it is limited to either monotonic loading conditions or undrained cyclic loading conditions. Verification of this model requires comparisons between model predictions and soil test results, and this will be studied in chapter two.

The modified Cam-clay model of Roscoe and Burland (1968) and the cap model of DiMaggio and Sandler (1971) are based on the concept of continuous yielding of soils. Both models assume the soils is an isotropic material, and differ only in the form of the yield condition, which is important in the quantitative description of a stress-strain response. It is noted that the so-called isotropic model considers that the principal stress rotations are neglected and also both the yield and potential surfaces are expressed in terms of stress invariants (i.e., symmetric functions of the principal stresses). In the modified Cam-clay model of Roscoe, the yield surface has the shape of an ellipse on the deviatoric stress versus pressure (p - q) plane but no elastic shear strain is considered. In 1978, a more general formulation including elastic shear strain has been introduced in this model by Banerjee and Stipho. In their model, plastic flow may occur when the stress state lies on the yield surface. For any stress state inside the yield surface, the material response is elastic. This model is efficiency in the sense that it requires only four soil parameters which can normally be obtained from standard soil tests. The modified Cam-clay model of Banerjee and Stipho (1978) has been employed to represent the behaviour of one dimensional normally to heavily over-consolidated soils for pile driving problems, by Randolph et al. (1978a,b) and by Wroth et al. (1978). Unfortunately, this model possesses certain disadvantages, such as it may predict excessive elastic response and cannot predict hysteretic behaviour beneath the yield surface.

The modified Cam-clay model has been extended, with some degree of modification, to describe cyclic soil response (Eekelen and Potts ,1978, and Carter et al., 1982). However, soils are always anisotropic to some degree because of their geological history. In an attempt to take account of an anisotropy in plastic constitutive equations of soils, Prevost (1977,1978) adopted the combined isotropic and kinematic hardening theory proposed by Mroz(1967) and by Iwan(1967) for metals. Prevost replaced the single yield surface by several nested yield surfaces. The locations and sizes of the yield surfaces reflect the past stress-strain history of the soil element. Similar to most of the anisotropic hardening soil models, Prevost's model assumes an associative flow rule. In the class of anisotropic hardening soil models, Provost's model can be considered as relatively simple. However, the model predicts only undrained soil behaviour and the effective stress state cannot be predicted. Furthermore, determination of the excess pore pressure during shearing requires an additional pore pressure model.

Beginning in 1975, Dafalias and Popov (1975,1976) and Krieg (1975) introduced the concept of "bounding surface" which is conceptually similar to that of Mroz (1967). This concept considered a yield surface which lies within a bounding surface. Both surfaces were allowed to translate in stress space subject to the isotropic/kinematic hardening rule. Mroz et al. (1978, 1979, 1981) adopted this concept and the critical state theory, and developed anisotropic hardening soil models with various degrees of sophistication. The yield surface of these models may degenerate into one point, (i.e., the current stress state), and the plastic flow direction is defined normal to the bounding surface at the intersection of the direction of the stress rate. However, this formulation may result in a plastic flow direction which is depends on the direction of the stress rate and the flow rule is non-linear in rate of stress.

On the other hand, Dafalias(1979) adopted another approach in applying bounding surface plasticity to clays. He assumed the yield surface has degenerated into one point and it coincided with the current stress state. This allows the soil model reduce to an isotropic hardening model. Dafalias derived his model from the modified Cam-clay model but he transformed the elliptical yield surface into the bounding surface. He also introduced a mapping rule which relates the current stress state to an image stress state on the bounding surface which in turn defines the plastic flow direction at the current state. As a result of these modifications, overconsolidated clays were able to experience plastic deformation; this was not predicted by the modified Cam-clay model. In 1980, Dafalias revised the shape of the bounding surface in order to improve the description of soil response for both normally consolidated and overconsolidated clays. We have found that this model performs reasonably well without the need of sophisticated solution techniques, but this model requires 11 model parameters.

In chapter two, we will investigate the modelling features of the modified Cam-clay model, the rate-type model of Davis and Mullenger (1979), and the bounding surface model of Dafalias and Herrmann (1980). The reason that we selected these three soil models is that in the case of static loading conditions, especially the pile problem that we consider later in this work, it may be convenient to employ isotropic hardening soil models to represent the soils. Furthermore,

both the modified Cam-clay model and the rate-type model are developed based on similar assumptions but different theories. Therefore it may be interesting to compare the resulting response obtained from both models. The bounding surface model adopted the advanced idea of the bounding surface plasticity theory without over-complicating the mathematical formulation. The modelling features of these models will be evaluated on the basis of soil test results.

In chapter three, the cylindrical cavity expansion approach and the recently developed simple pile method for investigating pile driving or cone penetration effects in soils will be studied. Because of the simplicity of the rate-type model of Davis and Mullenger (1979), this model will be used to represents the soil. It may be expected that pile driving may cause significant disturbance in soils which will eventually affect the subsequent pile load carrying capacity. However theoretical development for predicting pile capacity is made difficult by a variety of factors (i.e., soil types, details of pile installation such as pre-drilled pilot hole, pile wrapping, drag down of soil from upper layer to lower layer, stress changes in soils due to pile driving and subsequent reconsolidation). Among these factors affecting the pile capacity, the stress changes in soils due to pile installation may be important for theoretical development of pile capacity predictions.

For long piles in clay where no significant stronger strata lies beneath the pile tip, the pile load carrying capacity mainly come from the shaft. Empirical pile design rules, such as α, β and λ methods which will be discussed in chapter three, utilize coefficients which provide an estimate of the limiting skin friction for pile design. These coefficients are evaluated based on limited full scale pile load test results. All the factors affecting the limiting skin friction are lumped into these coefficients. In 1971, the petroleum industry initialized the idea of using the effective stress method for prediction of pile shaft capacity for driven piles in clays. Thereafter, extensive work involving both theoretical and experimental studies has been made in this area and several pile capacity models to compute the limiting skin friction have been proposed (Focht and Kraft 1981, Kraft 1982, Kirby et al. 1983). The development of these pile capacity models are based on the concept of the critical state soil mechanics. Pile driving is simulated by plane strain cylindrical cavity expansion approach. Reconsolidation processes are considered by assuming pore water flows radially outward from the pile.

The use of the cylindrical cavity expansion approach to simulate pile driving effects in soils is based on an idealized assumption that at depth pile whipping and surface effects due to pile driving may vanish. Furthermore, the pile tip effect is ignored. These assumptions greatly simplify the method and may allow more realistic soil models to be considered. Alternatively, the recently developed simple pile method (Baligh 1984) initially appeared to be an attractive approach to investigate the pile driving problem, because the pile tip effects due to pile advancement may be included. Baligh (1984, 1985, 1986a,b) assumed that, in the case of deep penetration, the strain field around the simple pile may be estimated by an ideal fluid flow field. The stress field around a simple pile is evaluated from a soil model and the pre-determined strain field. This method has also been extended to estimate the strain field around the pile or cone penetrometer with various tip conditions, Levadoux and Baligh(1980), Tumay et al. (1985). Both the cylindrical cavity expansion

approach and the simple pile method are strain control problems and require no complicated solution methods. However, the cylindrical cavity expansion approach may over simplify the deformation pattern experienced by the soil while the simple pile method ignores the resistance to distortion of soil in the displacement calculation. Solutions for both methods will be studied and compared with pile test results in chapter three, and we will show that the simple pile method predicts unrealistic pile-soil interaction around the pile shaft.

In chapters four and five, we will employ the modified Cam-clay model, the bounding surface model and the rate-type model in applying to the prediction of the response of a single axially loaded friction pile. A one-dimensional idealized pile model will be proposed in chapter four. The theoretical solutions will be compared with actual field measurements of three full size pile tests in lightly to heavily overconsolidated clay deposits. In this work, particular interest will be paid to the axial pile load versus displacement response and the load diffusion along the pile length.

Prediction of the response of axially loaded piles involves an analysis of a pile-soil interaction problem. Currently used methods in this area may be broadly categorized into three classes:

(1) Load-transfer method: This method was first introduce by Seed and Reese (1957) and extended by Coyle and Reese (1966). The relationship between the shear stress at the pile shaft and pile displacement, the so-called t-z curve, may be established from either measurement of instrumented pile test results, [Coyle and Sulaiman 1967, Reese et al. 1969, O'Neill et al. 1982a,b], or theoretical predictions, [Kraft et al. 1981, Heydinger and O'Neill, 1986].

(2) Elastic theory: The widely used method is mainly based on Mindlin's solution, a point load acting in an elastic-half space. Extensive work has been done in this area with the aid of Mindlin's solution may be attributed to Poulos and his co-worker, [Poulos and Davis 1968, Mattes and Poulos 1969, Poulos 1979].

(3) Finite element method: This method is mainly used for research purposes. Earlier work employing this method considered that soil is represented as a linearly elastic material,[Cooke and Price 1973, Randolph and Wroth 1977]. Recently, plasticity models have been widely used to represent the soils, [Ottaviani and Marchetti 1979, Potts and Martins 1982, Nystrom 1984].

Among these three methods, the load-transfer method may be the simplest one if the t-z curve is predetermined. The one-dimensional pile model that we will use belongs to this class. The t-z curves in our work will be determined from the soil models. However the major disadvantages in this method are that displacements in upper soil layers due to movements in lower layers are not taken into account and the three dimensional features of pile-soil behaviour are not incorporated. Nevertheless, the error induced from this one-dimensional idealization may be less than that

resulting from difficulty in accurate determination of soil properties, such as the shear modulus, as is commonly encountered in geotechnical problems.

Mullenger et al. (1984) approached the axially loaded pile problem assuming infinite pile length and a homogeneous stress field with no shear stress initially in the soil. Initial stress conditions corresponding to normally to heavily over-consolidated "undisturbed" clay as well as the stress state after cylindrical cavity expansion have been considered in their work. They demonstrated that the induced shear traction at the pile shaft due to pile displacement is relatively independent of the initial stress conditions. In this work, we assume that the pile is embedded in "undisturbed" layered clays. Results obtained from this simplified approach will be compared with actual pile test results. Although we assumed that the soil is unaffected by pile installation and the limiting skin friction problem has not been incorporated in our pile model, we find that the results of this idealized pile model compare favourably with the test data, particularly with regard to load diffusion behaviour and the low stress, load-displacement response.

CHAPTER TWO

EFFECTIVE STRESS SOIL MODELS

The concepts of critical state theory were developed (Schofield and Wroth 1968) based on the general observations of saturated soil response under triaxial loading conditions in laboratory tests. Many recently developed soil models employ these concepts to describe the mechanical behaviour of soils. A brief review of the concepts of critical state theory will be given and three existing soil models employing these concepts will then be studied. The first two models are the modified Cam-clay model of Banerjee and Stipho (1978) and the bounding surface model of Dafalias and Herrmann (1980). Both models were developed from ideas associated with classical theories of plasticity. The third model is the rate-type model of Davis and Mullenger (1979) founded upon the theory of hypoelasticity. Undrained, monotonic loading conditions for these three models are of particularly interest in this work, because the models will be adopted to study the monotonic loading conditions of an axially loaded pile. The response of the rate-type model under cyclic loading conditions will also be studied because the condition of continuity of the loading and unloading equations for this model have been violated. Further, comparisons of model predictions with triaxial test and direct simple shear test results will be discussed.

SECTION 2.1 Concept of Critical State Theory

2.1.1 The Critical Void Ratio

Casagrande (1936) proposed the concept of critical void ratio based on the results of direct shear tests on loose and dense sand with the same initial vertical effective stress. The vertical effective stress was held constant during shear in all tests. He suggested that the void ratio of a sand at large strain approached a constant value which was independent of its initial void ratio and vertical effective stress. The void ratio at this state was called the critical void ratio. Later findings of Taylor (1948) from the results of constant volume triaxial tests on sand indicated that the critical void ratio was in fact a function of the effective vertical stress, contrary to Casagrande's earlier belief.

2.1.2 The Critical State Concept

Roscoe (1958) developed the critical state theory using two stress parameters together with the void ratio. The two stress parameters were

$$q = \sigma_a - \sigma_r \qquad (2.1.a)$$

$$p = (\sigma_a + 2\sigma_r)/3 \qquad (2.1.b)$$

in which σ_a and σ_r represent the axial and radial effective stresses in triaxial conditions. The stress parameters p and q are derived from the first invariant of the stress tensor, and the second invariant of the deviatoric stress tensor. Physically, p represents the isotropic effective pressure while q is a measure of deviatoric stress in the soil. Using the parameters p and q together with e the void ratio, the state of a soil element can be defined in e-p-q space. During isotropic loading and unloading of an isotropically normally consolidated clay element, q is zero and the normal consolidation and swelling lines can be depicted as shown in Fig. 2.1. Both lines are approximated as straight lines in the e-ln p plane. The slopes of the normal consolidation and swelling lines are denoted by λ and κ respectively.

In an attempt to study the stress and strain behaviour of soils, Roscoe and his co-workers (1958, 1963, 1968) adopted the concepts of Casagrande (1936) and Taylor(1948). They analyzed HenKel's (1956) drained and undrained triaxial compression test results on saturated remoulded samples of Weald clay. Roscoe (1958) found that the clays monotonically sheared to sufficiently large strain would reach a state at which continuous deformation occurred with no further change in the parameters e, p and q. This state was referred to as the critical state (Roscoe 1968). Roscoe also proposed that there existed a unique critical void ratio line, also known as the critical state line (Schofield & Wroth 1968), in e-p-q space. For a given clay this line is independent of the consolidation history and of the drained or undrained loading conditions (except perhaps for very heavily overconsolidated clay). The projections of the critical state line into the e-ln p plane and the q-p plane are straight lines. The critical state line is parallel to and located on the left side of the normal consolidation line in the e-ln p plane as shown in Fig. 2.1. The slope of the critical state line in the q-p plane is denoted by M. Soil states located between the critical state line and the normal consolidation line in e-p or e-ln p plane are called 'wet' of critical while soil states on the left side of the critical state line are called 'dry' of critical.

2.1.3 The State Boundary Surface

In the development of constitutive relations for soils, the so-called state path in e-p-q space is extremely important. In limit analysis, only the final or critical state is of interest, but in the critical state theory, then entire state path must be considered.

From Gilbert's (1954) drained and undrained triaxial compression results on normally and over-consolidated Weald clay, Roscoe (1958) found that the state paths of the normally consolidated clay samples formed a continuous surface connecting the normal consolidation line with the critical state line. This surface became known as the Roscoe surface (Atkison & Bransby 1978). General soil responses of normally and heavily over-consolidated clay under drained and undrained tests together with the state boundary surface are depicted in Figs. 2.2. The state paths of the heavily overconsolidated clay samples climbed from the e-p plane and (the peak) reached a surface which joined the critical state line with the Roscoe surface from the 'dry' side. This surface had previously been referred to as the well known Hvorslev surface. The projection of the swelling line on the Roscoe and Hvorslev surfaces is shown in Fig. 2.3. The Roscoe and Hvorslev surfaces were

obtained from results of triaxial compression tests. One might expect that similar surface would be obtained from results of triaxial extension tests. Since the deviatoric stress q is negative for triaxial extension conditions, the Roscoe and Hvorslev surfaces determined from this type of test lie on the negative side of the p-q plane along the p axis as shown in Fig. 2.3. The slope of the critical state line in the q-p plane determined from triaxial compression tests may be denoted by M_c while the slope found from extension test is denoted by M_e. M_c and M_e may be given by

$$M_c = \frac{6 \sin \phi_c}{3 - \sin \phi_c} \qquad (2.2.)$$

and

$$M_e = \frac{6 \sin \phi_e}{3 + \sin \phi_e} \qquad (2.3)$$

where ϕ_c and ϕ_e are the effective angle of friction of the soil at critical state determined from triaxial compression and extension test respectively. The Hvorslev and the Roscoe surfaces formed a boundary surface which enclosed a region in e-p-q space where all possible states of the soil must lie. Therefore the Hvorslev and the Roscoe surfaces came to be called the state boundary surface.

The state path of a soil element inside the state boundary surface can be determined from the constitutive relations. Purely elastic or elastic-plastic deformations may occur depending on the particular assumptions used in development of soil models.

SECTION 2.2 Modified Cam-clay Model

The modified Cam-clay model of Banerjee and Stipho (1978) employed the classical theory of plasticity and assumed that the soil was an isotropic hardening material. The model was founded upon the concepts of critical state theory. In the original Cam-clay theory (Roscoe and Burland, 1968), no elastic shear strains were considered. However, the more general condition of including elastic shear strain has been introduced in the model formulation by Banerjee and Stipho (1978). They assumed that there exists a yield surface which encloses a purely elastic region. Hardening or softening may occur in the material when the stress state reaches the yield surface. This model was originally developed for normally to lightly over-consolidated clays, but it has been used (Wroth et al. 1978, Randolph et al. 1978a,b) to simulate stress changes in normally to heavily over-consolidated clays due to pile driving and subsequent reconsolidation process. However, the yield surface of this model encloses a relatively large purely elastic region. Thus the model may predict excessive purely elastic response or tensile stresses inside the yield surface before plastic deformation occurs; this is contrary to observations from test on overconsolidated soils, [Banerjee and Stipho 1979]. Clearly this model may not be good for soils under cyclic loading as large magnitude purely elastic cyclic response may occur inside the yield surface. Nevertheless it may be useful in modelling some aspects of soil behaviour under monotonic loading conditions. This is the

case in our study , and we will attempt to employ the model to simulate the soil response subject to monotonic pile loading.

The modified Cam-clay model assumes the yield surface has the following general expression

$$F= F(\sigma_{ij} , \varepsilon^{p}_{kk})= 0 \tag{2.4}$$

where σ_{ij} represents the effective stress while the plastic volumetric strain ε^{p}_{kk} provides a measure of hardening. Purely elastic deformation occurs when $F < 0$. Plastic deformation may occur when $F= 0$, however no meaning is associated with $F> 0$. During plastic deformation the strain rate $\dot{\varepsilon}_{ij}$ is decomposed into elastic and plastic parts

$$\dot{\varepsilon}_{ij}= \dot{\varepsilon}^{e}_{ij} + \dot{\varepsilon}^{p}_{ij} \tag{2.5}$$

in which the superscripts e and p denote elastic and plastic components respectively. If the plastic loading direction coincides with the direction of the unit normal vector n_{ij} to the yield surface, and H is defined as the plastic modulus associated with the stress rate $\dot{\sigma}_{ij}$, the loading function L is given by

$$L=\frac{\dot{\sigma}_{ij}\, n_{ij}}{H} \tag{2.6}$$

Here

$$n_{ij}= \frac{1}{g}\frac{\partial F}{\partial \sigma_{ij}} \qquad \text{and} \qquad g = \left[\frac{\partial F}{\partial \sigma_{ij}} \frac{\partial F}{\partial \sigma_{ij}} \right]^{1/2} \tag{2.7}$$

Plastic loading ,neutral loading and elastic unloading and can be defined by the sign of the loading function. Using the associative flow rule, the plastic strain rate can be expressed by

$$\dot{\varepsilon}^{p}_{ij} = \langle L \rangle\, n_{ij} \tag{2.8}$$

in which $\langle\ \rangle$ has the following definition

$$\begin{aligned} \langle L \rangle &= L \qquad \text{when } L> 0, \text{ Loading} \\ \langle L \rangle &= L \qquad \text{when } L= 0, \text{ neutral loading} \\ \langle L \rangle &= 0 \qquad \text{when } L< 0, \text{ unloading} \end{aligned} \tag{2.9}$$

Eq. 2.9 implies that the material is purely elastic during unloading. Using Eq. 2.4 and 2.6 to 2.8, the plastic modulus can be obtained by means of the consistency condition satisfying $\dot{F}$ equal to zero. We find

$$H = -\frac{\partial F}{\partial \varepsilon^{p}_{kk}} \frac{n_{jj}}{g} \tag{2.10}$$

The inclusion of H in the loading function allows Eq. 2.8 to describe plastic deformation for unstable (softening) materials. This may be the case when H is negative, however plastic loading may occur (i.e., $L> 0$) when both scalar quantities $\dot{\sigma}_{ij}\, n_{ij}$ and H are negative.

Substituting Eq. 2.8 into 2.5 and assuming undrained conditions (i.e., $\dot{\varepsilon}_{kk}$ is zero) as well as elastic incremental constitutive relations governed by Hooke's law, and finally inverting the resulting relationship, we arrive at the following equation

$$\dot{\sigma}_{ij} = 2\,G\,\dot{\varepsilon}_{ij} - \left[\, 2\,G\left(n_{ij} - \frac{1}{3}\, n_{kk}\delta_{ij} \right) + B\, n_{kk}\delta_{ij} \right] < L > \tag{2.11}$$

where δ_{ij} is the Kronecker delta. G and B denote the elastic shear and bulk modulii and L becomes

$$L = \frac{2\,G\,\dot{\varepsilon}_{kl}\, n_{kl}}{H + B\, n_{mm}^2 + 2\,G(\,1 - n_{mm}^2/3)} \tag{2.12}$$

During undrained deformation, the total stress may be determined from equilibrium considerations. The total stress σ_{ij}^t is related to the effective stress by

$$\begin{aligned} \sigma_{ij}^t &= \sigma_{ij} + u\,\delta_{ij} \\ u &= \Delta u + u_i \end{aligned} \tag{2.13}$$

in which u denotes the pore water pressure, Δu and u_i represent the excess and initial pore pressure, respectively. Eq. 2.11 is a general formulation of the isotropic elastroplastic soil model independent of the exact form of the yield surface itself. The choice of the yield surface may be choosen differently for each particular soil.

For general stress states, it is convenient to introduce the stress invariants

$$\begin{aligned} J_1 &= \sigma_{kk} \\ J_2 &= \sigma_{ij}^* \sigma_{ij}^* \\ \sigma_{ij}^* &= \sigma_{ij} - \sigma_{kk}\,\delta_{ij}/3 \end{aligned} \tag{2.14}$$

where σ_{ij}^* denotes the deviatoric part of σ_{ij} . J_1 represents the first invariant of σ_{ij} and J_2 denote the second invariant of σ_{ij}^*. J_1 and J_2 are equivalent to 3 p and $2/3\ q^2$ in triaxial conditions. In the modified Cam-clay model, purely elastic deformation would occur on the curved surface abcd of Fig. 2.2c, the so called elastic wall. The state bounding surface was choosen as the yield surface. In terms of stress invariants J_1 and J_2, a particular form of the yield surface for clay was earlier proposed by Roscoe (1968). It was

$$F = (\,J_1 - J_0\,)\,J_1 + J_2 / N^2 = 0 \tag{2.15}$$

where $J_0 = J_0\,(\,\varepsilon_{kk}^p\,)$, the hardening parameter, is the intersection of the yield surface with J_1 axis. Eq. 2.15 is the equation of an ellipse in the J_1 - $\sqrt{J_2}$ plane as shown in Fig. 2.4. For isotropic normally consolidation processes with no deviatoric stress initially in the soil, J_0 is equal to J_1. The soil state is considered to be "wet" of critical in this model when $J_1 > J_0/2$, or to be "dry" of critical when $J_1 < J_0/2$. N is the slope of the critical state line in the J_1 - $\sqrt{J_2}$ plane and is a constant in this model. The assumption that N remains constant requires that the material be isotropic in the sense that the projection of Eq. 2.15 in the π plane is a circle, (i.e., extended von Mises failure criterion), as shown in Fig. 2.5. Since N is a constant , M_c of Eq. 2.2 is equal to M_e of Eq. 2.3 and both are related to N by

$$M = M_c = M_e = 3\sqrt{\frac{3}{2}}\,N \tag{2.16}$$

However, this assumption requires that ϕ_e is much larger than ϕ_c, which is contrary to general experimental observations (Parry 1960, Wu et al. 1963, Parry and Nadarajah 1973)

During isotropic consolidation processes, the void ratio rate of change, $\dot{e}$, is given by

$$\dot{e} = -\lambda \frac{\dot{J}_1}{J_1} \tag{2.17}$$

Upon isotropic swelling process, the elastic void ratio rate of change, e^e is expressed as

$$\dot{e}^e = -\kappa \frac{\dot{J}_1}{J_1} \tag{2.18}$$

The plastic volumetric strain rate is given by

$$\dot{\varepsilon}^p_{kk} = -\frac{(\dot{e} - \dot{e}^e)}{1 + e_i} \tag{2.19}$$

where e_i is the initial void ratio. If we consider J_0 to be the value of J_1 for isotropic consolidation, then the change in the hardening parameter J_0 is related to $\dot{\varepsilon}^p_{kk}$ as follows

$$\dot{J}_0 = \left(\frac{1 + e_i}{\lambda - \kappa}\right) J_0\, \dot{\varepsilon}^p_{kk} \tag{2.20}$$

the plastic modulus can be determined from Eqs 2.10, 2.15 and 2.20. It is given by

$$H = \frac{(2J_1 - J_0)\, J_1\, J_0}{((2J_1 - J_0)^2 + \frac{4}{3} J_2 / N^4)} \left(\frac{1 + e_i}{\lambda - \kappa}\right) \tag{2.21}$$

The plastic modulus determined from Eq.2.21 may be positive or negative depending upon whether $J_1 > J_0/2$ or $J_1 < J_0/2$. During plastic loading, the yield surface may expand or contract in stress space depending upon whether the location of the stress state lies on the wet or dry side of the critical state.

Using Eqs. 2.7, 2.15, 2.20 and 2.21, the effective stress in undrained deformation may be obtained from Eqs. 2.11 and 2.12. The elastic shear and bulk modulii may be functions of stress invariants and may be expressed in the following form.

$$B = (1 + e_i)\, J_1 / 3\kappa \tag{2.22a}$$

and

$$G = \frac{J_1\,(1 + e_i)(1 - 2\upsilon')}{2\,\kappa\,(1 + \upsilon')} \tag{2.22b}$$

where υ' is the Poisson's ratio. Since Poisson's ratio is not easy to be measured accurately, it is commonly assumed that it is choosen to be a constant. In this case, both the bulk and shear modulii are proportional to J_1 or the effective pressure. It should be noted that when the stress state lies within the yield surface, the model predicts a purely non-linearly elastic response. However, for

elastic loading conditions, problems may arise because of the assumption of Eqs. 2.22; some energy is created or extracted from the soil during closed stress cycles and the energy may becomes dependent upon the stress path. This results in the model violating thermodynamics principles. An alternative formulation to overcome this contradiction is discussed by Zytynski et al. (1978). They assumes that a constant shear modulus be adopted. Further, Wroth (1971) analyzed the undrained triaxial test results on samples of "undisturbed" London clay. These results indicated that the ratio of shear modulus to J_1 increases with overconsolidation ratio increase. This implies Eq. 2.22b is not adequate to estimate the shear modulus from J_1. For these reasons, we will not use Eq. 2.22b to determine the shear modulus but instead we will assume G is a constant. However, a constant value of G combined with a variable bulk modulus B implies a variation of Poisson's ratio with effective pressure.

Finally we note that the modified Cam-clay model employs five model parameters, (λ, κ, G, N, e_i) and one initial value of the hardening parameter J_0. These parameters can be directly evaluated from conventional experiments.

SECTION 2.3 Bounding Surface Soil Model

The concept of the bounding surface was originally introduced by Dafalias and Popov (1975) for metals. Independently, Krieg (1975) also introduced a two-surface model which employed similar ideas to the concept of the bounding surface. Dafalias and Popov (1976) used the concept of the bounding surface and of the plastic internal variables. They proposed a general formulation of equations for rate-independent plasticity. Both formulations of Dafalias and Popov (1976) and Kreig (1975) incorporated a yield surface which lies within the bounding surface. The yield surface and the bounding surface were allowed to move in stress space subject to the isotropic / kinematic hardening rules. The bounding surface formulation was later extended to incorporate cohesive soils by Dafalias and Herrmann. It was the so-called 'Bounding surface soil plasticity model', Dafalias and Herrmann (1980, 1982). Similar to the modified Cam-clay model. This model was built within the frame work of the critical state soil theory.

Dafalias and Herrmann (1980) considered that the yield surface has been shrunk to the stress state inside the bounding surface. Their model assumes that the actual stress has an image stress point on the bounding surface, and the plastic flow direction is defined by this image stress. The plastic modulus associated with the actual stress is related to the image stress by the distance between these two stress points. As a result of these assumptions, the bounding surface model allows plastic deformation to occur inside the bounding surface and a purely elastic domain may not exist.

The general form of the bounding surface is expressed by

$$F = F(\bar{\sigma}_{ij}, \varepsilon^{p}_{kk}) = 0 \tag{2.23}$$

in which $\bar{\sigma}_{ij}$ is the 'image' stress state of the actual stress σ_{ij} projected on the bounding surface. The relationship between $\bar{\sigma}_{ij}$ and σ_{ij} may be given by the so-called 'radial mapping' rule, defined by

$$\bar{\sigma}_{ij} = \alpha(\sigma_{ij}, \varepsilon^{p}_{kk})\, \sigma_{ij} \tag{2.24}$$

The concept of the radial mapping rule is illustrated in Fig. 2.6. The distance factor α is determined from Eqs. 2.23 and 2.24, with realistic values of α ranging between 1.0 and infinity. Note that the image stress cannot be defined from Eq. 2.24 when the stress state is located at the origin. Other choices of mapping rules relating the image stress and the actual stress are possible; such as the image stress may be defined on the bounding surface by mapping from the actual stress and a pole situated outside the origin of the stress space. However this may require the existence of a small pure elastic region enclosing the pole, so that the image stress can be defined everywhere inside the bounding surface during plastic loading conditions. The distance δ between $\bar{\sigma}_{ij}$ and σ_{ij} in stress space is evaluated from

$$\delta = [\,(\bar{\sigma}_{ij} - \sigma_{ij})(\bar{\sigma}_{ij} - \sigma_{ij})\,]^{1/2} = (\alpha - 1)\,[\,\sigma_{ij}\,\sigma_{ij}\,]^{1/2} \tag{2.25}$$

For stress states inside the bounding surface, the plastic loading direction is defined by the normal vector to F at the " image " stress $\bar{\sigma}_{ij}$. Assuming an associative flow rule, Dafalias (1980) arrived at the following equations

$$L = \frac{\dot{\bar{\sigma}}_{ij}\, n_{ij}}{\bar{H}} = \frac{\dot{\sigma}_{ij}\, n_{ij}}{H}$$

$$n_{ij} = \frac{1}{g}\,\frac{\partial F}{\partial \bar{\sigma}_{ij}}\,, \quad g = \left[\frac{\partial F}{\partial \bar{\sigma}_{ij}}\,\frac{\partial F}{\partial \bar{\sigma}_{ij}}\right]^{1/2} \tag{2.26}$$

in which $\bar{H}$ and H are defined as the plastic modulii associated with $\dot{\bar{\sigma}}_{ij}$ and $\dot{\sigma}_{ij}$ respectively. $\bar{H}$ is determined from the condition of consistency satisfying $\dot{F}=0$, while H is interpolated from $\bar{H}$ dependent upon σ_{ij} and α as defined below.

The general formulations of Eqs 2.5 to 2.10 for elastroplastic soil are equally valid for the bounding surface model, but they are now determined using the bounding surface of Eq. 2.23 and the 'image' stress $\bar{\sigma}_{ij}$ instead of the yield surface of Eq. 2.4 and σ_{ij} . The plastic modulus H which appeared in Eqs. 2.6 and 2.10 should be replaced by $\bar{H}$. The effective stress in undrained conditions is determined from both Eqs. 2.11 and 2.12.

The bounding surface soil plasticity model does not employ the concept of a yield surface and therefore no purely elastic region is defined. However, a quasi-elastic domain enclosed by a surface of similar shape to the bounding surface is indirectly defined by Eqs. 2.8 and 2.26 at the stress point σ_{ij} . This quasi-elastic surface is considered as the neutral loading path emanating from σ_{ij} as shown by the dashed line in Fig. 2.6. Elastic deformation occurs when the stress point moves inward from the surface but plastic reloading occurs immediately if the loading direction is reversed. It may

also be possible to define a purely elastic domain of similar shape to the bounding surface by selecting a maximum value of α, α_{max}, so that if α is larger than α_{max} then the model allows elastic deformation only.

In the $\sqrt{J_2}$ versus J_1 invariant space illustrated in Fig. 2.7, the slope of the critical state line N may depend upon the stress invariants. One convenient form for such dependence uses the Lode angle ω which is defined by

$$-\frac{\pi}{6} \le \omega = \frac{1}{3}\sin^{-1}\left[3\sqrt{6}\,\frac{J_3}{J_2^{3/2}} \right] \le \frac{\pi}{6} \tag{2.27}$$

where J_3 is the third stress invariant of σ^*_{ij} (i.e., J_3=det(σ^*_{ij})). Specific values of N determined from triaxial compression and extension tests will be denoted N_c and N_e respectively. For other stress states, N may be expressed as a function of ω.

$$N(\omega) = \frac{2\,n\,N_c}{1 + n - (1 - n)\sin 3\omega} \tag{2.28}$$

where $n=N_e/N_c$. To ensure convexity of the bounding surface, n must range between 0.7 and 1. This is illustrated in Fig. 2.5. Thus the general shape of the bounding surface may depend upon the Lode angle. Two alternative shapes for the bounding surface have been used by Dafalias and Herrmann(1980). The choice of surface depends upon the current dimensionless stress $\eta = \sqrt{J_2}/J_1$. Whenever $0 < \eta \le N$, the bounding surface is elliptic in shape, defined by

$$F = \left(\bar{J}_1 - 2\frac{J_0}{R} \right)\bar{J}_1 + \left(\frac{R - 1}{N} \right)^2 \bar{J}_2 + \frac{2 - R}{R} J_0^2 = 0 \tag{2.29}$$

in which R is a new material parameter and $\bar{J}_1$, $\bar{J}_2$ are the invariants of $\bar{\sigma}_{ij}$. Similar to the modified Cam-clay model, the hardening parameter J_0 is again a function of ε^p_{kk} and the relationship between J_0 and ε^p_{kk} has been choosen identical to Eq. 2.20. When R=2, Eq. 2.29 has a similar form with Eq. 2.15 of the modified Cam-clay model. In contrast, if $\eta > N$, a hyperbolic surface is used, defined by

$$F = \left(\bar{J}_1 - 2\frac{J_0}{R} \right)\bar{J}_1 - \frac{\bar{J}_2}{N^2} + 2\,J_0\left(\frac{1}{R} + \frac{A_c}{N_c} \right)\frac{\sqrt{\bar{J}_2}}{N} - \frac{2}{R}\frac{A_c}{N_c} J_0^2 = 0 \tag{2.30}$$

Here A_c is also a material constant, representing the fraction of J_0 by which the critical state line lies below the asymptote to the hyperbolic surface for triaxial compression, as illustrated in Fig. 2.7. The ratio of A_e to A_c must be equal to the ratio of N_e to N_c maintaining compatibility of both surfaces. Using Eqs. 2.29 and 2.30, the analytic expressions for n_{ij}, α and H are summarized in Appendix (A) and are not repeated here. H is related to $\bar{H}$ by the so-called interpolation rule

$$H = \bar{H} + T\,\frac{\delta}{\delta_o - \delta} \tag{2.31}$$

where δ_o is a reference stress which may be used to capture the stress history of the soil, but it has been taken as the distance between $\bar{\sigma}_{ij}$ and the origin for simplicity (Dafalias 1980). Using Eq. 2.25, Eq. 2.31 becomes

$$H = \bar{H} + T\,(\alpha - 1) \tag{2.32}$$

in which T is the hardening shape function

$$T = P_a\, t(\omega)\,[\,1 + |\eta / N|^{-x}\,]\left\{ 9\left[\frac{\partial F}{\partial \bar{J}_1}\right]^2 + \frac{2}{3}\left[\frac{\partial F}{\partial \sqrt{\bar{J}_2}}\right]^2 \right\} \frac{1}{g^2} \tag{2.33}$$

and P_a is atmospheric pressure providing correct dimensions. Here $t(\omega)$ has the same form as $N(\omega)$ with t_c and t_e being parameters measured from triaxial compression and extension tests. The exponent x has been taken as 0.2 which ensures H becomes singular if η approaches zero, and hence purely elastic loading results.

The plastic modulus $\bar{H}$ evaluated from the elliptic surface is positive. It is negative for the hyperbolic surface. However, even if $\bar{H}$ is negative, H may be positive provided α is sufficientiy large. Also, when $\alpha = 1$, the stress point σ_{ij} has arrived at the bounding surface, and then H equals $\bar{H}$.

Dafalias and Herrmann(1980) assumed both G and B are given by Eqs. 2.22. For the bounding surface model, G is not necessarily assumed to be constant since no purely elastic domain is used and the second law of thermodynamics will not be violated under cyclic loading condition. However, since G value determined from Eq.2.22b may not be representative for most soils, we assume G is constant and B is defined by Eq. 2.22a as used in the modified Cam-clay model.

Using Eqs. 2.29 through 2.33, the effective stress during plastic loading in undrained conditions is determined from Eqs. 2.11 and 2.12. We note that the bounding surface model require six material parameters in addition to the five Cam-clay model parameters. These six new parameters may be determined from soil test results. Procedures are discussed in Dafalias(1980,1982).

In conclusion, the bounding surface soil plasticity model may be restricted to small deformation problems because a frame indifferent stress rate is not incorporated. The constitutive equations do not satisfy the principle of material frame-indifference for arbitrary motions. Incorporation of the co-rotational stress rate in this model may complicate the solution methods. The bounding surface expands or contracts subject the isotropic hardening rule while the stress state can experience plastic loading inside the bounding surface. This is one of the advantages of this model over the modified Cam-clay model. The model does not account for anisotropy which simplifies the formulations and reduces the number of model parameters required. Sophisticated anisotropic hardening soil models can be found in Mroz et al.(1978,79,81) where a relatively small yield surface is assumed inside a bounding surface. The bounding surface model may provide a wide range of possible responses, and this is reflected in the number of model parameters required.

SECTION 2.4 Rate-type Model

The rate-type model of Davis and Mullenger(1979) was founded upon the theory of hypoelasticity (Truesdell and Noll, 1965). It was proposed as an alternative to plasticity models for constitutive modelling of in elastic behaviour of soils

In 1956, Green discussed a special hypoelastic constitutive equation which he considered to be a generalization of incremental plasticity. It was found by Mroz(1980) that a full correspondence exists between Green's formulation of hypoelastic theory and the isotropic hardening model of classical plasticity theory during loading conditions. Romano(1974) combined the basic concepts of hypoelasticity and with those of critical state theory. He developed a model for granular material with the critical void ratio being the key parameter. Following similar ideas to Romano's model, Davis and Mullenger (1979) proposed a rate-type model in which a elliptic yield surface, similar to the yield surface for modified Cam-clay, was embedded in the model. The term yielding that we use here is defined as in the sense of classical plasticity theory. Inside the yield surface, it is assumed that loading and unloading processes may involve inelastic deformations and a linear elastic domain may not exist. Mroz (1980) and Hashiguchi (1980) pointed out that the rate type model of Davis and Mullenger(1978), violated the continuity condition between loading and unloading domains. However, the rate type model (Davis and Mullenger 1979) with which we are particularly concerned in this work is well founded for monotonic loading. Also, any discontinuities in both loading and unloading equations will vanish for isochronic or undrained deformation problems. This will be illustrated here.

2.4.1 Model Formulation

The constitutive equation of a hypoelastic material may be written (Truesdell and Noll, 1965) in the following form

$$\overset{\circ}{\sigma}_{ij} = \Gamma_{ij}(\sigma_{mn}) [D_{mn}] \qquad (2.34)$$

where $\overset{\circ}{\sigma}_{ij} = \dot{\sigma}_{ij} - W_{im}\sigma_{mj} + \sigma_{im}W_{mj}$ is the co-rotational stress rate. W_{ij} and D_{ij} are the components of spin and rate of deformation tensors. The tensor function Γ_{ij} is linear in D_{mn} and is isotropic in both σ_{mn} and D_{mn}. The general form of Eq. 2.34 is given by

$$\begin{aligned}\overset{\circ}{\sigma}_{ij} = &(a_1 D_{kk} + a_2 \sigma_{mk}D_{km} + a_3 \sigma_{mn}\sigma_{nk}\sigma_{km}) \delta_{ij} \\ &+ (a_4 D_{kk} + a_5 \sigma_{mk}D_{km} + a_6 \sigma_{mn}\sigma_{nk}D_{km}) \sigma_{ij} \\ &+ (a_7 D_{kk} + a_8 \sigma_{mk}D_{km} + a_9 \sigma_{mn}\sigma_{nk}D_{km}) \sigma_{il}\sigma_{lj} \\ &+ a_{10} D_{ij} + a_{11} (\sigma_{il}D_{lj} + D_{il}\sigma_{lj}) \\ &+ a_{12} (D_{il}\sigma_{ln}\sigma_{nj} + \sigma_{il}\sigma_{ln}D_{nj}) \end{aligned} \qquad (2.35)$$

in which the coefficients a_1 to a_{12} are functions of stress invariants.

Romano (1974) and later Davis and Mullenger (1979) assumed that Eq. 2.34 can be replaced by

$$\sigma_{ij} = \overset{*}{\Gamma}_{ij}(\sigma_{mn}, e) [D_{mn}] \tag{2.36}$$

for granular material. It follows that the coefficients a_1 to a_{12} become functions of the stress invariants and the void ratio e. The constitutive equation with the form of Eq. 2.36 has been classified as rate-type fluid by Truesdell and Noll (1965).

Following ideas similar to those employed in Romano (1974) and Davis and Mullenger (1978), we use the sign of the stress power $\Phi = \sigma_{ij} D_{ij}$ to define loading, neutral loading and unloading processes. A loading or neutral loading process is defined by $\Phi > 0$ or $\Phi = 0$ respectively, while $\Phi < 0$ indicates unloading.

Davis and Mullenger (1979) assumed that the non-zero coefficients of Eq. 2.35 are a_1, a_2, a_4, a_5, a_{10}, and are functions of e only. Based on the critical state theory, Davis and Mullenger made the following two assumptions in the rate type model for loading conditions.

$$\text{(i)} \quad p_c = p_c(e) = \frac{1}{2} p_e(e) \tag{2.37}$$

$$\text{(ii)} \quad \bar{M} = \bar{M}(e) = 3 N_c p_c \tag{2.38}$$

where p_c is the critical state pressure and p_e is the virgin consolidation pressure at void ratio e or the so-called equivalent pressure, [Atkinson and Bransby 1978]. The relationship between p_c and p_e in the e - ln p plane is depicted in Fig. 2.8. $\bar{M}$ represents the soil strength at the critical state. Employing the idea proposed by Tokuka(1971), Davis and Mullenger(1979) assumed that yielding is defined when the constitutive matrix becomes singular. Furthermore, they have choosen the non-zero coefficients a_1 to a_{10} to be

$$\begin{aligned} a_1 &= -\frac{2}{3} G \\ a_2 &= a_4 = \frac{2 G p_c}{\bar{M}^2} \\ a_5 &= -\frac{2 G}{\bar{M}^2} \\ a_{10} &= 2 G \end{aligned} \tag{2.39}$$

Using Eq. 2.39 in Eq. 2.35 the rate-type model for loading conditions has the form

$$\overset{\circ}{\sigma}_{ij} = \frac{2G}{\bar{M}^2}\left[\left(-\frac{1}{3}\bar{M}^2 D_{kk} + p_c \sigma_{mk} D_{km} \right) \delta_{ij} + \left(p_c D_{kk} - \sigma_{mk} D_{km} \right) \sigma_{ij} + \bar{M}^2 D_{ij} \right] \tag{2.40}$$

We refer the reader to the original reference cited above for details of the derivation of Eq. 2.40. In this model , G is the elastic shear modulus and is a function of void ratio only. It is noted that a bulk modulus has been indirectly introduced in Eq. 2.40 when choosing the coefficients a_1 to a_{10} in Eq. 2.39, and has the following form.

$$B = \frac{2G}{\bar{M}^2} (2 p_c p - p^2) \tag{2.41}$$

This expression of the bulk modulus allows this model predicts hydrostatic yielding when p approaches the virgin consolidation pressure p_e.

It should be mentioned that an elliptic yield surface having the following form is implicitly embedded into the loading equation of the rate type model. This is given by

$$F = (p - p_e) p + J_2 / (3N_c)^2 \tag{2.42}$$

and is illustrated in Fig. 2.9. Here p is equal to J_1 /3. The yield surface of this model has the identical shape to that of the modified Cam-clay model in the p - q plane for triaxial conditions, but they are different in e-p-q space. The yield surface of the rate-type model is located on the constant e plane, whereas that of the modified Cam-clay model is obtained from the projection of the isotropic swelling line on the state boundary surface. p_c and p_e used in the rate-type model are only functions of e and thus the yield surface remains stationary during undrained deformation. Note that J_0 defined in the modified Cam-clay model is a function of plastic volumetric strain ε^p_{kk}. It follows that the yield surface may expand (or possible contract) during undrained deformation. The relationship between J_0 used in the modified Cam-clay model and p_e defined in the rate-type model is also illustrated in Fig. 2.8.

Assuming that unloading follows non-linear elastic constitutive relationship, Davis and Mullenger derived that the non-zero coefficients of Eq. 2.35 are given by

$$a_1 = \frac{2\,G}{\bar{M}^2}\left(p_c^2 - \frac{1}{3}\bar{M}^2\right)$$
$$a_{10} = 2\,G \tag{2.43}$$

Using Eq. 2.43 into Eq. 2.35, the rate type model for unloading conditions has the form

$$\overset{\circ}{\sigma}_{ij} = \frac{2\,G}{\bar{M}^2}\left[\left(p_c^2 - \frac{1}{3}\bar{M}^2\right) D_{kk}\,\delta_{ij} + \bar{M}^2 D_{ij}\right] \tag{2.44}$$

The bulk modulus implicitly introduced in the unloading Equation 2.44 is given by

$$B = 2\,G\,\frac{p_c^2}{\bar{M}^2} \tag{2.45}$$

The bulk modulus in Eq. 2.45 is choosen to match the bulk modulus for loading conditions in Eq. 2.41 only at p= p_c. As a result of this adoption, a discontinuity in the bulk modulus occurs at the beginning of the unloading process. Further, for the neutral loading conditions, the condition of continuity requires that both the loading and unloading equations should coincide so that uniqueness can be ensured. However, for a general deformation problem, Eqs. 2.40 and 2.44 will not be equal when $\Phi = 0$. Therefore, for general problems, this model violates the condition of continuity. Use of Eqs. 2.40 and 2.44 to describe cyclic loading response should be limited to problems where this discontinuity does not exist. If we consider undrained conditions the rate-type model will not violate the continuity condition. The loading equation 2.40 reduces to

$$\overset{\circ}{\sigma}_{ij} = \frac{2\,G}{\bar{M}^2}\left[\bar{M}^2 D_{ij} - (\sigma_{ij} - p_c\delta_{ij})\,\sigma_{mk}D_{km}\right] \tag{2.46}$$

From Eqs. 2.37 and 2.38, we note that p_c M and G become constants in Eq. 2.46. The unloading equation 2.44 becomes

$$\overset{\circ}{\sigma}_{ij} = \frac{2\,G}{\bar{M}^2}\left[\bar{M}^2 D_{ij}\right] \tag{2.47}$$

Here Eq. 2.47 implies linear elastic unloading. Now we see that when $\Phi = 0$, the conditions of continuity and uniqueness can be satisfied by Eqs. 2.46 and 2.47. Since only undrained deformations are considered in this work, violation of the continuity condition will not be a problem.

2.4.2 Investigation of Undrained Cyclic Loading Responses

Davis and Mullenger (1984) have employed the loading equation 2.46 to solve some simple boundary value problems such as triaxial deformation, simple shear and pure torsion. Here we attempt to investigate the use of both loading and unloading equations 2.46 and 2.47 under undrained conditions. Two hypothetical examples for lightly and heavily overconsolidated soil subjected to arbitrary cyclic loading in triaxial conditions will be considered. The analytic solutions for this problem are summarized in Appendix (B). Two conditions will be used to clarify the initial state of the soil. They are

$$\beta = \frac{\sqrt{2}\,G}{\bar{M}} = \frac{G}{Cus} \tag{2.48}$$

and

$$\tilde{P}_i = \frac{p_i - p_c}{\sqrt{2}\,\bar{M}} = \frac{p_i - p_c}{2\,Cus} \tag{2.49}$$

where β represents the initial rigidity of the soil and is the rigidity index defined by Vesic (1972). The constant Cus denotes the undrained shear strength in plane strain shearing of the soil, and p_i is the initial effective pressure. $\tilde{P}_i$ may be used to classify the state of overconsolidation of soils. When p_i lies on the 'wet' side of p_c, then $\tilde{P}_i$ is positive for normally to lightly overconsolidated soils. In contrast, $\tilde{P}_i$ is negative for heavily overconsolidated soils.

We have choosen $\beta = 50$ for the lightly overconsolidated soil element with $\tilde{P}_i = 0.5$. For the heavily overconsolidated soil element we take $\beta = 50$ but set $\tilde{P}_i$ to -0.5. Using these initial conditions and the analytic solutions given in Appendix(B) for the rate type model, the cyclic loading responses of these two soil elements are obtained for this problem. We note from equations B.8 (see Appendix B) that the normalized deviatoric stress q / 2Cus versus axial strain response is independent of the initial effective pressure for isotropically consolidated soil. Also, the normalized expression for effective pressure (p - p_c)/ 2Cus versus axial strain is identical for both selected soils except the sign is different. For these reasons, only one curve will be shown for illustration. The results are given in Figs. 2.10 to 2.13. Fig. 2.10 to 2.13 indicated that

(a) The deviatoric stress response for reloading in triaxial extension (curve b'-b") is similar to that for initial loading in compression. Both triaxial compression and extension conditions predict identical magnitude of deviatoric failure stress.

(b) Unloading from compressive state at high deviatoric stress levels (line a'-b') results in relatively large magnitude linear elastic response.

(c) Repetitions loading at high deviatoric stress levels result in ratchetting such as curves b-c, c-d and d-e in Figs. 2.10.

(d) There is no change in effective pressure during unloading but each loading process brings the effective pressure closer to the critical pressure.

(e) The rate-type model exhibits positive pore water pressure for lightly overconsolidated soils and negative pore pressure for heavily overconsolidated soils.

From the above results, we note that the model does not reflect the preconsolidation history of the soils in their deviatoric stress and strain response. Large magnitude linear elastic response results from unloading and a ratchetting effect results from repeated loading which may not be realistic for general soil response. Therefore, use of this model to predict undrained cyclic loading should be limited to the case where the unloading and reloading stress reversal is not significant. The similarity between the deviatoric stress and strain response in compression and extension conditions may be attributed to the consideration that the soil is isotropic in the model formulation. However, the predicted excess pore pressure for both lightly and heavily overconsolidated soils during loading conditions exhibits some salient features of real soil response.

In conclusion, the rate type model employs the co-rotational stress rate and thus is not restricted to small deformation problems. In the sense of classical plastic theory, soil yielding and plastic flow are incorporated within the model without an additional flow rule or hardening rule. The rate-type model requires few material parameters which simplifies application of the model to the practical problems, but on the other hand this also means that the response of the model is less general. Despite this loss of generality, same salient features of real soil response are captured by the model. The rate type model does not allow translation of the yield surface, it thus cannot account for anisotropy. The continuity condition limits the model to predictions of monotonic loading or undrained cyclic loading conditions. The ratchetting effect predicted by the model for cyclic loading response may not be realistic for cyclic loading of real soils. However, if unloading and reloading reversal is not significant or is of limit extent, the model may remain valid.

SECTION 2.5 Determination Of Soil Parameters

In order to make use of the Modified Cam-clay model, the bounding surface model or the rate type model, we must define the initial stress state, stress history, and material parameters for the soils. For initially isotropically consolidated and one-dimensionally consolidated soils, the soil parameters may be obtained from the following formulation.

2.5.1 Isotropically Consolidated Soil

The slopes of the isotropic normal consolidation and swelling lines λ and κ, may be related to more familiar compression and swelling indices C_c and C_s. They are given by

$$\lambda = C_c / \ln 10$$
$$\kappa = C_s / \ln 10 \qquad (2.50)$$

If the soil is unloaded isotropically from the normally consolidated state, the overconsolidation ratio is given by

$$OCR = \frac{p_0}{p_i} \qquad (2.51)$$

where p_0 is the virgin consolidation pressure. Note that p_0 is equal to J_0 /3 for both the modified Cam-clay and the bounding surface model.

The undrained shear strength in triaxial compression, Cu, is required to characterize the soil's strength. It is given by

$$Cu = \frac{3}{2}\sqrt{\frac{3}{2}} N_c p_c \qquad (2.52)$$

We assume that elastic unloading from virgin consolidation state follows the isotropic swelling line, as illustrated in Fig. 2.8. From Eqs. 2.37, 2.42 and Fig. 2.8, the critical pressure p_c for the rate-type model is predicted by

$$p_c = \frac{1}{2} p_i (OCR)^{(1 - \kappa/\lambda)} \qquad (2.53)$$

Similarly, for the modified Cam-clay and the bounding surface models, p_c may be obtained from Eq. 2.29. It is given by

$$p_c = p_i (\frac{OCR}{R})^{(1 - \kappa/\lambda)} \qquad (2.54)$$

in which R is equal to 2 for the modified Cam-clay model.

When κ or λ are not available from existing test results, it may be possible to assume that

$$\sqrt{6} N_c = 1 - \kappa / \lambda \qquad (2.55)$$

for soils with ϕ_c less than 35° Schofield and Wroth(1968) suggested that Eq. 2.55 may be appropriate for most clays. We have used 87 existing data of clay samples from Mayne(1980) to check the validity of Eq. 2.55. The results are summarized in Appendix (C). We find that Eq. 2.55 successfully predicted 54 data with less than 25% error. Therefore assumption of Eq. 2.55 is, in general, valid for most clays.

2.5.2 One-Dimensionally Consolidated Soil

The naturally deposited soil history may be considered to consist of one-dimensional consolidation and (possibly) swelling processes. If we assume no vertical and horizontal shear stress initially in the soil,it may be possible to characterize the stress history of naturally deposited soil by the vertical stress σ_{zi} , the coefficient of lateral earth pressure at rest, K, and the overconsolidation ratio $\overline{OCR}$. For one-dimensionally consolidated soil, the $\overline{OCR}$ is defined as

$$\overline{OCR} = \frac{\sigma_{znc}}{\sigma_{zi}} \tag{2.56}$$

where σ_{znc} is the preconsolidation pressure. The overburden stress σ_{zi} may be obtained directly from measurement of soil bulk unit weight and pore pressure, and the value of K may be measured by means of oedometer tests or pressuremeter tests.

The value of K and $\overline{OCR}$ are not independently determined. For normally consolidated soils, K may be estimated using Jaky's formula

$$K_{nc} = 1 - \sin \phi \tag{2.57}$$

For overconsolidated soils, K may be approximate by, (Parry 1977)

$$K_{oc} = K_{nc} \sqrt{\overline{OCR}} \tag{2.58}$$

During a one-dimensional virgin consolidation process, the state path of the soil should be located on the state boundary surface. The hydrostatic pressure p_{nc} and the deviatoric stress q_{nc} experienced by the soil are given by

$$p_{nc} = \frac{1}{3} \sigma_{znc} (1 + 2 K_{nc}) \tag{2.59}$$

and

$$q_{nc} = \sigma_{znc} (1 - K_{nc}) \tag{2.60}$$

The one-dimensional consolidation line, p_{nc} and q_{nc}, is shown in Figs 2.14. When one-dimensional unloading occurs, the state path departs from the state boundary surface but remains on the elastic wall, as illustrated in Figs. 2.14.

The projections of the one-dimensional consolidation and swelling lines in the e - ln p plane are theoretically parallel to the isotropic normal consolidation and swelling lines, respectively. Therefore λ and κ can be used for both isotropically consolidated and one-dimensionally consolidated soils.

The undrained shear strength Cu is also given by Eq. 2.52. But the critical pressure is obtained as follows. For the rate-type model, p_c is obtained from Eqs 2.37, 2.42 and 2.56 through 2.60 with the aid of Figs. 2.14. It is given by

$$P_c=\frac{p_i}{2}\left[\overline{OCR}\left(\frac{1+2K_{nc}}{1+2K_{oc}}\right)\right]^{(1-\kappa/\lambda)}[x_{nc}^2+1] \tag{2.61}$$

where

$$p_i=\frac{1}{3}\sigma_{zi}(1+2K_{oc}) \tag{2.62}$$

and

$$x_{nc}^2=\frac{2}{3}\frac{(1-K_{nc})^2}{N_c^2(1+2K_{nc})^2} \tag{2.63}$$

In contrast, the critical pressure predicted from the modified Cam-clay and the bounding surface model is obtained from Eq. 2.29. It is given by

$$p_c=p_i\left[\frac{\overline{OCR}}{R}\left(\frac{1+2K_{nc}}{1+2K_{oc}}\right)\right]^{(1-\kappa/\lambda)}\left[\frac{R(1+(R-1)^2x_{nc}^2)}{1+(R-1)\sqrt{1+R(R-2)x_{nc}^2}}\right]^{(1-\kappa/\lambda)} \tag{2.64}$$

or

$$p_c=p_i^{\kappa/\lambda}\left(\frac{J_0}{3R}\right)^{(1-\kappa/\lambda)} \tag{2.65}$$

Again, R is equal to 2 for the modified Cam-clay model.

SECTION 2.6 Comparison Of Model Predictions

In this section, two sets of test results will be used to evaluated the performance of the soil models. The first set of test results is obtained from triaxial compression tests and direct simple shear tests on normally consolidated (undisturbed) Drammen clay. The model parameters evaluated from results of triaxial compression tests will then be used in the soil models to predict the results of the direct simple shear tests. The second set of the test results is obtained from triaxial compression and extension tests on normally to heavily over consolidated (remoulded) Kaolin.

2.6.1 Triaxial Tests

(i) Drammen Clay

Shown in Figs. 2.15 and 2.16 are triaxial compression test results of isotropic normally consolidated Drammen clay. The soil was consolidated up to 400 kpa before being sheared to failure. Typical properties of this soil have been summarized in Table 2.1. This set of test results is available from Anderson (1976), Eekelen and Potts(1978) and from Dyvik et al.(1987).

The results predicted from all three soil models are also shown in Figs 2.15 and 2.16 for comparisons. The selected model parameters for the models have been summarized in Tables 2.2 to 2.3. It is notable that, in this case, for isotropic normally consolidated soils, the predicted results of

the bounding surface model will be identical to that of the modified Cam-clay model if the selected bounding surface model parameter R is taken to be 2 instead of 2.55 .

From results given in Figs. 2.15 and 2.16, we find that both the bounding surface model and the rate-type model predict the test results reasonably well. However, the modified Cam-clay model overestimates the failure strength of the soil and predicts the effective stress path to be significantly different from the measured results at high stress levels.

(ii) Kaolin

The test soil that we consider here is normally to heavily over-consolidated Kaolin, reported by Banerjee and Stipho(1978,1979). The soil was fully remoulded into a slurry and was subsequently allowed to consolidate vertically in a special consolidation cell. Specimens of diameter 7.5cm by 15cm in height were trimmed from the consolidated samples. Each specimen was installed in a triaxial cell for further consolidation to a predetermined isotropic consolidation pressure. For overconsolidated tests, the specimens were allowed to swell isotropically from the normally consolidated state. Typical properties of this soil, reported by Banerjee and Stipho, are summarized in Table 2.4. Further, the initial pressure p_i, overconsolidation ratio OCR, and the void ratio for all these specimens are summarized in Tables 2.5 and 2.6.

Shown in Figs. 2.17 to 2.26 are triaxial compression and extension test results reported by Banerjee and Stipho(1978,1979). All tests were conducted under stress controlled conditions. The cell pressure was held constant during shearing (i.e., the total radial stress remains constant), while the applied total vertical stress was increased or decreased for triaxial compression or extension, respectively.

This set of test results was previously used to verify the modified Cam-clay model by Banerjee and Stipho(1978), and the bounding surface model by Dafalias and Herrmann(1980). In their work, the G modulus has been assumed to be function of J_1 and was evaluated from Eq. 2.22b. However, in this work we assume G is constant and evaluate the G value from the initial slope of the deviatoric stress and strain curves (q vs ε_a) as has been summarized in Tables 2.5 and 2.6. All the necessary parameters for these three soil models have been summarized in Tables 2.7 to 2.9. In Table 2.7, the bounding surface model parameter t_e/t_c has been taken to 1.5 [instead of 2 used by Dafalias and Herrmann(1980)] to provide a reasonably close prediction to the triaxial extension test results. Note that the elementary assumptions of both the modified Cam-clay model and the rate-type model make N independent of the Lode angle. We therefore assumed N_e is equal to N_c for these two models.

The results predicted by these three models are compared with the measured test results in Figs. 2.17 to 2.26. It is found that the modified Cam-clay model predicts unrealistic tensile stresses for samples with OCR larger than 5, and thus these results will be rejected. From Figs. 2.17 to 2.26, we note that

(a) The bounding surface model

--The sophisticated bounding surface model provided remarkable predictions to all test results of the normally to heavily overconsolidated Kaolin.

--In these comparisons, the deviatoric failure stresses q are predicted quite close to the measured results from both triaxial compression and extension tests. Because this model allows the N value to depend upon the Lode angle and the critical pressure p_c can be adjusted by the parameter R to provide reasonable deviatoric failure stresses to fit the test results.

--Since the shape of the response curves may be adjusted by the parameter t_c, t_e, A_c, R and n, a wide range of possible responses are covered by this model to fit the test results.

(b)The rate-type model

--In the comparisons of model response with triaxial compression test results, response of the rate type model compared favourably with the test results. However, as the failure stress is approached, stiffer response deviating from measured results were obtained. Therefore, we find that, in this range, the rate-type model trends to overestimate or underestimate the pore pressure response for lightly or heavily overconsolidated clays respectively.

--The model response compares less favourably with extension test results. This is mainly attributed to the basic model assumption that the strength parameter M is determined from N_c, Eq. 2.38, for all conditions. Thus the rate-type model provided better predictions for triaxial compression results than for extension results.

--This model demonstrated that it captured some realistic features of the real soil response and it provided reasonable predictions for normally to heavily over-consolidated clays.

(c)The modified Cam-clay model

--This model suffered excessive strength softening in predicting the response for heavily overconsolidated soils.

--The model significantly over-predicted the deviatoric failure stresses in these comparisons. However, it may be improved by allowing the from of elliptic yield surface to be controlled by an additional parameter (i.e., such as the form of Eq. 2.29 of the bounding surface model).

--The model was less successful in these comparisons, but it also demonstrated the capability to capture some salient features of the response of normally to lightly over consolidated clay.

--This model requires fewer parameters than does the bounding surface model, therefore, in many cases where insufficient test results exist to evaluate the model parameters for more sophisticated models, the modified Cam-clay model remains an efficient model to

provide comprehensive studies on general geotechnical engineering problems for normally to lightly over-consolidated clays.

2.6.2 Direct Simple Shear Tests

In section 2.6.1, the soil models are verified under conditions where the directions of the principal stresses remain unchanged during the tests. In the case of simple shear conditions (i.e., plane strain deformation), rotations of the principal stress axes will occur during shearing. The direct simple shear test is one of the standard soil tests that is capable of applying this condition. Therefore in this section, we will attempt to predict the simple shear test results.

The test results that we consider here are available from Dyvik et al.(1987). The test soil is undisturbed Drammen clay. The soil properties have been summarized in Table 2.1. Circular specimens were consolidated under one-dimensional conditions. The consolidation pressure, σ_{znc}, is equal to 255kpa which is about twice the in situ preconsolidation stress. The measured value of K_{nc} is 0.49 which agrees well with that predicted from Eq. 2.57. During the test, the specimen was sheared allowing for shear distortion, γ_{xz} , in the horizontal direction and the applied total vertical stress was held constant. The pore pressure and horizontal shear stress, σ_{xz}, were measured.

In modelling these tests, we assume that the stress condition and shear distortion of the specimen in a direct simple shear device are identical to those in an idealized simple shear strain conditions as shown in Fig. 2.27. Ideally, the direct simple shear test should develope a condition of uniform simple shear strain in the sample under undrained conditions. However, inside the direct simple shear device, the complementary shear stress may not be developed on the vertical sides of the specimen, and slippage may occur between the clay sample and the upper and lower cap. Hence, the stress conditions in the specimen may be different from those in an idealized simple shear strain conditions.

Figs. 2.28 to 2.30 compare predictions of the soil models with the test results. The required model parameters have been shown in Table 2.1. Both the modified Cam-clay model and the bounding surface model require numerical integration. Fortunately, analytic solution for the rate-type model for this problem are possible and are summarized in Appendix (B). Predicted results indicate that all three soil models over-estimate the horizontal shear stress, σ_{xz}. However, the bounding surface model provides a better prediction to the test results than the other two models. The difference between the predicted and measured results may be due to

(a)Lack of complementary shear stresses developed on the vertical sides of the specimen and, more important, the stress conditions in the specimen during the test which are, in general, non-uniform [Airey and Wood (1987)]. These may alter the distributions of shear and effective normal stresses and prevent the idealized simple shear strain conditions from taking place during the test.

(b)Strength anisotropy exhibited by the soil has not been incorporated in both the modified Cam-clay model and the rate-type model (i.e., the deviatoric stress at failure

is the same in both triaxial and simple shear strain conditions). Therefore these two models significantly over-estimate the soil strength under simple shear strain conditions.

The bounding surface model allows the predicted soil strength to vary depending upon the loading stress path (i.e., N depends upon the Lode angle). However, we find that because the bounding surface model follows an associative flow rule, the Lode angle of the stress state at failure is governed by the shape of the bounding surface in the deviatoric plane, or by the ratio $n=N_e/N_c$. Similar findings have been extensively discussed by Eekelen (1980) and Potts and Gens (1984). We note that the Lode angle is zero when n=1, the stress condition corresponding to the intermediate principal stress being equal to the mean value of the major and minor principal stresses. From above analysis, we selected n=0.72, the predicted Lode angle of the stress state at failure is approximately equal to 19° as shown in Fig. 2.31. Therefore the predicted deviatoric stress at failure in plane strain deformation is not significantly different from that in triaxial compression conditions. The model predicts the deviatoric stress at failure in simple shear conditions is lower than that in triaxial compression conditions, and provides a better prediction of σ_{xz} than the other two models. However, a 25% over prediction of measured σ_{xz} has been found.

SECTION 2.7 Summary

In this section, the modified Cam-clay model, the bounding surface model and the rate-type model have been studied. All three soil models consider that the soil is an isotropic material. Anisotropy has not been included within these models. Only the rate-type model employes the co-rotational stress rate and thus may not be restricted to small deformation problems. In the class of simple boundary value problems that we have considered here, analytic solutions have been obtained from the rate-type model while the other two models require numerical integration. The rate-type model has been criticized in that it violates the conditions of continuity. However, we have found that any discontinuities in both loading and unloading equations of this model vanish for isochronic or undrained deformation problems. Also, this model may be valid to describe cyclic response of soils under undrained conditions if unloading and reloading reversal is not significant.

The model predictions have been compared with test results in triaxial and simple shear strain conditions. In the case of triaxial conditions, the bounding surface model provides remarkable predictions to fit all test results of normally to heavily over-consolidated soils. However, the bounding surface model requires more model parameters, which need sufficient test results to be evaluated than that of the modified Cam-clay model and the rate-type model. The rate-type model predicts reasonable results for the normally to heavily over-consolidated soils. The predictions of the modified Cam-clay model are less successful in these comparisons, and are restricted to the application to normally to lightly over-consolidated soils.

In comparisons of the model predictions with truely undrained direct simple shear test results, both the modified Cam-clay model and the rate-type model significantly over-estimate the measured horizontal shear stress. This is mainly because the extended von Mises failure criterion has been adopted in these two model. Since the bounding surface model allows the projection of the bounding surface model on the deviatoric stress plane or the π plane to be adjusted by inclusion of the Lode angle, more reasonable results than those of the modified Cam-clay model and the rate-type model have been achieved.

The disadvantage of the modified Cam-clay model shown in these comparisons can be easily removed by changing the shape of the yield surface on both the 'wet' and 'dry' side of the critical state. However, the model parameters required by both the modified Cam-clay model and the rate-type model are essentially similar. The advantages demonstrated by the rate-type model may indicate that it may be an alternative for the modified Cam-clay model especially for undrained deformation problems. The bounding surface model provides more reasonable response than do the other two models, but it requires numerous model parameters. The rate-type model and the modified Cam-clay model are useful because of the few parameters which need to be specified in order that the model may be used.

Material Parameters	
λ	0.14
κ	0.05
ϕ_c	30°
N_e	0.326
K_{nc}	0.49
liquid limit	55
plasticity index	28
natural water content	45%

Table 2.1 Soil properties of Drammen clay , (after Eekelen 1978, Dyvik 1987)

	triaxial compression test	simple shear test
G (kpa)	16000.0	13000.0
p_i (kpa)	400.0	168.3
σ_{zi} (kpa)	400.0	255.0
e_i	1.02	1.15

Table 2.2 Initial conditions of Drammen clay for undrained triaxial compression and simple shear tests.

	triaxial compression test	simple shear test
p_c (kpa)	200.0	119.0
$\bar{M}$ (kpa)	195.0	117.0

Table 2.3 Rate-type model parameters for Drammen clay

Material Parameters	
λ	0.14
κ	0.05
N_e	0.231
N_c	0.286

Table 2.4 Soil properties of Kaolin, (after Banerjee & Stipho, 1978).

OCR	p_0 (kpa)	p_i (kpa)	G (kpa)	e_i
1	366.0	366.0	10650.0	0.94
1.2	366.0	304.0	6350.0	0.95
5	380.0	76.0	2750.0	0.95
8	386.0	48.0	1670.0	0.95
12	413.0	35.0	1100.0	0.95

Table 2.5 Initial conditions of Kaolin for undrained triaxial compression tests, (after Banerjee & Stipho, 1978 ,1979).

OCR	p_0 (kpa)	p_i (kpa)	G (kpa)	e_i
1	414.0	414.0	11000.0	0.93
1.2	414.0	345.0	10150.0	0.93
6	551.0	92.0	3675.0	0.95
10	414.0	41.4	1932.0	0.95

Table 2.6 Initial conditions of Kaolin for undrained triaxial extension tests, (after Banerjee & Stipho, 1978 ,1979).

Model Parameters	
n	0.8
Ac	0.085
tc	11.0
te/tc	1.5
R	2.6

Table 2.7 Bounding surface model parameters for Kaolin, (after Dafalias & Herrmann 1980).

OCR	p_c (kpa)	$\bar{M}$ (kpa)
1	183.0	157.0
1.2	171.0	147.0
5	107.0	92.0
8	92.0	79.0
12	85.0	73.0

Table 2.8 Rate-Type model parameters for Kaolin, (undrained triaxial compression tests).

OCR	p_c (kpa)	$\bar{M}$ (kpa)
1	207.0	178.0
1.2	194.0	166.0
6	145.0	124.0
10	91.0	78.0

Table 2.9 Rate-Type model parameters for Kaolin, (undrained triaxial extension tests).

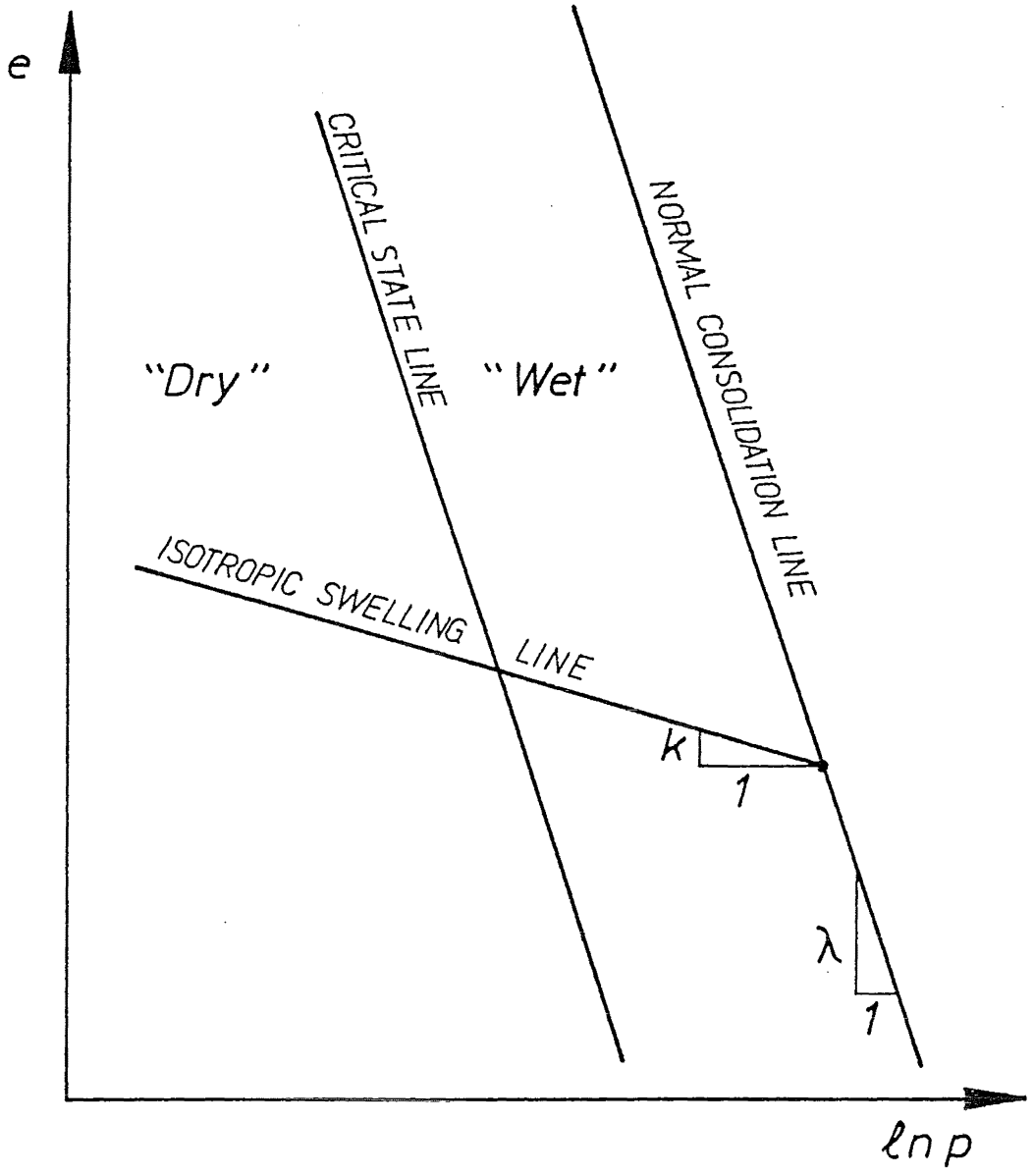

Figure 2.1 The normal consolidation, swelling and critical state lines in e - ln p plane.

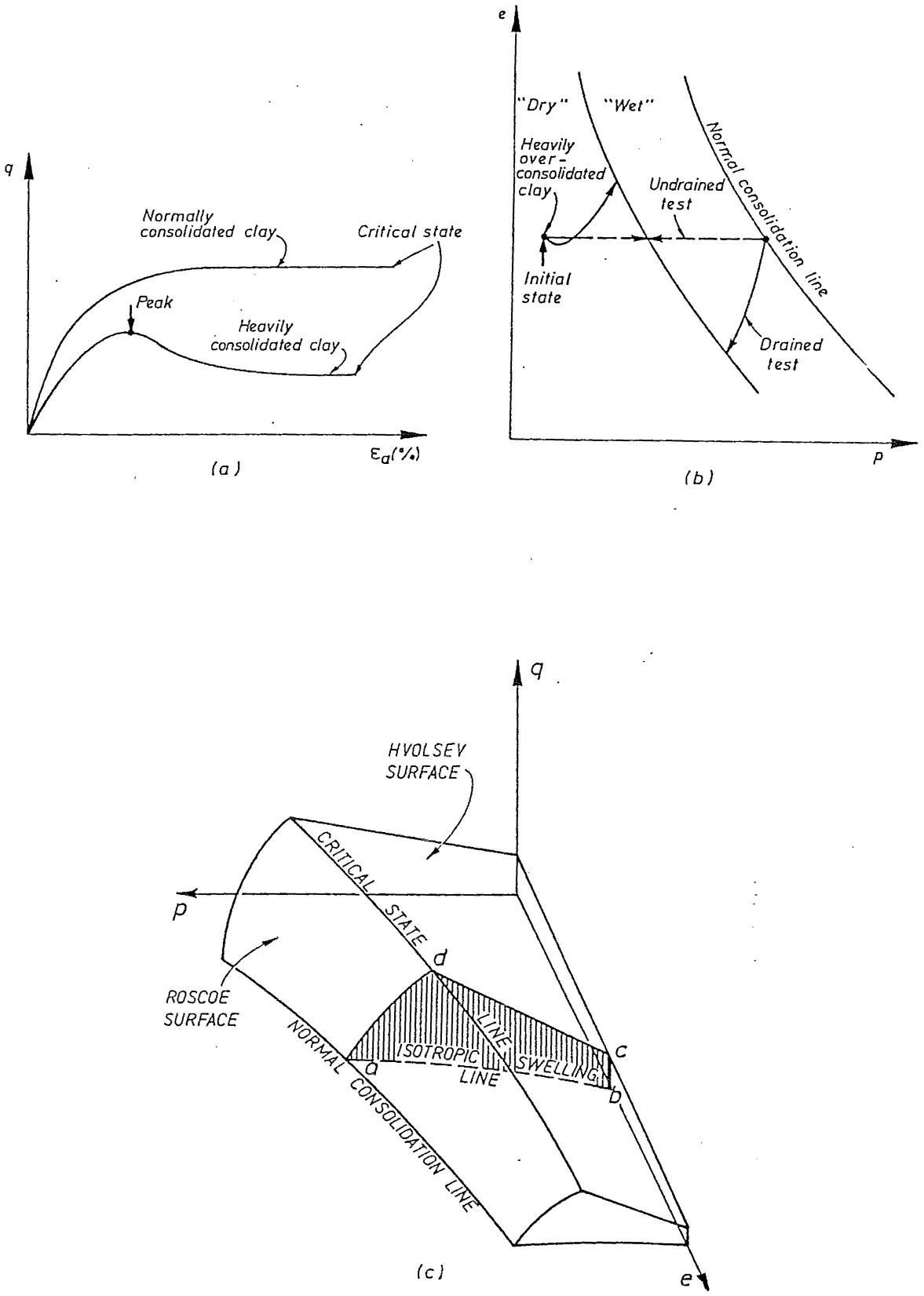

Figure 2.2 General behaviour of clay, (a) stress and strain response (b) state path in e-p plane and (c) the state boundary surface.

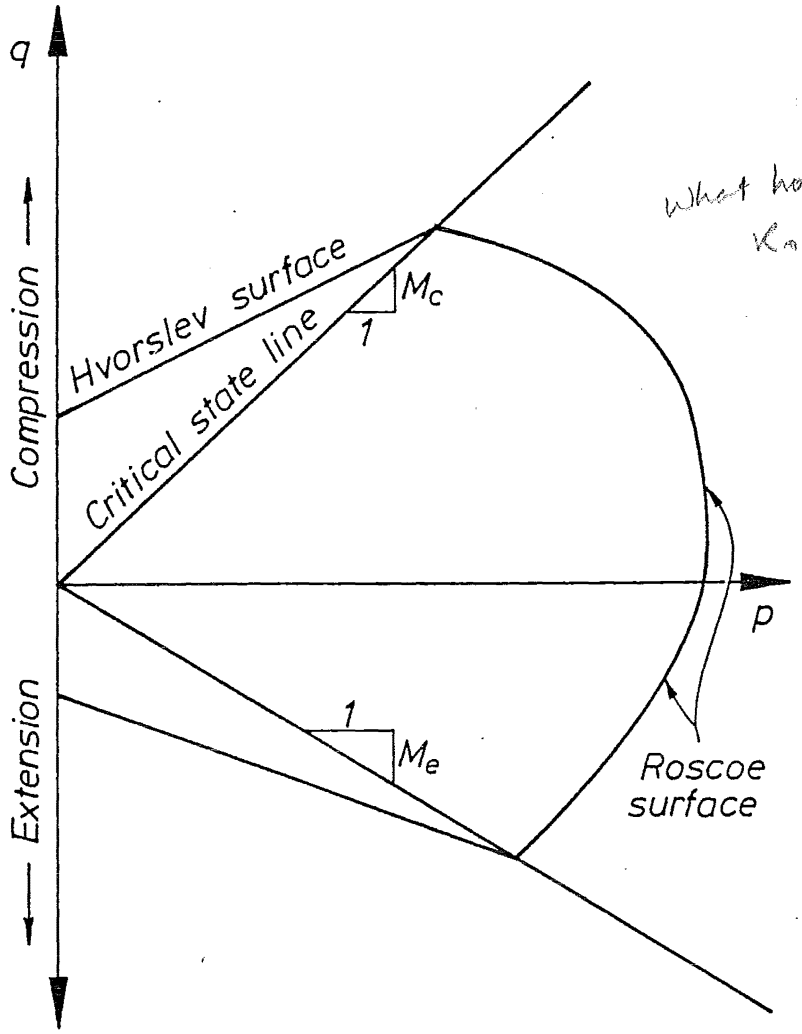

Figure 2.3 State boundary surface in p - q plane.

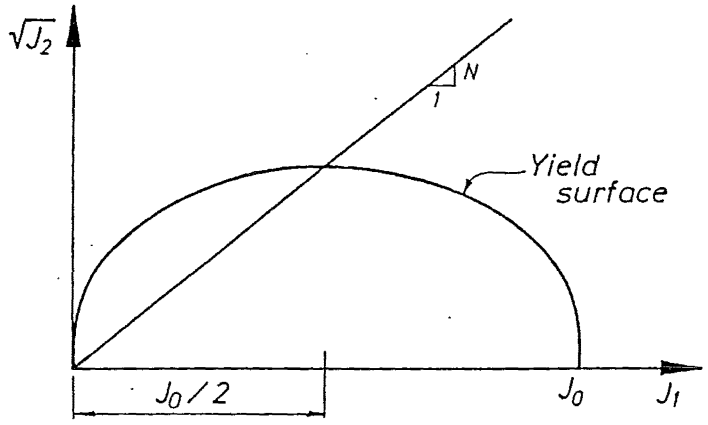

Figure 2.4 Elliptic yield surface of modified Cam-clay model.

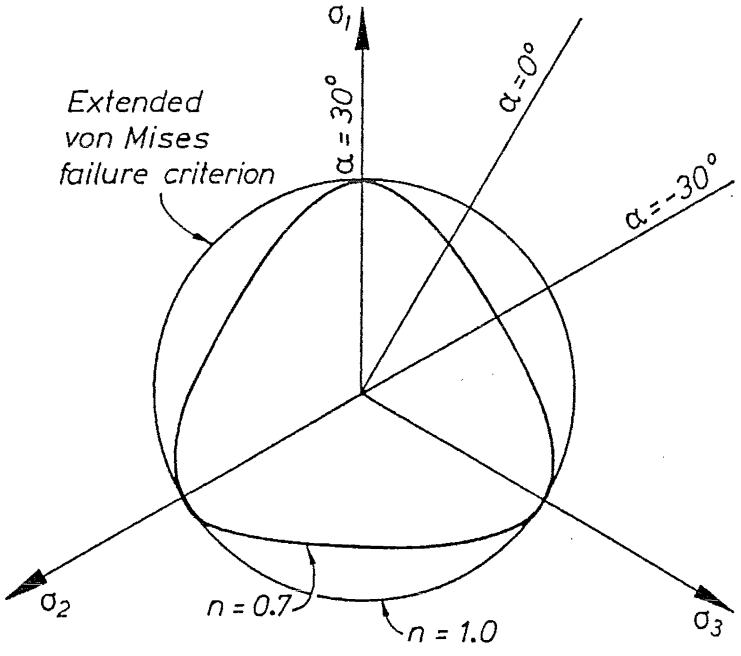

Figure 2.5 Projection of the failure surfaces on π plane.

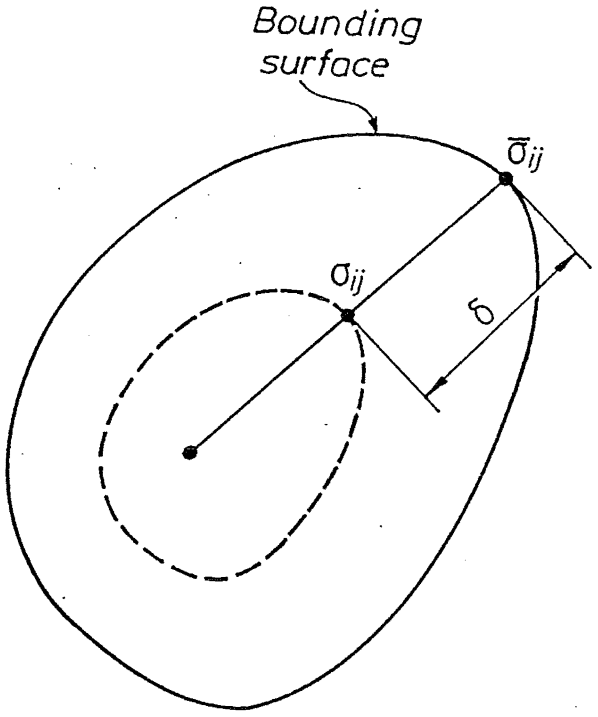

Figure 2.6 Bounding surface and radial mapping rule in generalized stress space.

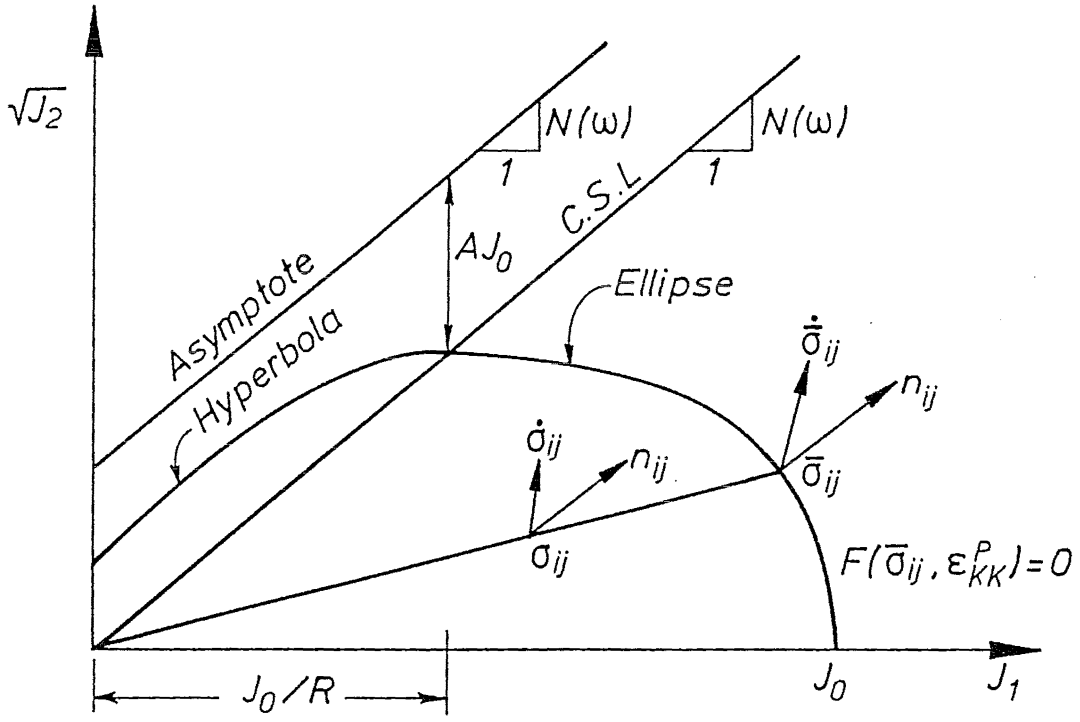

Figure 2.7 Bounding surface in J_1 - $\sqrt{J_2}$ plane.

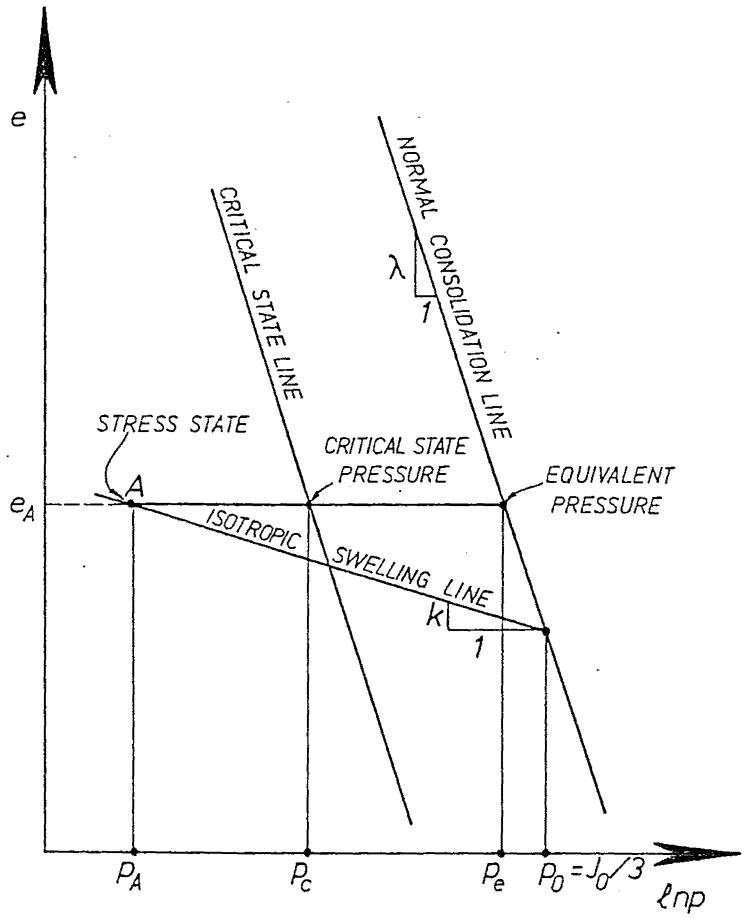

Figure 2.8 Relationship between critical pressure and equivalent pressure in e - ln p plane.

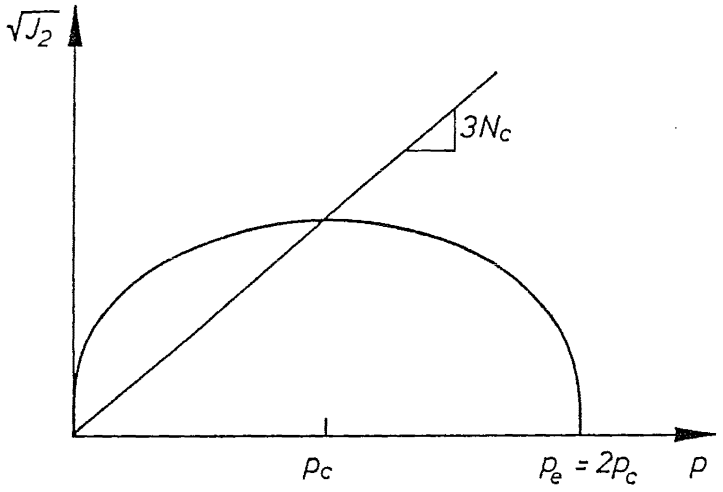

Figure 2.9 Elliptic yield surface of the rate-type model in p - $\sqrt{J_2}$ plane.

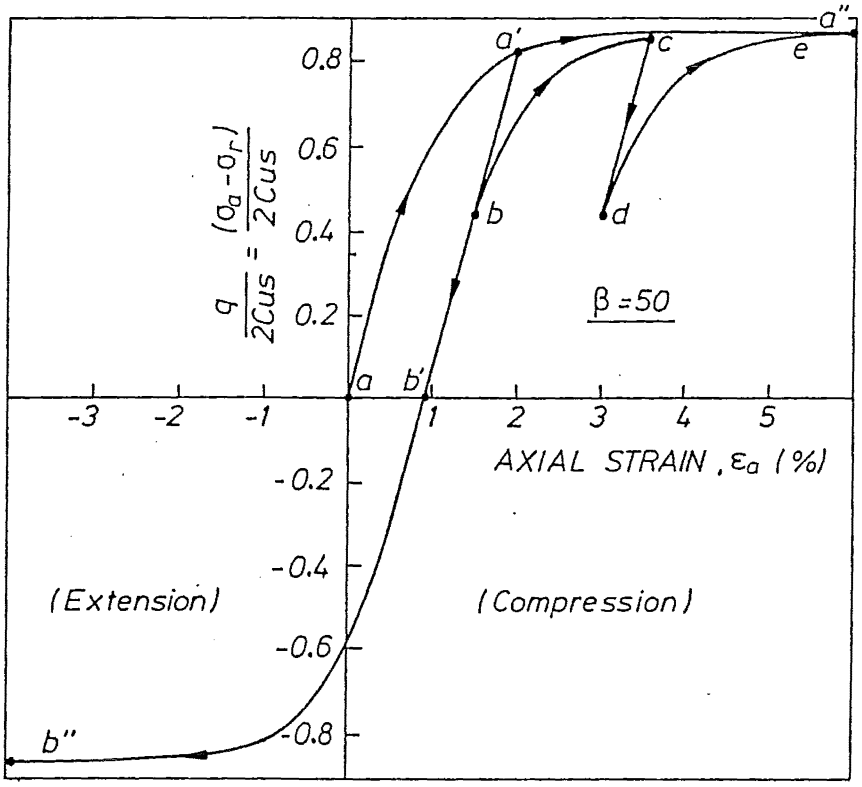

Figure 2.10 Deviatoric stress and axial strain response of the rate-type model under undrained triaxial and cyclic loading conditions.

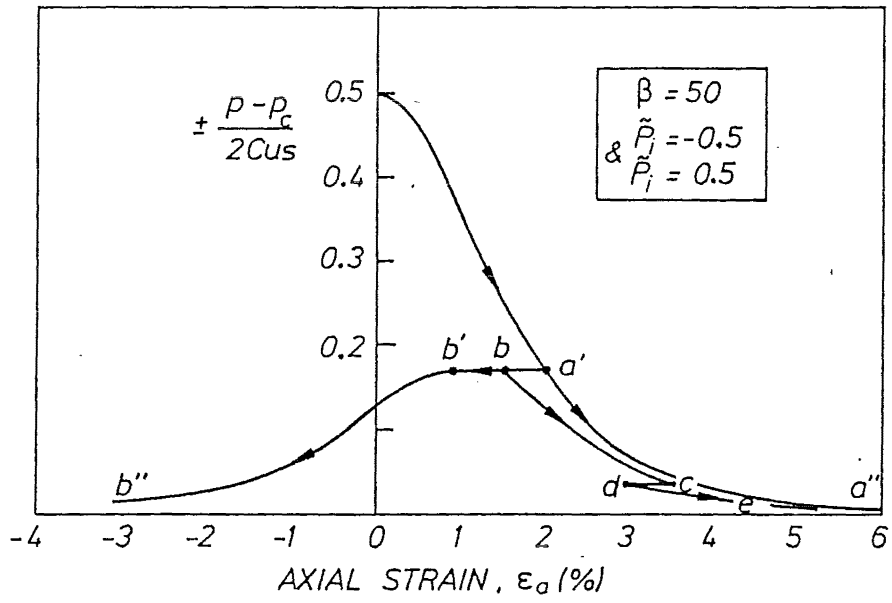

Figure 2.11 Effective pressure and axial strain response of the rate-type model under undrained triaxial and cyclic loading conditions.

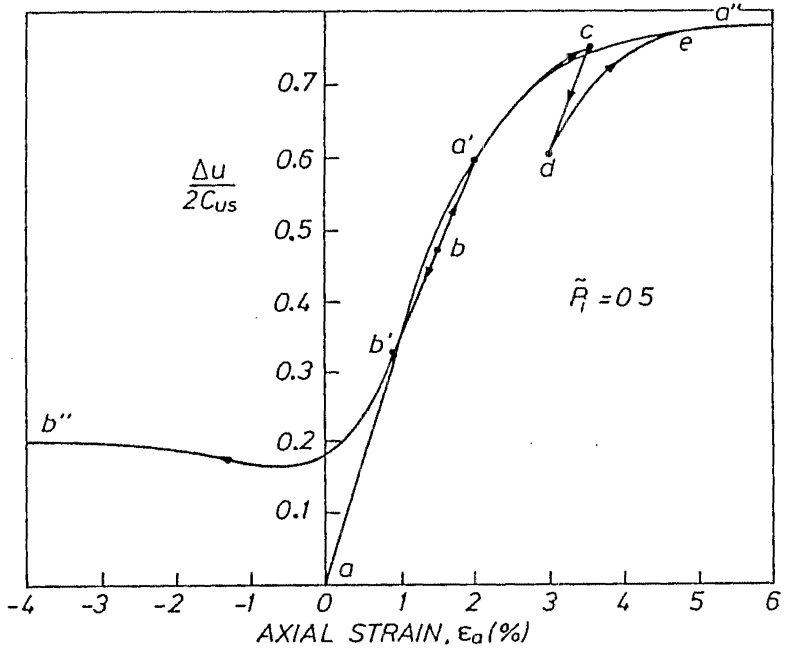

Figure 2.12 Pore pressure and axial strain response of the rate-type model for lightly overconsolidated soil under triaxial and cyclic loading conditions.

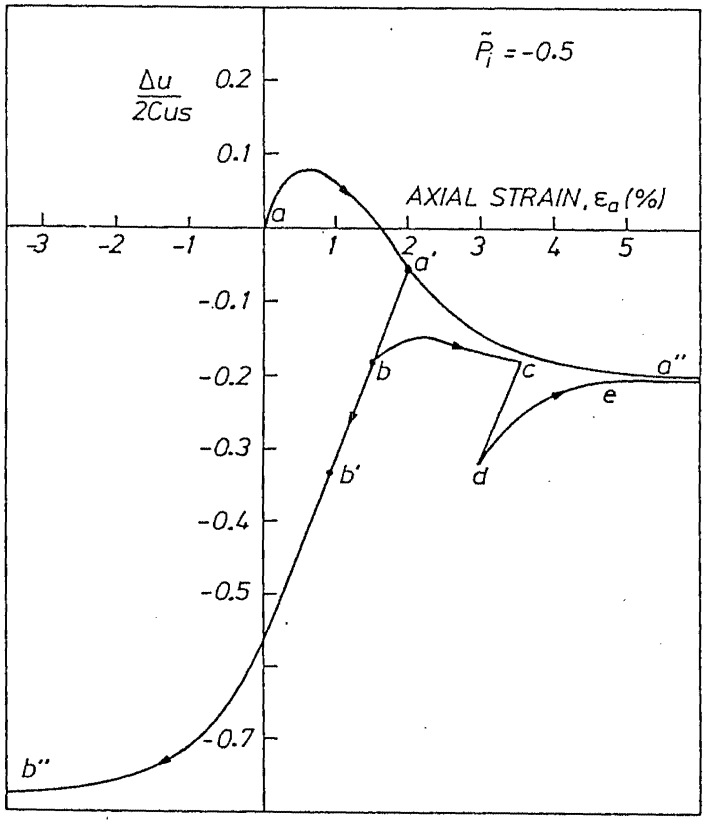

Figure 2.13 Pore pressure and axial strain response of the rate-type model for heavily overconsolidated soil under triaxial and cyclic loading conditions.

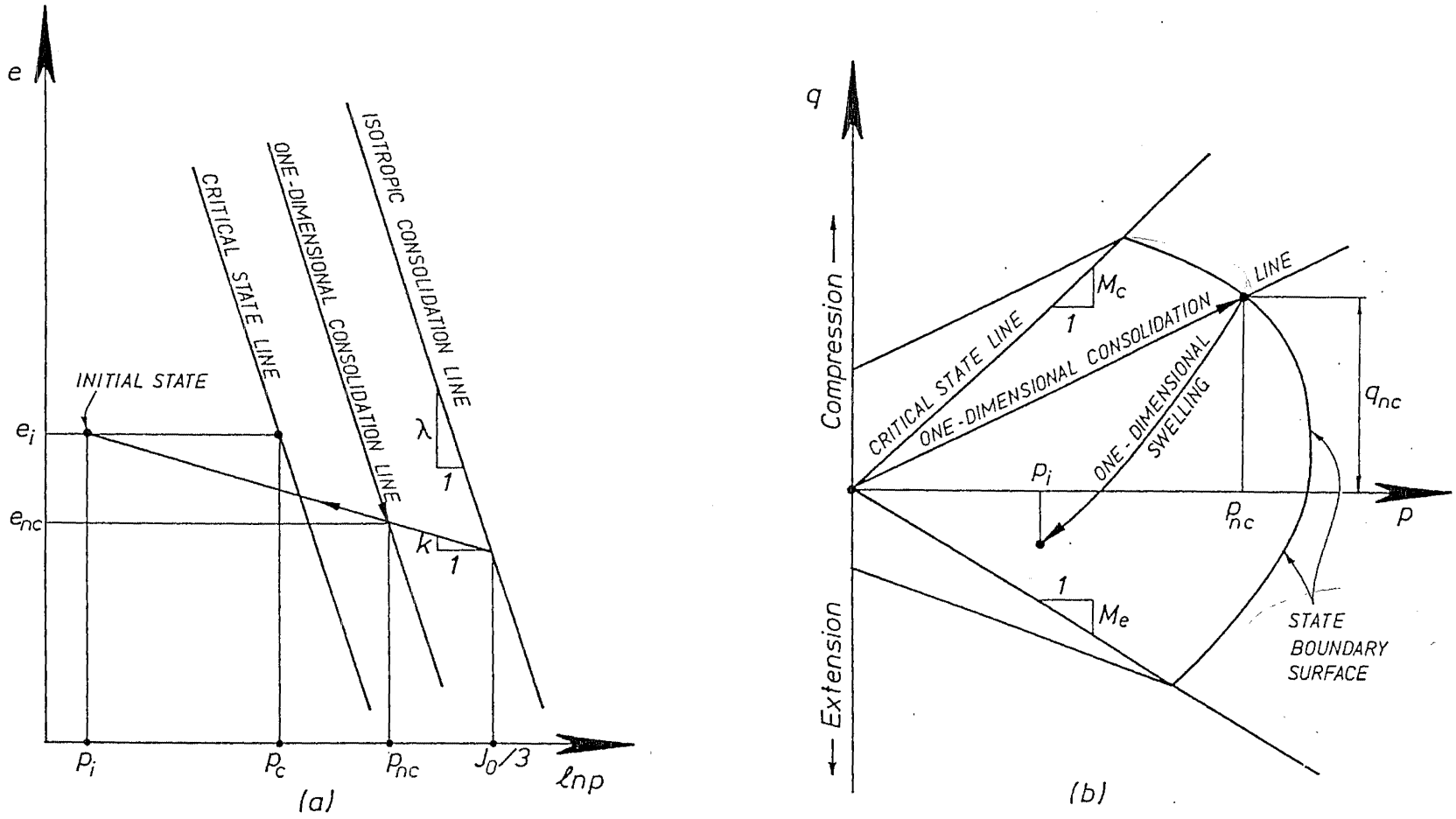

Figure 2.14 One-dimensional consolidation line in (a) e - ln p plane (b) q - p plane

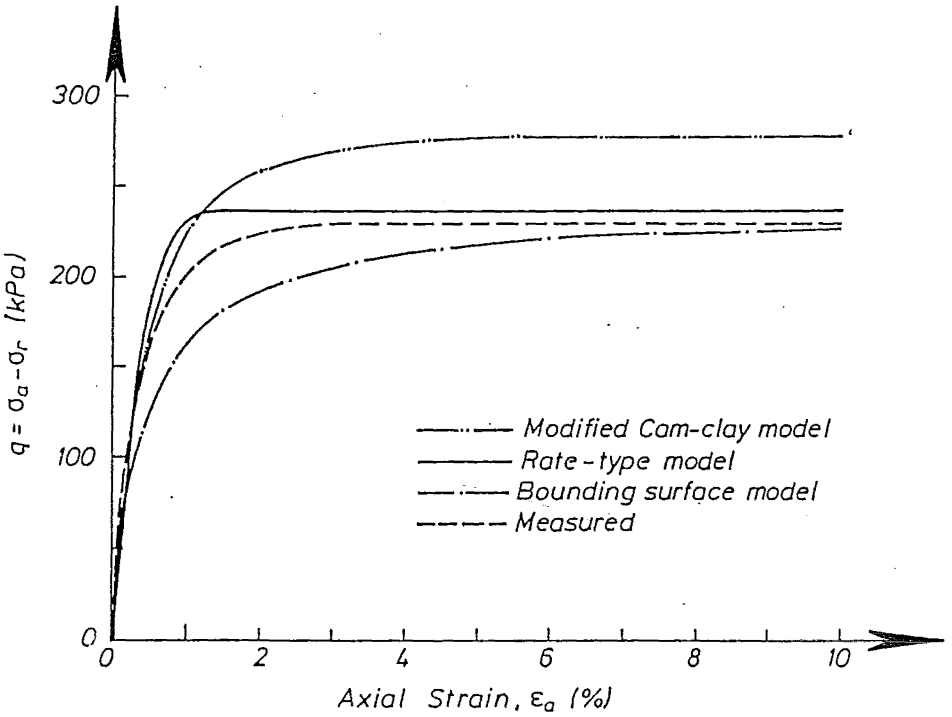

Figure 2.15 Predicted and measured stress-strain curves for undrained triaxial test on normally consolidated Drammen clay.

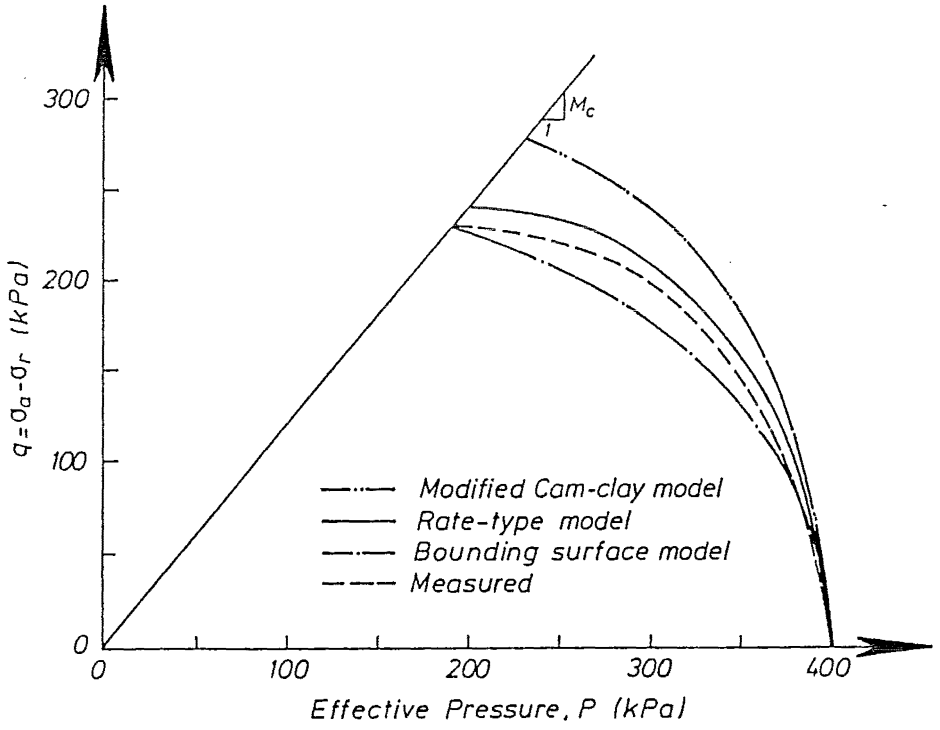

Figure 2.16 Predicted and measured effective stress path for undrained triaxial test on normally consolidated Drammen clay.

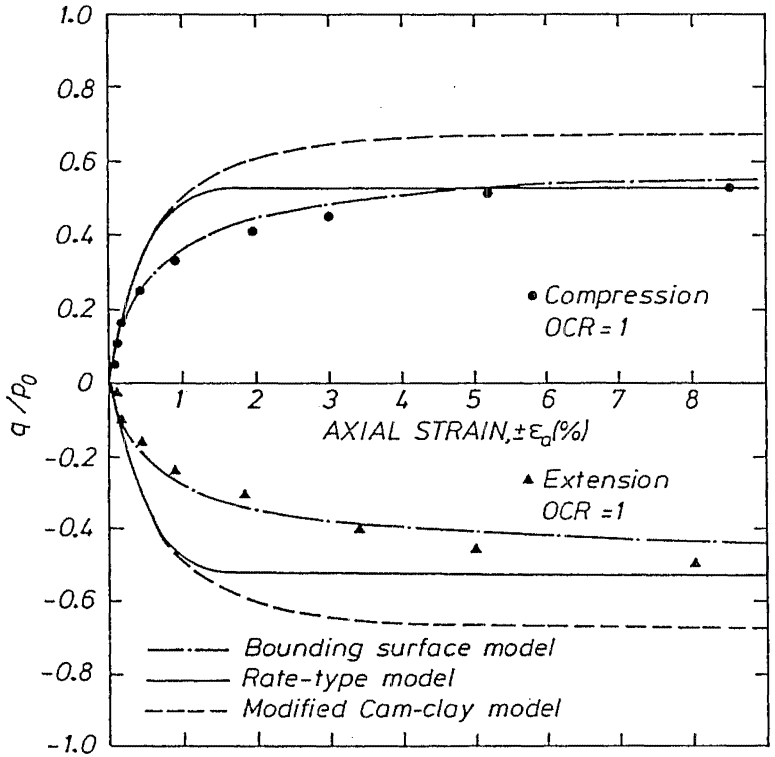

Figure 2.17 Predicted and measured stress-strain curves for undrained triaxial tests on Kaolin (OCR= 1).

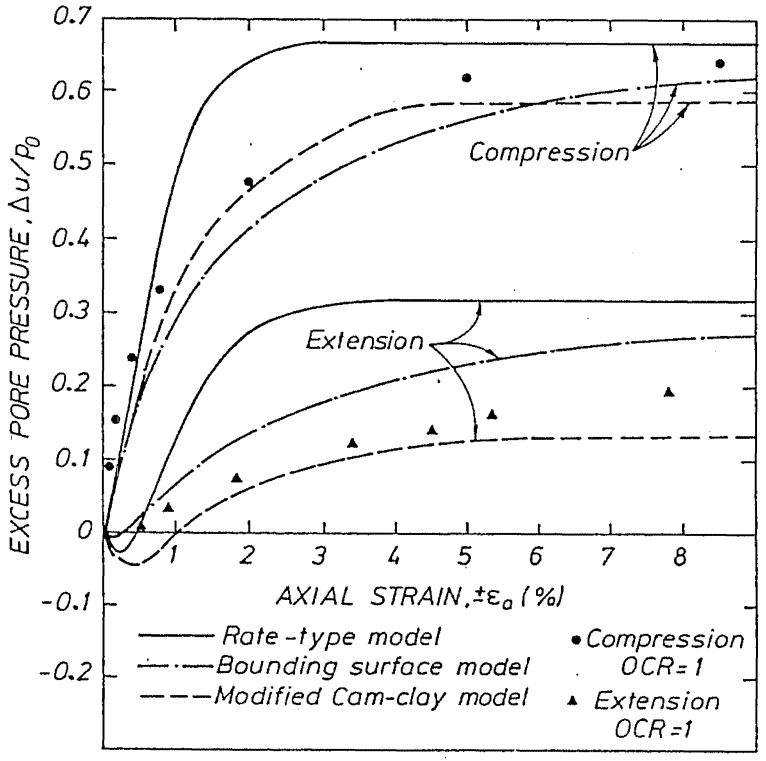

Figure 2.18 Predicted and measured pore pressure-strain curves for undrained triaxial tests on Kaolin (OCR= 1).

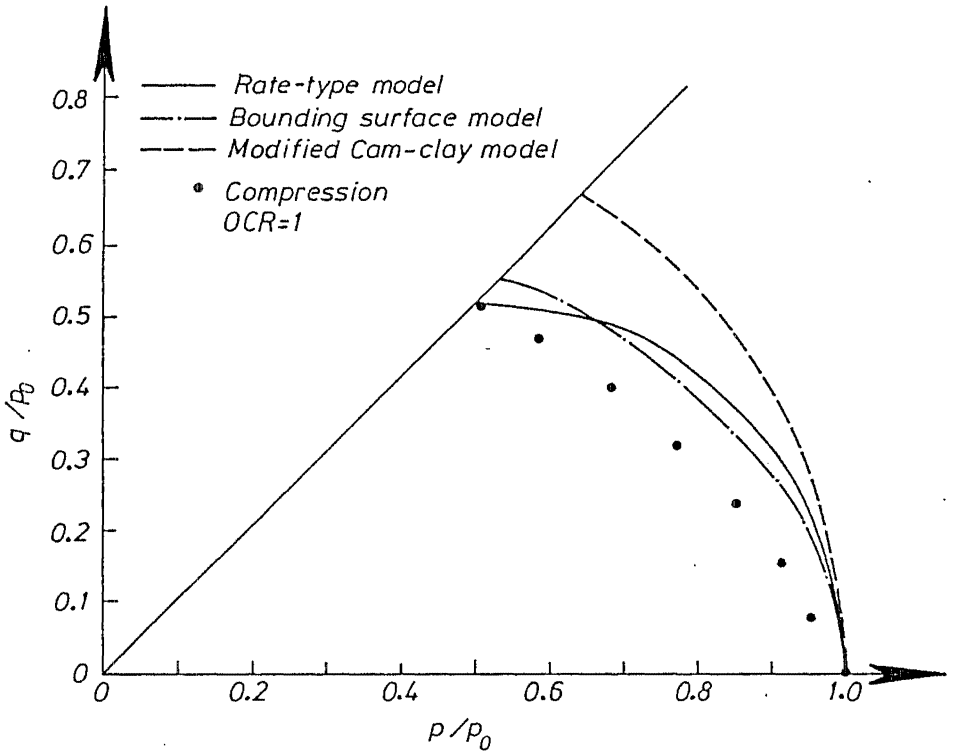

Figure 2.19 Predicted and measured effective stress path for undrained triaxial compression test on Kaolin (OCR= 1).

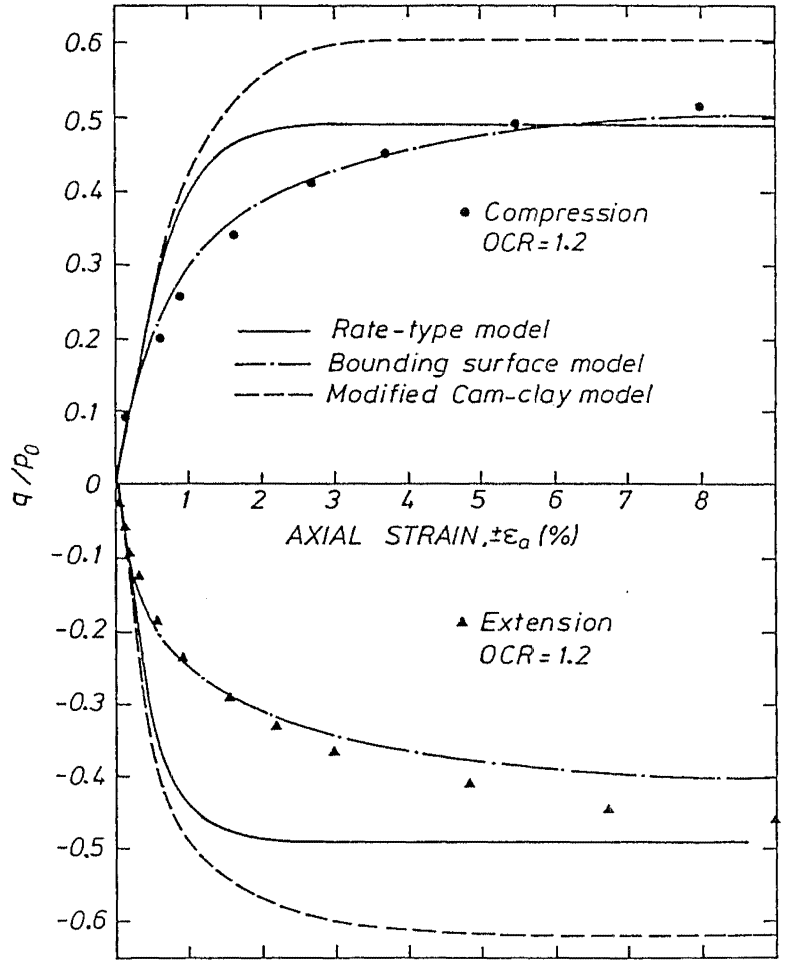

Figure 2.20 Predicted and measured stress-strain curves for undrained triaxial tests on Kaolin (OCR= 1.2).

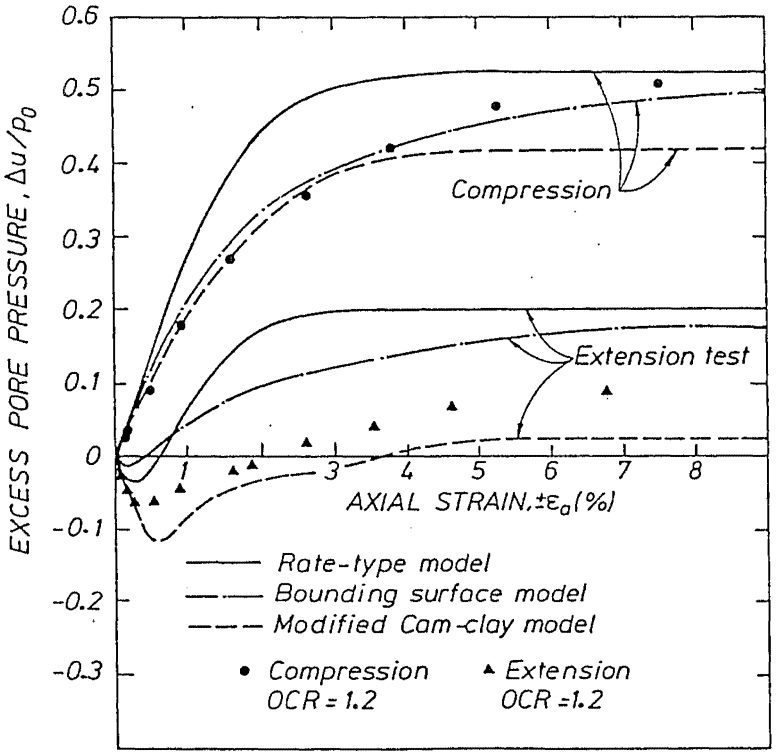

Figure 2.21 Predicted and measured pore pressure-strain curves for undrained triaxial tests on Kaolin (OCR= 1.2).

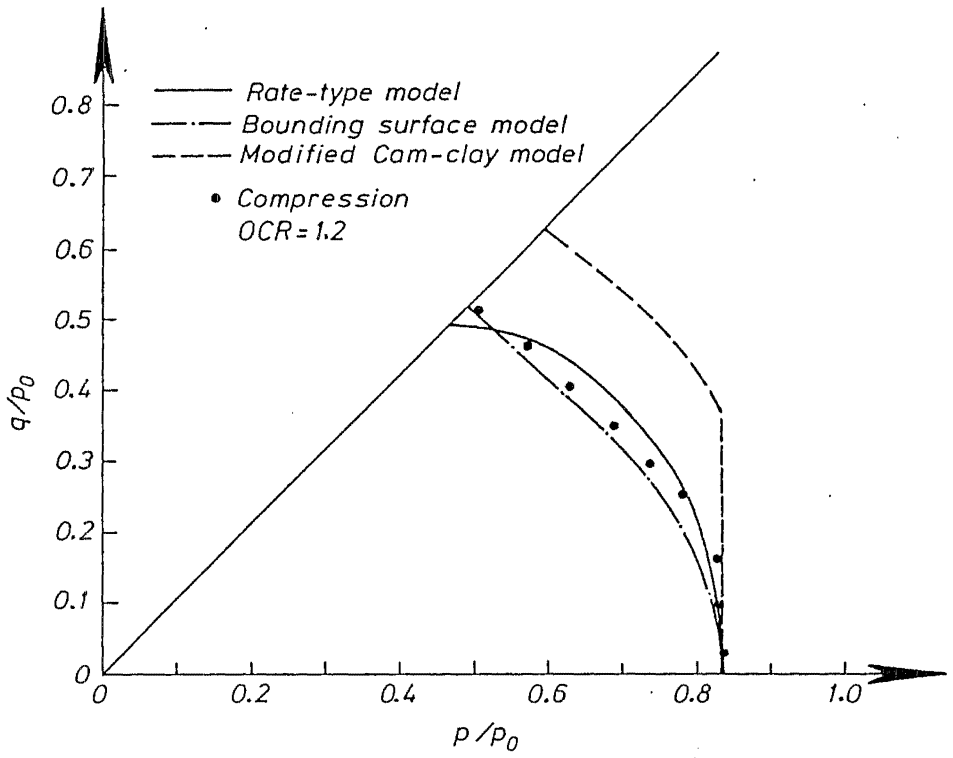

Figure 2.22 Predicted and measured effective stress path for undrained triaxial compression test on Kaolin (OCR= 1.2).

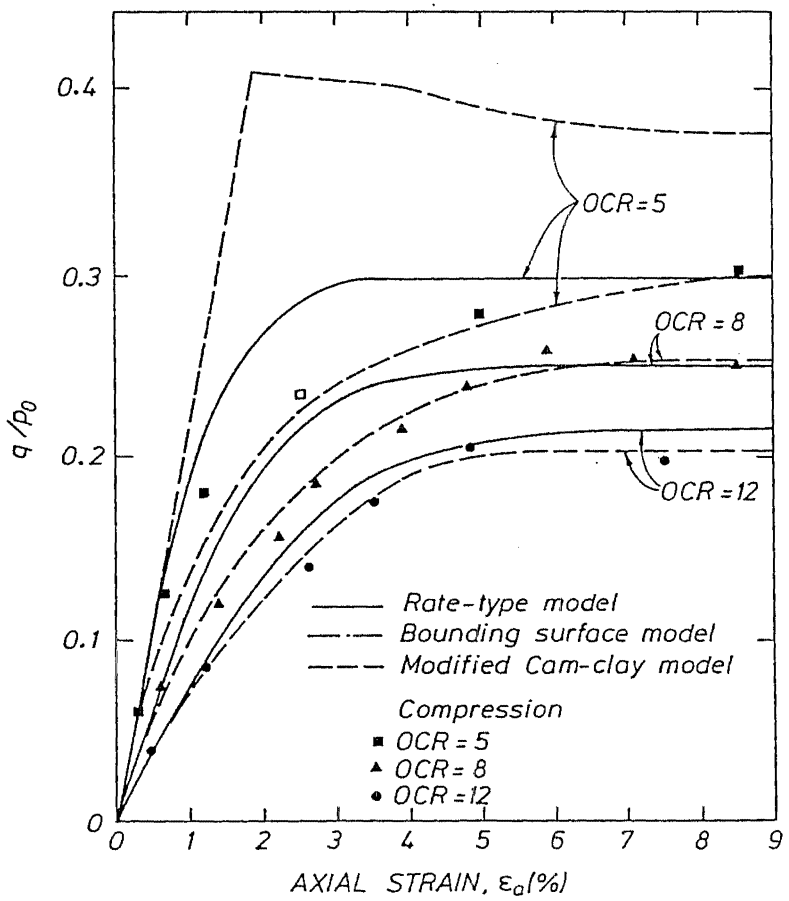

Figure 2.23 Predicted and measured stress-strain curves for undrained triaxial compression tests on Kaolin (OCR= 5, 8, 12).

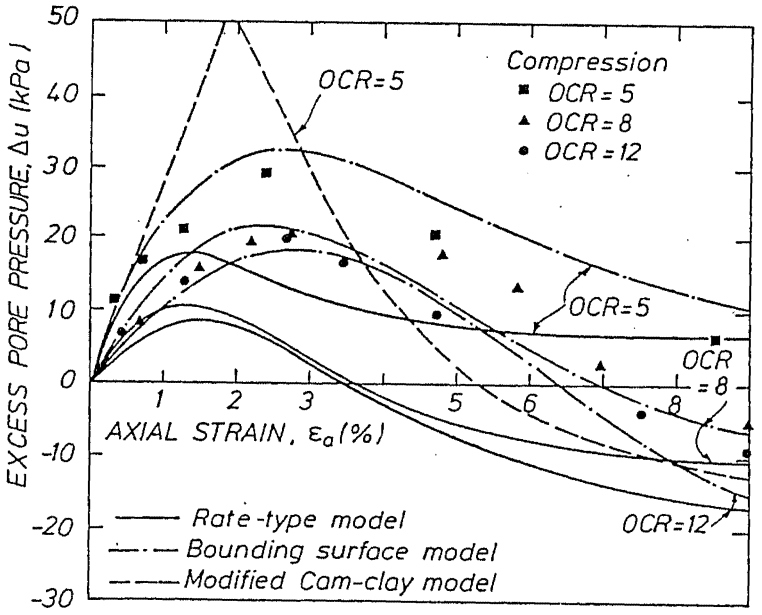

Figure 2.24 Predicted and measured pore pressure-strain curves for undrained triaxial compression tests on Kaolin (OCR= 5, 8, 12)

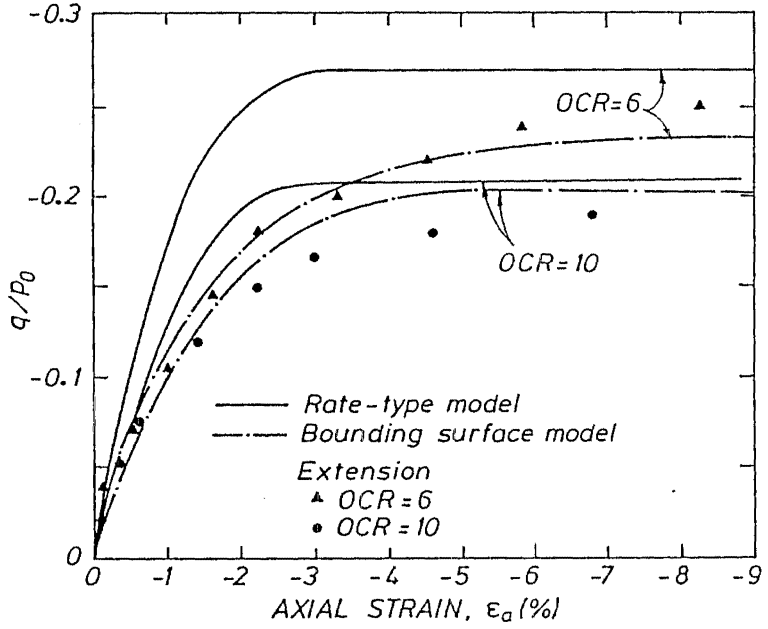

Figure 2.25 Predicted and measured stress-strain curves for undrained triaxial extension tests on Kaolin (OCR= 6,10).

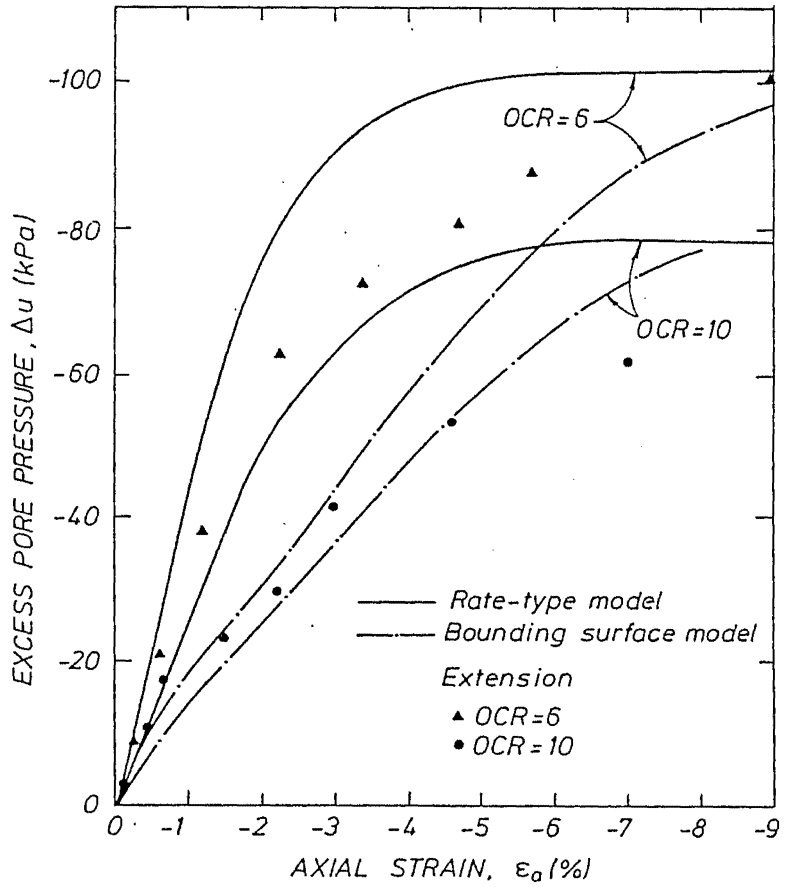

Figure 2.26 Predicted and measured pore pressure-strain curves for undrained triaxial extension tests on Kaolin (OCR= 6,10).

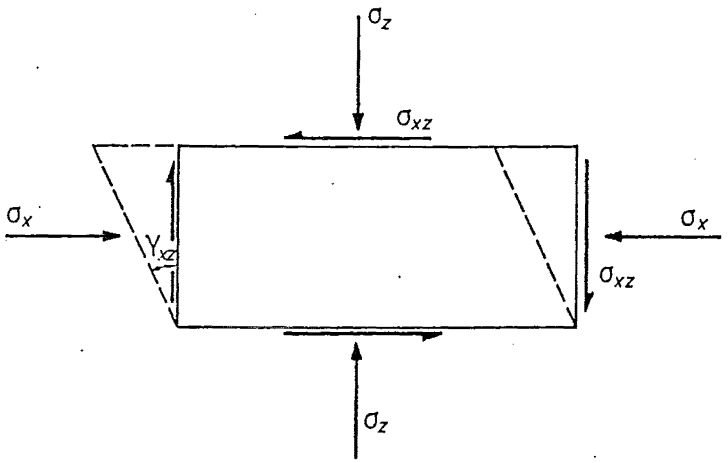

Figure 2.27 Simple shear strain conditions.

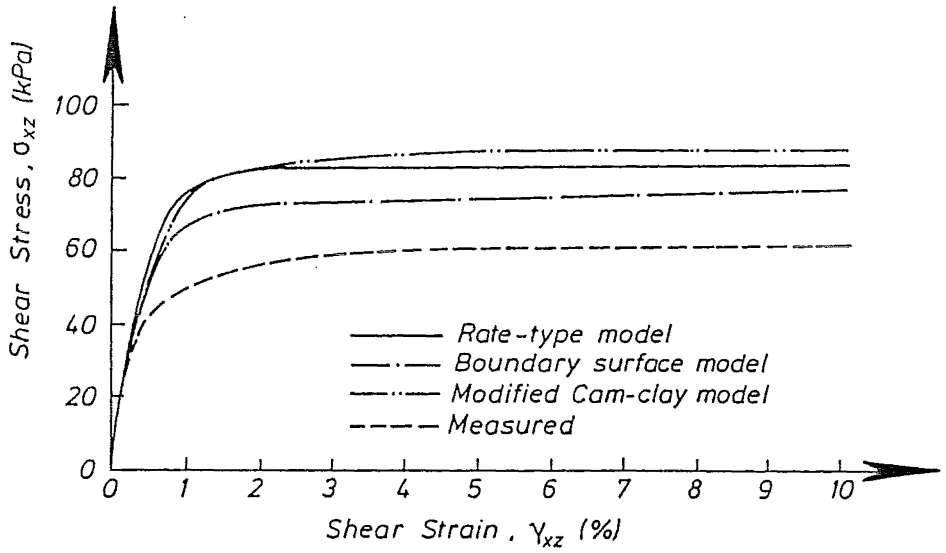

Figure 2.28 Predicted and measured stress-strain curves for undrained direct simple shear test on one-dimensionally normally consolidated Drammen clay.

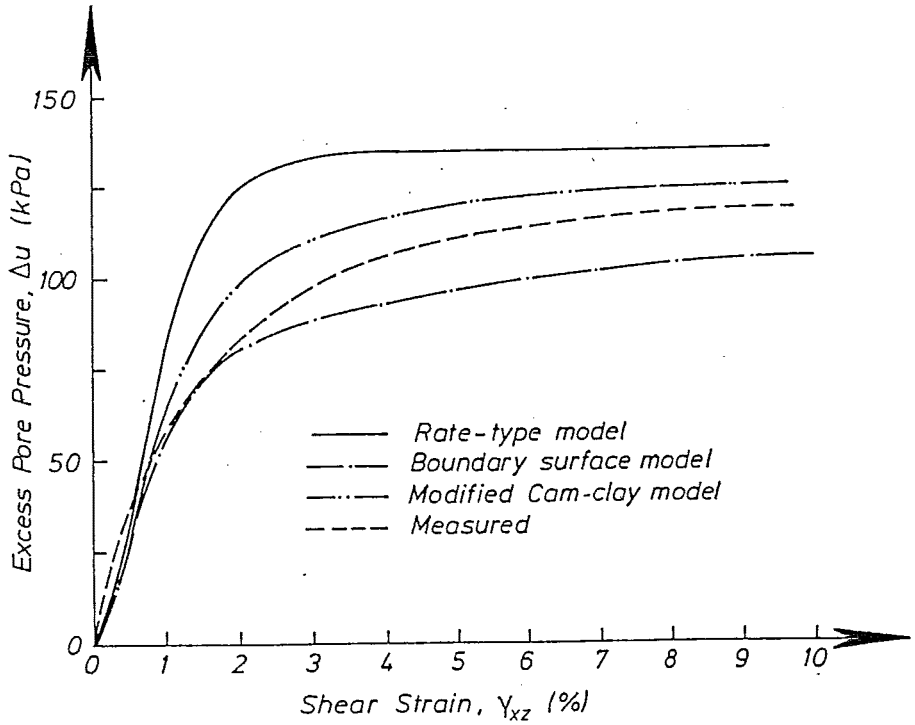

Figure 2.29 Predicted and measured pore pressure-strain curves for undrained direct simple shear test on one-dimensionally normally consolidated Drammen clay.

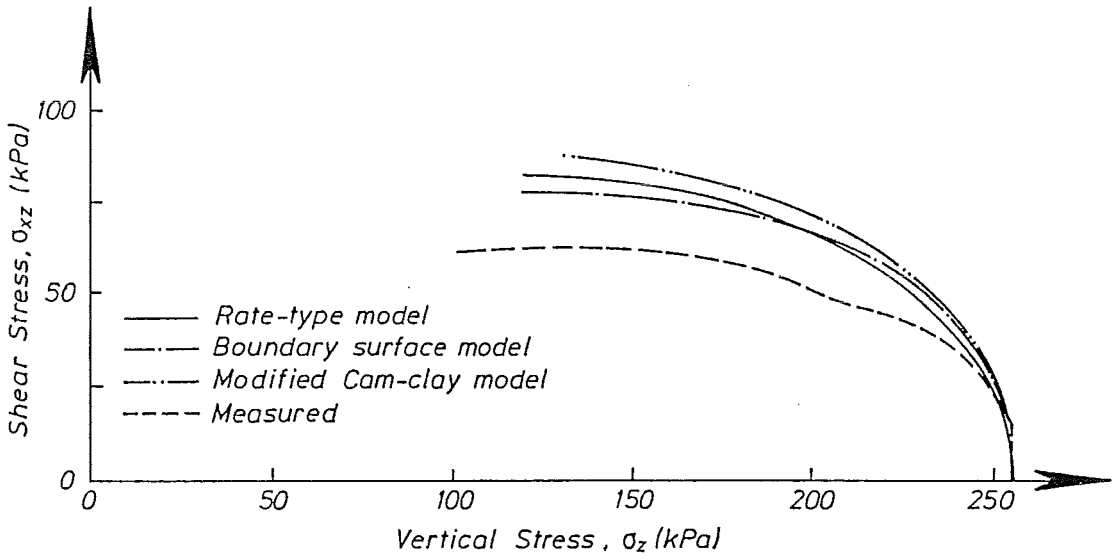

Figure 2.30 Predicted and measured effective stress path for undrained direct simple shear test on one-dimensionally normally consolidated Drammen clay.

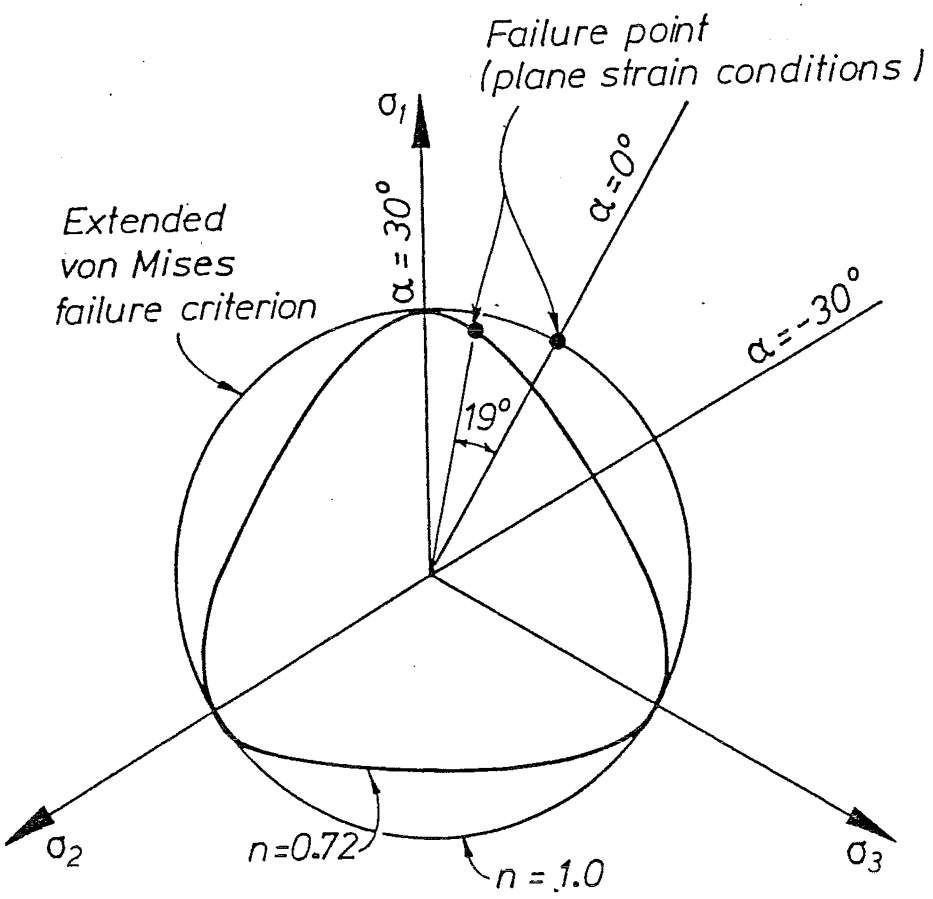

Figure 2.31 Lode angle of stress state at failure on π plane due to plane strain shearing

CHAPTER THREE

EFFECTS OF PILE INSTALLATION:
The Cylindrical Cavity Expansion Approach and The Simple Pile Method

SECTION 3.1 Introduction

It has long been recognized that pile driving processes may significantly alter the initial stress state in a soil. Pile driving in saturated clay generates significant pore pressure in surrounding soils and may cause remoulding around the pile (see for example: Lo and Stermac 1965, Koizumi and Ito 1967, Bakholdin and Bolshakov 1973, Meyerhof 1976). Dissipation of pore water pressure follows immediately after pile driving. At completion of the reconsolidation process, a gain in soil shear strength around the pile may govern the ultimate capacity (Kraft 1982, Kirby et.al 1983).

Traditional pile design methods which have been used to estimate pile shaft capacity largely rely on empirical coefficients deduced from limited numbers of full scale pile test results in various soil conditions. Various factors (i.e., details of pile installation, pile type, and soil type, etc) affecting the subsequent load carrying capacity are included in these empirical coefficients. Among these factors, the effect of pile installation in soils appeared to be important. Recently developed effective stress methods in predicting pile shaft capacity (Focht and Kraft 1981, Kraft et.al 1982, Kirby et.al 1983) employ a theoretical approach to investigate the effect of the pile driving on subsequent shaft capacity. Hence, in this section, we will briefly review some empirical and theoretical pile design methods, and then we discuss the recently developed methods in simulating the pile installation effects in soils.

The popular empirical "α " method for pile design work (Tomlinson 1971, API 1981) relates the limiting skin friction on the pile shaft to the average in-situ undrained shear strength Cu of clay over each soil layer by an empirical 'adhesion factor α'. API 1981 defined the value of α to range from 1 for soft clay to 0.5 for stiff clay. The value of Cu is normally determined from unconfined compression tests. Tomlinson (1971) analyzed 93 pile load test results. He concluded that drag down of overlying soil into a lower layer may affect the skin friction developed between the pile and the soil. He therefore considered that α is a function of soil profile, average undrained strength and penetration depth of the pile. The effects of pile installation, subsequent reconsolidation, and pile length effects, as well as other factors are lumped in this adhesion factor. Thus the choice of the value α in practical pile design work depends largely upon judgement and experience of the design engineer.

Burland (1973) considered that the limiting skin friction at the pile shaft for driven piles is governed by effective stress at the pile-soil interface. For a normally consolidated clay, he deduced a simple expression correlating the limiting skin friction to the in-situ average effective overburden pressure σ_{zi} by a factor " β " which depends upon the coefficient of lateral earth pressure

at rest and angle of friction between pile material and soil. This method is the so called "β " method. Meyerhof (1976) extended this concept to predict driven pile shaft capacity in overconsolidated clay. However, it might be expected that after pile installation the coefficient of lateral earth pressure on the pile shaft may be differ from the coefficient of lateral earth pressure at rest. From pile test results on soft to stiff clay, Tomlinson (1971) found that at a greater depth, failure due to vertical pile loading was found to have occurred in the soil and not at the pile-soil interface. The rupture surface in the soil was comprised of numerous vertical laminations similar to those occurring in one dimensionally normally consolidated clay in the simple shear test at large strain (Randolph and Wroth 1981, Airey and Wood 1987). Therefore, the pile material may have a comparatively minor effect on ultimate pile capacity.

Relying on the concept of Rankine passive earth pressure theory, Vijayvergiya and Focht (1972) estimated the skin friction for long pile explicitly with inclusion of the effect of initial overconsoldation of soil through the ratio of Cu/σ_{zi} by a dimensionless coefficient λ. The values of λ are evaluated based on 47 load tests on pipe piles embedded in clays. This method is referred to as the "λ " method and is claimed to be especially useful in offshore pile design. However, the stress state in soil after pile installation may not be similar to that in a Rankine passive state. Therefore, this correlation between the pile shaft capacity and soil state appears arbitrary.

The α , β and λ methods have been widely used in both past and current design practice. However, individual effects (such as details of pile driving, reconsolidation, pile length, etc) on pile shaft capacity are not fully understood, while all these factors have been lumped in the coefficients α, β or λ.

Details of pile installation (i.e., jacking, driving and pre-drilled pilot holes, etc.) may have considerable influence in subsequent pile shaft capacity. Especially for overconsolidated stiff clay, based on some field evidence obtained by excavating soil from around piles after pile loading to failure, Tomlinson (1971) found that the effects of lateral vibrations or movement (i.e., whipping) of the pile during driving may form a gap between the soil and the upper part of the pile. Water and debris infiltration may close the gap with little adhesion between pile and soil, or result in a lack of pile-soil contact. However, the pile and soil at a greater depths remain in good bonding contact. A tightly-adhering clay coating on the pile shaft was discovered. This may be due to high constraining pressures on pile movement at greater depths. For piles in overconsolidated soils, it can be found from Aurora et.al (1980) and O'Neill et.al (1982a,b) that pile driving generally results in a very low skin friction to undrained shear strength ratio at the upper part of the embedded pile length. Tests results of jacked piles in overconsolidated clay reported by Cooke (1979) indicate that the effect of pile lateral movement is less severe for jacked piles than for driven piles.

Originated by the petroleum industry in 1970's, based on the concept of critical state soil mechanics and a modified Cam-clay model, Randolph et.al (1978a, b) and Wroth et.al (1978) carried out a systematic approach to simulate the stress changes in soil due to pile driving and reconsolidation. In their work, pile driving was represented by a cylindrical cavity expansion

problem, while drainage during reconsolidation was assumed to occur in the radial direction only with no straining of the soil in the vertical and hoop directions. These assumptions are based on the consideration that at a greater depth pile whipping and surface effects due to pile driving may vanish. The pile tip effect in soil has also been ignored. This concept has been used to develop new generation pile capacity models (Focht and Kraft 1981, Kraft 1982, Kirby et.al 1983) to estimate pile shaft capacity for offshore piles. However, the cylindrical cavity expansion method may not correctly include the strain path history of the surrounding soil caused by pile advancement. Therefore it may be questionable that cavity expansion methods can provide sufficient details of pile driving effects.

Baligh (1984, 1985) introduced the so-called "simple pile method". He considered that in the case of the deep penetration problem, the strain field around the rigid 'simple pile' may be determined by an ideal fluid flow field. This method may be used to investigate the effects of pile driving, since the complicated strain path experienced by the soil due to pile advancement is given in advance. However, the simple pile method is an approximation, because the strain field around the simple pile has been assumed identical to that in an ideal fluid.

Both the cylindrical cavity expansion approach and the simple pile method are efficient in investigating effects of pile driving in the sense that no complicated numerical procedure is required. Therefore, it is our attempt in this chapter to study the solutions of these two methods and compare their results with existing test results.

The rate-type model (Davis and Mullenger 1979) will be used to represent the soil in this chapter. This model is a rate-independent soil model, the strain rate effects and strain softening characteristics in soils under undrained conditions are not incorporated. The rate-type model may not, in general, provide sufficient flexibility to model any particular soil. Nevertheless, the model was built within the frame work of the critical state soil mechanics. It requires fewer model parameters than many other soil models and it possesses some salient response features exhibited by many soils as we have shown in chapter two. Therefore, the rate-type model becomes a useful tool in this work to investigate the pile driving problem.

The strain, effective stress and pore pressure fields in a infinite soil mass predicted from the cylindrical cavity expansion approach and the simple pile method will be compared in this chapter. Pile driving is considered as steady driving or steady pile penetration.

SECTION 3.2 The Deformation Field

3.2.1 General

Palmer (1972) and Vesic (1972) considered an infinite cylindrical cavity expanding from an finite radius in infinite soil mass. This method has previously been used to determine the in-situ soil properties from results of pressuremeter tests (Ladanyi 1972, Windle and Wroth 1977). Also, the method has been used to study pile driving effects in surrounding soils by other researchers (Butterfield and Bannerjee 1970, Desai 1978, Wroth et.al 1979, Kraft et.al 1982). Ignoring the precise detail of soil movement near the pile tip due to pile advancement and assuming soil particles are displaced radially outward only, the one dimensional idealized cylindrical cavity expansion provided a simplified approach to the study of pile driving effects. Since pile driving displaces the soil rapidly, the saturated soil can be assumed incompressible. The strain field during cylindrical cavity expansion is predetermined and is independent of shearing characteristics of soils. Because of this simplification, analytic solutions for this problem are sometimes possible using soil models with various degree of complexity (Vesic 1972, Prevost and Hoeg 1975, Davis et.al 1984).

In contrast to the cavity expansion methods, Baligh (1984, 1985) introduced the 'simple pile solution' to investigate the deep penetration problem in saturated soft clay. He considered that in the case of deep penetration, the strain field around the pile tip is not very sensitive to soil behaviour because of high constraint in the surrounding soil. Therefore he assumed that the deep penetration problem is essentially strain controlled. This is contrary to the shallow foundation problem where it is basically stress controlled (Lambe 1967, Lambe and Marr 1979). The simple pile method may be used to simulate pile installation effects. This method retained the advantages of the cavity expansion approach in that the problem is completely strain-controlled. The simple pile method incorporates the strain path history of the soil as it passes around the so-called 'simple pile' without over-complicating the problem. The strain field around the simple pile is determined by superposition of solutions of a spherical source and a uniform flow field within an ideal fluid. This is the so-called 'Rankine half-body' problem in fluid mechanics (Eskinazi 1962). The velocity field around the simple pile is also predetermined. It follows that the stress field can be immediately obtained from the adopted constitutive relationship without using complicated numerical methods.

The major disadvantage is that the simple pile method determines the strain field within the fluid without considering the constitutive relation or shearing responses of the medium and therefore the strain field is an approximation and will not provide a stress field which in general satisfies the equilibrium conditions. Further, the surface roughness of the simple pile has not been considered, therefore realistic pile-soil behaviour may not be predicted. This will be investigated in this work.

In concurrent developments, the strain field around a driven pile, sampling tube or penetration cone with various end conditions may be found in Levadoux and Baligh (1980), Baligh (1985) and Tumay et.al (1985, 1986).

3.2.2 Cylindrical Cavity Expansion

A solution for the strain field resulting from a cylindrical cavity expansion in the infinite soil mass is available in Davis et.al (1984). The results given there are summarized in this section. The sign convention of strain components in a cylindrical coordinate system is shown in Fig. 3.1 for our later illustration. The sign convention we define here is choosen to coincide with that which will be used in the 'simple pile method'.

We consider an infinite length cylindrical cavity with its center located on the z axis, expanding from zero radius to a cavity with radius a at time t. We assume that expansion occurs sufficiently rapidly so that no drainage in the soil is allowed and thus incompressibility is implied. After expansion, a particle initially located at a_0 has moved radially outward to a position $r=r(a_0,t)$. The relationship between a_0 and r, is given by, as shown in Fig. 3.2,

$$r^2 = a_0^2 + a^2 \tag{3.1}$$

where a is the radius of the cavity and is a function of time t. From Eq. 3.1, we note that only radial deformation will occur in the soil mass. The radial velocity of the particle is given by differentiating Eq. 3.1 . It is

$$v_r = \frac{a}{r}\dot{a} \tag{3.2}$$

In a cylindrical coordinate system, with compressive deformation considered to be positive, the non-zero components of the rate of deformation tensor obtained from Eq. 3.2 are given by

$$D_{rr} = -\frac{\partial v_r}{\partial r}$$
$$D_{\theta\theta} = -\frac{v_r}{r} \tag{3.3}$$

where the subscript θ denotes the tangential or the hoop component. For an incompressible material, the continuity equation (Malvern 1969) requires that $D_{kk} = 0$. Applying this condition to Eq. 3.3, we obtain

$$\dot{\xi} = -\frac{\partial v_r}{\partial r} = \frac{v_r}{r} \tag{3.4}$$

Using Eqs. 3.1 and 3.2 and integrating Eq. 3.4, the natural radial strain ξ_{rr} and hoop strain $\xi_{\theta\theta}$ in the soil are given by

$$\xi_{rr} = -\xi_{\theta\theta} = -\frac{1}{2}\ln\left(1 - \frac{a^2}{r^2}\right) \tag{3.5}$$

We note that infinite strain results on the cavity surface. The strain field in the soil mass is described by the analytic expression in Eq. 3.5.

3.2.3 Simple Pile Penetration

In this section, we describe the strain field around the so-called 'Simple pile' following the development of Baligh (1984, 1985). The usual sign convention adopted in penetration problems, considering the positive z-direction pointing upward and the origin of coordinates near the pile tip, will be used in this chapter.

To investigate the deep penetration problem, Baligh (1984) considered a semi-infinite slender object being pushed into an infinite soil mass. He represented the soil deformation during penetration by inserting a spherical source into a uniform flow field of an ideal fluid with constant velocity V_z in the z direction, as shown in Figs. 3.3. and 3.4. The spherical source discharges an incompressible material at a volumetric rate VR. The pile shaft radius is then given by $a^2=VR/(\pi V_z)$. In a cylindrical coordinate system, the non-zero velocity components are given by

$$v_r = \frac{a^2 V_z}{4\rho^2} \sin\varphi$$
$$v_z = \frac{a^2 V_z}{4\rho^2} \cos\varphi + V_z \qquad (3.6)$$

where

$$\rho^2 = r^2 + z^2 \qquad (3.7)$$

and

$$\varphi = \tan^{-1}(r/z) \qquad (3.8)$$

Here, v_r and v_z denote the velocity components of soil in r and z directions respectively. The stream line of a soil particle initially located at a_0 may be obtained from integration of Eqs. 3.6. This is given by

$$\frac{r^2}{a^2} = \frac{a_0^2}{a^2} + \frac{1}{2}(1 + \cos\varphi) \qquad (3.9)$$

Here, we have used the boundary condition $r = a_0$ at $\varphi = \pi$ to obtain Eq. 3.9. As the soil particle moves along the stream line, the angle φ changes from π to 0. The shape of the simple pile is also described by Eq. 3.9 by setting a_0 to zero, as shown in Fig. 3.4. We find that the simple pile tip is located at z=-0.5a below the origin of the coordinate system. The pile radius increases from zero at the tip to a at a distance far above the tip in the z direction. The deformation field described by Eqs. 3.6 to 3.9 is well known in fluid mechanics; the Rankine half body problem. Since the flow considered is nonviscous, the flow in the internal part of the Rankine body can be considered solid without altering the configuration of the flow on the outside.

Considering compressive deformation to be positive and using soil velocity components given in Eqs. 3.6, the components of the rate of deformation tensor in the soil mass are given by

$$
\begin{aligned}
D_{rr} &= \frac{a^2 V_z}{4\rho^3}\left(2\sin^2\varphi - \cos^2\varphi\right) \\
D_{\theta\theta} &= -\frac{a^2 V_z}{4\rho^3} \\
D_{zz} &= \frac{a^2 V_z}{4\rho^3}\left(2\cos^2\varphi - \sin^2\varphi\right) \\
D_{rz} &= \frac{a^2 V_z}{4\rho^3}\left(\frac{3}{2}\sin 2\varphi\right)
\end{aligned}
\qquad (3.10)
$$

The components of the spin tensor W_{ij} are all zero. Therefore, the flow field is irrotational. Variation of the components of the rate of deformation tensor with respect to angle φ are depicted in Fig. 3.5. Integration of Eqs. 3.10 along each stream line gives the natural strain components ξ_{rr}, $\xi_{\theta\theta}$, ξ_{zz} and ξ_{rz} experienced by a soil particle.

We have shown the stream lines of three soil particles initially located at a_0 =0.2, 1 and 3a, respectively, beneath the simple pile tip in Fig. 3.4. The strain paths experienced by these three particles are shown in Fig. 3.6. The final strain predicted by the cylindrical expansion approach are also given in Fig. 3.6 for comparison. For soil particles with a_0 larger than 3a, the strain path is basically similar to that experienced by the particle at a_0 =3a but it experiences a lower strain level. From these results, we note that

(a) Approximately within the range from φ =165° to 180°,a region beneath the tip, the strain field is found to be similar to that found in undrained triaxial compression conditions, where $\xi_{rr} = \xi_{\theta\theta} = -\xi_{zz}/2$. This is similar to the findings given in Baligh (1985).

(b) Only the hoop strain $\xi_{\theta\theta}$ decreases monotonically during the penetration process. This is because after the particle has passed around the tip, the radial distance between the particle and the pile shaft is reduced. In order to maintain constant volume, the soil mass has to expand laterally. This is similar to the cylindrical cavity expansion.

(c) As the soil particle moves along the stream line, the radial strain ξ_{rr} reverses from extension to compression. Far behind the tip, for a soil particle initially located at a_0>a, the strain components ξ_{rr} and $\xi_{\theta\theta}$ approximately arrive at the final strain values predicted by the cylindrical cavity expansion approach. This does not imply that the simple pile method and cylindrical cavity expansion approach will predict similar stress fields because the stress state of a soil particle is strain path dependent.

(d) The soil particles were compressed vertically beneath the tip; however, reversal of vertical strain ξ_{zz} may bring the particles to an extension state as motion occurs along the stream line. Note that in the far field (say $a_0 \geq 3a$), ξ_{zz} vanish above the tip. In

contrast, the cylindrical cavity expansion approach assumes no vertical deformation occurs everywhere within the soil mass.

(e) The shear strain ξ_{rz} reaches its maximum value at $\varphi = 90°$. Far above the tip, as φ approaches zero, ξ_{rz} approaches zero in the far field while in the near field, ξ_{rz} approaches a finite value despite D_{rz} approaching zero at $\varphi = 0$.

It is notable that the strain field is completely independent of the uniform flow velocity, V_z, and the strain level depends upon the particle position , r and z only. Thus the strain field around the simple pile is rate independent.

For engineering purposes, the quantity called the octahedral shear strain, γ_{oct}, is often used as a measure of deviatoric strain level. Here, γ_{oct} is defined by

$$\gamma_{oct}^2 = \frac{1}{9}\left[(\xi_{rr} - \xi_{\theta\theta})^2 + (\xi_{\theta\theta} - \xi_{zz})^2 + (\xi_{rr} - \xi_{zz})^2 \right] + \frac{2}{3}\xi_{rz}^2 \qquad (3.11)$$

The octahedral shear strain around the simple pile is shown in Fig. 3.7. From this result we note that γ_{oct} is increasing monotonically for each stream line without reversing level.

In this section we have briefly reviewed some particular characteristics of the strain field obtained from the simple pile method. The strain field around the 'simple pile' has been studied extensively by Baligh (1985). For further details, the reader is referred to original references cited above.

Finally, we note from Fig. 3.4, the simple pile shape may initially appear to be unrealistic for most driven piles. In fact, the shape may be a reasonable representation. Soil conditions beneath a flat-ended pile after driving into dense sands and clays as reported by the BCP committee (1972) and by Randolph et.al (1979) are shown in Fig. 3.8 and Fig. 3.9, respectively. We note that a core of soil was formed beneath the pile tip. Similar findings from model jacked piles in soft clay can also be found in Vesic (1977). Vesic (1977) suggested that during driving, the soil beneath a flat ended pile is carried downward from the upper soil layers. A relatively rigid core is formed beneath the pile tip. Considering the soil core beneath the tip, we see that the tip condition of a flat ended pile may be similar to that of the simple pile. Therefore, from a practical point of view, the idealized shape of the simple pile may remain a valid approximation to model a flat ended pile. However, the resulting stresses around the simple pile require further investigation in a later section.

SECTION 3.3 The Effective Stress Field

3.3.1 Stress and Strain Relationship due to Cylindrical Cavity Expansion

Following Davis et.al (1984), we use the following dimensionless stress components

$$S_{ij} = \frac{1}{\sqrt{2}\,\bar{M}} (\sigma_{ij} - p_c \delta_{ij}) = \frac{1}{2\,Cus} (\sigma_{ij} - p_c \delta_{ij}) \tag{3.12}$$

where S_{ij} are the components of the dimensionless stress tensor. Using Eq. 3.12 in the undrained loading equation 2.44 for the rate-type model, we obtain the following expression for the loading equation

$$\overset{\circ}{S}_{ij} = \beta [D_{ij} - 2 S_{ij} (S_{mn} D_{mn})] \tag{3.13}$$

Upon unloading, the form of Eq. 2.47 becomes

$$\overset{\circ}{S}_{ij} = \beta D_{ij} \tag{3.14}$$

where the co-rotational stress rate is given by

$$\overset{\circ}{S}_{ij} = \dot{S}_{ij} - W_{im} S_{mj} + S_{im} W_{mj} \tag{3.15}$$

The term $S_{mn} D_{mn}$ in Eq. 3.13 is the stress power.

It is convenient at this point to introduce dimensionless stress invariants for this model. They are

$$\begin{aligned} \tilde{P} &= \frac{1}{3} S_{kk} \\ \tilde{J}_2 &= S^*_{ij} S^*_{ij} \\ S^*_{ij} &= S_{ij} - P\delta_{ij} \end{aligned} \tag{3.16}$$

where S^*_{ij} denotes the deviatoric part of S_{ij}. Here, $\tilde{P}$ is the first invariant of S_{ij} and $\tilde{J}_2$ is the second invariant of S^*_{ij}. It is notable that the initial pressure $\tilde{P}$ has the form of Eq. 2.49 expressed as $\tilde{P}_i$. Soil arrives at the critical state when $\tilde{P}$=0 and $\tilde{J}_2$= 0.5. Use of these two dimensionless invariant forms will simplify later comparisons.

Davis et.al (1984) assumed the dimensionless effective stresses due to cylindrical cavity expansion have the form

Assumed Zero mean stress at casing wall ?

$$[S_{ij}] = \begin{bmatrix} S_{rr} & 0 & 0 \\ 0 & S_{\theta\theta} & 0 \\ 0 & 0 & S_{zz} \end{bmatrix} \tag{3.17}$$

The sign convention of stress components in a cylindrical coordinate system is also shown in Fig. 3.10. The dimensionless total stress T_{ij} is related to the effective stress S_{ij} by

$$T_{ij} = S_{ij} + U \delta_{ij} \tag{3.18}$$

where U is the dimensionless pore pressure given by

$$U = \frac{u}{\sqrt{2}\,M} = \frac{u}{2\,Cus} \tag{3.19}$$

Suppose the initial dimensionless effective stresses when time t= 0 are given by

$$S_{rr} = S_{\theta\theta} = S_{rri} \tag{3.20}$$

$$S_{zz} = S_{zzi}$$

where the subscript i denotes initial state. Since no unloading occurs during expansion, only the loading equation 3.13 will be used. Integration of Eq. 3.13 with the use of Eqs.3.3, to 3.5 and 3.17 as well as 3.20, leads to the following analytic expressions for the dimensionless effective stresses.

$$S_{rr} = \frac{1}{2}\left[\frac{-\left(1-\frac{a^2}{r^2}\right)^{2\beta} + 4\,S_{rri}\left(1-\frac{a^2}{r^2}\right)^{\beta} + 1}{\left(1-\frac{a^2}{r^2}\right)^{2\beta} + 1}\right] \tag{3.21a}$$

$$S_{\theta\theta} = \frac{1}{2}\left[\frac{\left(1-\frac{a^2}{r^2}\right)^{2\beta} + 4\,S_{rri}\left(1-\frac{a^2}{r^2}\right)^{\beta} - 1}{\left(1-\frac{a^2}{r^2}\right)^{2\beta} + 1}\right] \tag{3.21b}$$

$$S_{zz} = \frac{2\,S_{zzi}\left(1-\frac{a^2}{r^2}\right)^{\beta}}{\left(1-\frac{a^2}{r^2}\right)^{2\beta} + 1} \tag{3.21c}$$

To illustrate stress changes in soils due to a cylindrical cavity expansion, we have adopted two dimensionless initial stress conditions, $\tilde{P}_i$= 0.5 and -0.5, for lightly and heavily over-consolidated soils, respectively, with β =50 and 200. The results are shown in Figs. 3.11 and 3.12. We find

(a) Inside the critical state region, the effective stress is only affected by the undrained shear strength and effective angle of friction at the critical state. The stresses are completely independent of the initial stress state and the soil rigidity.

(b) Remote from the critical state region, the hoop stress $S_{\theta\theta}$ trends to reduce because the soil mass expands laterally. The radial stress S_{rr} increases due to radial compression caused by the outward movement of the soil particles.

(c) Throughout the soil mass, the vertical stress remains the intermediate principal stress. The radial stress and the hoop stress are major and minor principal stresses, respectively. For one-dimensionally consolidated soils, this may occur only in the critical state region.

(d) For heavily overconsolidated soils, dilation trends to increase the radial effective stress around the pile shaft.

3.3.2 Stress and Strain Relationship due to Simple Pile Penetration

In this section, we will use the rate-type model to investigate the stress field around a simple pile. The results obtained here will also be compared with Baligh's existing solutions. The shortcomings of the 'simple pile' method will be investigated.

(i) Stress and Strain Relationship

During a simple pile penetration, four non-zero dimensionless stress components in a cylindrical coordinate system are present. They are

$$[\,S_{ij}\,] = \begin{bmatrix} S_{rr} & 0 & S_{rz} \\ 0 & S_{\theta\theta} & 0 \\ S_{rz} & 0 & S_{zz} \end{bmatrix} \qquad (3.22)$$

Using the components of the rate of deformation tensor, Eq. 3.10, and the dimensionless stress tensor, Eq. 3.22, in the constitutive equation 3.13 or 3.14, it is possible to obtain the stress and strain relationship in the soil by integrating along each stream line, Eqs. 3.9. However, analytic solutions may not be obtained, and numerical integration is required. The details of integration to obtain the stress field around the simple pile are summarized in Appendix (D).

(ii) Soil Parameters

Baligh (1986a) used a hyperbolic elastic-perfectly plastic model to investigate the penetration of a simple pile in Boston Blue clay. We will use the rate-type model and compare the deviatoric stress field around the simple pile with Baligh's (1986a) results. Note that the hyperbolic model is a total stress model. Before yielding occurs, the model predicts non-linear elastic soil response. Soil yielding is defined by the von-Mises yield criterion. The post-yield behaviour of the soil follows the associative flow rule. Since the hyperbolic model is an elastic-perfectly plastic model, we assume the soil arrives at the critical state when yielding occurs. This model cannot predict the total pressure in the soil, therefore the total pressure must be determined from equilibrium considerations. Further, the effective stress in the soil cannot be predicted by this model, thus an additional pore pressure model (Bishop and Henkel 1964, Baligh 1986b) is required in determining the effective stress and pore pressure.

Baligh (1986a) used the test results of resedimented Boston Blue clay to evaluate soil parameters for the hyperbolic model. The samples were isotropically normally consolidated before being sheared to failure. All samples were tested under undrained triaxial compression or extension conditions.The results are shown in Figs.3.13 and 3.14. Baligh (1986a) made two assumptions.

(a) The isotropic consolidation pressure p_i is equal to 3Cus.

(b) The non-linear elastic response of the hyperbolic model is controlled by varying the soil rigidity from β =1000 at the beginning of the loading process to β =20 when yielding occurs.

The response of the hyperbolic model is also shown in Figs.3.13 and 3.14.

In evaluating the model parameters for the rate type model, we assume an effective angle of friction in triaxial compression of ϕ_c =28°. Using Eqs. 2.37, 2.38, and 2.49, we find the dimensionless initial effective pressure $\tilde{P}_i$ = 0.78, which also gives $p_i \approx$ 3Cus. We have chosen β =200 for the rate-type model. The response of the rate-type model is also illustrated in Figs.3.13 and 3.14. Comparisons in these figures indicate

(a) Reasonable agreement is obtained from the prediction of the rate-type model in triaxial compression, while the hyperbolic model predicts a higher initial stiffness for the sample.
(b) Both models predicted the deviatoric stress, q, at failure close to the test results in triaxial compression as they were selected to match the test results.
(c) The rate-type model predicts soil failure at a lower strain level while the hyperbolic model predicts failure at a higher strain level.
(d) Both models are isotropic in the sense they predict identical magnitude of deviatoric failure stress in both triaxial compression and extension conditions. Therefore both models over-predict the extension failure stress. However, the hyperbolic model exhibits better agreement for the test result at low strain level ($-\varepsilon_a$<0.1%) than does the rate-type model.

(iii) Stress Distribution

Fig. 3.15 shows the dimensionless deviatoric stress $\sqrt{\tilde{J}_2}$ contours around the simple pile evaluated from the rate-type model and from the hyperbolic model available from Baligh(1986a). The selected parameters $\tilde{P}_i$=0.78 and β =200 have been used for the rate-type model. Comparing these figures, we find

(a) The size of the critical state region predicted from the rate-type model covers a larger region than that from the hyperbolic model. This is because the rate-type model approaches critical state at a lower strain level.
(b) Both models predicted similar $\sqrt{\tilde{J}_2}$ distribution at the contour level $\sqrt{\tilde{J}_2}$ =0.6.
(c) Outside the region bounded by the $\sqrt{\tilde{J}_2}$ =0.6 contour, the hyperbolic model predicts higher $\sqrt{\tilde{J}_2}$ levels than are predicted by the rate-type model. This is mainly due to the fact that the initial soil rigidity of the hyperbolic model is five times larger than the value selected for the rate-type model.
(d) Assuming initially isotropic stress conditions throughout the soil mass no soil particle experiences a decrease in $\sqrt{\tilde{J}_2}$. No unloading occurs in the rate-type model (the stress power $S_{ij}\, D_{ij}$ remains larger than zero).

The effective stress distribution around the simple pile is not predicted from Baligh's hyperbolic model. We therefore only present the results obtained from the rate-type model for Boston Blue clay in Fig 3.16. In order to illustrate the effects of stress history, the effective stress around the simple pile for a soil with initial isotropic overconsolidated stress state, $\tilde{P}_i$ =-0.25 and β =200 (which approximately corresponds to a one-dimensionally overconsolidated soil with ϕ_c=28° and $\overline{OCR}$=3) are also shown in Fig. 3.17. It is noted that the deviatoric stress $\sqrt{\tilde{J}_2}$ contours and the shear stress S_{rz} contours around the simple pile are independent of initial isotropic stress state. Results obtained from Figs.3.16 and 3.17indicate

(a) Within four pile radii around the pile, well inside the critical state region, the effective stress distributions are identical for both normally and over-consolidated soils; the soil history has been completely erased in this region. This is slighty different to the results of the cavity expansion appproach as we have mentioned in section 3.3.1 where the "erasing" of stress history covers the entire critical state region.

(b) Around the pile shaft, both S_{rr} and $S_{\theta\theta}$ are less than the value of the S_{zz} stress component; this is significantly different from the result for the cylindrical cavity expansion.

(c) Beneath the tip, soil failure occurs in a triaxial compression mode.

Results obtained above appear different to those evaluated from the cavity expansion approach as may be expected. It is notable that simple pile penetration predicts non-zero shear stresses in the surrounding soil. Beneath the tip, negative shear stress indicate that inner soil particles are being pushed down with respect to outer particles. However, close to the pile shaft, the S_{rz} stress component changes sign. This implies that the shear stress may produce "*tensile* " stress in the pile at some distance above the tip. Therefore, we will first investigate the stress changes along the stream line predicted by the rate-type model. Later we will consider the effective stress distribution and surface tractions to evaluate the effectiveness of the simple pile model. Further evaluation of the simple pile method in predicting penetration resistance will be shown in a later section where the solution for pore pressure is found.

(iv) Stress Changes along a Stream Line

In order to investigate the stress changes along a stream line using the rate-type model, we will use the following variables to represent the components of deviatoric stress as proposed in Baligh (1986a).

$$\begin{aligned} \tilde{S}_1 &= \sqrt{\frac{2}{3}}\left[S_{zz} - \frac{1}{2}\left(S_{rr} + S_{\theta\theta} \right) \right] \\ \tilde{S}_2 &= \frac{1}{\sqrt{2}}\left(S_{rr} - S_{\theta\theta} \right) \\ \tilde{S}_3 &= \sqrt{2}\, S_{rz} \end{aligned} \tag{3.23}$$

We note that

$$\tilde{J}_2 = \tilde{S}_1^2 + \tilde{S}_2^2 + \tilde{S}_3^2 \tag{3.24}$$

From the deviatoric stress tensor, S^*_{ij}, in Eqs. 3.16 , we find that $\tilde{S}_1$ denotes a measure of vertical deviatoric stress, S^*_{zz}, and $\tilde{S}_2$ represents the difference of deviatoric stress components S^*_{rr} and $S^*_{\theta\theta}$ in the radial and hoop directions. $\tilde{S}_3$ measures the stress due to simple shear. As we have demonstrated in section 3.3.1 for the cylindrical cavity expansion approach, $\tilde{S}_1$ and $\tilde{S}_3$ are zero for soils with initial isotropic stress conditions. Therefore $\tilde{S}_2$ is a measure of the deviatoric stress due to cylindrical cavity expansion. It should be noted that the stress paths of the $\tilde{S}_1$, $\tilde{S}_2$ and $\tilde{S}_3$ components and the deviatoric stress components S^*_{ij} of Eq. 3.16 predicted from the rate-type model are independent of the isotropic initial stress state in the soil.

To illustrate stress changes along the stream line we have choosen three soil particles initially located at a_0=l, l0, and 20a respectively. β is choosen to be 200 as used for a Boston Blue clay. With reference to the $\sqrt{\tilde{J}_2}$ contours given in Fig. 3.15(b), the particle initially located at a_0 =a remains close to the pile, well inside the critical state region. The stream line of the particle with a_0 =l0a passes outside the edge of the critical state region. The particle with a_0 =20a is sheared to a $\sqrt{\tilde{J}_2}$ level about half of that experienced by the particle at a_0 =10a, and is mainly within the elastic range .

Results for deviatoric stress components $\tilde{S}_1$, $\tilde{S}_2$ and $\tilde{S}_3$ for each soil particle moving along each of the stream lines are plotted against the angle φ in Figs. 3.18. From these figures, we note

(a) For soil beneath the tip, the action of simple pile penetration is similar to a combination of vertical compression and cylindrical cavity expansion.

(b) Close to the pile shaft, the cavity expansion stress $\tilde{S}_2$ and the vertical compression stress $\tilde{S}_1$ arrive at their maximum and minimum values at φ =90° respectively. The shear stress vanishes near this depth. Far above the tip (as φ approaches zero), the $\tilde{S}_2$ component nearly vanishes.

(c) As the soil particle initially located at a_0 =10a moves along the stream line, significant reversal of $\tilde{S}_1$ and $\tilde{S}_3$ occurs. However, for φ < 90°, the effect of $\tilde{S}_1$ is significantly reduced, and the stress state is mainly governed by the cavity expansion stress $\tilde{S}_2$ and shear stress S_{rz}.

(d) The soil response experienced by the particle initially located at a_0 =20a is mainly elastic. When the soil particle moves above the tip, both $\tilde{S}_1$ and $\tilde{S}_3$ become negligible small and the stress state is dominated by the cylindrical cavity expansion stress $\tilde{S}_2$.

The above results predicted from the rate-type model are very similar to those findings discussed in Baligh (1986a) for soils response outside the critical state region (a_0 >10a). But the results we obtain here indicate that the shear stress component $\tilde{S}_3$ for the soil particle initially located at a_0=a does not reduce to a negligibly small value when φ approaches zero. Therefore,a further investigation of the effective stress distribution along the "simple-pile" shaft is given below.

Figs.3.19 show the effective stress distribution along the pile shaft. Values of soil rigidity of β =10, 100, 200 are used. Since soil failure beneath the pile tip (i.e., φ =180°) occurs in a triaxial compression state, $S_{rr} = S_{\theta\theta} = - S_{zz}/2$, independent of soil rigidity and initial stress state, the stress states for all three cases at φ =180° are the same. These results are obtained by numerical integration. Soil with β equal to 10 corresponds to a very soft clay while a soil with β equal to 200 corresponds to a medium stiff clay. From these figures we find that

(a) Within the region between φ values of 145° and 180°, the soil rigidity has no effect on the effective stress distribution (i.e., around the tip).
(b) As the soil moves along the shaft, the shear stress, S_{rz}, reverses sign from negative to positive at 90°.
(c) For the β= 10 case, the residual value of shear stress S_{rz} as φ approaches zero exceeds 60% of the undrained shear strength, Cus. When β increases the residual value of S_{rz} reduces but remains finite.
(d) For a stiffer clay, the stress state at a depth far above the tip is similar to a triaxial compression state.

Also, comparing Figs. 3.19 with Fig.3.5, we realize that the effective stresses along the pile shaft are directly related to the components of rate of deformation, D_{ij}.

The shear stress, S_{rz}, in the range between φ equal to 90° and 180° appeared reasonable as it may provide an upward resistance to the simple pile during penetration. But, above the tip, the shear stress is unrealistic. Our results are different from the analytic solution obtained by Baligh (1986a).The difference mainly lies in the fact that Baligh ignored the importance of the elastic strain rate in his model; resulting in a rigid plastic constitutive relationship. However, the results given here demonstrate that the elastic strain rate must not be ignored. In fact, the similarity between the stress distribution and the rate of deformation components clearly suggests that a more accurate velocity field model is required for the penetration problem.

(v) Surface Tractions

The surface roughness has not been incorporated into consideration of the simple pile method. The stress distribution along the simple pile is directly governed by the soil model and the velocity field determined from the ideal fluid. It is possible to directly evaluate the surface tractions acting on the simple pile.

We consider the unit normal vector, $\overrightarrow{NV}$, to the simple pile as shown in Fig. 3.20,

$$\overrightarrow{NV} = \cos\mu\,\vec{i} - \sin\mu\,\vec{k} \tag{3.25}$$

in which $\vec{i}$ and $\vec{k}$ are the unit vectors in positive r and z directions, respectively. Here, μ, represents the slope angle of the simple pile and is obtained from Eq. 3.9. It has the form of

$$\tan\mu = \frac{\left(\frac{1}{2}\frac{a^2\sin\varphi}{y}\right)}{\left(2+\frac{1}{2}\frac{a^2\cos\varphi}{y}\right)} \tag{3.26}$$

where

$$y = \frac{1}{2}(1+\cos\varphi)(1+\cot^2\varphi) \tag{3.27}$$

Let the normal and shear tractions due to the effective stresses σ_{nv} and τ_{nv} be non-dimensionalized by the following expressions.

$$S_\sigma = \frac{\sigma_{nv} - P_c}{2Cus} = S_{rr}\cos^2\mu + S_{zz}\sin^2\mu - S_{rz}\sin 2\mu \tag{3.28}$$

and

$$S_\tau = \frac{\tau_{nv}}{2\,Cus} = \frac{1}{2}(S_{rr} - S_{zz})\sin 2\mu + S_{rz}\cos 2\mu \tag{3.29}$$

where S_σ and S_τ are dimensionless normal and shear tractions, respectively. The directions of σ_{nv} and τ_{nv} are indicated in Fig. 3.20.

Using the effective stress distribution along the pile given in Figs 3.19 and Eqs. 3.26 to 3.29, the surface tractions S_σ and S_τ for soils with β = 10, 100 and 200 are shown in Figs. 3.21. Note that negative S_σ does not necessary imply tensile normal stress, but it implies that normal traction is less than the critical pressure of soils. Figs. 3.21 indicate that

(a) The simple pile methods results in relatively low effective normal stress acting on the pile shaft (when $\varphi \le 40^\circ$).

(b) The shear traction is acting *downward* along the pile everywhere.

(c) A maximum downward shear traction as high as 85% of Cus is found.

(d) For soft clay, the downward shear traction is significantly higher than for stiff clay.

These results demonstrate that the shear traction on the pile surface will eventually produce a tensile stress in the pile at some distance above the tip. This is physically unacceptable.

Furthermore, the resulting surface condition does not correspond to a smooth pile condition; this is contrary to the discussion given in Baligh (1986a). The idea of the simple pile method is founded upon the assumption that the velocity field in soft clay due to pile penetration can be closely approximated by that in an ideal fluid flow. However, we have found that an unrealistic downward shear traction results the effect for a soft clay is significantly higher than that in a stiffer clay.

SECTION 3.4 Pore Pressures

During undrained deformation, changes in effective stress in the soil mass will normally be associated with changes in pore water pressure. Since the rate-type model is an effective stress soil model, the pore pressure in the soil mass must be determined from equilibrium considerations. In this section, we will investigate the pore pressure distribution evaluated from both the cylindrical cavity expansion method and the simple pile method.

3.4.1 Equilibrium Consideration

Equilibrium of the undrained deformation problem is governed by the total stress, T_{ij}, Eq.3.18. We may assume that the dimensionless pore pressure U is composed of two parts. They are

$$U = \Delta U + U_i \tag{3.30}$$

where

$$\Delta U = \frac{\Delta u}{2Cus} \tag{3.31}$$

and

$$U_i = \frac{u_i}{2Cus} \tag{3.32}$$

Here, ΔU is the dimensionless excess pore pressure due to shearing and U_i is the dimensionless initial pore pressure in the soil. U_i may be a function of r and z in a cylindrical coordinate system, but we will assume it is a constant. For axially symmetric problems, assuming zero body forces and using Eqs.3.18 and 3.30, we arrive at the following two equilibrium equations. In the r direction

$$\frac{\partial \Delta U}{\partial r} = -\left(\frac{\partial S_{rr}}{\partial r} + \frac{\partial S_{rz}}{\partial z} + \frac{1}{r}(S_{rr} - S_{\theta\theta}) \right) = f^* \tag{3.33}$$

and in the z direction

$$\frac{\partial \Delta U}{\partial z} = -\left(\frac{\partial S_{zz}}{\partial z} + \frac{\partial S_{rz}}{\partial r} + \frac{S_{rz}}{r} \right) = g^* \tag{3.34}$$

In general, integration of either Eqs.3.33 and 3.34 along the r or z direction, respectively, would lead to a solution for ΔU in the soil mass. A unique solution for ΔU can be obtained from Eqs.3.33 or 3.34 only when the following condition is satisfied.

$$\frac{\partial f^*}{\partial z} = \frac{\partial g^*}{\partial r} \tag{3.35}$$

However, if Eq.3.35 is not satisfied, then equilibrium is violated and the solution for ΔU is not unique but is integration path dependent.

3.4.2 Pore Pressure Around a Cylindrical Cavity

During cylindrical cavity expansion in an infinite soil mass, the equation of equilibrium in the z direction is trivially satisfied. Thus the excess pore pressure, ΔU, is uniquely determined from the equation of equilibrium in the r direction, Eq. 3.33. Using the effective stresses given in Eqs. 3.21 for the rate-type model, we can evaluate ΔU by carrying out the integration of Eq. 3.33. The theoretical boundary condition for this problem is $\Delta U = 0$ at ∞. However, the analytic solution for ΔU may not be obtained even through analytic expressions for the effective stress distribution have been found. Thus, we have carried out the integration numerically.

The excess pore pressure associated with the effective stress field for the initial conditions we have used in the cylindrical cavity expansion problem, section 3.3.1, are given in Figs.3.22 and 3.23, from which we note that

(a) Cylindrical cavity expansion generates higher ΔU in normally or lightly over-consolidated soil than in heavily over-consolidated soil.
(b) Heavily over-consolidated soil exhibits slightly negative excess pore water pressure outside the critical state region, while lightly over-consolidated soils exhibit positive excess pore water pressure everywhere.
(c) The generated ΔU distribution in the soil decreases log-linearly as r increases. Thus large generated pore pressure can only exist close to the pile shaft.
(d) As soil rigidity increases, the generated ΔU increases as expected.

3.4.3 Pore Pressure Around the Simple Pile

In this section, we will first compare the so-called 'shear induced pore pressure' predicted by the rate-type model with that measured in Boston Blue clay under triaxial conditions and results obtained by Baligh's (1986b) " shear induced pore pressure model ". The excess pore pressure around a simple pile obtained by the rate-type model will then be investigated, and these results will also be compared with Baligh's existing solution (1986b).

(i) Shear Induced Pore Pressure

Baligh's (1986a) hyperbolic model is a total stress model, hence he requires an additional so-called shear induced pore pressure model to determine the excess pore pressure in the soil. More precisely, the so-called "shear induced pore pressure", Δu_s, is the difference in effective pressure before and during shearing. Therefore, when an effective stress model is used, the effective pressure and excess pore pressure during shearing can be directly predicted. However, if a total stress model is used, the excess pore pressure is composed of two parts : (1) the increase in total pressure which is determined from equilibrium considerations and (2) the shear induced pore pressure.

Fig.3.24 shows the 'shear induced pore pressure' measured for Boston Blue clay under triaxial conditions as reported in Baligh (1986b). Since the test results for Δu_s in Boston Blue clay are

similar in both triaxial compression and extension conditions, we only show the triaxial compression results here. Baligh (1986b) used these results to evaluate the values of two soil parameters for the shear induced pore pressure model. His shear induced pore pressure model predicts equal magnitudes of Δu_s in both triaxial compression and extension conditions. This feature is similar to the rate-type model. Thus only the prediction of the rate-type model and results of Baligh(1986b) for triaxial compression conditions are shown for comparison, but we note that no additional soil parameters are required for the rate-type model in predicting the shear induced pore pressure. Fig. 3.24 shows that

(a) The rate-type model over-estimates Δu_s when the axial strain ε_a is less than 3.5% and it under-estimates Δu_s for ε_a greater than 3.5%.

(b) Baligh's shear induced pore pressure model gives a better fit to the test results. This is expected since two additional soil parameters are used.

(ii) Integration Path

Unlike the cylindrical cavity expansion approach, the equation of equilibrium in the z-direction is not trivially satisfied by the simple pile method. The terms in the right hand of equilibrium equations 3.33 and 3.34 may be obtained from the known effective stresses for the rate-type model. However, since analytic expressions for the effective stresses around the simple pile are not obtained from the rate-type model, the partial derivatives of the effective stress components in Eqs. 3.33 and 3.34 must be estimated by using numerical differentiation. The numerical differentiation scheme that we have used in this problem provides the exact solution for a quadratic function. In regions close to the pile tip, where high gradients of stress occur, intervals of increment in the r and z directions have been taken to be 0.025a for numerical differentiation.

Recalling that the strain field around the simple pile is approximated by an ideal flow field, it follows that the effective stress associated with this strain field will in general not satisfy the condition of equilibrium, Eq. 3.35. The resulting value of ΔU evaluated from Eqs.3.33 and 3.34 is integration path dependent. Therefore we will use two integration schemes and compare the resulting ΔU distribution around the simple pile. The integration schemes we will use are

(1) Integrating both of Eqs.3.33 and 3.34 along the stream line of each soil element

(2) Carrying out the integration of only Eq.3.33 along the r-direction, as discussed by Levadoux and Baligh(1980).

The discrepancy between the resulting ΔU values estimated from the above integration schemes may be a good measure of the validity of equilibrium for this problem.

When the integration is carried out along the steam line, it is necessary to obtain ΔU from the following expression.

$$d(\Delta U) = \frac{\partial(\Delta U)}{\partial r} dr + \frac{\partial(\Delta U)}{\partial z} dz \qquad (3.36)$$

Note that Eq.3.36 is mainly governed by the term $\partial(\Delta U)/\partial z$, because the stream lines are basically vertical except in the region close to the tip.

When the excess pore pressure is to be determined from the equilibrium equation 3.33 in the r-direction only, we find that it is convenient to evaluate the term $\Delta U+S_{rr}$ directly from the integration of Eq.3.33. The ΔU distribution is then obtained from the known effective stress field S_{rr}. This is because only one numerical differentiation for the term $\partial S_{rz}/\partial z$ is required.

Finally we will assume the boundary condition $\Delta U = 0$ at z=-200a and r=200a where the theoretical boundary condition at $z=-\infty$ and $r=\infty$. is imposed.

(iii) Results

Figs. 3.25 show the excess pore pressures resulting from both integration schemes mentioned in section 3.4.3(ii). The soil parameters evaluated from the isotropically normally consolidated Boston Blue clay for the rate-type model have been used. From Figs. 3.25 we note that

(a) For depth z<-6a and r>15a, reasonable agreement for ΔU is found from both integration schemes. This indicates that equilibrium is essentially satisfied in this region.
(b) Within one pile radius around the pile tip, the integration scheme carried out along the r-direction predicts higher excess pore pressures than those obtained from the integration scheme carried out along the stream lines.
(c) Inside the critical state region, integrating the equilibrium equations along the stream line predicts significant negative ΔU (i.e., $\Delta u < -3Cus$) around the pile shaft. Contrary to this, no negative excess pore pressures are obtained by carrying out the integration in r-direction.

Similar findings have also previously been reported by Levadoux and Baligh (1980). From our discussion given in section 3.3.2, we have found that the 'simple pile' method gives an unrealistic S_{rz} distribution, especially close to the pile shaft. This results from the fact that the simple pile solution ignores the shearing resistance within the soil in its basic formulation. The rate of deformation component D_{rz} is evidently poorly modelled leading to an incorrect shear stress S_{rz}. This may be a central cause of path dependence of solutions for Δu.

It should be noted that the difference of the solutions for ΔU from the two integration schemes may be a measure of validity of equilibrium for this problem. We have found that significant discrepancy of ΔU occurs close to the pile shaft where the critical state has been reached. In this region, we may expect that the inaccurate shear stress distribution may also effect the S_{rr}, $S_{\theta\theta}$ and S_{zz} distributions, especially inside the critical state region.

Further examination of the path dependence of solutions for ΔU can be carried out. We may compare the equilibrium equations 3.33 and 3.34 with reference to the effective stress contours in Figs. 3.16. We note that

(a) When we evaluate ΔU from the integration along the stream line, the effect of the term $\partial S_{zz}/\partial z$ in the equilibrium equation 3.33 diminishes above z>8a. It follows that solutions for ΔU are mainly governed by the term $\partial S_{rz}/\partial r + S_{rz}/r$, thus slightly inaccuracies in S_{rz} may directly affect the resulting ΔU distribution

(b) When equilibrium is satisfied in the r-direction only, the resulting ΔU distribution is less affected by the S_{rz} distribution because the term $\partial S_{rz}/\partial z$ in Eq.3.33 is generally small; except in the region around the pile tip.

Of the two equilibrium equations, Eq. 3.33 is less dependent upon the shear stress S_{rz} for this problem. Also, only one numerical differentiation for the term $\partial S_{rz}/\partial z$ is required. Thus the inherent error from numerical differentiation is minimized, and therefore the solution for ΔU estimated from Eq.3.33 in the r-direction would in general be expected to provide a better approximation in this problem. Note that a similar method has also been used in Baligh (1986b) to estimate ΔU.

Again, using the rate-type model, and satisfying equilibrium in r-direction, the dimensionless excess pore pressure of isotropically overconsolidated clay with initial state $\bar{P}_i$= -0.25 and β =200 which has been discussed in section 3.3.2 (iii) is given in Fig.3.26. Comparing this result with those in Fig.3.25(b) evaluated from the rate-type model for normally consolidated Boston Blue clay, we note that

(a) No negative excess pore pressure was predicted for both soils inside the critical state region.

(b) Simple pile penetration causes higher dimensionless excess pore pressure, ΔU, in isotropically normally consolidated soil than in overconsolidated soil with the same rigidity. This is indicative that the shear induced pore pressure in a normally consolidated soil is higher than that in a overconsolidated soil,(i.e., shear induced pore pressure is negative for this overconsolidated soil).

(c) Both soils show the same trend that maximum excess pore pressure is generated around the tip, with ΔU gradual reducing in magnitude along the pile shaft.

Further, Fig. 3.27 shows the results obtained by Baligh(1986b) using his hyperbolic soil model with the shear induced pore pressure relationship for Boston Blue clay. Comparing results given in Fig.3.27 and the prediction of the rate-type model given in Fig. 3.25(b), we note that

(a) Outside the critical state region state region, Baligh's results predict higher excess pore pressure than does the rate-type model. This is because the hyperbolic model predicts stiffer response at low strain level (c.f. Figs. 3.15) and thus predicts a higher increase in total pressure.

(b) Along the boundary of the critical state region, both models predicted similar ΔU distributions.

(c) Within the area of one pile radius around the tip, the ΔU distributions obtained from both models are similar

(d) Along the pile shaft, the excess pore pressure predicted from the rate-type model decreases in magnitude gradually in the z-direction and approaches a constant value above z=20a.

The discrepancies found here may be due to the numerical procedures used and individual features of the models. The use of either total stress or effective stress models in predicting response in the undrained penetration problem will have different advantages. Both the hyperbolic model and the rate-type model are simple in the sense that only a few model parameters and no complex curve fitting procedures are required to determined these soil parameters. In our calculations with the rate-type model, we have used three model parameters ϕ, Cus and G, and one initial stress parameter p_i. The hyperbolic model with the shear induced pore pressure relation uses a total of four soil parameters and, additionally, an initial stress parameter p_i and the soil shear strength Cus.

SECTION 3.5 Evaluation of the Simple Pile Method in Prediction of Penetration Resistance

In the previous section, we found that the simple pile method results in unrealistic surface shear tractions, and tensile stress in the pile is inevitable. However, we also noted that the simple pile penetration induced significant high excess pore pressure around the pile tip, which may lead to high total stress around this region. Therefore, it may be interesting to investigate the maximum penetration resistance predicted from this method and the point at which tensile stress first occurs in the pile. The results obtained here may be an indication of error resulting from this method.

Let us assume that no initial pore pressure exists in the soil and define the penetration resistance of the simple pile by

$$Q_{sp} = \frac{1}{\pi a^2} \int_{A_{sp}} [(\sigma_{nv} + u) \sin \mu - \tau_{nv} \cos \mu) \, d A_{sp} \qquad (3.37)$$

Here Q_{sp} is the force in the pile divided by the cross sectional area of the pile shaft and has units of stress. A_{sp} is the surface area of the pile which may be obtained from

$$A_{sp} = -\pi a^2 \int_{\pi}^{\varphi} \sqrt{1+ \cot^2 \mu} \left(\frac{1}{2} \sin \psi \right) d\psi \qquad (3.38)$$

It is reminded that μ is obtained from Eq.3.26. We will use the initial stress state of the isotropically normally consolidated Boston Blue clay with β equal to 10, 100 and 200 to illustrate the results. Using Eq. 2.53 and p_i of 3Cus for this soil, the critical pressure p_c is 1.5Cus. Results for Q_{sp} are plotted against the angle φ in Fig. 3.28. From this figure, we note that

(a) Tensile stress occurs in the pile when φ is less than 12°, 4.5° and 3.5° (i.e., when z is larger than 5, 13 and 16.5a), for soil with β equal to 10, 100, 200, respectively.

(b) The maximum penetration resistance Q_{sp} ranges from 5 to 9 Cus for β between 10 and 200. This occurs approximately at φ= 40° or z=1.2a.

Since the pile shaft radius at depth z=1.2a is approximately equal to 0.95a, we will assume that the region below this depth is effectively the tip of the pile and the maximum penetration resistance Q_{sp} corresponds to the tip resistance of the pile. It is possible to rearrange Eq. 3.37 into the following form.

$$Q_{sp} = B_{cf}\, Cus + p_i \qquad (3.39)$$

where B_{cf} may be considered a bearing capacity factor, Terzaghi(1943). Note that B_{cf} determined here is independent of the OCR and the initial stress state for isotropically consolidated soils. Using the maximum value of Q_{sp} obtained above in Eq.3.39, B_{cf} ranges from 2 to 6 for β, ranging between 10 and 200. These values are lower than those obtained by Vesic(1972, and 1977) using the spherical cavity expansion approach, but may be representative for some clays.

Since the simple pile method predicts tensile stress in the pile at depths not far above the tip, the resulting effective stresses distribution close to the pile shaft may be less than reliable. Results obtained here warn against using the velocity field evaluated from an ideal fluid to approximate the response of soils.

SECTION 3.6 Comparisons of The Methods

3.6.1 Theoretical Solutions

(i) Comparison of Effective Stresses

In order to directly compare the results of the cylindrical cavity expansion approach and the simple pile method, we will use the results for the normally and over-consolidated soils that were discussed in section 3.3.2 (iii). The results of the simple pile method are evaluated at various depths : z=0, 5 and 20a. Comparisons for the dimensionless deviatoric stress $\sqrt{\tilde{J}_2}$ and effective pressure $\tilde{P}$ are shown Figs.3.29. The effective stresses are given in Figs.3.30 and 3.31. These figures indicate the following

(a) Despite the strain paths predicted by both methods being quite different, the deviatoric stress $\sqrt{\tilde{J}_2}$ and effective pressure $\tilde{P}$ distributions in the surrounding soil are similar.

(b) Above the pile tip, the critical state region predicted from the simple pile method is only slightly larger (i.e., about 2a) than that from the cylindrical cavity expansion approach.

(c) For depths of z=0 and z=5a similarity in the effective stress distributions is found only in the low stress region, where soil response is mainly elastic.

(d) For the depth z=20a, the effective stress distributions outside the critical state region from both methods are very similar.

(e) Inside the critical state region, the predicted stress distributions are quite different at all depths.

Both methods have been used by recent researchers to investigate pile driving in soils. The simple pile method includes the pile tip effect due to pile advancement, while the cylindrical cavity expansion approach ignores the details of the strain path in the soil and considers the final radial strain only. In this study, during pile penetration, the stream lines outside the critical state region (r >15a) are essentially straight lines. Thus, in this region, the strain field determined from an ideal fluid may be similar to that experienced by a soil with shearing resistance, and both methods result in similar effective stress distributions. Inside the critical state region, especially within a few pile radii of the pile shaft, the strain field estimated from the simple pile method may not be an appropriate approximation for the strain field for a material such as soil with shearing resistance. Therefore, the strain and stress distribution close to the pile shaft predicted from both methods are suspect. Both methods retain the advantage of simplicity, with no sophisticated or time consuming numerical procedure required.

(ii) Comparison of Pore Pressures

Figs 3.32 show the excess pore pressure generated around the simple pile and a cylindrical cavity. The isotropically normally and overconsolidated soils mentioned in section 3.3.2 (iii) have again been used. The results of the simple pile method are evaluated at various depths : z=0, 5, 20 and 50a. These results indicate that

(a) Outside the critical state region, (r>9a), the excess pore pressure distributions predicted from both methods are essentially small and similar.

(b) High excess pore pressures predicted from both methods are mainly generated within the critical state region.

(c) Both methods predict similar excess pore pressure at the pile shaft near the depth z=5a. Little similarity in the excess pore pressure distributions can be observed away from the pile shaft.

(d) The cylindrical cavity expansion method predicts a higher excess pore pressure than does the simple pile method at the pile shaft, but these are lower than the excess pore pressures around the tip in the simple pile method.

Here, we find that both methods predict high excess pore pressures mainly generated inside the critical state region. Since the excess pore pressure is mainly governed by the effective stress, a realistic estimate of the effective stress distribution inside the critical state region becomes important. However, both methods considered may not provide sufficiently good modelling to estimate the effective stress distribution in this region.

3.6.2 Field Test Results

(i) Soil Description and Pore Pressure Measurements

Well documented pile test results with pore pressure measurements were reported by Roy et al. (1981). The tests were carried out using jacked piles in a sensitive clay at St.Alban, Canada. Sensitivity of St.Alban clay is reported as 14 and 22 measured at 3 and 6m below the ground surface, respectively (Tavenas and Leroueil 1977). The soil is lightly over-consolidated. Immediately after pile driving, in-situ vane tests indicated a 25% to 40% decrease in undrained shear strength close to the pile shaft. In regions outside six pile radii, no decrease in undrained shear strength was indicated.

The piles were 0.22m diameter, 7.7m long flat ended circular steel pipe. Six piles were used in this test. The excess pore pressure was measured by means of pore pressure cells and a piezometer cell beneath the tip and at various locations along the pile shaft as well as in the surrounding soil. Before jacking, a 0.3m diameter and 1m deep pilot hole was drilled. The free water surface was found at 0.45m below the ground surface. The rate of penetration was varied for each pile. Excess pore pressures in the surrounding soil reported by Roy et al. are obtained for the piles with rate of penetration approximately equal to 2cm/min. A 20% increase in tip resistance occurred when the rate of penetration was increased from 2cm/min to 7cm/min. This suggests a rate effect involved in penetration resistance in this soil.

The soil profile at this site is shown in Fig.3.33. The overconsolidation ratio for the soil is less than 2.4 at depths below 2m from the ground surface. A ratio of shear modulus, G, to shear strength, Cu, in undrained conditions of 300 is suggested (Roy et al. 1981). This corresponds to β equal to 260 for the rate-type model. The excess pore pressure at 3 and 6m below the ground surface was reported. Measurements of excess pore pressure when the tip and the shaft pass through these depths are also given in Figs.3.34. Roy et al. reported that the piezometer cell measured a maximum excess pore pressure when the pile tip is 0-2 pile radius above the cell. The excess pore pressure decreases and reaches an equilibrium value after the pile tip has penetrated to a depth 15 or 20 pile radii below the cell. This is a general feature of pore pressure predicted from the simple pile method as we have shown in Sec 3.4.3(iii).

(ii) Soil-Parameters

Tavenas and Leroueil (1977) conducted consolidated undrained triaxial compression tests on undisturbed St.Alban clay under various confining pressures. Their results indicate that this clay exhibits a peak strength at low strain levels and there is strain softening after the peak. The soil arrives at the critical state at very large strain levels. Although this type of response cannot be closely simulated by the rate-type model under undrained conditions, we estimate the necessary soil parameters directly from available information in Tavenas and Leroueil (1977), and Roy et al. (1981).

The effective angle of friction for St. Alban clay at critical state is ϕ =27°, this gives N_c=0.29. Using Eqs.2.55 to 2.61 for the rate-type model and using the effective overburden pressure as well as the preconsolidation pressure from Fig.3.33, we obtain the parameters for the rate-type model given in Table 3.1. We note that St. Alban clay is one dimensionally lightly overconsolidated clay. The initial stress state of this soil is close to hydrostatic conditions.

The coefficient of earth pressure at rest, K_{oc}, decreases with depth from about 0.9 at 2m to 0.7 at 8m, Roy et al. (1981). This coincides with the K_{oc} value predicted from Eq.2.58. We note from Fig.3.33 and Table 3.1 that Eq.2.61 predicts Cu values which agree well with the in situ vane strength. However, vane measurements often underestimate the peak strength obtained from undrained triaxial tests.

(iii) Model Predictions

In this section, both solutions of the cylindrical cavity expansion approach and the simple pile method will be used to compare with the measured excess pore pressure. We have evaluated the excess pore pressure from the simple pile method at z=0 and 20a to compare with the measured excess pore pressure around the pile tip and the shaft respectively. The predicted results are also shown in Fig.3.34 for comparison, where it can be seen that

(a) The cylindrical cavity expansion method highly underestimates the excess pore pressure around the pile tip. Also, this method overestimates ΔU at the shaft but under estimates the excess pore pressure in regions outside 2 pile radii from the pile shaft.

(b) The simple pile method predicts excess pore pressures around the pile shaft which are close to the measured test results. However, this method also underestimates the excess pore pressure by about 2Cus outside one pile radius from the tip.

In this comparison, the simple pile method gives a better prediction for excess pore pressure around the pile shaft than does the cylindrical cavity expansion approach. Also, outside the region 3 pile radii from the pile shaft, comparing both measured and predicted ΔU distributions, we find that the cylindrical cavity expansion method predicts excess pore pressures dissimilar to measured values. Although unrealistic pile soil interaction has been found, especially in regions close to the pile shaft in the simple pile method; the simple pile method remains a better approximation to the excess pore pressure distribution than does the cylindrical cavity expansion approach.

SECTION 3.7 Summary

In this chapter, two existing methods, the cylindrical cavity expansion approach and the simple pile method, are used to investigate pile installation effects. The rate-type model has been used to represent the soil. Results obtained from both methods have been compared. Also, the predicted pore pressure has been compared with measured field test results.

The cylindrical cavity expansion approach is a simple method and allows analytical solutions to be obtained. However, the tip effects due to pile advancement cannot be considered. Both the cylindrical cavity expansion and simple pile method yield similar effective stress distributions outside the critical state region, but quite different results inside the critical state region.

The simple pile method attempts to include the tip effect, but results in unrealistic pile-soil interaction. The surface conditions of the simple pile do not correspond to a smooth surface, but we have found that the surface shear traction is acting downward along the pile body and results in tensile stress in the pile. The simple pile method is founded upon the idea that the velocity field in an ideal fluid flow may be provide sufficient approximation to that in a soil due to pile penetration. Contrarily, we find that the unrealistic surface traction is significantly higher in soft clay than that in stiff clay. Because of the unrealistic shear distribution along the pile, it may be expected that the effective stress distribution in the critical state region may be not reliable.

Since equilibrium conditions are violated in the simple pile method, the excess pore pressure is evaluated based on a selected integration path which is less reliant on the shear stress. From our results, high excess pore pressures are generated within the critical state region. However both the cylindrical cavity expansion and simple pile methods may not provide sufficiently good modelling of the effective stress distribution in this region and thus may affect the predicted pore pressure. Nevertheless, comparison of predicted pore pressures with measured field test results indicated that the simple pile method predicts more satisfactory results than does the cylindrical cavity expansion method.

Depth (m)	σ_{zi} (kpa)	σ_{znc} (kpa)	$\overline{OCR}$	K_{oc}	p_c (kpa)	Cu (kpa)	Cus (kpa)
3	20.0	48.0	2.4	0.9	19.2	10.3	11.9
6	37.5	82.0	2.2	0.85	33.5	18.0	20.7
Remark				Eq. 2.58	Eq. 2.61	Eq. 2.52	

Table 3.1 Rate-type model parameters for St. Alban test site.

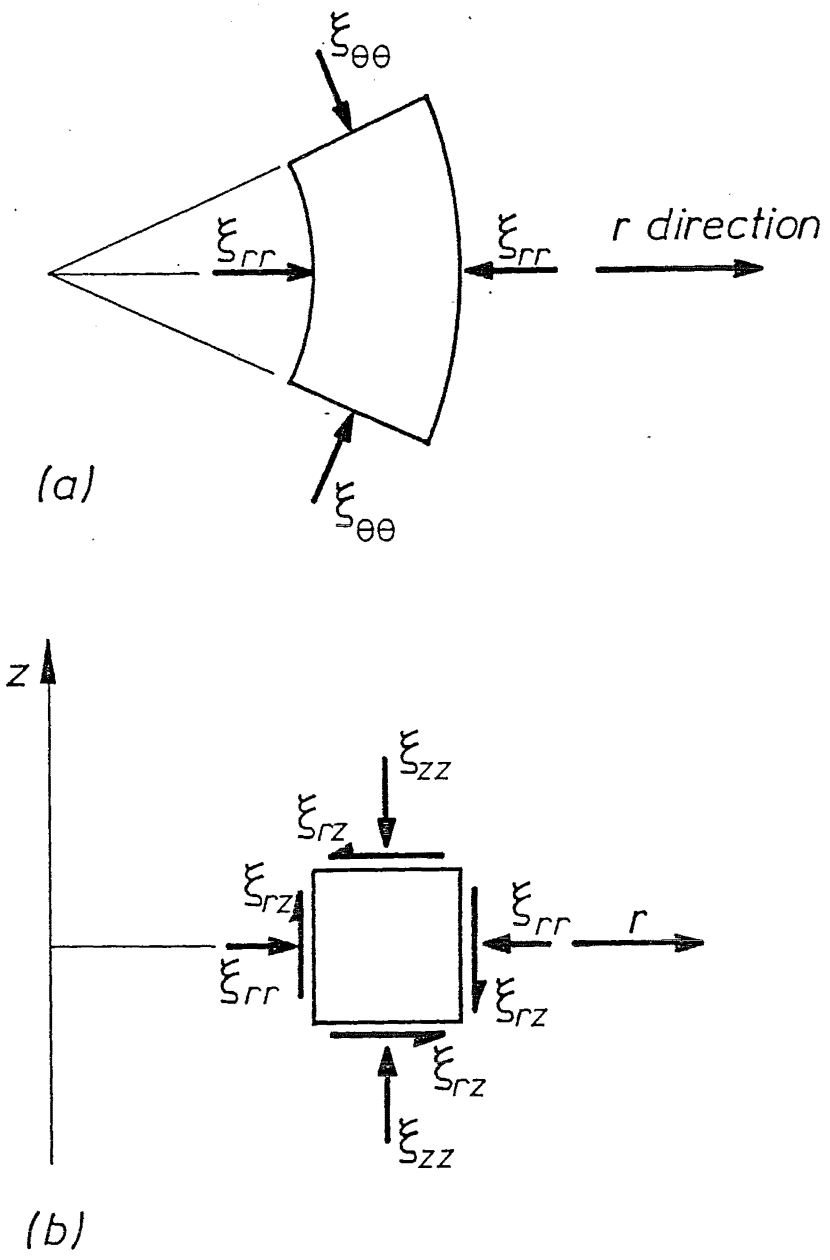

Figure 3.1 Sign convention of strain components in a cylindrical coordinates.

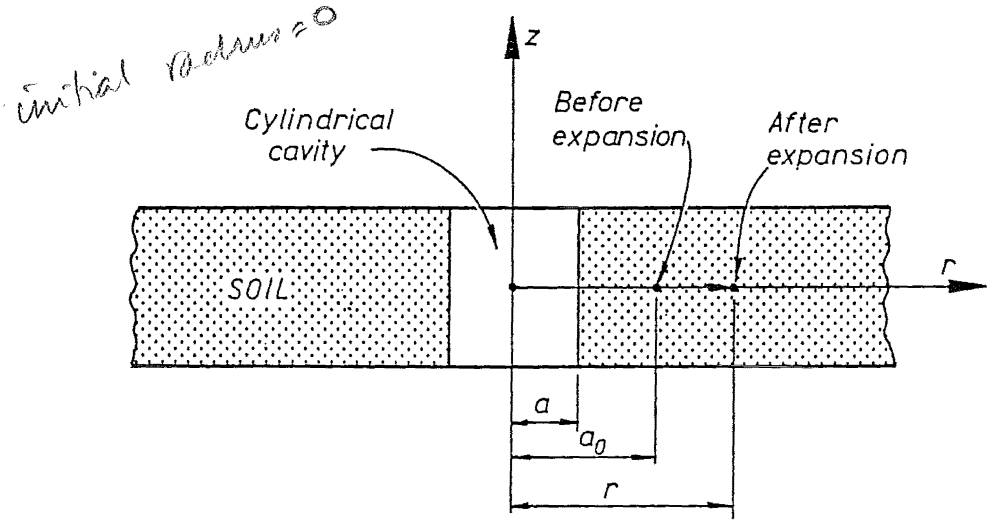

Figure 3.2 Cylindrical cavity expansion.

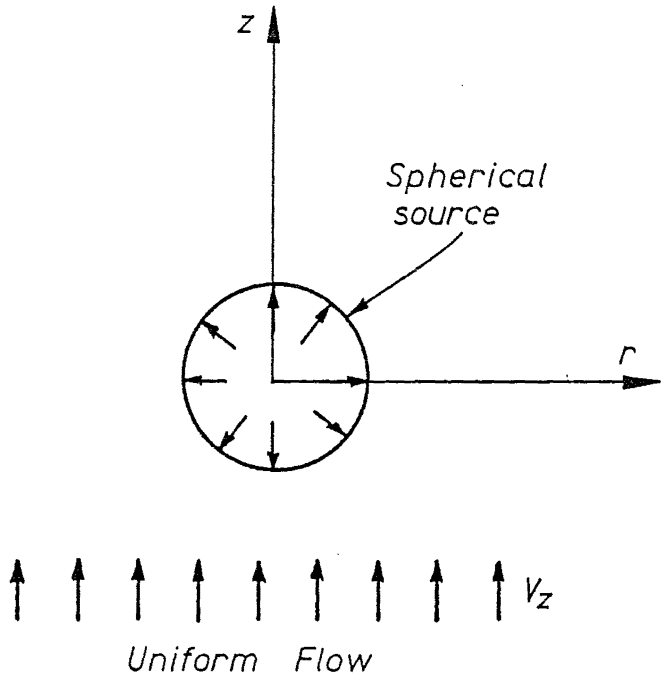

Figure 3.3 Concept of the simple pile method.

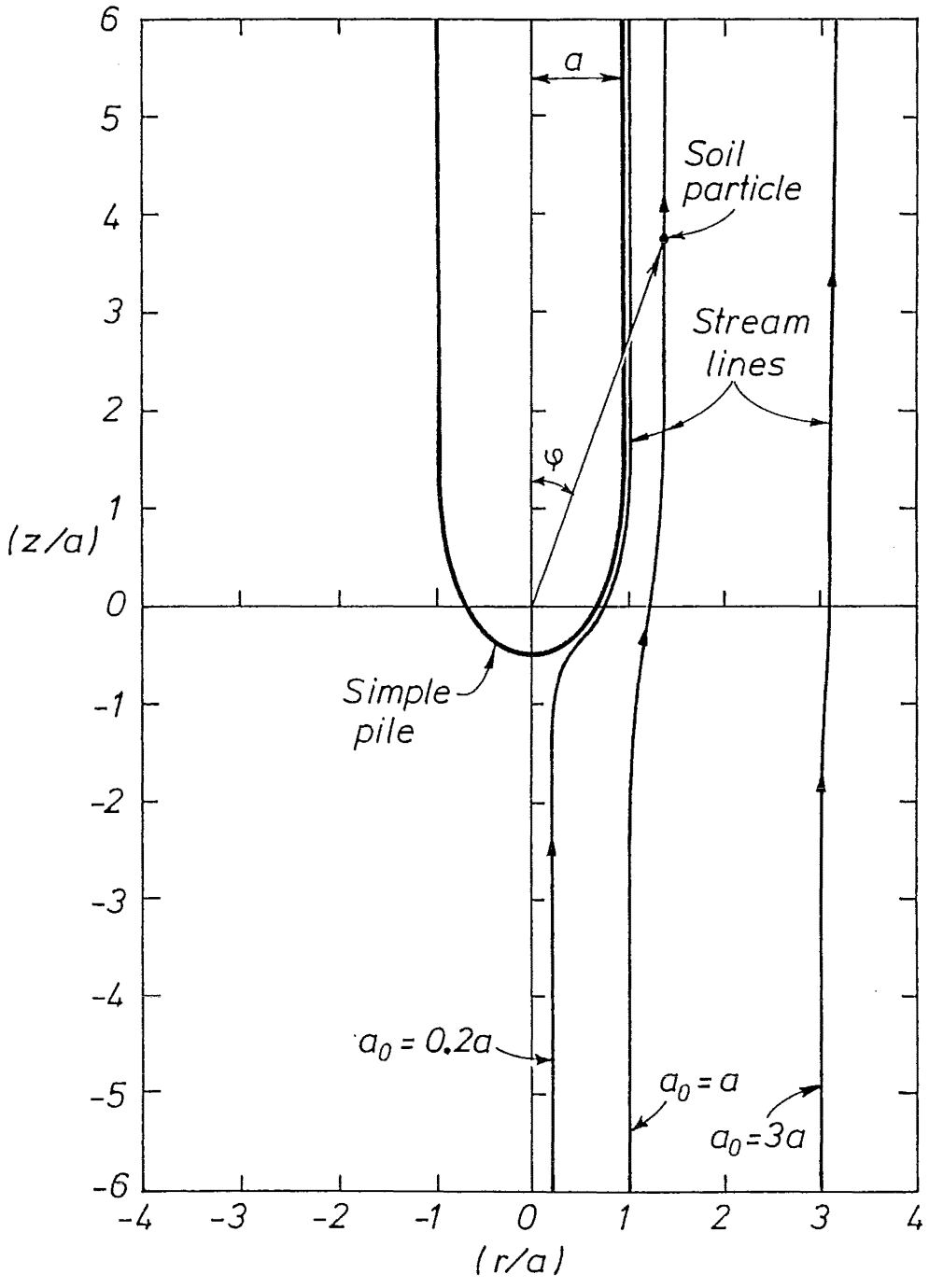

Figure 3.4 Simple pile and stream lines.

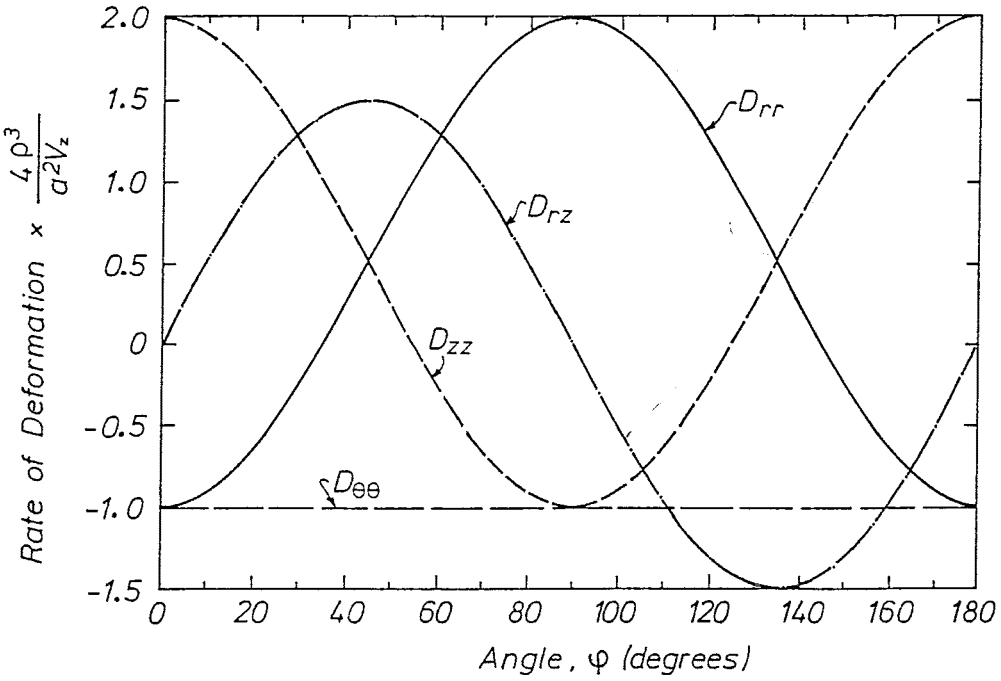

Figure 3.5 Variation of components of the rate of deformation tensor with angle φ.

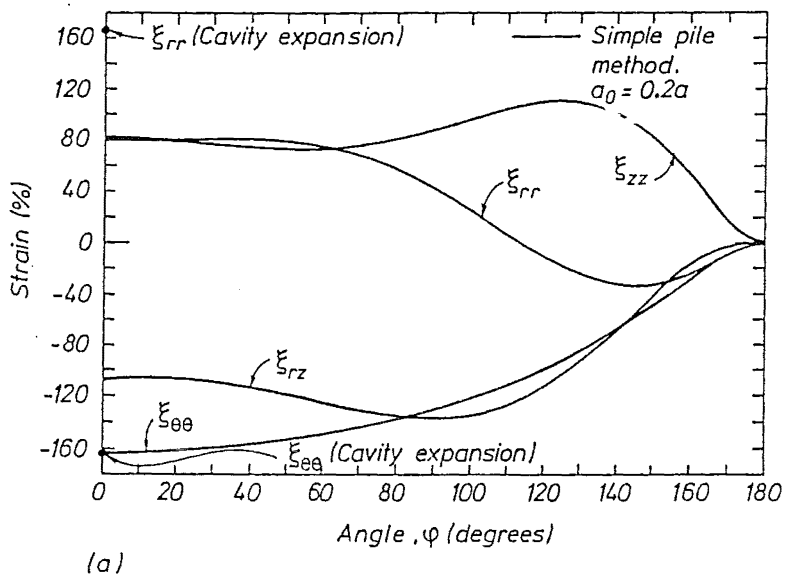

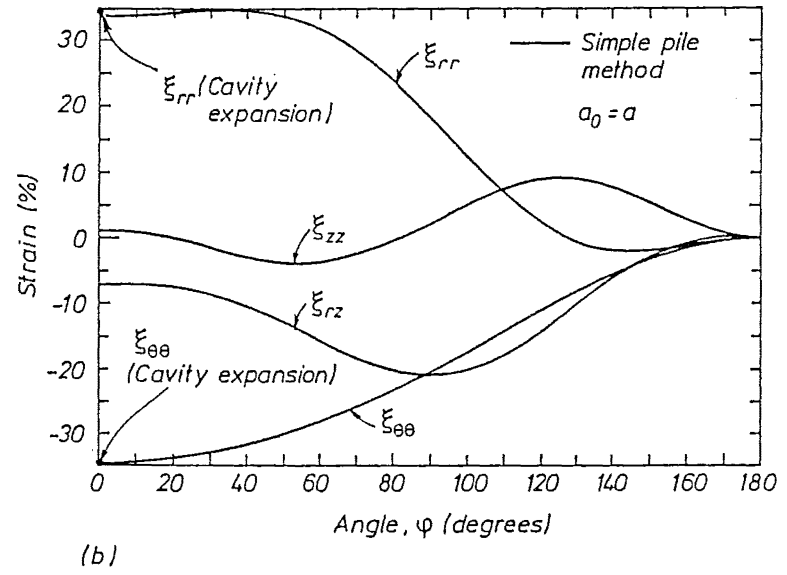

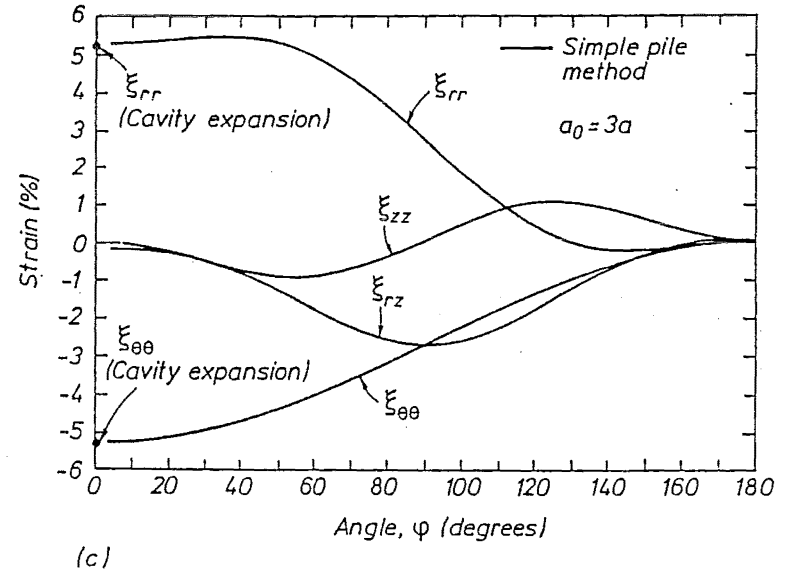

Figure 3.6 Strain path of soil initially located at (a) a_0= 0.2a (b) a_0= a and (c) a_0=3a.

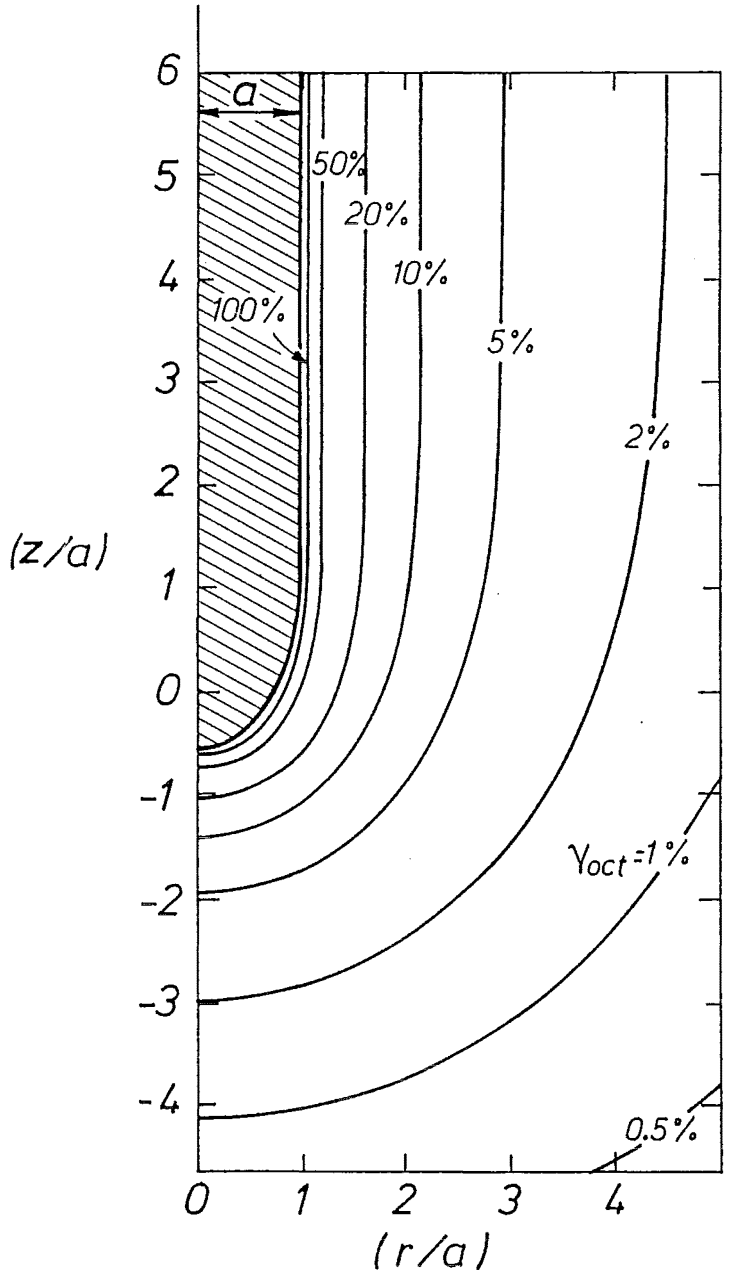

Figure 3.7 Contours of octahedral shear strain around a simple pile, (after Baligh 1984).

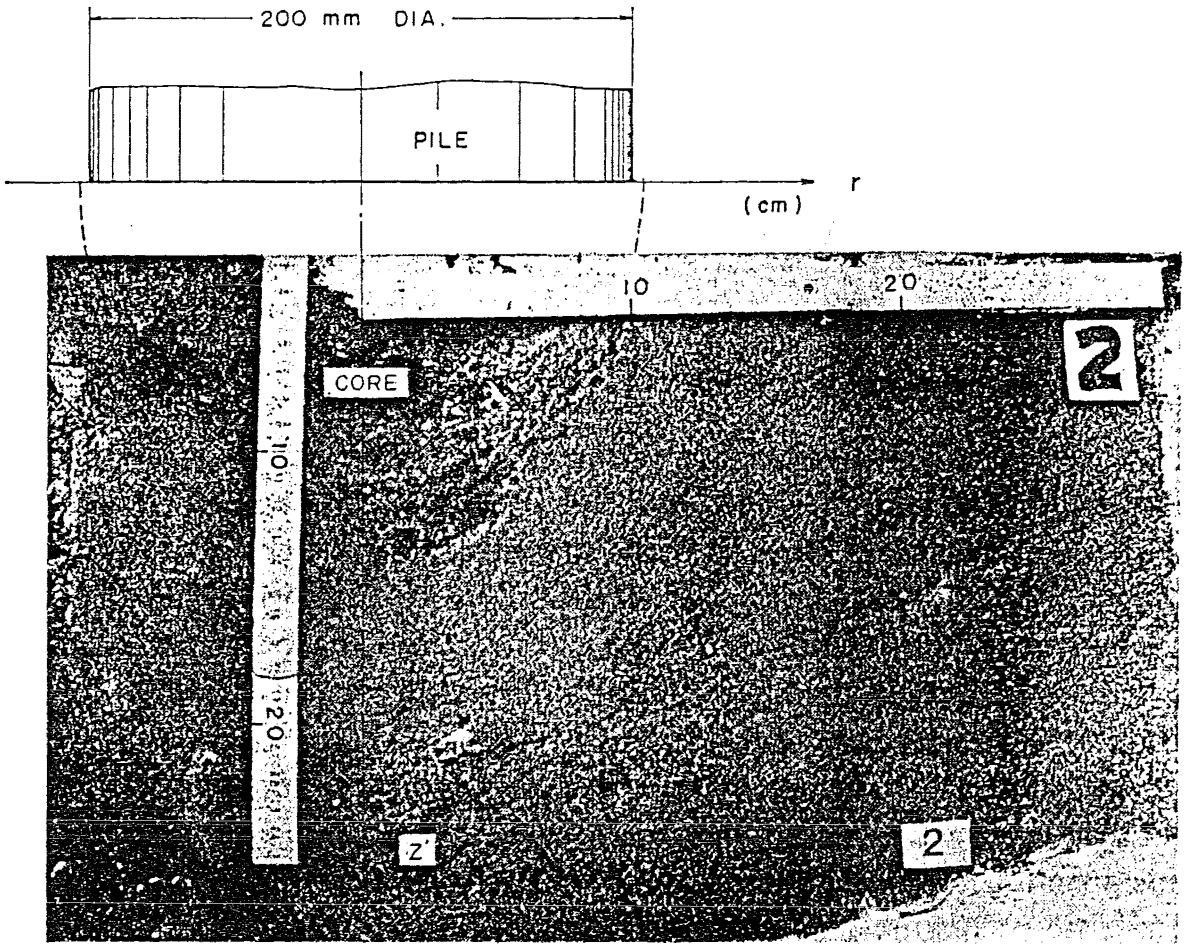

Figure 3.8 Soil conditions beneath a flat-ended pile in sand, (after BCP Committee 1971).

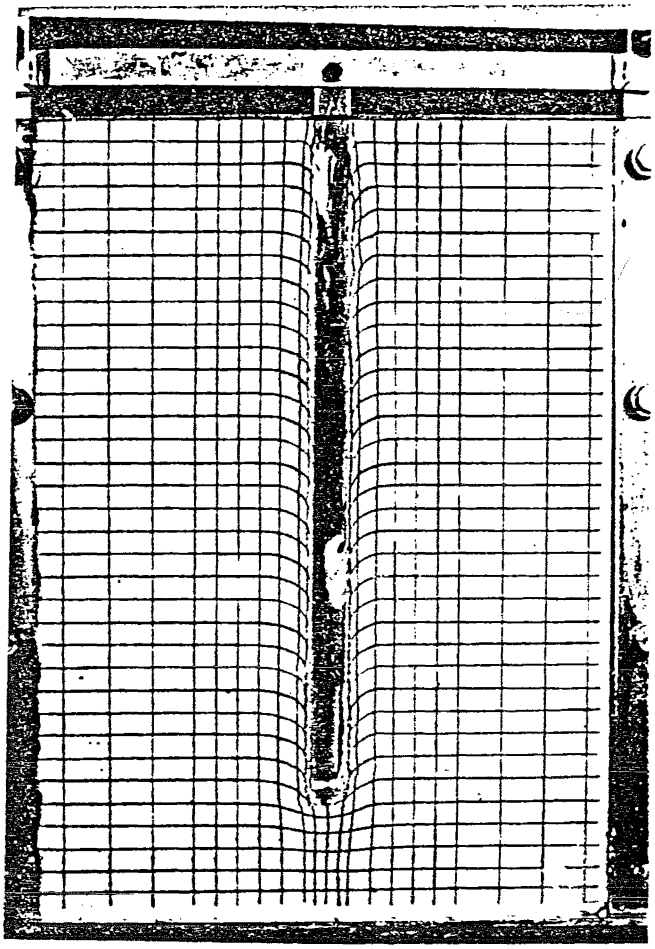

Figure 3.9 Soil conditions beneath a flat-ended model pile in clay, (after Randolph et al. 1979).

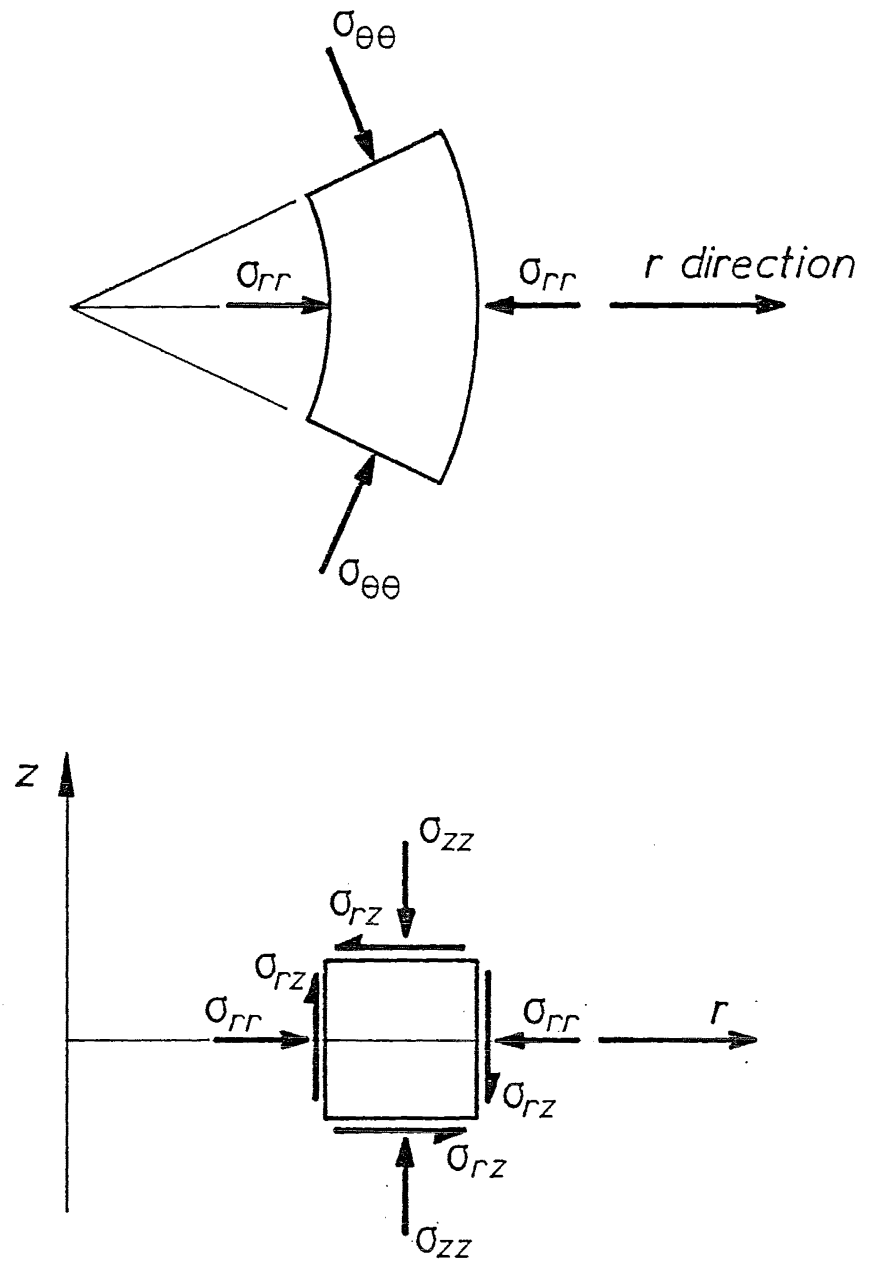

Figure 3.10 Sign convention of stress components in a cylindrical coordinates.

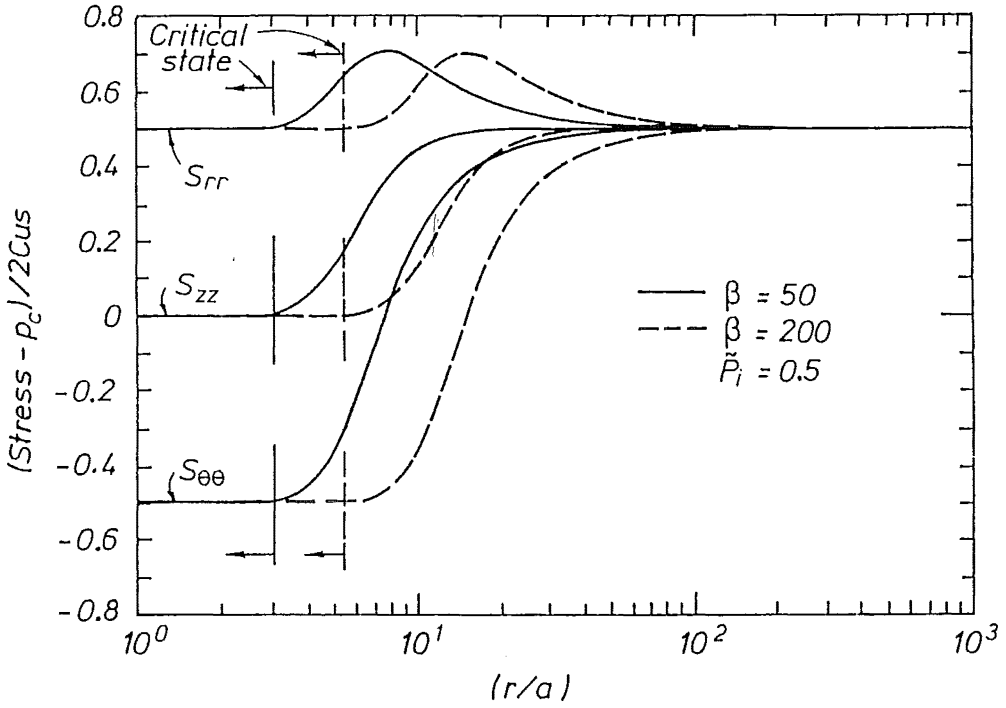

Figure 3.11 Effective stresses in lightly overconsolidated soil due to cylindrical cavity expansion.

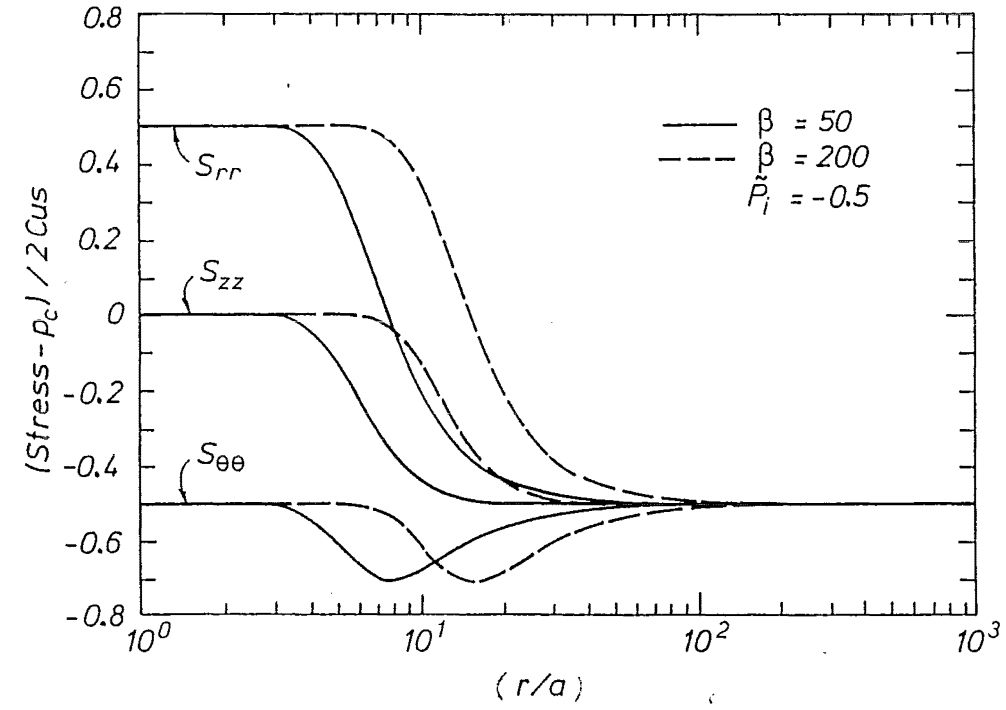

Figure 3.12 Effective stresses in heavily overconsolidated soil due to cylindrical cavity expansion.

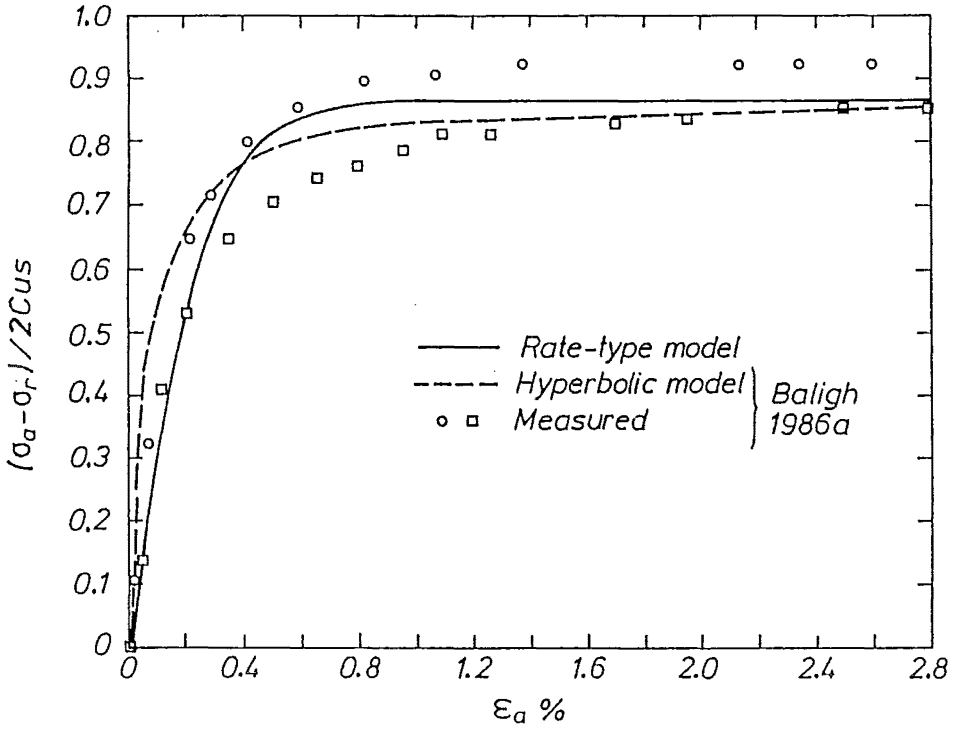

Figure 3.13 Comparison of rate-type model prediction with measured stress-strain curves for triaxial compression tests on Boston Blue clay, (after Baligh 1986a).

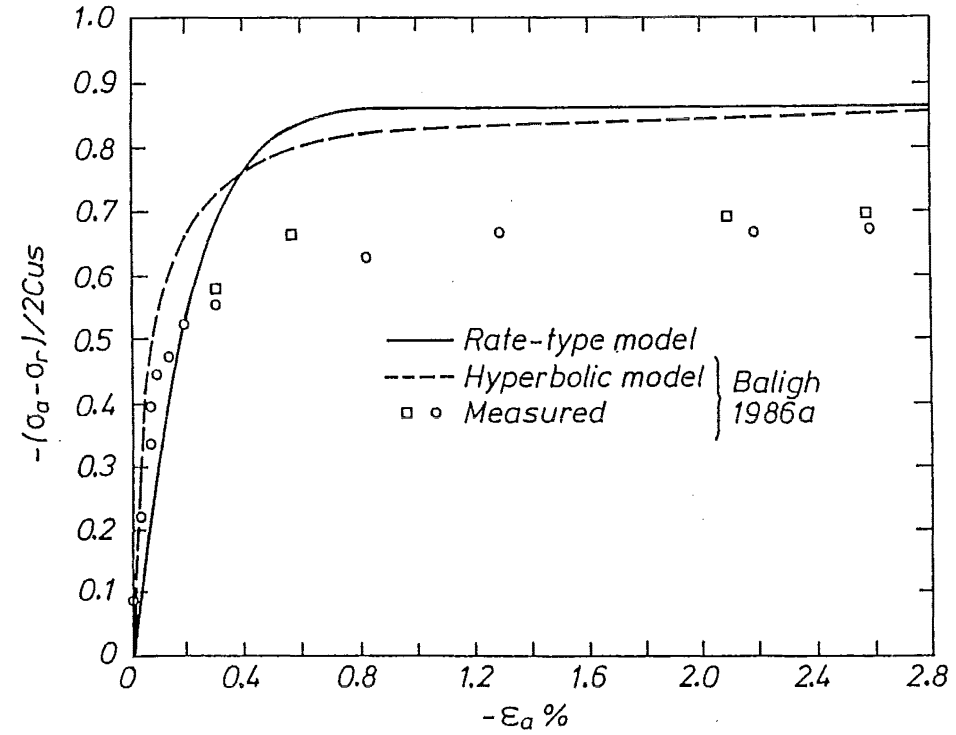

Figure 3.14 Comparison of rate-type model prediction with measured stress-strain curves for triaxial extension tests on Boston Blue clay, (after Baligh 1986a).

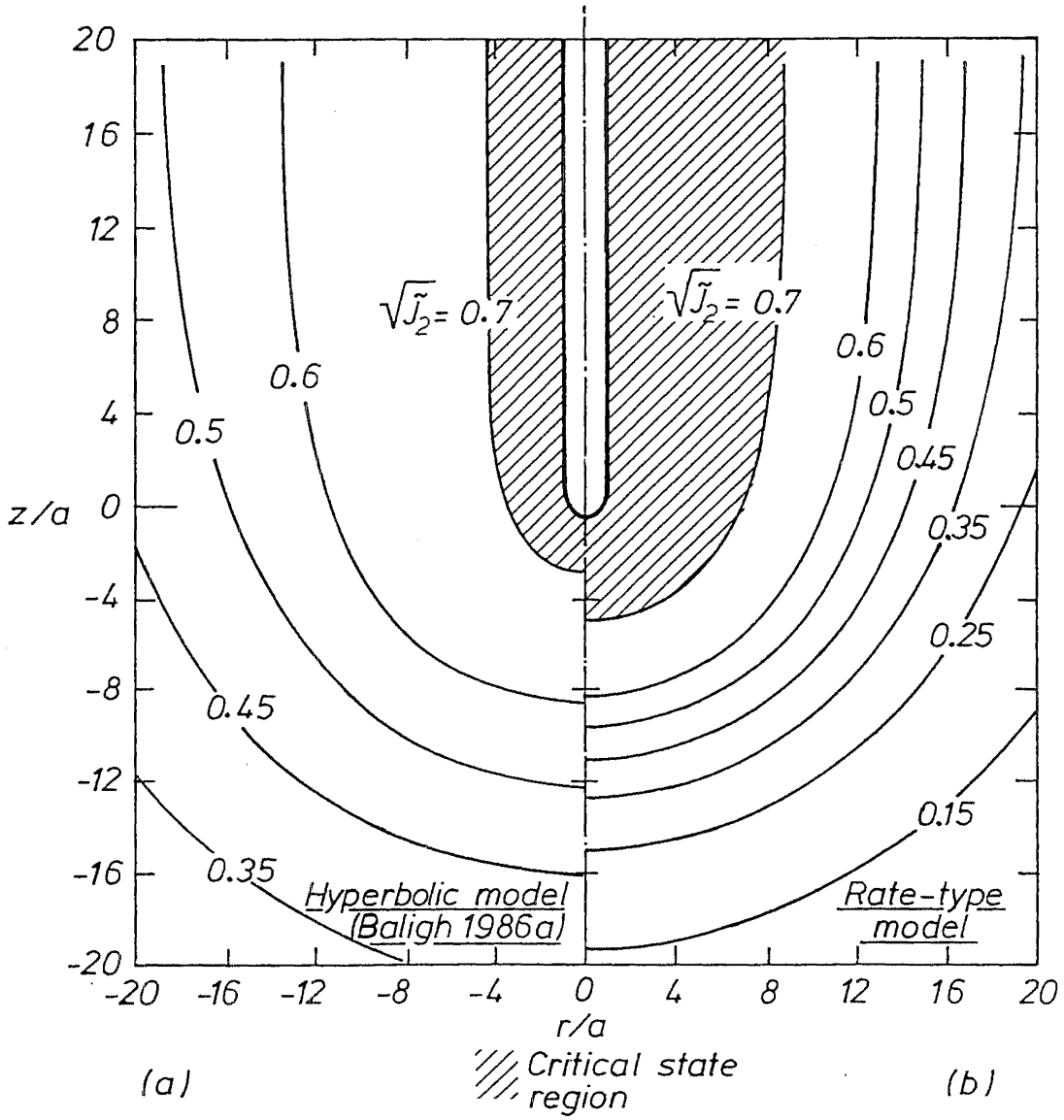

Figure 3.15 Comparison of predicted deviatoric stress contours around a simple pile, (a) hyperbolic model,after Baligh 1986a (b) rate-type model.

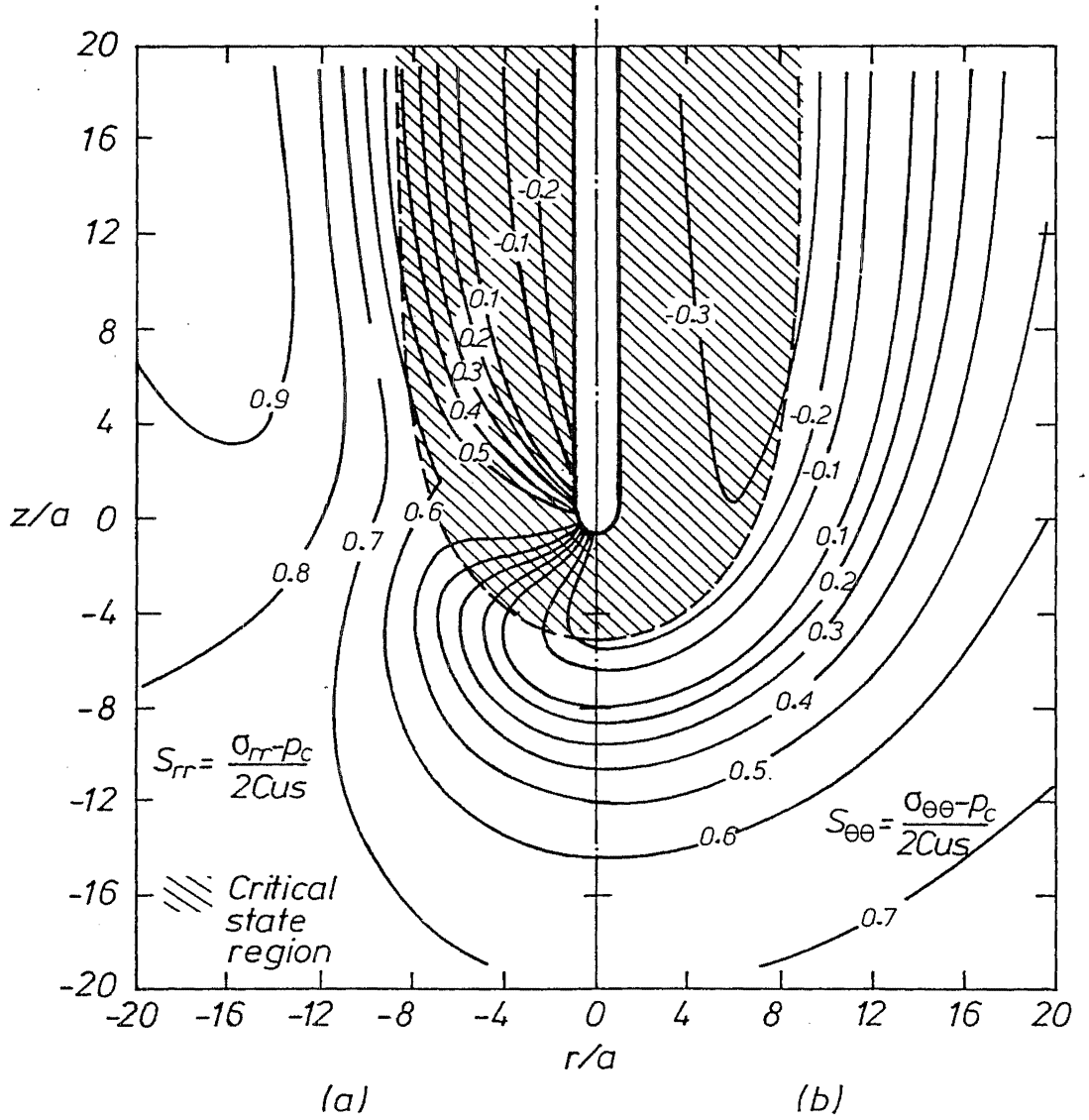

Figure 3.16 Predicted dimensionless effective stress contours due to simple pile penetration in normally consolidated Boston Blue clay (a) radial stress S_{rr} (b) hoop stress $S_{\theta\theta}$ (c) vertical stress S_{zz} and (d) shear stress S_{rz}.

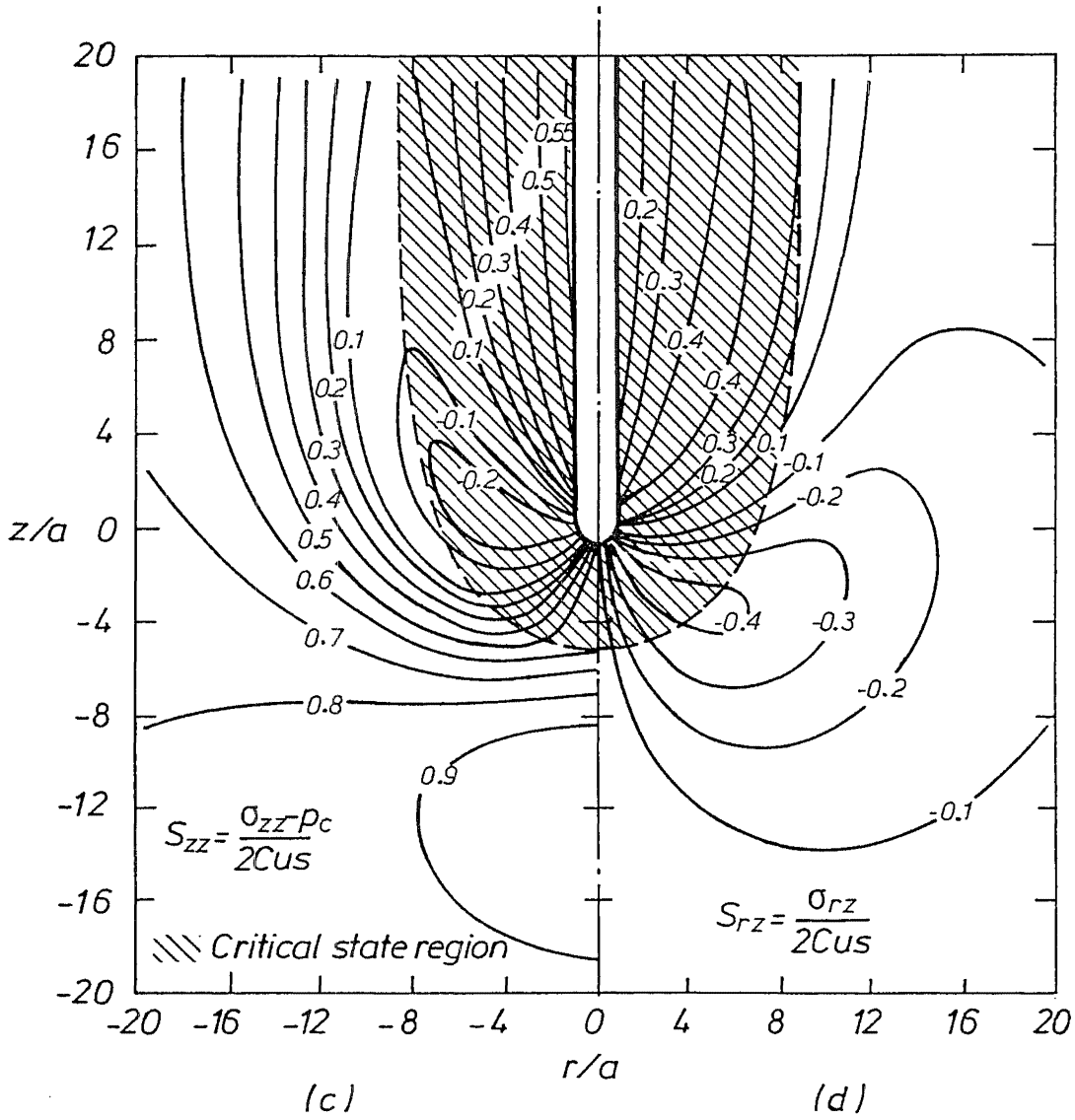

Figure 3.16 (continued) Predicted dimensionless effective stress contours due to simple pile penetration in normally consolidated Boston Blue clay .

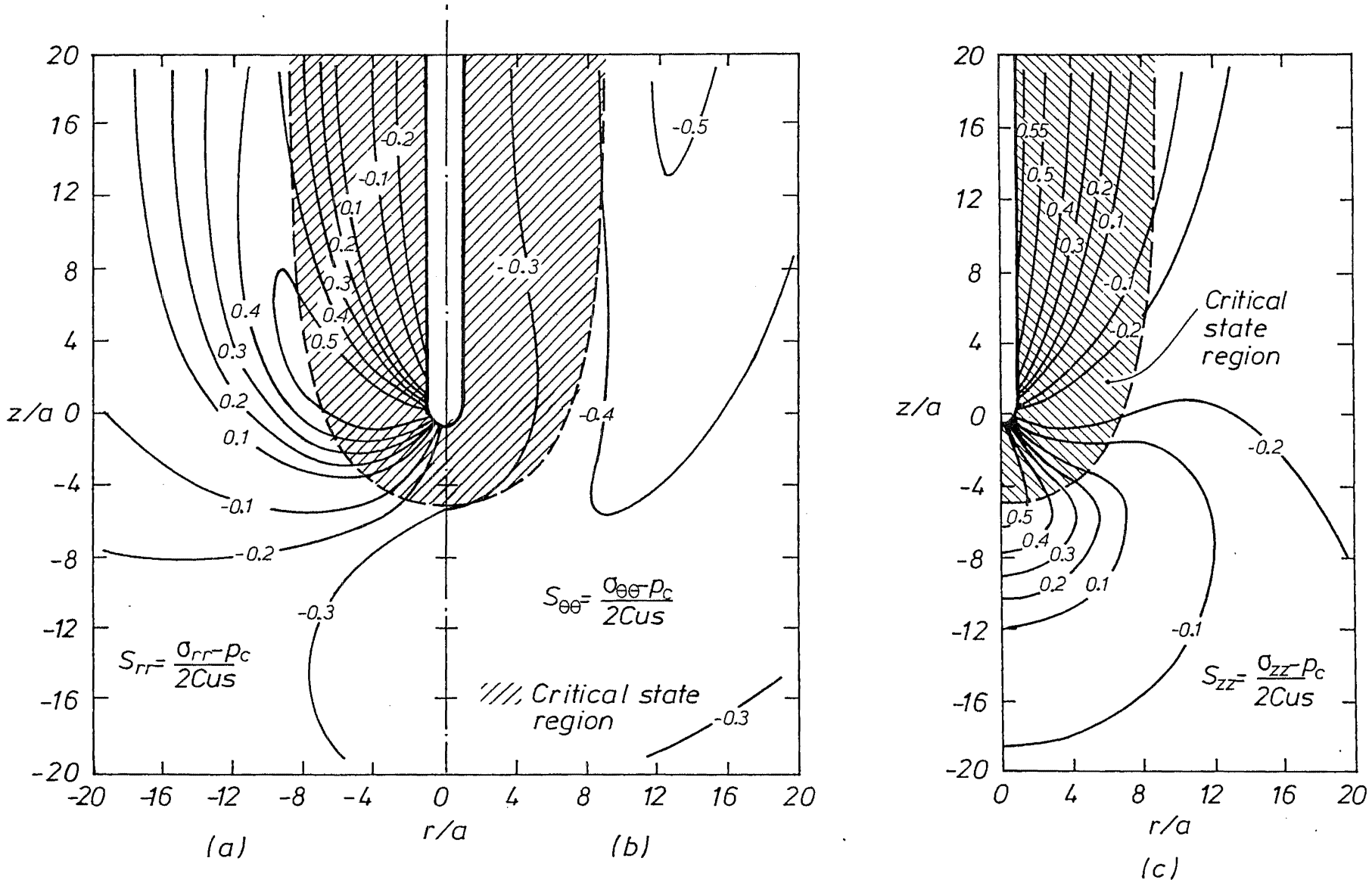

Figure 3.17 Predicted dimensionless effective stress contours due to simple pile penetration in overconsolidated soil (a) radial stress S_{rr} (b) hoop stress $S_{\theta\theta}$ and (c) vertical stress S_{zz} .

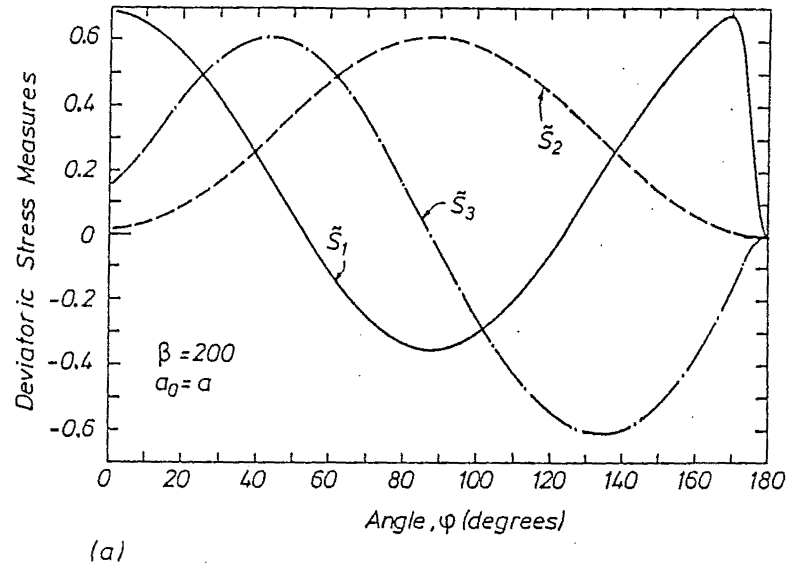

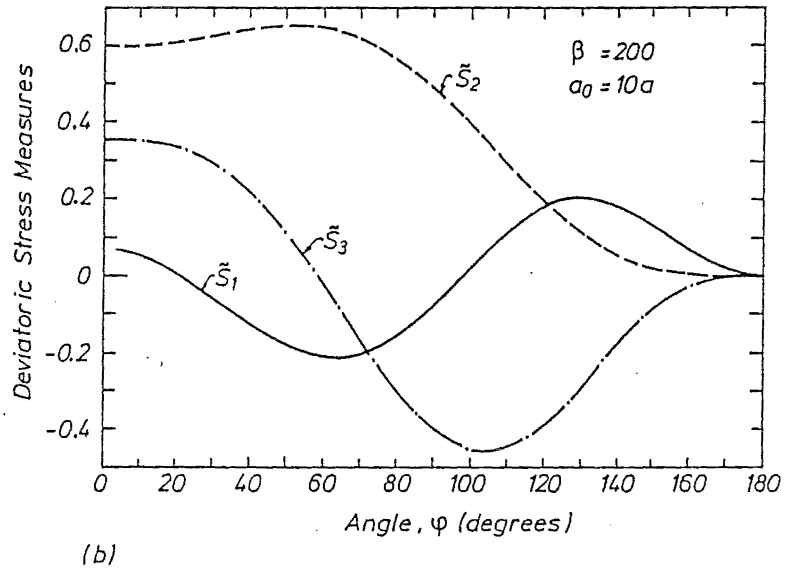

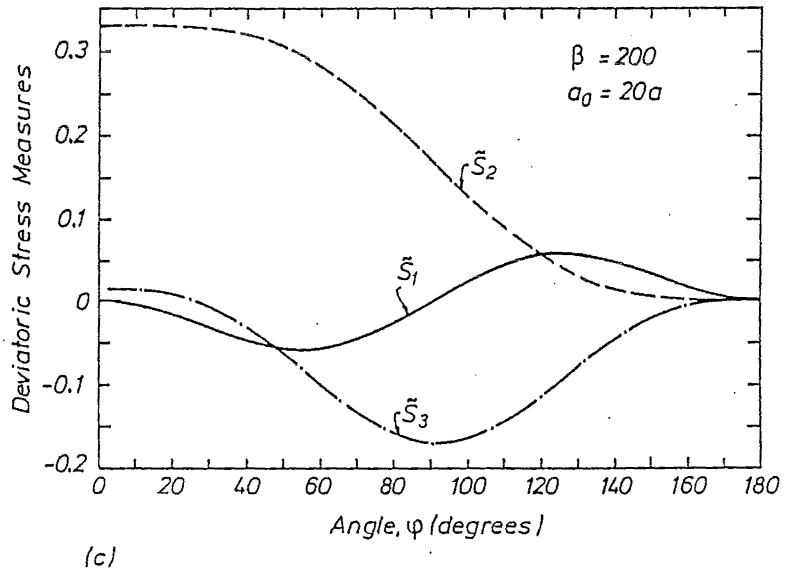

Figure 3.18 Deviatoric stresses along the stream line for a soil particle initially located at (a) a_0= a (b) a_0= 10a and (c) a_0=20a.

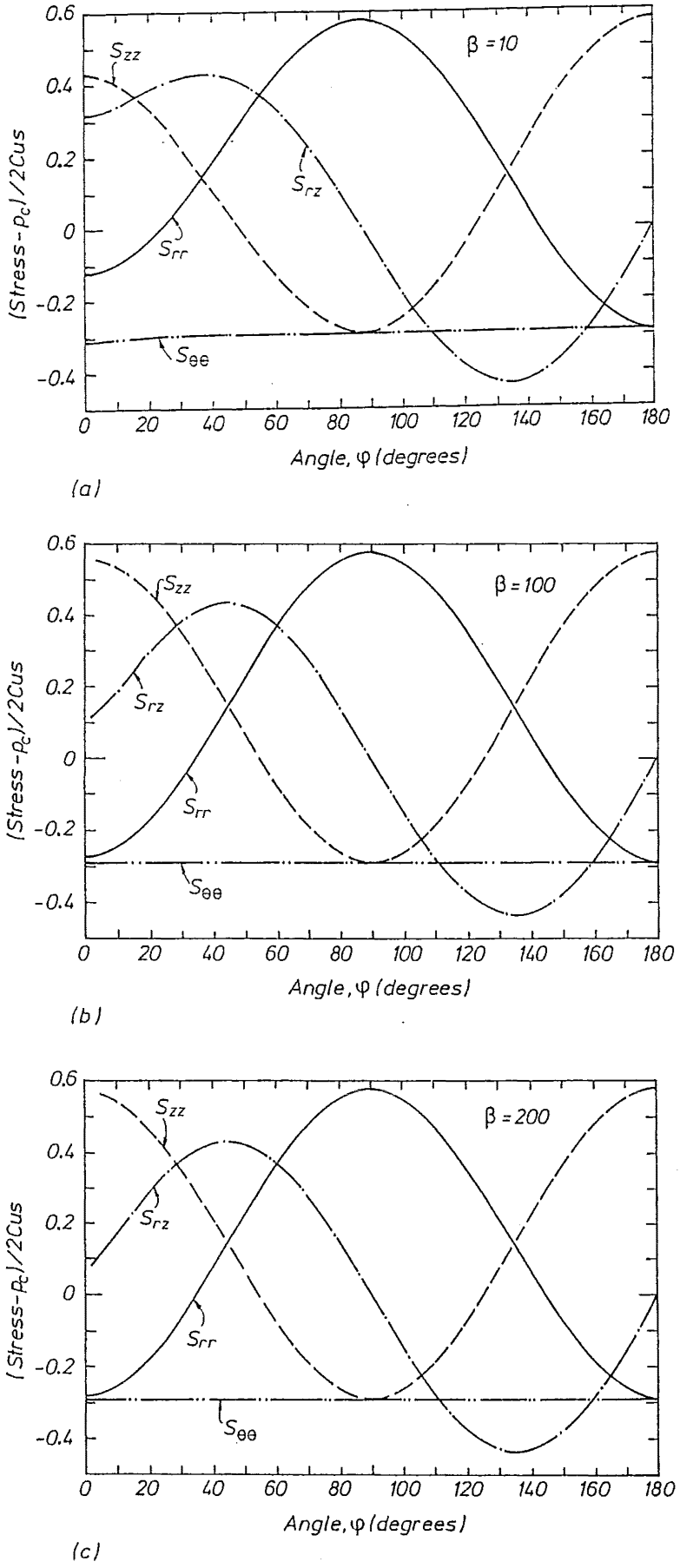

Figure 3.19 Effective stresses distribution along the pile shaft for soil with (a) β= 10 (b) β= 100 and (c) β=200.

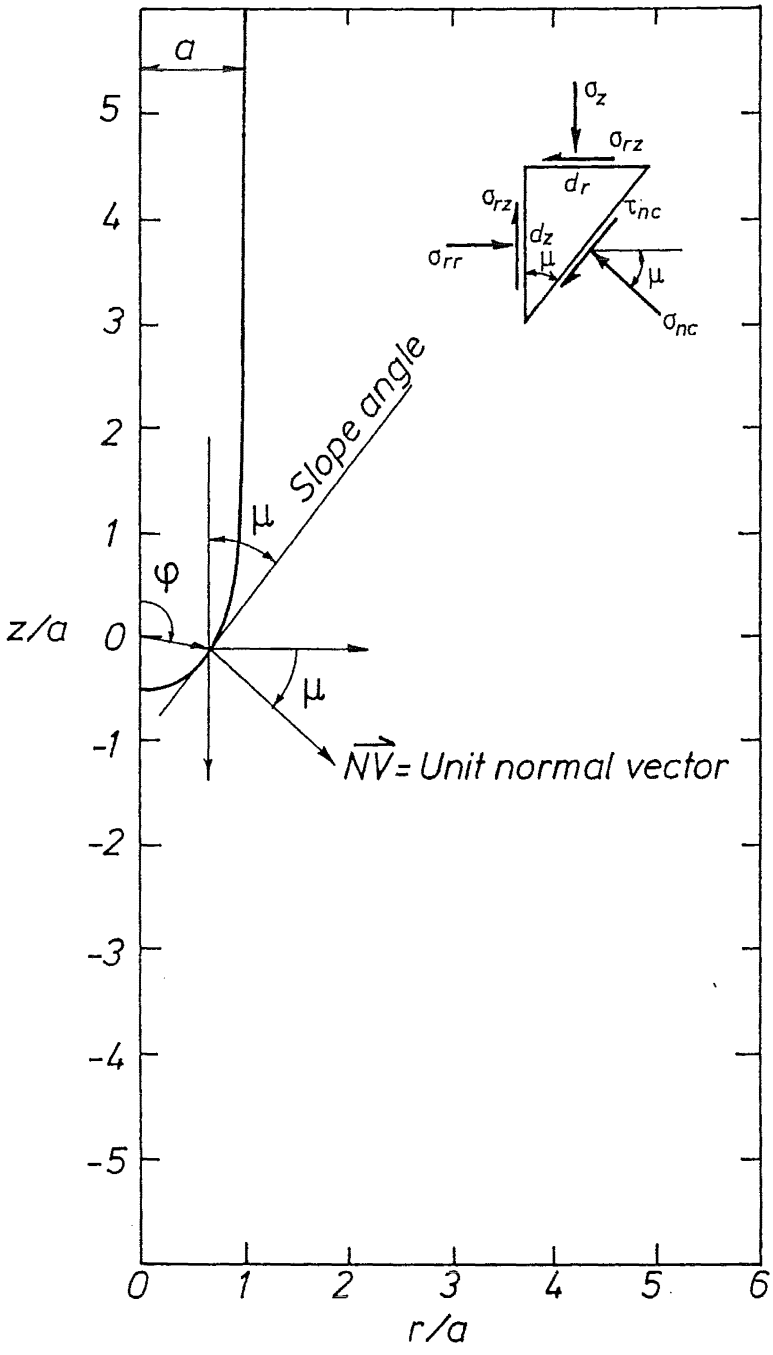

Figure 3.20 Unit normal vector and sign convention for surface tractions.

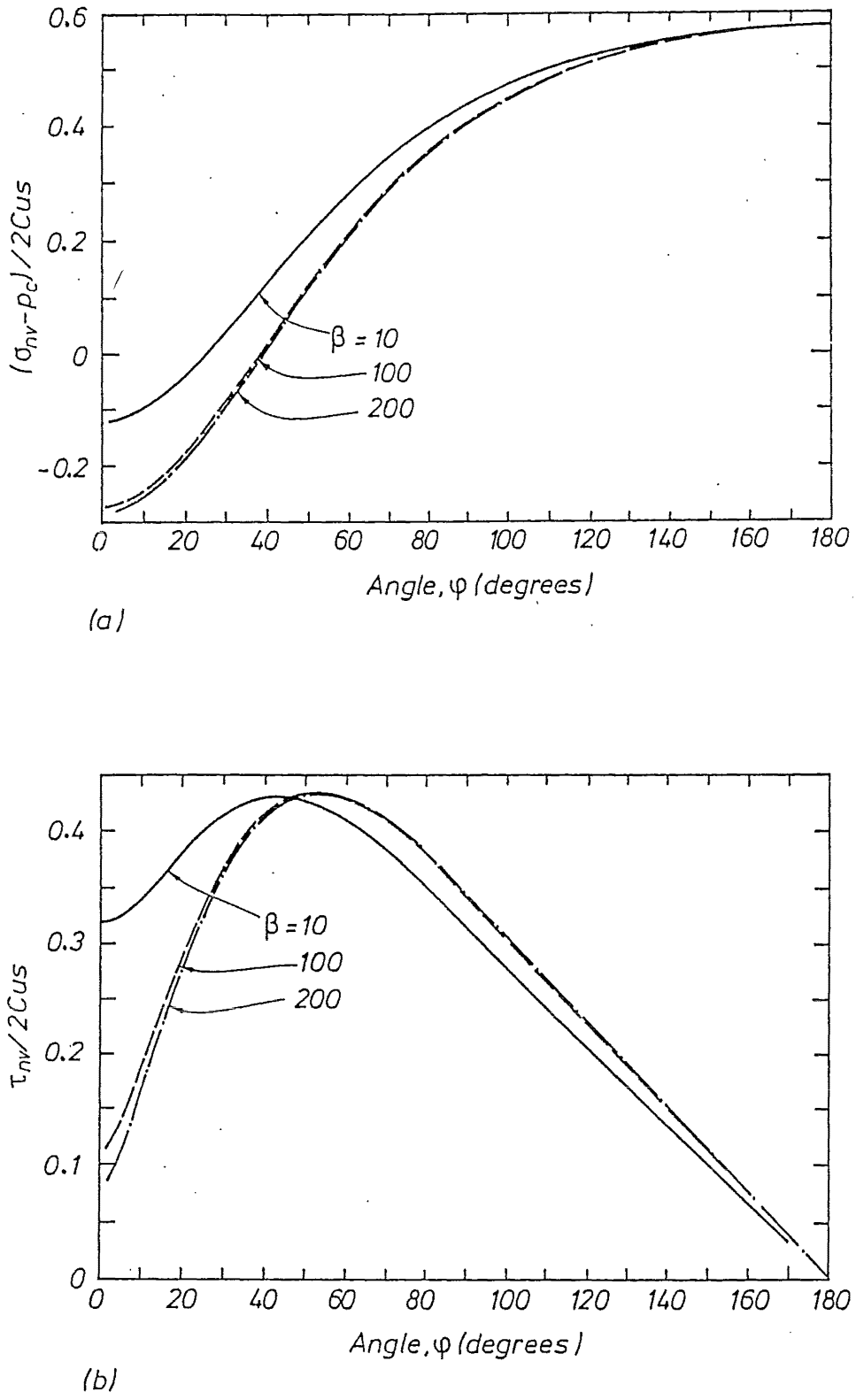

Figure 3.21 Dimensionless surface tractions on the simple pile (a) normal traction (b) shear traction.

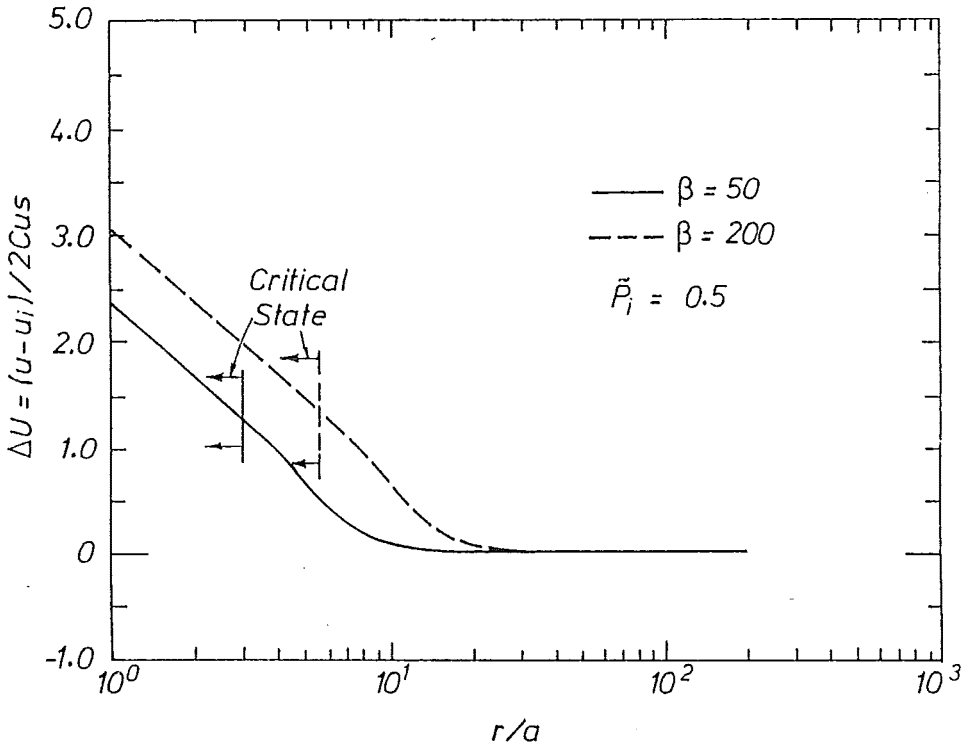

Figure 3.22 Predicted excess pore pressure in lightly overconsolidated soil due to cylindrical cavity expansion.

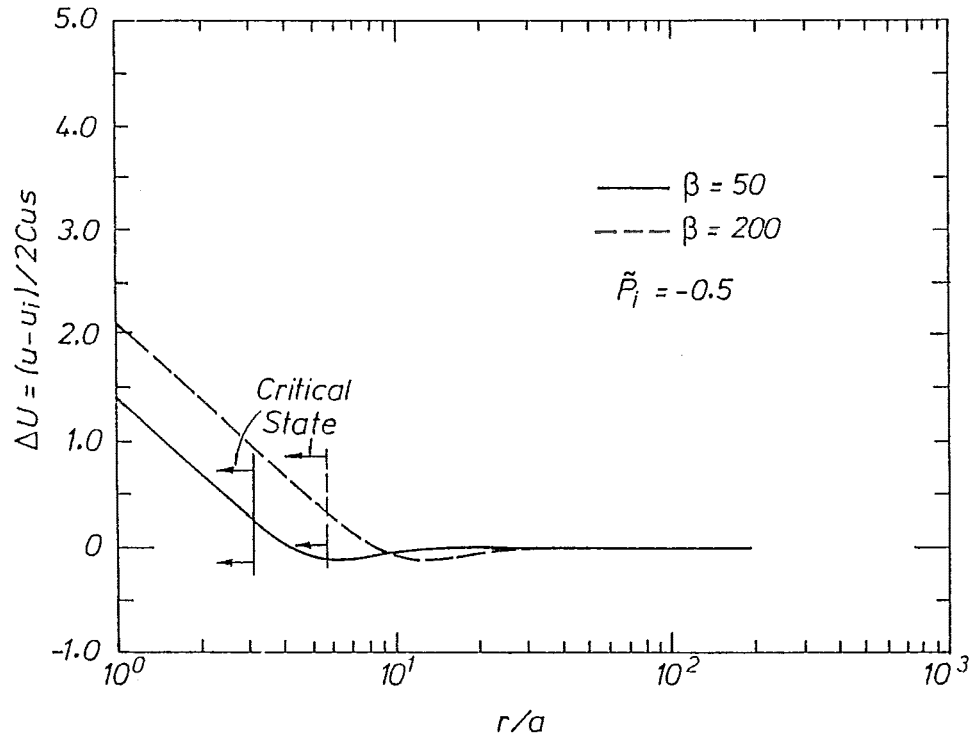

Figure 3.23 Predicted excess pore pressure in heavily overconsolidated soil due to cylindrical cavity expansion.

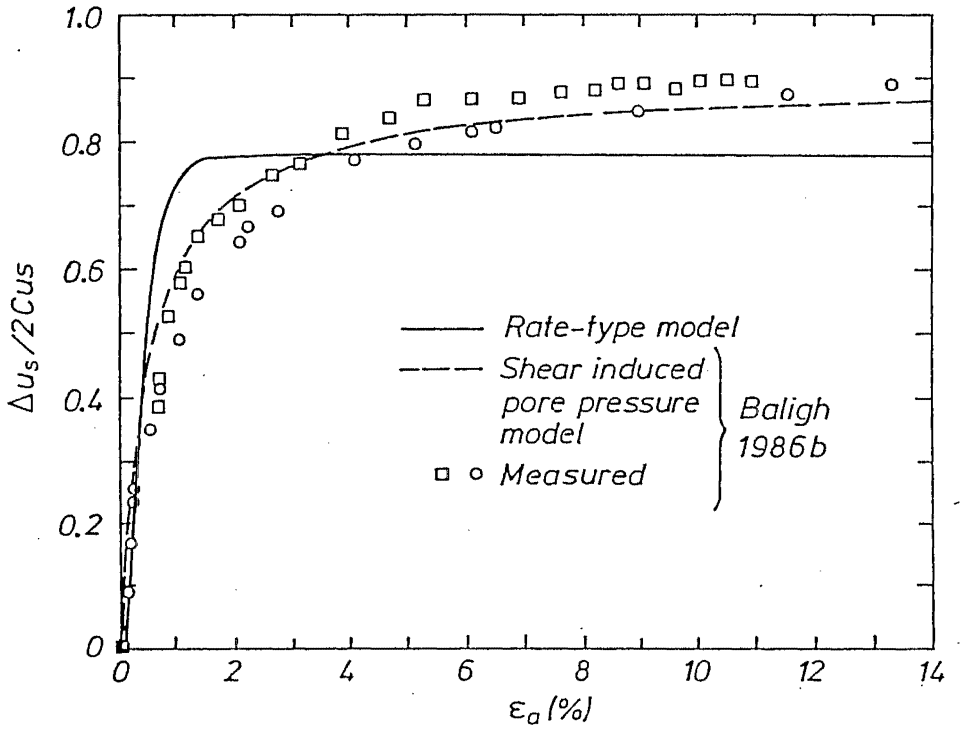

Figure 3.24 Comparison of rate-type model prediction with measured excess pore pressure for triaxial compression tests on Boston Blue clay (after Baligh 1986b).

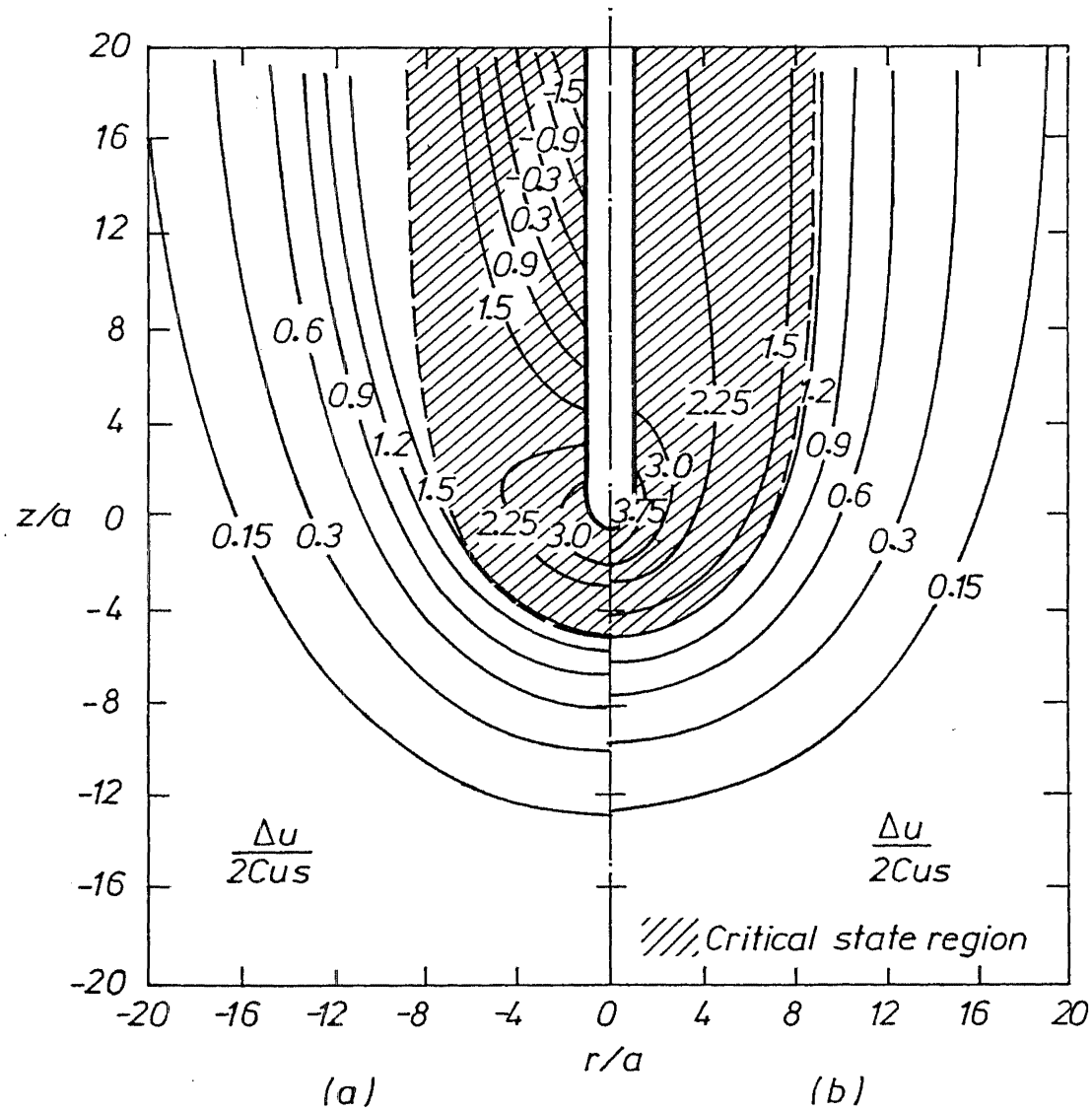

Figure 3.25 Predicted excess pore pressure contours due to simple pile penetration in normally consolidated Boston Blue clay by integrating the equilibrium equation along (a) stream line and (b) radial direction.

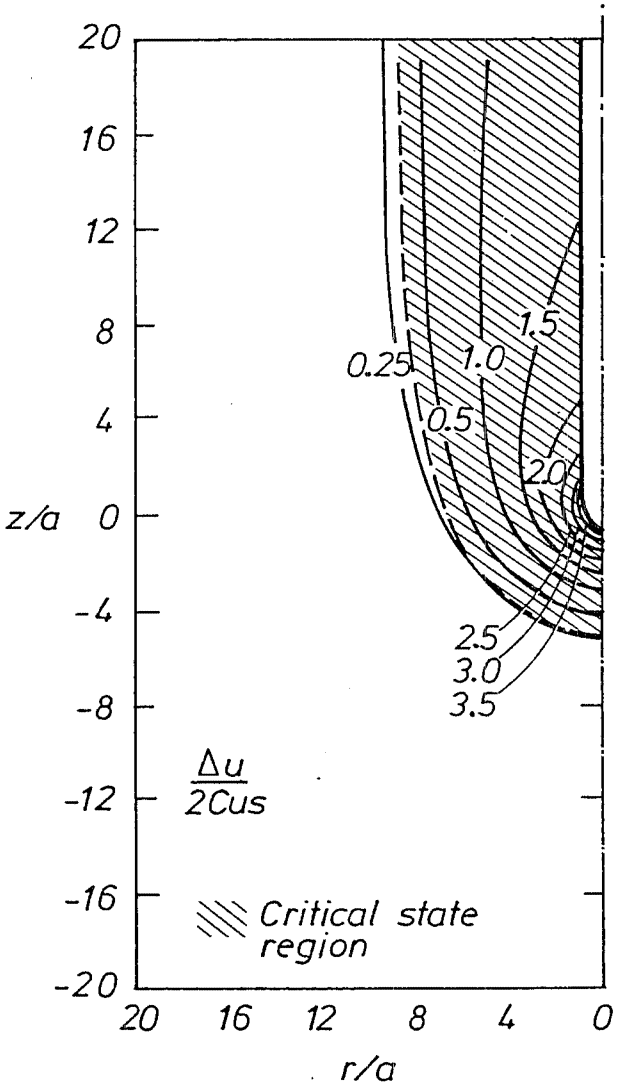

Figure 3.26 Predicted excess pore pressure contours due to simple pile penetration in heavily overconsolidated soil.

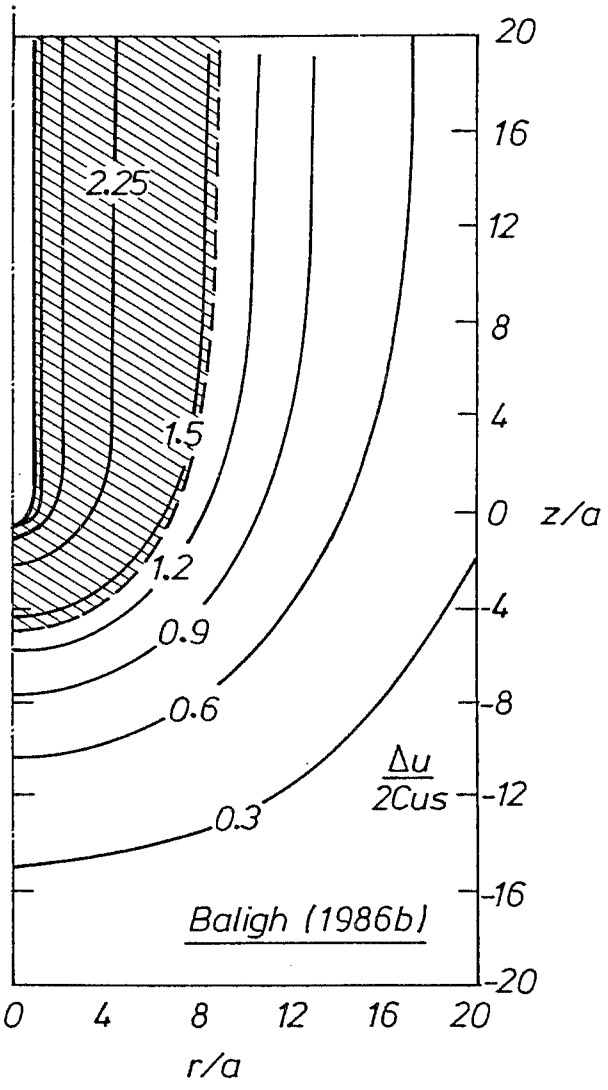

Figure 3.27 Excess pore pressure contours due to simple pile penetration in Boston Blue clay, (after Baligh 1986b).

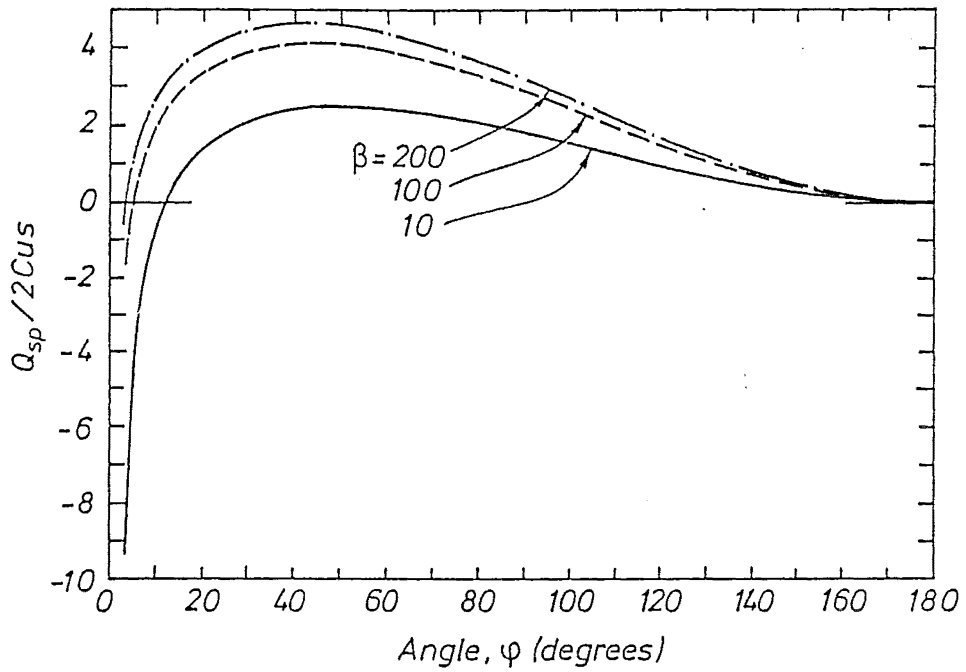

Figure 3.28 Dimensionless penetration resistance for the simple pile.

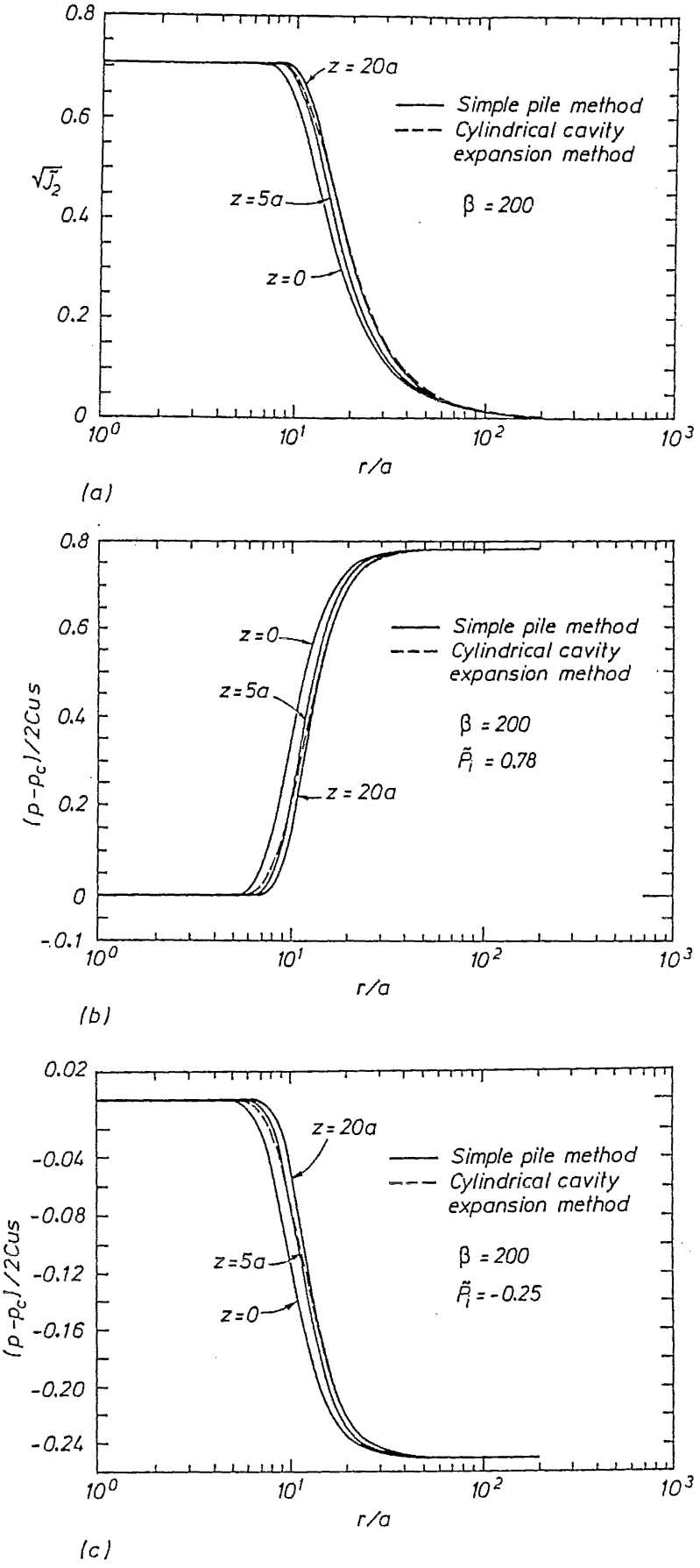

Figure 3.29 Comparison of solutions of the cylindrical cavity expansion method and the simple pile method (a) dimensionless deviatoric stress $\sqrt{\tilde{J}_2}$ (b) dimensionless effective pressure in normally consolidated soil (c) dimensionless effective pressure in overconsolidated soil.

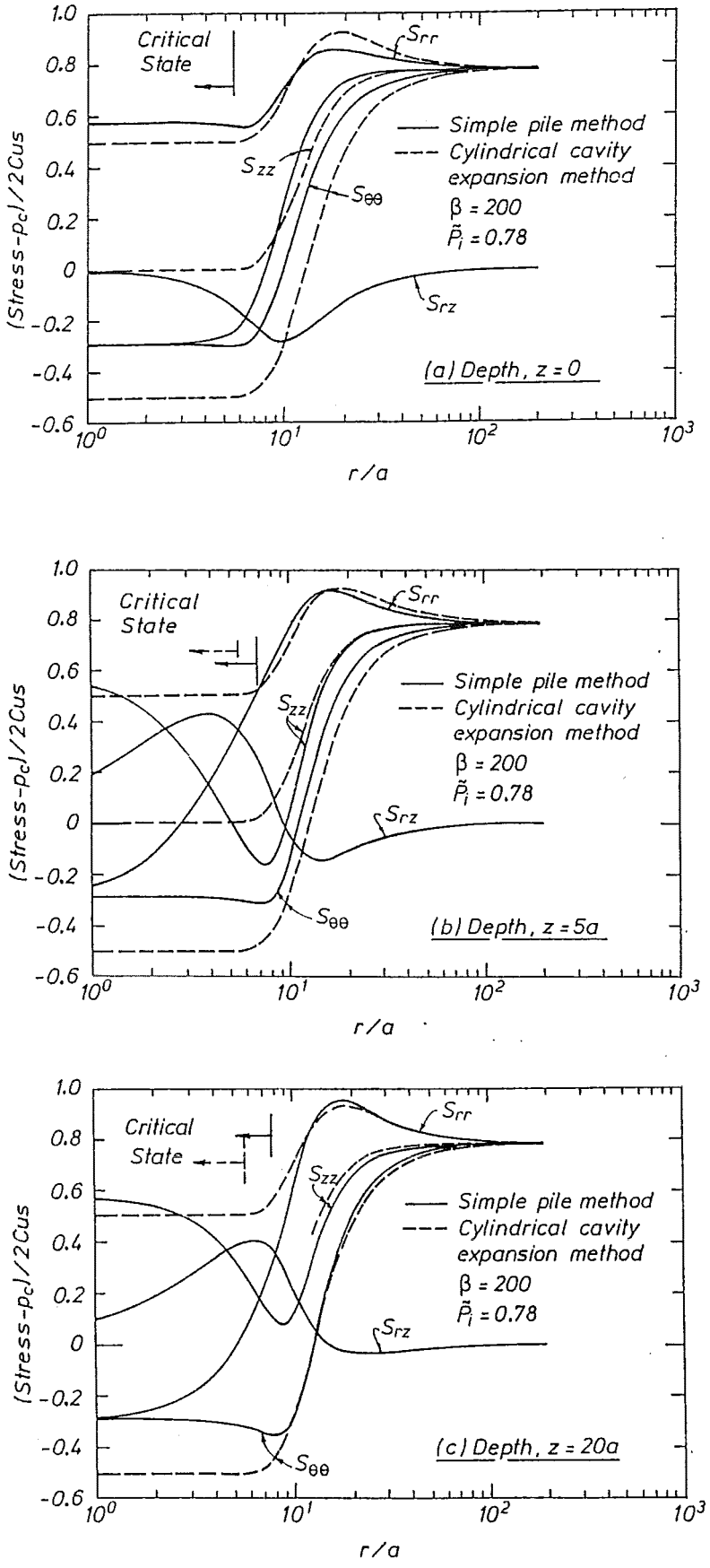

Figure 3.30 Comparison of dimensionless effective stress in normally consolidated Boston Blue clay due to cylindrical cavity expansion and simple pile penetration at depths (a) z= 0 (b) z= 5a and (c) z=20a.

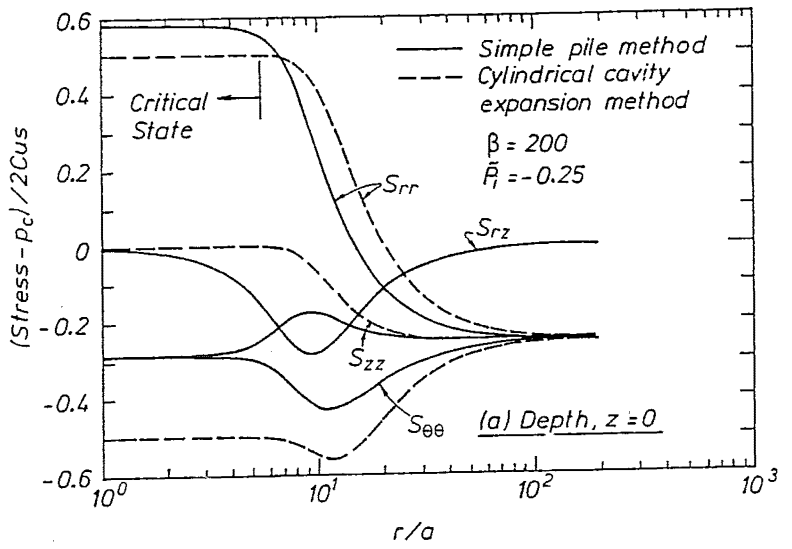

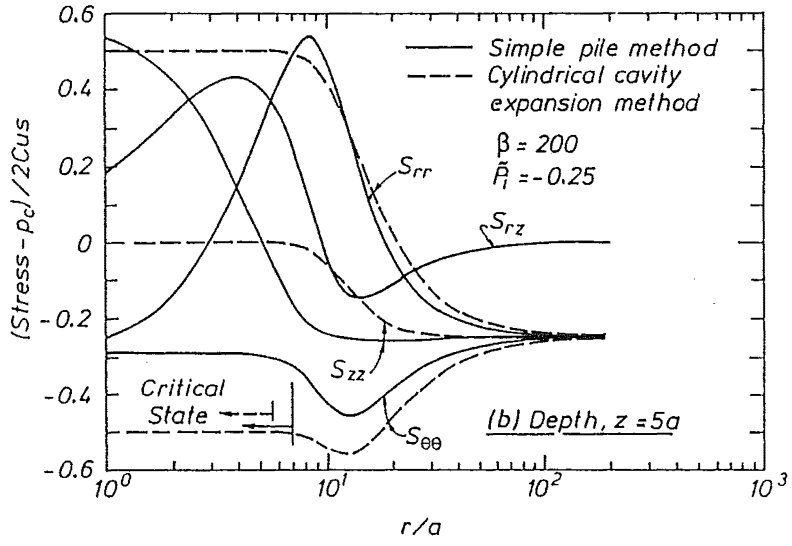

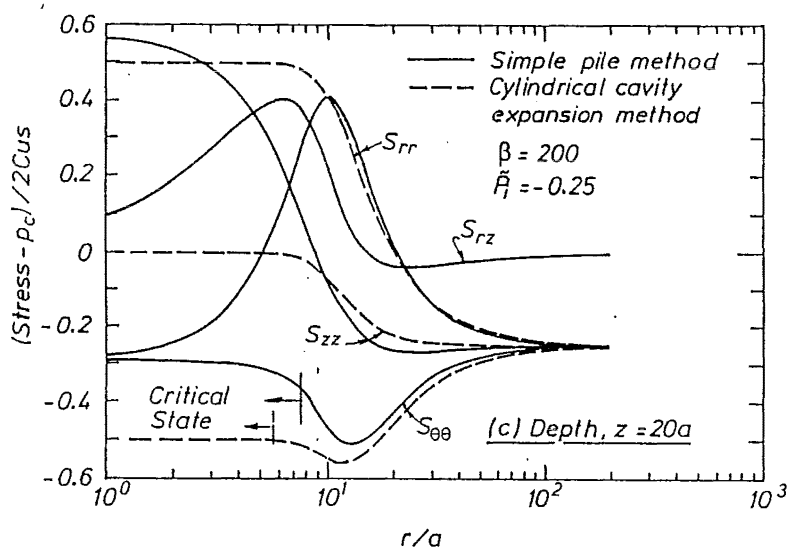

Figure 3.31 Comparison of dimensionless effective stress in overconsolidated soil due to cylindrical cavity expansion and simple pile penetration at depths (a) z= 0 (b) z= 5a and (c) z=20a.

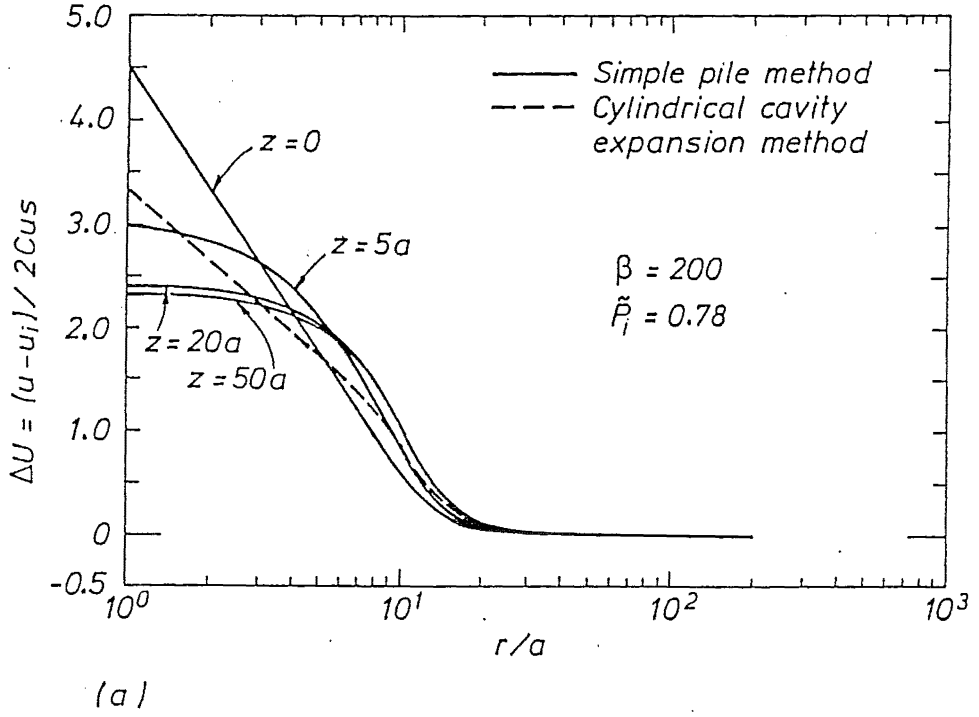

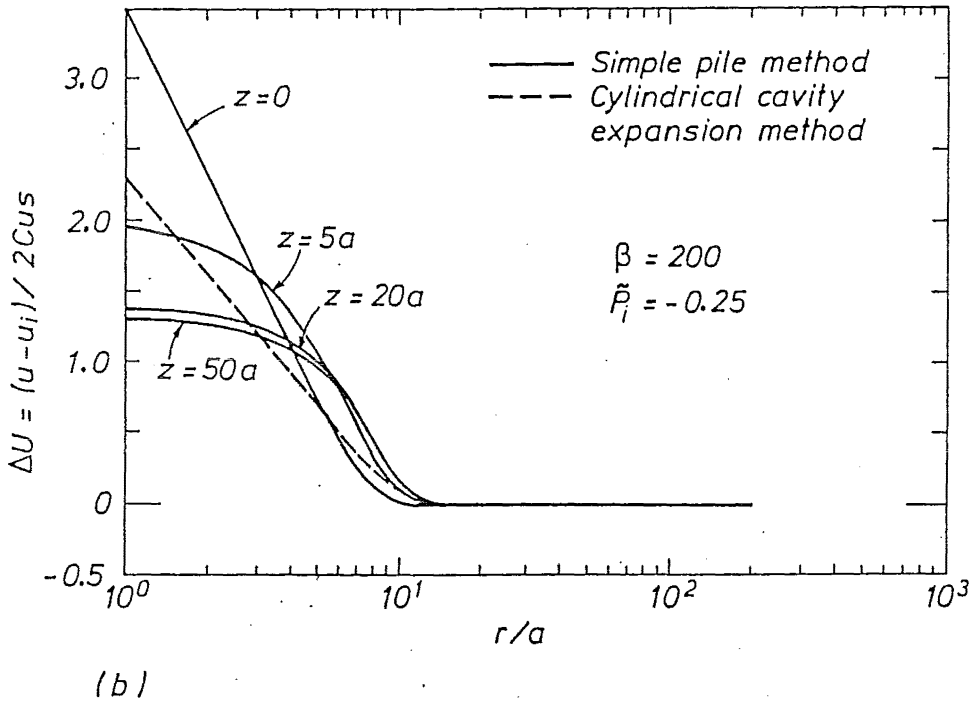

Figure 3.32 Comparison of dimensionless excess pore pressure due to cylindrical cavity expansion and simple pile penetration in (a) normally consolidated Boston Blue clay (b) overconsolidated soil

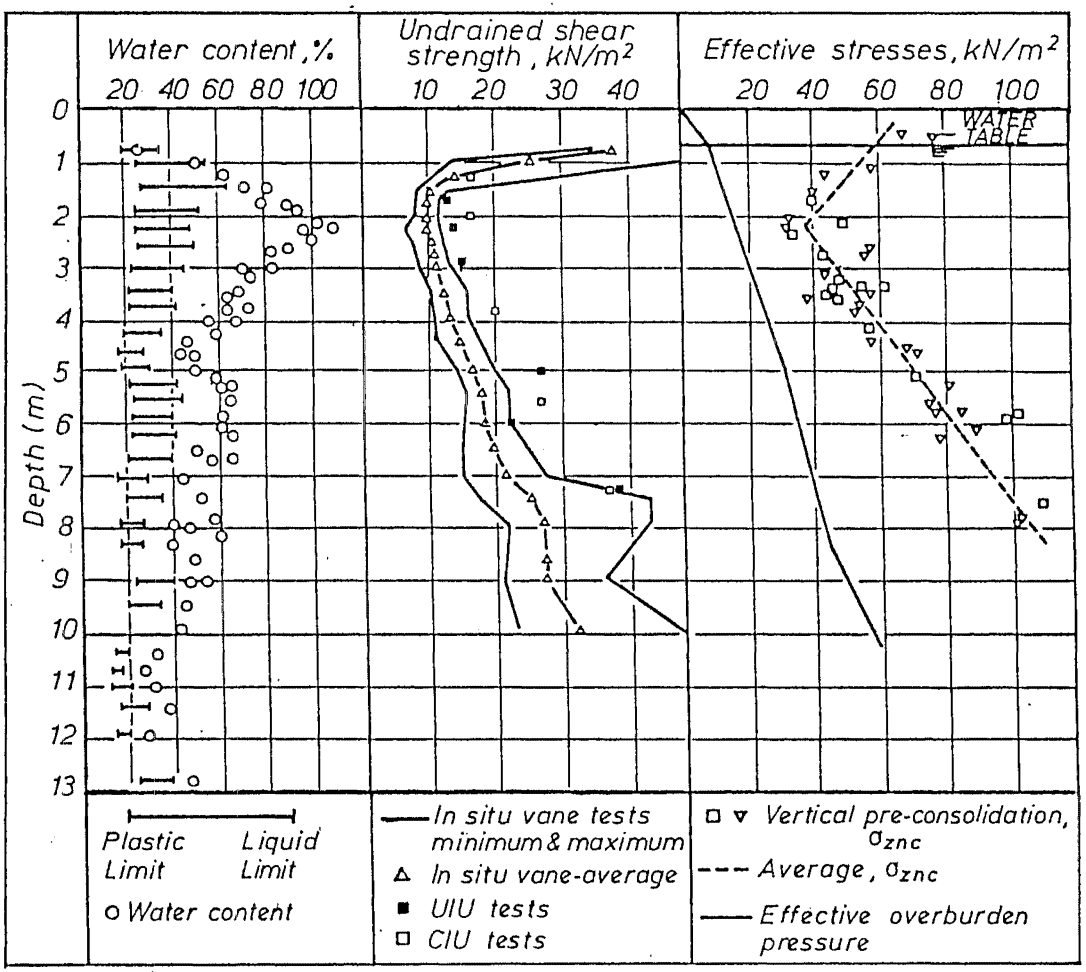

Figure 3.33 Soil profile at the Saint- Ablan test site.

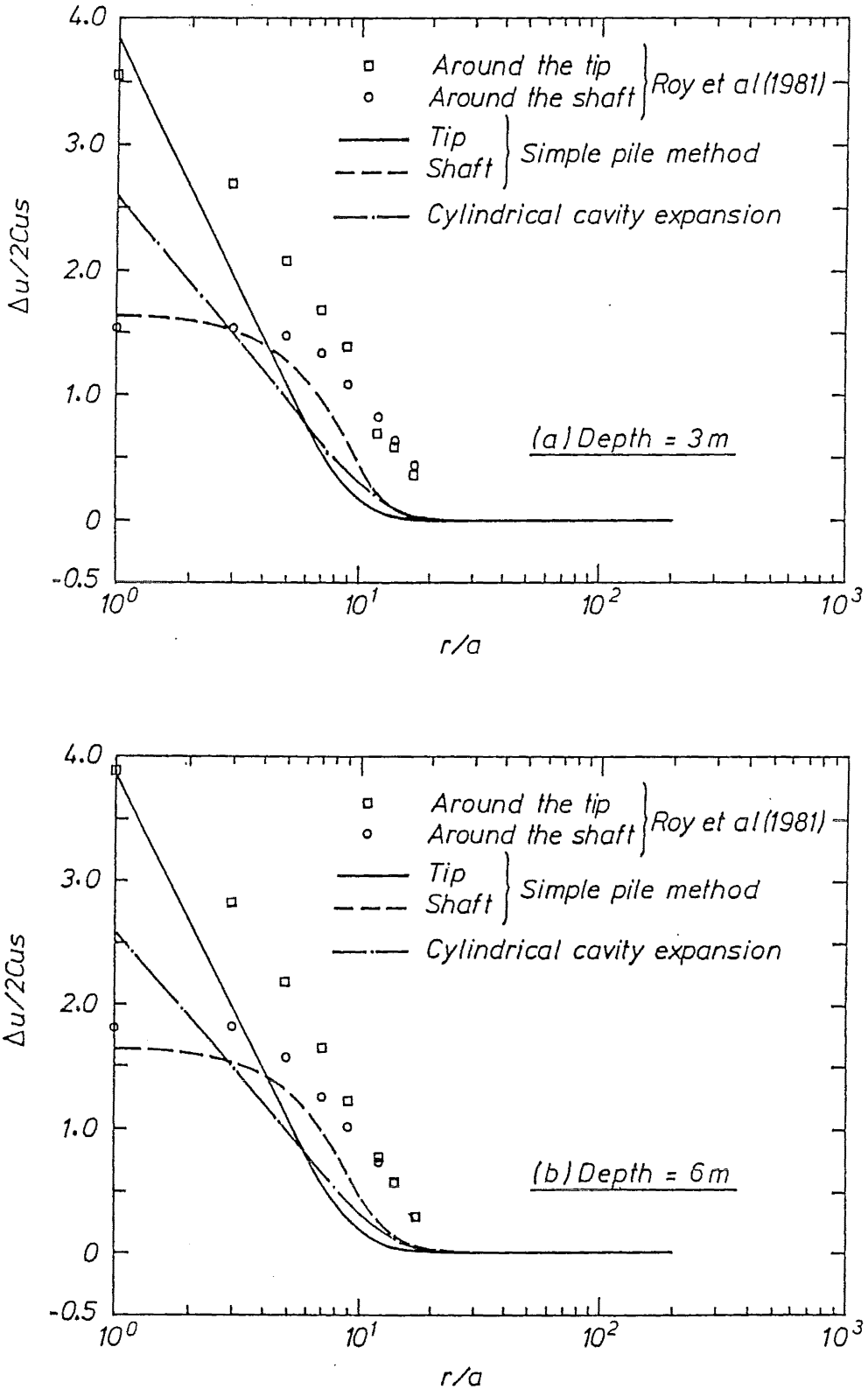

Figure 3.34 Predicted and measured excess pore pressure at depths (a) 3m and (b) 6m, due to pile jacking in Saint-Ablan test site.

CHAPTER FOUR

ONE DIMENSIONAL INFINITE PILE MODEL

In this chapter, a one-dimensional model for the axially loaded elastic pile will be proposed. The pile tip resistance is assumed to be negligible, therefore the pile model is applicable to pile-soil behaviour for a so-called 'floating' pile where no significantly stronger strata lies beneath the tip. Three soil models discussed in chapter two will be used to represent the soils around the pile shaft. The solution method for the problem will be discussed. Even though the pile itself is of finite length, the modelling procedure initially assumes it is infinitely long. Quantities of interest such as load versus displacement response and load diffusion along the pile length are determined by considering a finite segment of the infinite pile shaft.

SECTION 4.1 Relationship Between Shear Traction and Pile Displacement

Recent researchers (Randolph 1977, Ottaviani and Marchetti 1979, Potts and Martins 1982, Nystrom 1984) have employed finite element methods to investigate pile-soil behaviour of axially loaded piles. The finite element method may be used to represent the three dimensional nature of the pile problem, but this method requires complex solution techniques especially for elastro-plastic soils (Nayak and Zienkiewicz 1972). Also required is a large effort on data preparation for computer analysis. Because of these shortcomings, we will not use the finite element method. Instead we assume the pile has infinite length. This assumption reduces the problem to one spatial dimension. From this one dimensional idealization, the induced shear distribution in the surrounding soil due to vertical pile displacement can be easily determined. It follows that the induced shear traction at the pile shaft and the pile displacement response, the so-called t-z curve (Seed and Reese 1957, Coyle and Reese 1966, Kraft et al. 1981), can be determined from the modified Cam-clay model, the bounding surface model, or the rate-type model.

Davis et al. (1984) adopted the cylindrical cavity expansion to simulate pile driving effects, using the rate-type model to represent the soil. At the same time, Mullenger et al. (1984) approached the axially loaded pile problem assuming infinite pile length and a homogeneous stress field with no shear stress initially in the soil. Considering the initial stress conditions corresponding to normally and heavily over consolidated 'undisturbed' clays as well as the stress states of soil after cylindrical cavity expansion, Mullenger et al. (1984) demonstrated that the induced shear traction at the pile shaft due to pile displacement is relatively independent of the initial stress conditions. From Mullenger's work, we note that the vertical pile displacement will only seriously affect the stress state of the soil within approximately one pile radius from the pile shaft. For simplicity, we therefore consider only homogeneous initial stress states surrounding the

pile and assume a pre-existing cylindrical cavity in the "undisturbed" semi-infinite soil mass. The assumption that the surrounding soil is 'undisturbed' with zero shear stress may not be realistic for driven piles, but it does provide a simplified attempt to study the pile load behaviour of the axially loaded pile problem.

In this chapter, we following the used sign convention of soil mechanics and take the z-axis pointing downward, and further assume all soil displacements are vertical so that the only non-vanishing strain is

$$\varepsilon_{rz} = -\frac{1}{2}\frac{\partial u_z}{\partial r} \tag{4.1}$$

where u_z is the vertical component of displacement within the soil at a radial distance r from the pile axis.

If we further assume that the gradient of total vertical stress in the z-direction is equal to the total unit weight of the soil, equilibrium in the z-direction requires that (Butterfield and Bannerjee 1970, Mullenger, et al. 1984)

$$\sigma_{rz} = \frac{a}{r}(\sigma_{rz})_a \tag{4.2}$$

where a denotes the pile radius, and $(\sigma_{rz})_a$ is the induced shear traction at the pile-soil interface. Eq. 4.2 implies that the shear diffusion from the pile shaft to the soil in the radial direction is independent of soil properties. Using the modified Cam clay model, the bounding surface model or the rate-type model, we may construct a relationship of the following form

$$\sigma_{rz} = \chi(\varepsilon_{rz}) \tag{4.3}$$

To arrive at Eq. 4.3 it is necessary to integrate the constitutive equations for the special case where ε_{rz} is the only non-zero strain. Using the rate-type model, analytic expressions for the function $\chi(\varepsilon_{rz})$ of soils with various initial stress conditions were obtained by Mullenger et al. (1984). From their results, it has been verified by Cheung (1985) that the following analytic expressions can provide a sufficient approximation to $\chi(\varepsilon_{rz})$ for the case of one-dimensionally normally to heavily over-consolidated soils. This is given by

$$\varepsilon_{rz} = \frac{1}{2\sqrt{\beta^2 - 1}} \tanh^{-1}\left(\frac{\beta}{\sqrt{\beta^2 - 1}}\frac{\sigma_{rz}}{Cus}\right) \tag{4.4}$$

Here, β and Cus have been assumed constant and are referred to the "undisturbed" state of the soil in r direction. Solutions of Eq. 4.3 using the modified Cam-clay model or the bounding surface model require numerical integration. We have used the Runge-Kutta-Fehlberg method with equal step size (Burden et al. 1981) to carry out the numerical integration. Because of the high resolution power of this method, the accuracy of the numerical solution can be maintained at a high level.

Integration of Eq. 4.1 in the r direction will lead to a relationship between vertical displacement u_z and shear strain ε_{rz} . If that relationship is then used in Eq. 4.3; and further, Eq. 4.2 is used to eliminate σ_{rz} , there results an expression of the form

$$u_z = -\int_{r_m}^{r} 2\,\varepsilon_{rz}\,dr \;=\; \Omega\left[\frac{a}{r}\,(\sigma_{rz})_a\right] \tag{4.5}$$

Also, when r is equal to a, Eq. 4.5 can be expressed as

$$\Delta_a = \Omega[\,(\sigma_{rz})_a\,] \tag{4.6}$$

where Δ_a is the displacement at the pile shaft. Here, r_m is the so-called 'radius of influence'. We assumed u_z is zero at this radius. The pile-soil displacement associated with the idea of Eqs. 4.5 and 4.6 is depicted in Fig. 4.1. For an infinitely long pile embedded in a semi-infinite soil mass, r_m should theoretically be infinity. However, integration of Eq. 4.5 with $r_m = \infty$ leads to infinite displacement. Assuming an elastic soil, Randolph and Wroth (1977) analyzed a finite length pile which was embedded in a semi-infinite soil mass, and compared the results with that of Eq. 4.5. For incompressible soil, they suggested that the radius of influence could be correctly estimated by

$$r_m = 1.25\,L_p\,[\,G(L_p/2)\,/\,G(L_p)\,] \tag{4.7}$$

Here, L_p is the embedded pile length and the shear modulus G is assumed to vary linearly with depth z.

The functional relationship between Δ_a and $(\sigma_{rz})_a$ is the so-called t-z curve. Using Eq. 4.4 of the rate-type model in Eq. 4.5, we may arrive at the following analytic expression

$$u_z = \frac{r\,C_1}{\sqrt{\beta^2 - 1}}\left[\ln\left(\frac{r_m}{r}\right) + \frac{\tanh^{-1}(C_2)}{C_2} - \frac{1}{2}\ln\left(\frac{1 - C_1^2}{1 - C_2^2}\right) - \frac{\tanh^{-1}(C_1)}{C_1}\right] \tag{4.8}$$

where

$$C_1 = \frac{2\,a\,\beta}{r\sqrt{\beta^2 - 1}}\left[\frac{(\sigma_{rz})_a}{2\,Cus}\right]$$
$$C_2 = \frac{r}{r_m}\,C_1 \tag{4.9}$$

The pile shaft displacement Δ_a is also obtained from Eqs. 4.8 and 4.9 by setting r equal to a. We note that Eq. 4.8 is independent of initial stress state. For the modified Cam-clay model and the bounding surface model, numerical integration is required to obtain Eqs. 4.5 or 4.6.

It is noted that Eq. 4.6 may be expressed as a function of depth, z, so that it is possible to consider the load diffusion from the pile into non-homogeneous and layered soils and to predict the load-displacement response of the pile.

SECTION 4.2 Basic Analysis For a Single Floating Pile

We have derived the t-z curve for the infinitely long pile in section 4.1. For pile problems with finite length, we shall consider the pile length to be a segment of the infinitely long idealization.

Consider a cylindrical pile with length L_p, uniform shaft radius a, and loaded with an axial force Q_o at the ground surface, as shown in Fig. 4.2. We assume the pile is acted upon by a field of uniform shear traction $(\sigma_{rz})_a$ around its periphery and that the tip resistance is negligibly small. The surface of the pile shaft is assumed to be rough, implying perfect bonding between pile and soil.

Vertical equilibrium of a small pile element,as shown in Fig. 4.3, is given by

$$\frac{\partial Q_p}{\partial z} = -2 \pi a (\sigma_{rz})_a \tag{4.10}$$

where, Q_p represents the axial load in the pile at depth z . Using Hooke's law, the axial strain in the pile is given by

$$\frac{\partial \Delta_a}{\partial z} = \frac{Q_p}{E_p A_p} \tag{4.11}$$

where

$$A_p = \pi (a^2 - a_i^2) \tag{4.12}$$

in which a_i represents the inside radius if the pile is hollow and A_p is the cross sectional area of the pile Here E_p is Young's modulus of pile material. The pile displacement in Eq. 4.11 can be decomposed into

$$\Delta_a = \Delta_p + \Delta_b \tag{4.13}$$

where Δ_p and Δ_b denote the elastic shortening of the pile at depth z and pile tip displacement respectively. Then Eq. 4.11 becomes

$$\frac{\partial \Delta_p}{\partial z} = \frac{Q_p}{E_p A_p} \tag{4.14}$$

The boundary conditions for a floating pile are

$$Q_p(0) = Q_o \tag{4.15}$$

$$Q_p(L_p) = 0 \tag{4.16}$$

$$\Delta_p(L_p) = 0 \tag{4.17}$$

Once the t-z curve of Eq. 4.6 and the pile tip displacement Δ_b are known, integration of Eqs. 4.10 and 4.14 with the use of Eq. 4.13 will yield

(a) The load diffusion in the pile at any depth.

(b) The shortening of the pile at any depth.

(c) The pile displacement at any depth.

The shear traction acting on the pile shaft can be obtained from inversion of Eq. 4.6.

Eqs. 4.10 and 4.14 must be integrated numerically, even in the case where an analytic representation for Δ_a is available. One method which has been found to be efficient is integrating from the pile tip to the pile head and using Eqs. 4.16 and 4.17 as initial conditions. The constant stiffness method (Zienkiewicz 1977) may be used to evaluate the pile tip displacement Δ_b which may be used to yield a solution Q_p from Eq. 4.10 satisfying the boundary condition of Eq. 4.15.

SECTION 4.3 Summary

In this section, a one dimensional pile model was proposed. The surrounding soil was assumed to be " undisturbed" due to pile driving. The t-z curves for the pile can be obtained for the modified Cam-clay model, the bounding surface model and the rate-type model. We have obtained an analytic expression for the t-z curve using the rate-type model, while the modified Cam-clay model and the bounding surface model require numerical integration. This pile model can be used to analyze the pile-soil behaviour of the finite length floating pile.

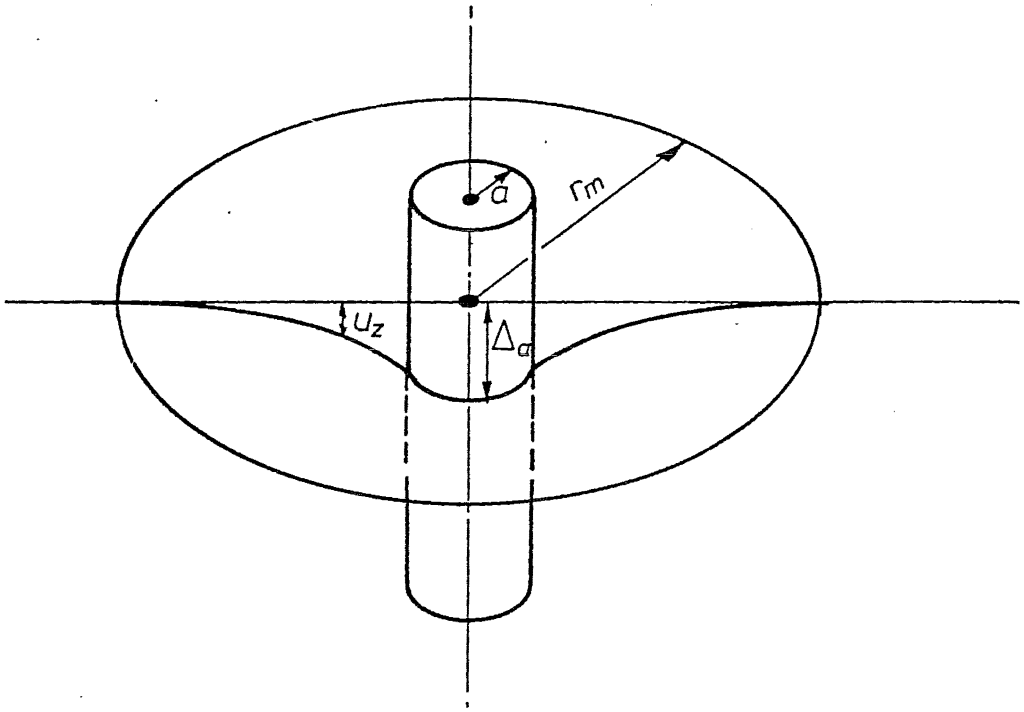

Figure 4.1 Vertical soil displacement in a infinite soil mass.

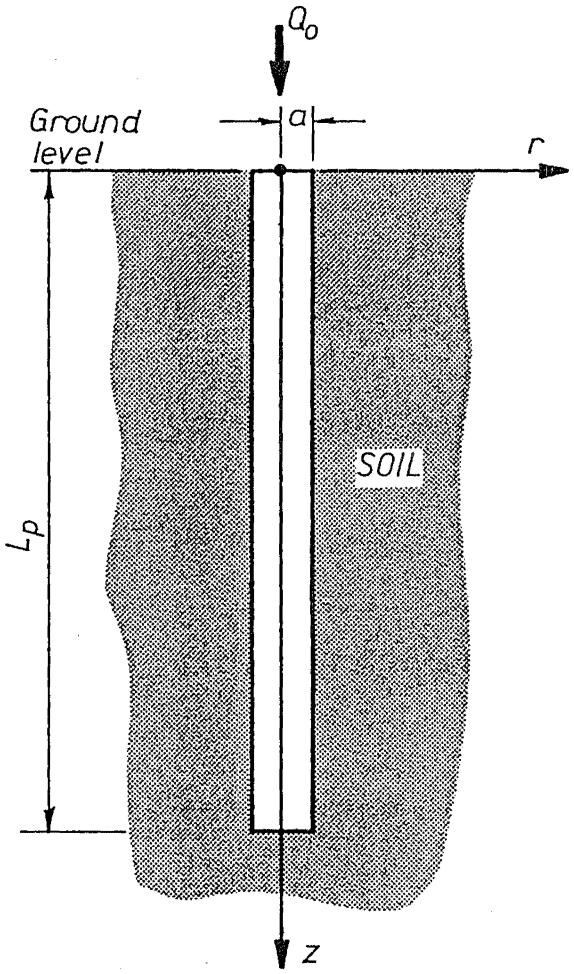

Figure 4.2 An axially loaded pile.

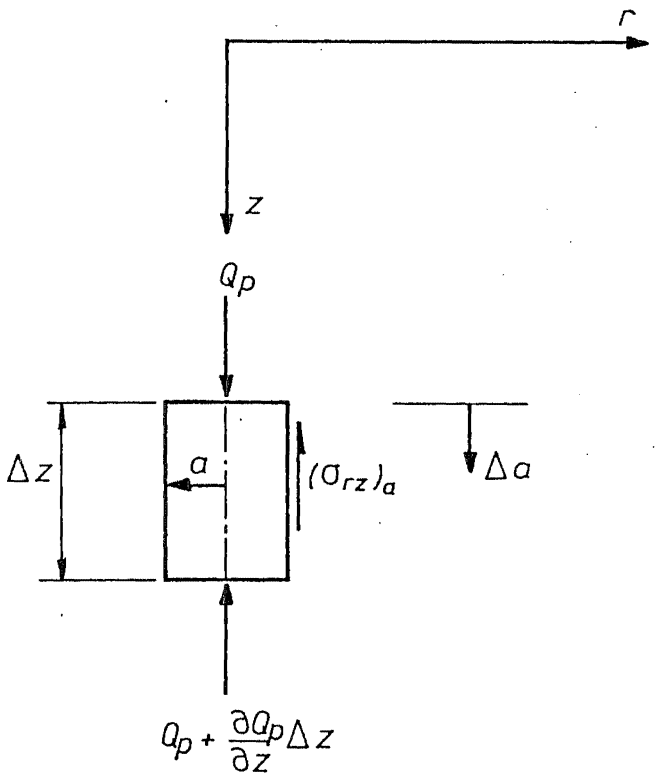

Figure 4.3 Equilibrium of a pile element in vertical direction.

CHAPTER FIVE

VERIFICATION OF THEORETICAL PILE MODEL WITH TEST RESULTS

Three pile tests previously reported in the literature are used for comparison with the model predictions. The first test was carried out at Hendon, in London clay, and was reported by Cooke et al.(1979). The second test was carried out near Houston and described by O'Neill et al. (1982a,b, 1983). In these two pile tests, closed end steel piles were used and were placed in heavily overconsolidated clay deposits. The Houston soil profile included three district strata, whereas the Hendon profile exhibited a more smoothly varying inhomogeneity. In both cases relatively complete descriptions of the soils involved are available, and shear transfer and load-displacement data were obtained during the tests. Since the soils are heavily over-consolidated, only the rate-type model and the bounding surface model will be used to describe the soil response. The third pile test (Cox et al. 1979 & Kraft et al. 1981) involved a open-ended steel pile driven into a relatively uniform lightly overconsolidated soil. All three soil models can be used to represent the soil response. However, only the t-z curves and the load-displacement relationships during these tests are available for our comparisons.

SECTION 5.1 Hendon Test Site

5.1.1. General Description

The pile test reported by Cooke et al. (1979) was carried out at Hendon, North London. London clay at this test site extends from the ground surface to a depth of 30m. The clay is heavily overconsolidated. Properties for this soil are available from several sources (Cooke et al. 1979, Windle and Wroth 1977, Marsland and Randolph 1977). The liquid limit and the plastic limit lie in the range 60-80 and 25-30, respectively. The water content is found to be approximately equal to the plastic limit. Observations at the site indicate that the free standing water table is located 0.75 to 1.0m below the ground surface. The bulk unit weight is approximately equal to 19kN/m^3.

Three 168mm diameter closed-end steel pipe piles were used in this test. The pile wall thickness is 6.4mm. Young's modulus of the pile material is approximately equal to 2.1×10^8 kN/m^2. The piles were jacked into London clay up to a depth of 4.6m. The first pile (pile "A") was load tested up to 80% of installation load, ten weeks after its installation. During the loading test, soil displacement and shear stress transfer along the pile shaft were recorded. After completion of the load test on pile A, the second and third test piles ("B" and "C") were then installed 500mm on each side of pile A. After 18 months following the installation of pile C, piles B and C were load tested to failure. The load-displacement curves of these two piles were also reported.

5.1.2 Soil Properties

Shown in Table 5.1 is the effective angle of friction at critical state for London clay. The slopes of isotropic consolidation and swelling lines λ and κ also shown are taken from Schofield and Wroth(1968). All these data are obtained for remoulded London clay, and will be used for the model predictions in our later discussion.

The undrained shear strength, Cu, profile for the test site is shown in Fig. 5.1. The measured data are obtained from tests of 98mm diameter soil specimens by Cooke et al. (1979) and by Marsland and Randolph (1977). Fig. 5.1 suggests that Cu increases linearly from about 35kN/m^2 at the surface to about 90kN/m^2 at a depth of 6m.

Fig. 5.2 shows the measured shear modulus for this test site. Two sets of data have been shown. The first set of data are measured below a depth of 6m by Marsland and Randolph (1977) by means of 865mm diameter plate bearing test. The tangent and secant shear modulus were also measured. We have extrapolated these results to the top 6m in Fig. 5.2. The second set of data are available from Windle and Wroth (1977). They conducted self-boring pressuremeter tests at the test site and evaluated the shear modulus from the initial slope of the measured pressure vs. radial strain curve. Fig. 5.2 indicated that despite the anisotropic nature of this clay, Windle's results agree closely with the results of secant shear modulus obtained from the plate bearing test.

Finally, the measured coefficient of lateral pressure at rest, K_{oc}, available from Windle and Wroth is shown in Fig. 5.3. The values of K_{oc} were calculated based on the measured pressure at which the membrane of the pressuremeter starts to expand radially. These values range from 1.5 to 3.0, indicating that the soil is heavily overconsolidated.

5.1.3 Pile Test Results

The first test pile (pile A) was load tested up to 65kN, about 80% of its installation load, or about 55% of its ultimate load carrying capacity, about ten weeks after installation. The measured shear stress transfer and load diffusion along the pile shaft at different loading stages are shown in Figs. 5.4 and 5.5.

Figs. 5.6 shows the measured soil displacements for the applied load equal to 20 and 60kN. The displacements are measured at depths 0.45, 1.87, 3.16 and 4.34m by means of inclinometers installed horizontally in the radial direction of the pile.

Fig. 5.7 is the measured t-z curve at the working load. We construct these t-z curves based on the measured shear transfer and pile shaft displacement available from Cooke et al.(1979). However, since the pile was not loaded to failure, the complete t-z curve for this test is not known.

Finally, we have shown in Fig. 5.8 the load-displacement response of the second and third test piles B and C. These two piles were installed after finishing the loading test of pile A. Also these two piles were load tested until failure, 18 months after installation.

5.1.4 Model Prediction

(i) In Situ Stress Conditions

Table 5.2 summarizes the values of effective overburden stress σ_{zi}, coefficient of lateral earth pressure at rest K_{oc}, and overconsolidation ratio $\overline{OCR}$ for the top 4.6m for the Hendon site. The selected values of K_{oc}, are also compared with measure data in Fig. 5.3. The values of $\overline{OCR}$ are determined based on Eqs. 2.57 and 2.58.

(ii) Undrained Shear Strength

Predicted values of undrained shear strength, Cu, are compared with measured values in Fig. 5.1. We obtained these values from Eqs. 2.52 and 2.64 of the bounding surface model by assuming R equal to 2 and using the data available from Tables 5.1 and 5.2. Average values of Cu were used over 1.0m interval giving the block-like distribution shown in Fig. 5.1. Comparison of these values with measured results in Fig. 5.1 indicates that the predicted Cu profile agrees closely with the measured data.

We will not use the rate-type model to predict the undrained shear strength profile in this chapter, because the predicted t-z curve, Eq. 4.8, of the rate-type model requires only two soil parameters, Cus and G, and also these two parameters can be easily determined from measured test results. However, we will adopt the predicted Cu values of the bounding surface model to evaluate the parameter Cus for the rate-type model to provide a consistent comparison with the bounding surface model.

(iii) Shear Modulus

Fig. 5.2 also shows the selected shear modulus profile for the top 5m at the Hendon site. These selected values will be adopted for our later model prediction. From Fig. 5.2, we note that the selected G values are higher than those resulting from the pressuremeter tests, but the selected values are lower than those extrapolated from results of plate bearing tests.

(iv) Model Parameters

Table 5.3 summarizes the model parameters required for the rate-type model while the initial value of J_0 required by the bounding surface model is summarized in Table 5.2. J_0 is calculated from Eqs. 2.64 and 2.65. To evaluate the model parameters for the bounding surface model, we have assumed that the effective angle of friction ϕ is approximately the same in both triaxial compression and extension conditions; this gives n approximately equal to 0.8 but we have assumed that $t_e=t_c$ for simplicity.

It would be possible to evaluate the remaining bounding surface model parameters A_c and t_c from the predicted and measured t-z curve. However, the complete t-z curve of this test is not known, (only the t-z curves at low stress level is given). We therefore evaluated these two parameters by

fitting the model response to agree with the rate-type model. We selected that A_c and t_c equal to 0.05 and 180 respectively. The shear stress and strain response of the two models are illustrated in Fig. 5.9. The responses predicted from both models are basically similar at low stress level as expected, but rate-type model predicts a higher failure strength. This is because the inherent assumption of strength isotropy for the rate-type model.

(v) Radius of Influence

The expression for the radius of influence given in Eq. 4.7 will be examined here. Observing Figs. 5.6 of the measured soil displacement, it is interesting to find that the radius of influence, r_m, at varies depths is approximately the same. This suggests that it may be appropriate to assume that the radius of influence is constant throughout the pile depth. Also, we have found that the radius of influence only slightly increased, by about four pile radii, when the applied load increased from 20 to 60kN.

From our selected shear modulus profile, Fig. 5.2, the ratio of $G(L_p/2)$ to $G(L_p)$ is 0.65, which gives r_m=45a. However, the measured soil displacements vanish at about r=22a. This suggests that the use of the radius of influence evaluated from Eq. 4.7 will result in overestimating the soil displacement in regions remote from the pile shaft in this case. Using the measured shear transfer along the pile shaft given in Fig. 5.5 and r_m=45a, a trial analysis was carried out. It was found that the calculated soil displacement using Eq. 4.5 obtained from both models only overestimated the pile shaft displacement about 20%, but highly overestimated the displacement in the surrounding soil. For this reason, we will adopt a more appropriate value of r_m=25a.

(vi) Prediction of Shear Transfer and Soil Displacement

Figs 5.6 and 5.7 show the comparisons between calculated and measured results. Eqs. 4.5, 4.6 and 4.8 were used to obtain the soil displacement shown in Figs. 5.6, and the calculated t-z curves of Fig. 5.7 for both soil models. In Figs. 5.6, because the soil displacement and the induced shear stress on the shaft are measured at working load conditions (less than 50% of the ultimate pile capacity) and mainly within the elastic range, both soil models predicted basically similar results and thus only one line will be shown. Comparisons of theoretical solutions with measured results in Figs. 5.6 and 5.7 indicate that

(a) For soils above 2m and at low stress levels, reasonable agreement between the predicted and measured displacement at the pile shaft was obtained. The soil displacements outside r=2a were generally overestimated; resulting from underestimation of the shear modulus at these shallow depths.

(b) Below a depth of 3m, good matching between the predicted and measured displacements was found.

(c) The rate-type model predicted an abrupt failure point in the calculated t-z curves. The failure points are marked (f). Once the failure point is reached the shear transfer remains constant as the pile shaft displacement increases.

(d) The predicted shear transfer and pile shaft displacement response from both soil models are essentially linear up to 75% of the maximum shear transfer. They compared favourably with the measured t-z curves at low stress level.

An examination of these results suggests that, at a greater depth, after pile installation and completion of reconsolidation, the soil shear modulus probably returns to a value close to its original value, perhaps with the exception of the region within 1 or 2 pile radius of the pile shaft. Therefore assuming a constant shear modulus in the radial direction for a jacked pile may be valid.

On the other hand, for soils at shallow depths, perhaps because of relatively low confining pressure and dilatancy due to overconsolidated soils, the pile installation process probably causes excessive disturbance or possibly with cracks occurring in the soil in a region close to the pile. This may results in a significant reduction in soil shear modulus. We have used Eq. 4.8 of the rate-type model to calculate the soil displacement which matches the measured soil displacement outside r=7a for soils at depths of 0.45 and 1.87m. It was found that a G value approximately equal to 30MN/m^2 is required. This value is close to the tangent modulus obtained from the plate-bearing tests. This suggests that reduction of shear modulus due to pile installation at shallow depths is more severe than that at greater depths.

(vii) Prediction of Load Diffusion and Shear Transfer along the Pile

The predicted load diffusion and shear transfer along the pile are compared with measured results in Figs. 5.4 and 5.5. The theoretical solutions are obtained from Eqs. 4.6, 4.10 and 4.14. The predicted results from both soil models are essentially the same, therefore only one line will be shown. The eight pairs of curves shown in these figures represent values at different increasing applied loads. From Figs.5.4 and 5.5, we note that

(a) In the range of working load, the tip resistance is less than 10% of the applied load.
(b) Good agreement between predicted and measured load diffusion and shear transfer were obtained up to about half the ultimate load.

From these results, we conclude that within the range of the working load, the tip resistance may be ignored and reliable results still be obtained. In spite of the simplicity of our one-dimensional pile model and the assumption of initial stress state corresponds to "undisturbed" clay, reasonable simulation of load transfer in the range of the working load is clearly possible. Finally, despite the reduction in shear modulus caused by pile installation at the top 2m of the soil, the measured shear transfer throughout the pile depth suggests that sufficient bonding between pile and soil has been developed, at least up to 50% of the ultimate load.

(viii) Prediction of Pile Load and Displacement Response

Illustrated in Fig. 5.8 are the predicted and measured pile load vs. head displacement response. These results indicate that the rate-type model predicts abrupt failure in the load-displacement curves. The load-displacement curve remains relatively linear nearly to the ultimate load. When the failure point is reached, the curve becomes horizontal immediately. The failure points are marked (f) in Figs. 5.8. The predicted results from both models exhibit only slight differences at high stress levels. The theoretical pile model correctly predicts the pile load and displacement response up to about 70% of the ultimate load. Both models slightly over-predict the ultimate load of the test pile, possibly because limiting skin friction has not been considered in the theoretical pile model. In general, measurements show that when approaching the ultimate load, the mobilized tip resistance will increase rapidly (see for example: Brand and Juta-Sirivmgse 1972, Vesic 1977).In this comparison we have ignored the tip resistance but this evidently results in the predicted ultimate load coming quite close to the measured ultimate load.

SECTION 5.2 Houston Test Site

5.2.1 General Description

Test results and soil descriptions are available from O'Neill et al. (1982 a, b), O'Neill (1983) and Heydinger and O'Neill (1986). The test involved a closely driven pile group, and two driven and separately tested single piles. The piles are closed-end steel pipe with 273mm outside diameter and 9.3mm wall thickness. All piles are driven through heavily overconsolidated clays and into a sandy clay. 200mm diameter and 3m deep pilot holes were drilled prior to driving the piles. The embedded length of all piles was 13.1m. In this study, we will consider the results reported for the single piles.

5.2.2 Site Description and Soil Properties

The Houston test site was composed of three distinct strata. The soils in these three strata are insensitive.Soil properties are summarized in Table 5.4. The measured undrained shear strength profile is shown in Fig. 5.10. The undrained shear strengths are measured by means of undrained triaxial tests and pressuremeter tests, while the shear modulii shown in Table 5.4 are evaluated from the pressuremeter test results. The angle of friction for these soils shown in Table. 5.4 are measured from the peak strength of the samples. The soils in strata B and C exhibited little effective cohesion and possibly reached the critical state, therefore the measured angle of friction may refer to the value at a critical state. The soil in stratum A shows an effective cohesion approximately equal to 20% of the measured shear strength and the soil may not be sheared to its critical state. Because the angle of effective friction of this soil at critical state is not available, we thus will adopted the reported value in our later calculation.

Strata A and B are very stiff, saturated heavily overconsolidated Beaumant clays. The free standing water table was located about 2m below the ground surface. The plastic limit and liquid limit for stratum A are approximately equal to 10 - 15 and 35 - 50 respectively, while the plastic limit and liquid limit for stratum B are roughly 15 -25 and 50-70 respectively. The water content of these soils has been found to be about 2-8% higher than the plastic limit.

At the top of stratum C, a 1.5m thick layer of silty clay with relatively low shear strength, as shown in Fig. 5.10, has been reported. Below this lies a very stiff sandy clay. The sand content increases from 15% to 40% moving from top to bottom of this stratum. Since no available soil properties for this silty clay have been reported, we will ignore the silty clay and consider that stratum C is composed of stiff sandy clay only. However, the existence of the silt layer does affect the measured pile shaft capacity in the region close to this layer, and thus will be discussed in a later section. The plastic limit and liquid limit of the sandy clay are 10-20 and 28-33 respectively, while the water content is close to the plastic limit.

5.2.3 Pile Test Results

Fig. 5.11 shows the load-displacement response of the test piles. The load-displacement response is taken from the combined data of two single piles during loading tests. Two response curves are shown in Fig. 5.11. The response curve exhibiting the lower load capacity is taken from the pile test (test 1) which was carried out 18 days after pile installation. The second curve is also obtained from these two piles, but from a later test (test 2) carried out 90 days after completion of test 1, (or 108 days after installation).

The load diffusion and shear transfer along the pile at working load, 273KN, are shown in Figs. 5.12 and 5.13, respectively. These reported results were obtained from test 1. The shear transfer measured when the pile plunged to failure, and the maximum shear transfer adjacent to pile occurring at various loading stages, are shown in Fig 5.14. It should be noted that the residual stress which occurs at the pile-soil interface has been excluded from the test results that we have summarized in this section.

Finally, illustrated in Figs. 5.15 are the measured t-z curves for stratum A to C at depths 1.5, 4.5 and 11.5m below the ground surface. These curves were obtained from test 1.

5.2.4 Model Predictions

(i) Prediction of Undrained Shear Strength

Summarized in Table 5.5 are the selected soil parameters for the Houston soils. The ratio $n=N_e/N_c$ is evaluated based on the assumption that the effective angle of friction ϕ is approximately the same in both triaxial compression and extension conditions.

The unit weight of the test site soil was 20.1 $\pm$0.8kN/m^3 and relationships for K_{oc} and $\overline{OCR}$ were reported as

$$K_{oc} = 3.5z^{-0.55}$$
$$\overline{OCR} = 16.0z^{-0.55}$$

for depths z in excess of 3m. Using Eq. 2.64 and assuming the parameter R = 2, the predicted undrained shear strength is directly compared with experimental values in Fig.5.10. Measured strengths seemed to agree well with calculated values except in stratum A. The relatively high measured strength in stratum A is possibly due to drying of the surface soils.

(ii) Model Parameters

The model parameters prepared for the rate-type and the bounding surface models are summarized in Table 5.6. In this section, we maintained the assumption $t_e=t_c$,similar to that discussed in section 5.1.4, for the bounding surface model. We evaluated the parameters A_c and t_c by adjusting the response curve which will later give a close simulation to the measured t-z curve and by comparing its response with that of the rate-type model. Using data in Tables 5.5 and 5.6, the

shear stress and strain response at three selected depths, 1.5, 4.5 and 11.5m, where the t-z curves are measured, for both models.are illustrated in Figs. 5.16. From these results, we note that the rate-type model provides relatively stiff response compared with the bounding surface model. The rate-type model predicts that the stress state arrives at the critical state at very low strain levels, while the bounding surface model predicts the stress state approaches the critical state at relatively high strain levels.

(iii) Prediction of Shaft Displacement and Shear Transfer

Before we establish the shaft displacement and shear transfer curves from the soil models, it is necessary to reexamine the radius of influence of Eq. 4.7 for this pile test. We will assume that the radius of influence is constant throughout the pile depth. Using Eq. 4.7 and the ratio $G(L_p/2)/G(L_p)$ equals 0.61, and the radius of influence is given by r_m=10m or 75a. No measurements of soil displacement during these tests has been reported, however O'Neill (1982b) has measured displacements around a pile group during loading tests at this test site. These results suggest that the soil displacement during the loading test may vanish at a distance about 6-7m from the edge of the pile group. Since the size of the pile group is significantly larger than the radius of the single pile, we estimate that the radius of influence for a single pile in this soil may not be larger than r_m = 6m or r_m=45a. Therefore, r_m=45a will be used in establishing the t-z curves from the soil models.

Shown in Figs. 5.15 are the shear transfer and shaft displacement responses predicted from the two soil models. These theoretical solutions are also directly compared with measured results at depths 1.5, 4.5 and 11.5m. Comparing these results, we note that

(a) All theoretical solutions significantly overestimate the maximum shear transfer at the pile shaft,except at depth 4.5m for soils in stratum B.
(b) The rate-type model gives better predictions at low stress levels than does the bounding surface model.
(c) The bounding surface model provides a smooth transition from the initial loading state to the ultimate stress state, while an abruptly failure point is predicted by the rate-type model.

From the measure t-z curve at depth 1.5m, a significant degradation of shear transfer is apparent as the shaft displacement increases after the peak shear transfer. This probably suggests slipping between pile and soil occurs at this depth. Contrary to this, the measured t-z curves at greater depths indicate no significant degradation in shear transfer after the peak was reached. This observation may imply that the soils at a greater depth were strained to a state close to the critical state so that large deformation could not cause significant reductions in shear transfer.

The theoretical shear transfer and pile displacement at depths 4.5 and 11.5m can be improved to give a closer fit to the measured t-z curves by doubling in-situ measured value of the shear modulus. This probably implies that the pressuremeter test underestimated the in-situ soil modulus for these soils.

A trial calculation with increased radius of influence from r_m=45a to r_m=75a only increased by 15% the predicted shaft displacement at the same shear stress level. This suggests that Eq. 4.7 giving the radius of influence proposed by Randolph and Worth (1977), remains a valid approximation for soil displacement calculations at the pile shaft.

The overestimation of maximum shear transfer at the pile shaft results mainly due to the fact that we assumed the soil is undisturbed. Therefore effects in the soil due to pile installation and subsequent consolidation have not been incorporated in our one-dimensional pile model.

(iv) Prediction of Pile Load and Displacement Response

Illustrated in Fig. 5.11 are comparisons of theoretical solutions of pile load and displacement response with measured test results.

The theoretical solutions resulting from both models again show only slight differences at high stress levels. The theoretical solutions compare favourably with test results obtained from test 2 (tested 108 days after pile installation), while significantly overestimating the ultimate load measured from test 1.

Surprisingly, in spite of the simple assumptions of our theoretical model, without considering the actual three-dimensional pile-soil system, the theoretical solutions correctly predicted the pile load and displacement relationship up about 80% of the ultimate load measured from the pile tests. Further, the bounding surface model predicted the ultimate load quite closely.

(v) Prediction of Load Diffusion and Shear Transfer

The load diffusion and shear transfer along the pile predicted from both soils models and the measured values of test 1 at working load, 273kN, will be compared. The theoretical solutions are also shown in Figs. 5.12 and 5.13. Clearly, these results obtained from both soil models show quite good agreement with measured data.

Comparison of predicted maximum shear transfer from the bounding surface model with the measured maximum shear transfer adjacent to the pile shaft at various loading stages and the measured shear transfer when pile plunged to failure are shown in Fig. 5.14. This result indicates that the bounding surface model predicts reasonable maximum shear transfer along the pile from stratum A and B. Over prediction of the pile shaft capacity mainly comes from overestimation of maximum shear transfer within stratum C. Nevertheless, the overall results appear to be reasonbly good.

SECTION 5.3 Empire Test Site

5.3.1. General Description

In this section, the test results from a 35.6cm (14in) diameter open-ended steel pipe pile will be compared with model prediction. The wall thickness of this pile was 9.5mm (0.375in). The pile test was conducted at a site one mile south of Empire, Louisiana. At this site, the lightly overconsolidated plastic Empire clay extends from a depth of 30m to 54m, (zone 1), below the ground surface. The pile was driven into this clay and embedded between depth 35 to 50.3m. The pile was tested 7 days after installation. The test results and site description are available from several sources (Cox, et al. 1979, Kraft, et al. 1981, Heydinger and O'Neill 1986, Azzonz and Lutz 1986). The t-z curves and the pile load-displacement response are available for later comparisons.

5.3.2 Soil Properties

Summarized in Table 5.7 are soil properties for the Empire clay. These data are available from Kraft et al. (1981), and from Azzonz and Lutz (1986). The plastic limit and liquid limit of this clay are found to be 20-27 and 80-100, respectively. The water content ranges between 40 and 50%.

Based on measured total unit weight and static pore pressure, the effective overburden pressure has been found to increase linearly from 150kN/m^2 at a depth 33.5m to 260kN/m^2 at 50.3m.

Fig. 5.17 shows the undrained shear strength of the clay obtained by different methods (Azzonz and Lutz 1986). Both results of unconsolidated-undrained (UU) and vane tests exhibit significant scatter, without a clear trend with depth, while the SHANSEP DSS (Direct simple shear) strength profile (Ladd and Foott 1974) exhibits a clear trend that the undrained strength increases with depth.

5.3.3 Pile Test Results

Figs. 5.18 shows the t-z curves measured during pile testing. These two curves represent the average shear transfer and shaft displacement relationship over the pile sections 40 to 45.75m and 45.75 to 50.33m, respectively. These two curves are reproduced from Heydinger and O'Neill (1986). Kraft et al. (1981) analyzed stress-strain curves for Empire clay from simple shear tests, reporting that this clay exhibits some strain softening behaviour. However, the strain softening behaviour that may occur in the measured t-z curves has probably been ignored by Heydinger and O'Neill in their work.

Fig 5.19 shows the load-displacement response during the compression testing. This measured result may involve 15% error due to malfunction in the data logging device (Kraft, et al. 1981). This result indicates a slight amount of strain-softening behaviour.

5.3.4 Model Prediction

(i) Predicted Undrained Shear Strength

The predicted values of Cu are shown and compared with test results in Fig. 5.17. These values are evaluated from Eq. 2.64 for the bounding surface model, using soil properties given in Table 5.7 and the effective overburden pressure given in section 5.3.2. The parameter R in Eq. 2.57 has been chosen to be 2.75 while the $\overline{OCR}$ value has been taken to be 1.3 instead of the measured $\overline{OCR}$ value 1.7, in order to provide a more reasonable strength profile when compared with the SHANSEP strength profile.

(ii) Selected Shear Modulus Profile and Radius of Influence

Since the shear modulus profile of this site is not found from available engineering literature, we therefore will assume that the rigidity index $\beta = G/Cus$ is taken to be 150 throughout the soil layer. This assumption may be reasonable for the lightly overconsolidated plastic clay. Based on this assumption and the predicted Cu profile, (Fig. 5.17), the calculated G profile is summarized in Table 5.8.

Finally, the radius of influence is calculated to be $r_m=85a$ which is obtained from Eq. 4.7 and from the assumed shear modulus profile given in Table 5.8.

(iii) Model Parameters

Summarized in Table 5.8 are the model parameters required for the rate type model and for the bounding surface model. In our calculations, we will use the parameters $N_e=0.75N_c$, $t_e=t_c$ and $t_c=230$ for the bounding surface model. Additional parameters for this model have been given in Table 5.7.

From Eq. 2.64, we find that the initial stress state of the Empire clay is located on the 'wet' side of the critical state. We, therefore, will also use the modified Cam-clay model in this comparison. Further, we will assume the yield surface of the modified Cam-clay model has the same form as the elliptical bounding surface, Eq. 2.29, of the bounding surface model, so that the stress parameters given in Table 5.8 are identical for both the modified Cam-clay and bounding surface models.

Figs. 5.20 shows the shear stress and strain response of all three soil models the pile at two selected depths 42.5m and 48.5m. Both the rate-type model and the bounding surface model provide smooth responses but the modified Cam-clay model predicts a distinguishable yield point at around 0.5% shear strain. Also, the rate-type and modified Cam-clay models should predict identical maximum shear stresses, but the modified Cam-clay predicts the stress state approaching the critical state at very large strain (about 15%).

(iv) Prediction of Shaft Displacement and Shear Transfer Response

Figs. 5.18 shows the comparisons between the measured and predicted t-z curves from all three soil models for soils at depths of 42.5m and 48m. From results in Figs. 5.18, we note that all three models predict reasonable agreement with measured results, except the rate-type model and the modified Cam-clay model overestimate the shear transfer by 20-35% at large displacements

In this comparison, response of the rate-type model and the modified Cam-clay model come quite close together, while the bounding surface model predicts remarkable good results especially for soils at the greater depth, 48.5m.

(v) Prediction of Pile Load and Displacement Response

Fig. 5.19 shows the comparison between the measured and predicted pile load and displacement response from all three soil models. All models predicted reasonable ultimate pile load carrying capacity when compared with the measured peak capacity. Since the measured pile load-displacement response curve exhibits strain softening behaviour after the peak capacity was reached, it is believed that the measured t-z curves should also exhibit strain softening behaviour, but this has evidently been ignored by Heydinger and O'Neill (1986) in producing the t-z curves for this test.

SECTION 5.4 Summary

The results of the one-dimensional idealized pile model have been compared with results from three separate pile tests. The rate-type model and the bounding surface model have been used to represent lightly to heavily overconsolidated soils, while the modified Cam-clay model has only been used to represent the lightly overconsolidated soil at the Empire test site.

Comparisons of theoretical solutions with measured pile test results in heavily overconsolidated clays, at the Hendon and Houston test sites, suggest that

(a) The theoretical expression Eq. 4.7, for the radius of influence will generally over-estimating the vertical soil displacement outside one pile radius during pile loading (i.e., the actual radius of influence is much smaller).
(b) At a greater depths, the elastic soil shear modulus around a jacked pile probably returns to a value close to its original disturbed value after the reconsolidation process.
(c) Good agreement between theoretical predictions of load diffusion, shear transfer and actual measured data is found for both Hendon and Houston test piles at working loads.
(d) The predicted pile capacity compared favourably with measured long term pile capacity in heavily overconsolidated clays.

Further, reasonable agreement between the theoretical solutions and measured results is found for the pile test in lightly overconsolidated clay at Empire.

From the results of this chapter, the selected value of the elastic shear modulus appeared to be an important factor affecting the predicted shear transfer, load diffusion along the pile and the pile load-displacement response. It may be more appropriate to consider the elastic shear modulus is expressed as a function of radial direction but this value may be difficult to determine; both experimentally and theoretically. Therefore, assuming a constant G distribution in the radial direction may be reasonable from a practical point of view. The radius of influence predicted from Randolph's (1977) equation 4.7 generally provides reasonable representation of shear transfer and pile shaft displacement relationship.

Finally, the one-dimensional pile model which used has grossly oversimplified the actual three dimensional pile-soil system. Nevertheless, surprisingly overall agreement between theoretical predictions and actual measured data is found.

For the class of problems considered here, however, all soil models appear to give roughly equally good predictions. This is only slightly surprising in light of the relatively simple but non-homogeneous, deformation field which has been used, nevertheless it emphasizes the point that use of more complex modelling methods is not always justified.

Soil Properties	
e_i	0.795
ϕ_c	22.5°
N_c	0.238
λ	0.161
κ	0.062
bulk unit weight, kN/m^3	19.0

Table 5.1 Soil properties of London clay at Hendon test site.

Depth (m)	K_{oc}	$\overline{OCR}$	σ_{zi} (kN/m^2)	J_0 (kN/m^2)
0.5	3.3	28.5	9.5	815.3
1.5	2.5	16.5	23.5	1156.6
2.5	2.3	14.0	32.5	1355.7
3.5	2.1	11.5	41.5	1444.7
4.3	2.0	11.0	48.8	1607.6

Table 5.2 Initial stress state of London clay at Hendon test site.

		Rate- type model parameter
Depth (m)	Shear modulus, G, (kN/m^2)	Cus (kN/m^2)
0.5	12750.0	35.4
1.5	18750.0	56.7
2.5	24750.0	69.0
3.5	30375.0	76.6
4.3	34500.0	86.3

Table 5.3 Model parameters for London clay at Hendon test site.

Stratum	Depth (m)	ϕ_c	λ	G (kN/m^2)
A	0 - 2.6	22°	0.06 - 0.144	24000
B	2.6 - 7.9	23°	0.06 - 0.144	35000
C	7.9 - 14.6	27°	0.04 - 0.057	57500

Table 5.4 Summary of soil properties at Houston test site.

Stratum	λ	κ	N_c	n	e_i
A	0.13	0.06	0.233	0.8	0.53
B	0.14	0.06	0.245	0.8	0.72
C	0.057	0.016	0.292	0.75	0.45

Table 5.5 Selected soil parameters for Houston test site.

		Rate-type model parameters	Bounding surface model parameter				
Stratum	Depth (m)	Cus (kN/m^2)	A_c	t_c	σ_{ri} (kN/m^2)	σ_{zi} (kN/m^2)	J_0 (kN/m^2)
A	0.5	14.9	0.08	12.0	20.8	10.1	288.0
	1.5	44.9			62.4	30.2	864.0
	2.3	65.6			91.6	44.2	1267.0
B	3.3	77.7	0.05	35.0	98.6	54.3	1346.0
	4.5	81.5			101.7	66.5	1388.0
	5.5	85.0			104.9	76.5	1432.0
	6.5	88.7			108.3	86.7	1478.0
	7.45	92.3			111.6	96.3	1524.0
C	8.5	128.3	0.1	100.0	122.0	127.0	1559.0
	10.5	132.2			125.3	137.1	1599.0
	11.5	136.4			128.5	147.3	1642.0
	12.55	140.5			132.1	158.9	1684.0

Table 5.6 Initial values of the soil models for Houston test site.

Soil Properties	
e_i	1.22
ϕ_c	25.0°
N_c	0.267
λ	0.234
κ	0.058
Knc	0.61
Koc	0.75
$\overline{OCR}$	1.3 **
** measured $\overline{OCR} = 1.7 \pm 0.5$	

Table 5.7 Soil properties of Empire test site.

Depth (m)	G (kN/m^2)	Cus (kN/m^2)	σ_{zi} (kN/m^2)	σ_{ri} (kN/m^2)	J_0 (kN/m^2)
35.5	8630	57.5	162.9	122.2	757.5
36.5	8970	59.8	169.5	127.1	787.7
37.5	9310	62.1	176.0	132.0	817.8
38.5	9660	64.4	182.4	136.8	848.0
39.5	10000	66.7	188.9	141.7	878.1
40.5	10350	68.9	195.4	146.5	908.2
41.5	10690	71.2	201.9	151.4	938.3
42.5	11030	73.5	208.4	156.3	968.5
43.5	11370	75.8	214.8	161.2	998.6
44.5	11720	78.1	221.3	166.0	1028.8
45.5	12060	80.4	227.8	170.0	1059.0
46.5	12400	82.7	234.3	175.7	1088.9
47.5	12750	85.0	240.8	180.6	1119.2
48.5	13090	87.3	247.3	185.5	1149.4
49.5	13430	89.6	253.8	190.3	1179.5

Table 5.8 Initial values of the soil models for Empire test site.

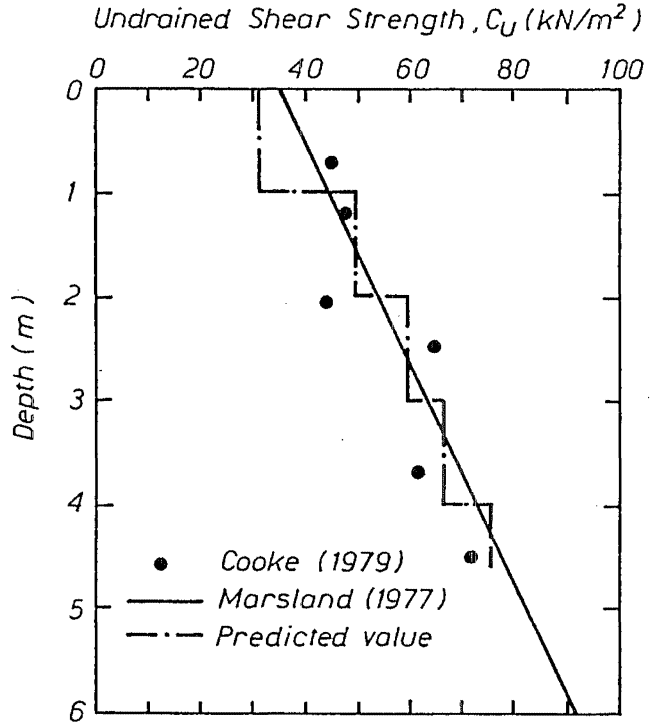

Figure 5.1 Predicted and measured undrained shear strength, Hendon test site.

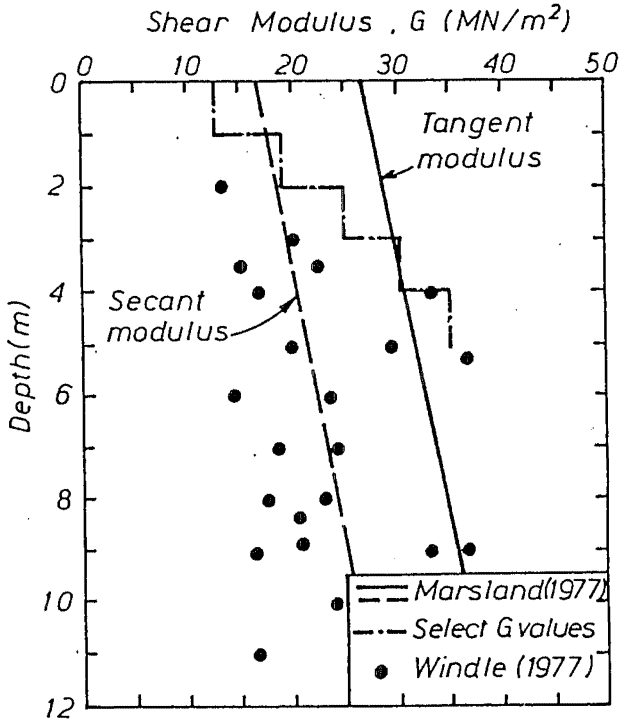

Figure 5.2 Selected and measured shear modulus, Hendon test site.

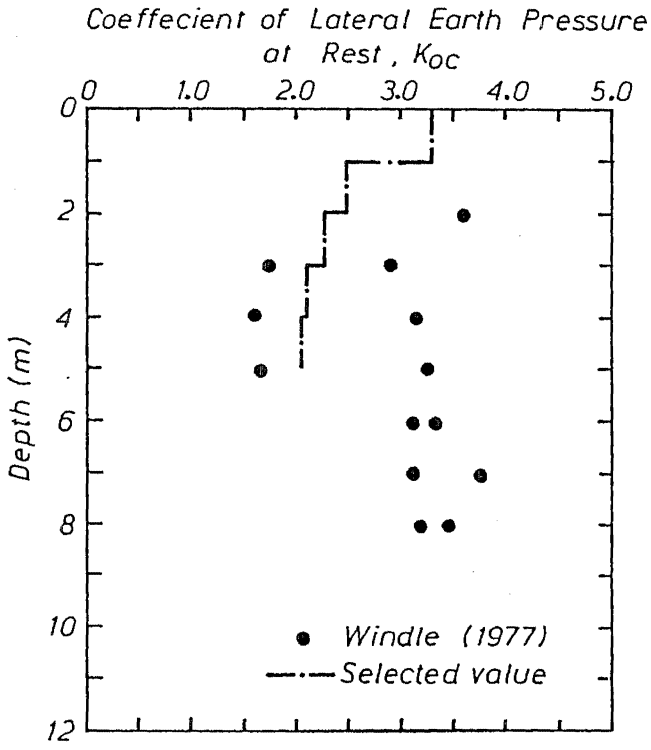

Figure 5.3 Selected and measured coefficient of lateral earth pressure at rest, Hendon test site.

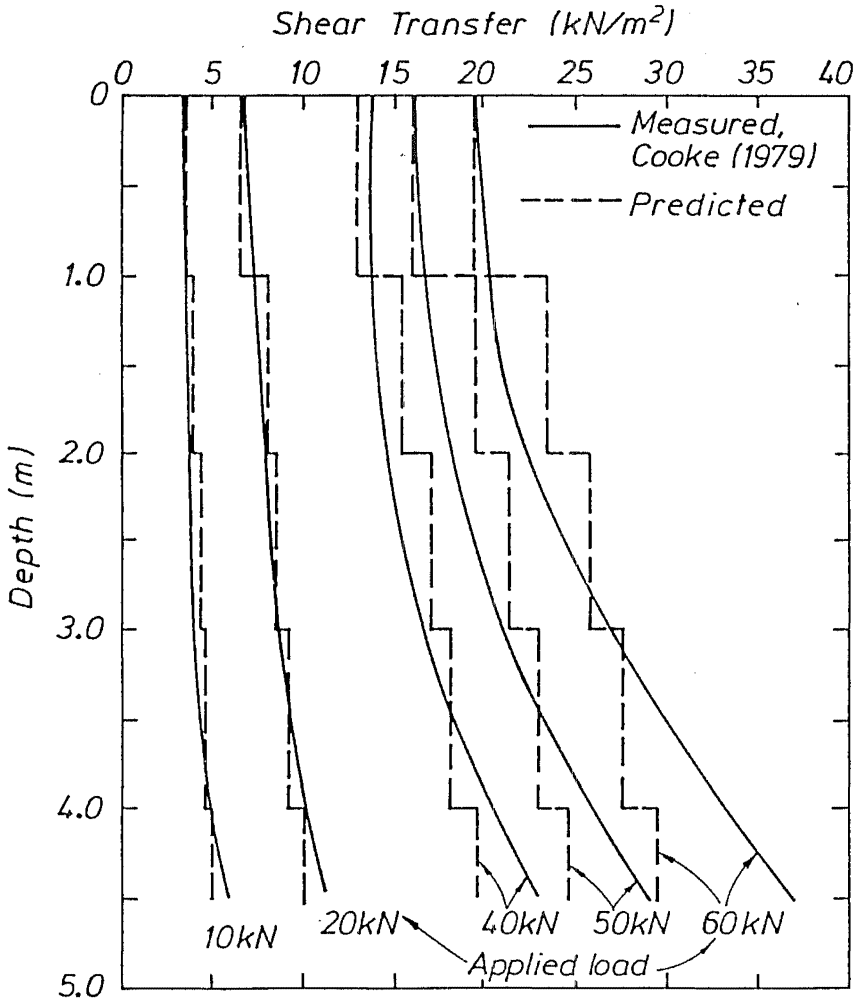

Figure 5.4 Predicted and measured shear transfer along the pile shaft, Hendon test site.

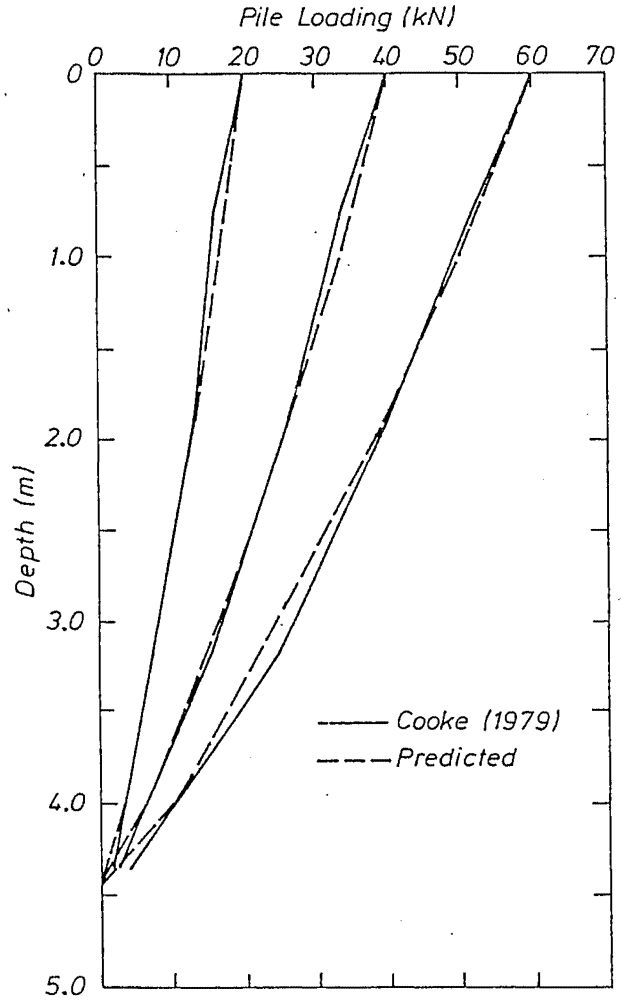

Figure 5.5 Predicted and measured load diffusion along the pile, Hendon test site.

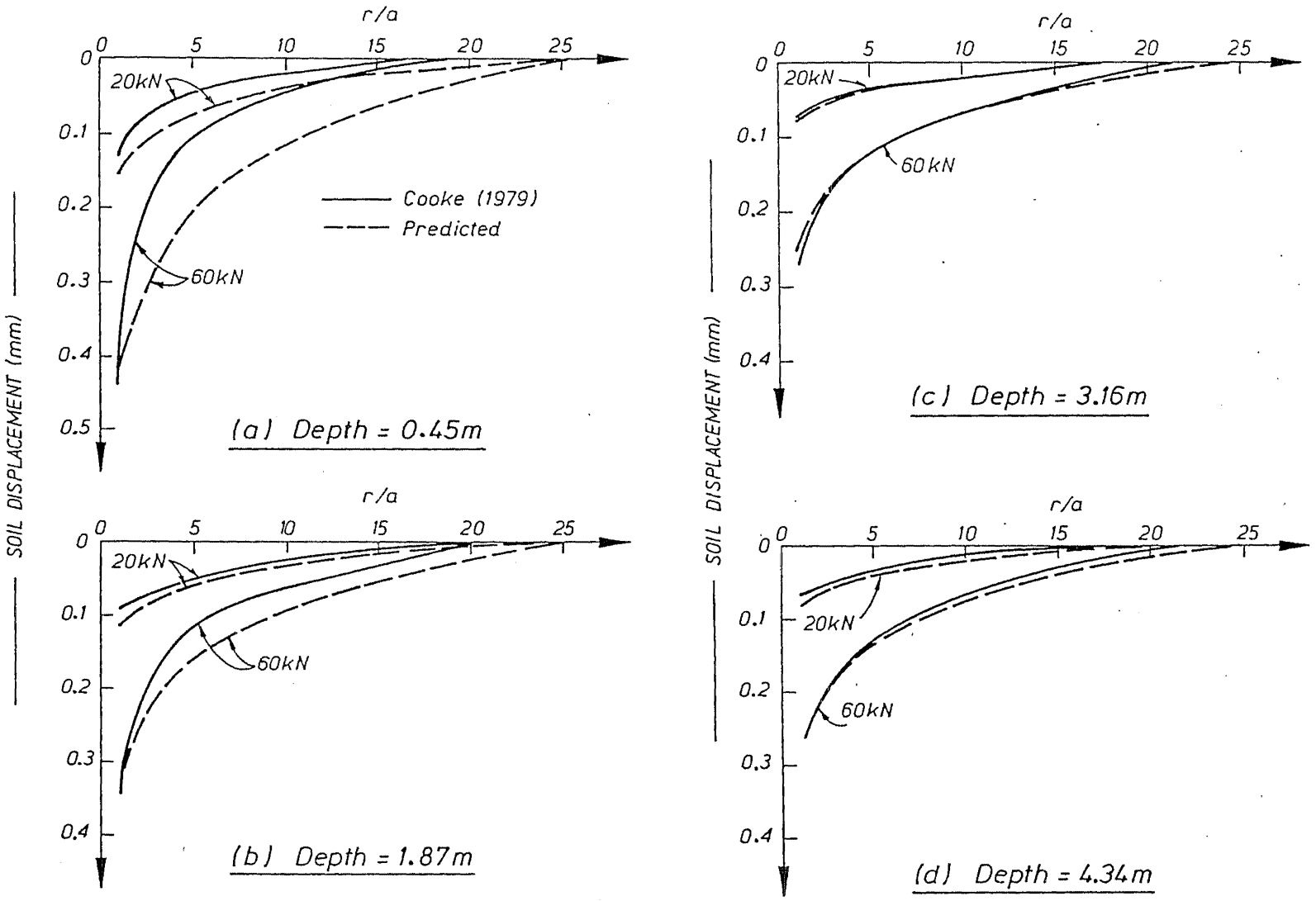

Figure 5.6 Predicted and measured soil displacement at depths (a) 0.45m (b) 1.87m (c) 3.16m and (d) 4.34 during pile loading, Hendon test site.

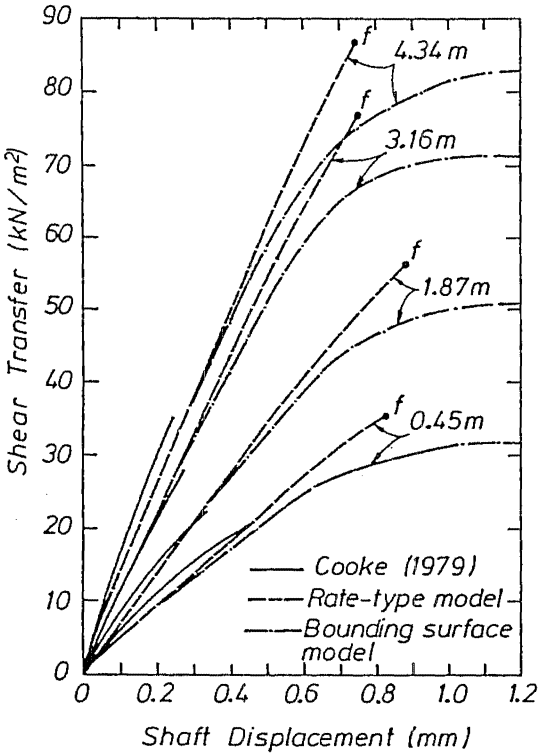

Figure 5.7 Predicted and measured shear transfer and pile shaft displacement relationship, Hendon test site.

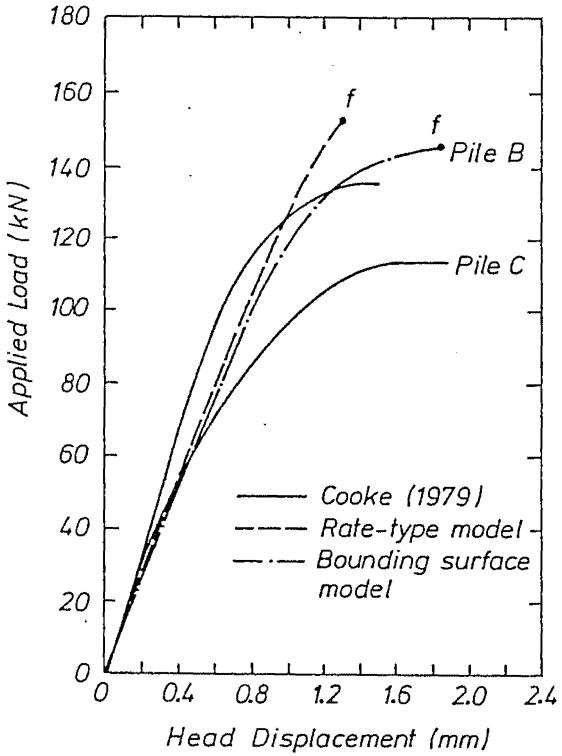

Figure 5.8 Predicted and measured pile load and displacement responses, Hendon test site.

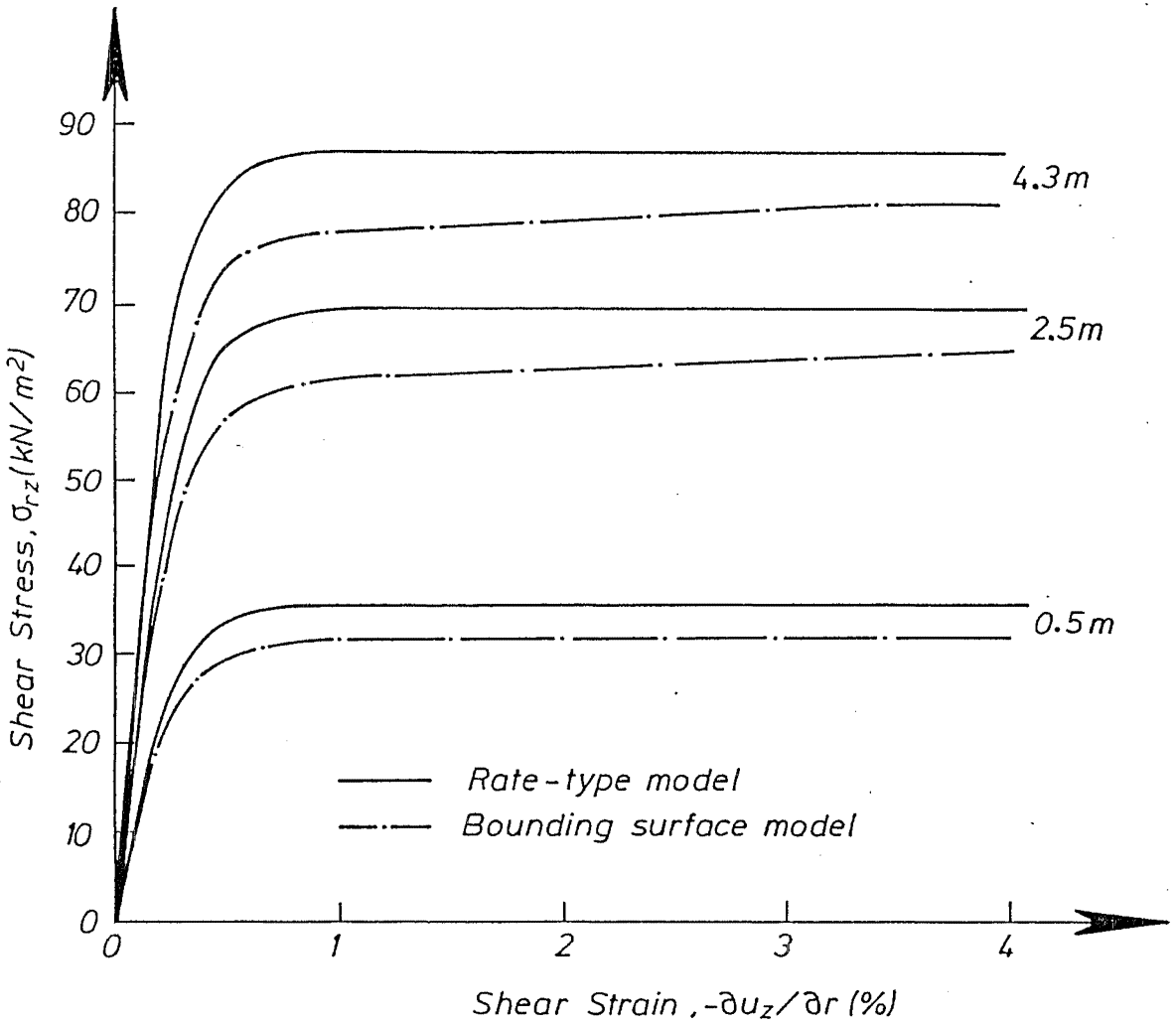

Figure 5.9 Shear stress and strain response of Bounding surface model and rate-type model for soils at Hendon test site.

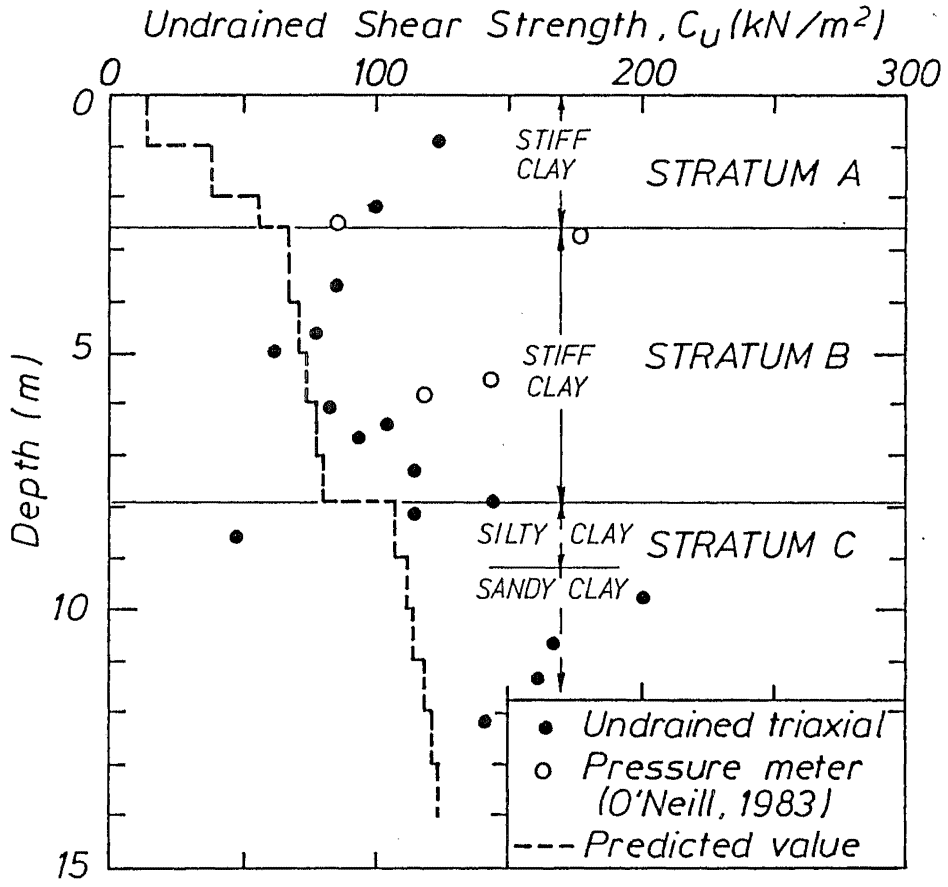

Figure 5.10 Predicted and measured undrained shear strength, Houston test site.

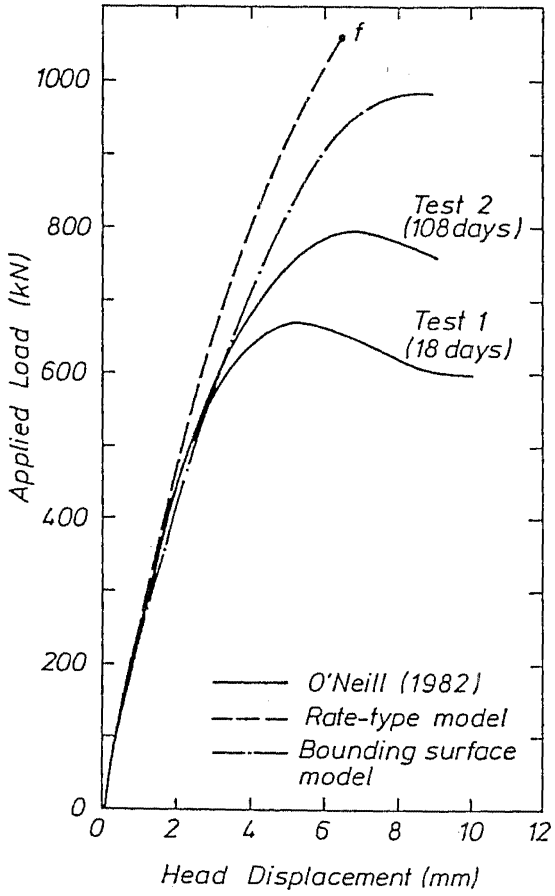

Figure 5.11 Predicted and measured pile load and displacement response, Houston test site.

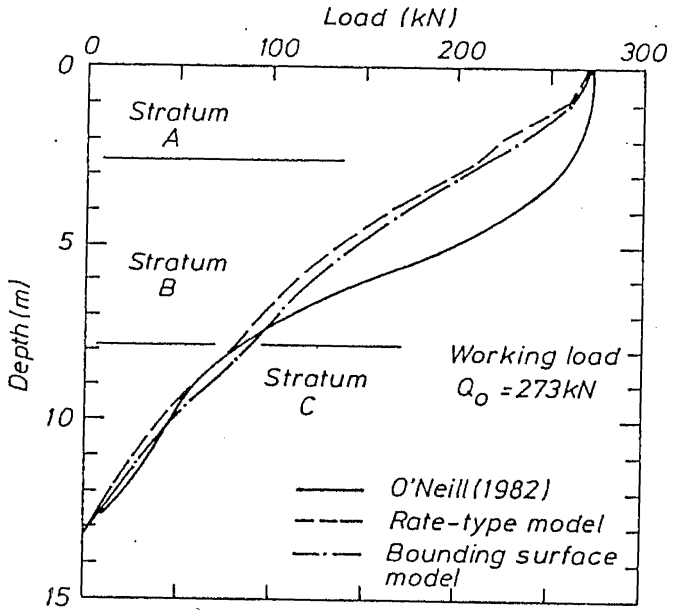

Figure 5.12 Predicted and measured load diffusion along the pile, Houston test site.

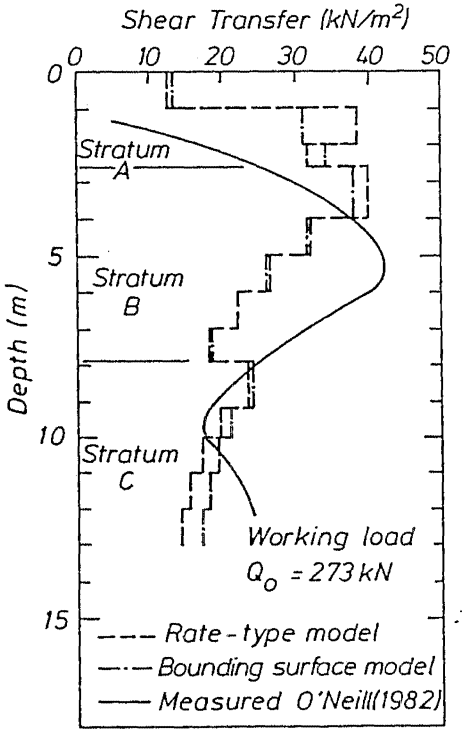

Figure 5.13 Predicted and measured shear transfer along the pile shaft, Houston test site.

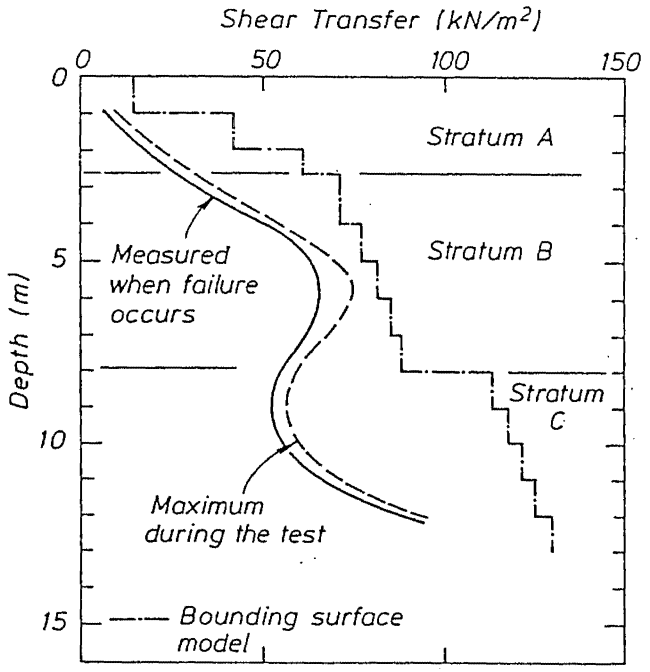

Figure 5.14 Comparison between predicted maximum shear transfer and measured shear transfer when the pile plunged failure, and maximum shear transfer at various loadings, Houston test site.

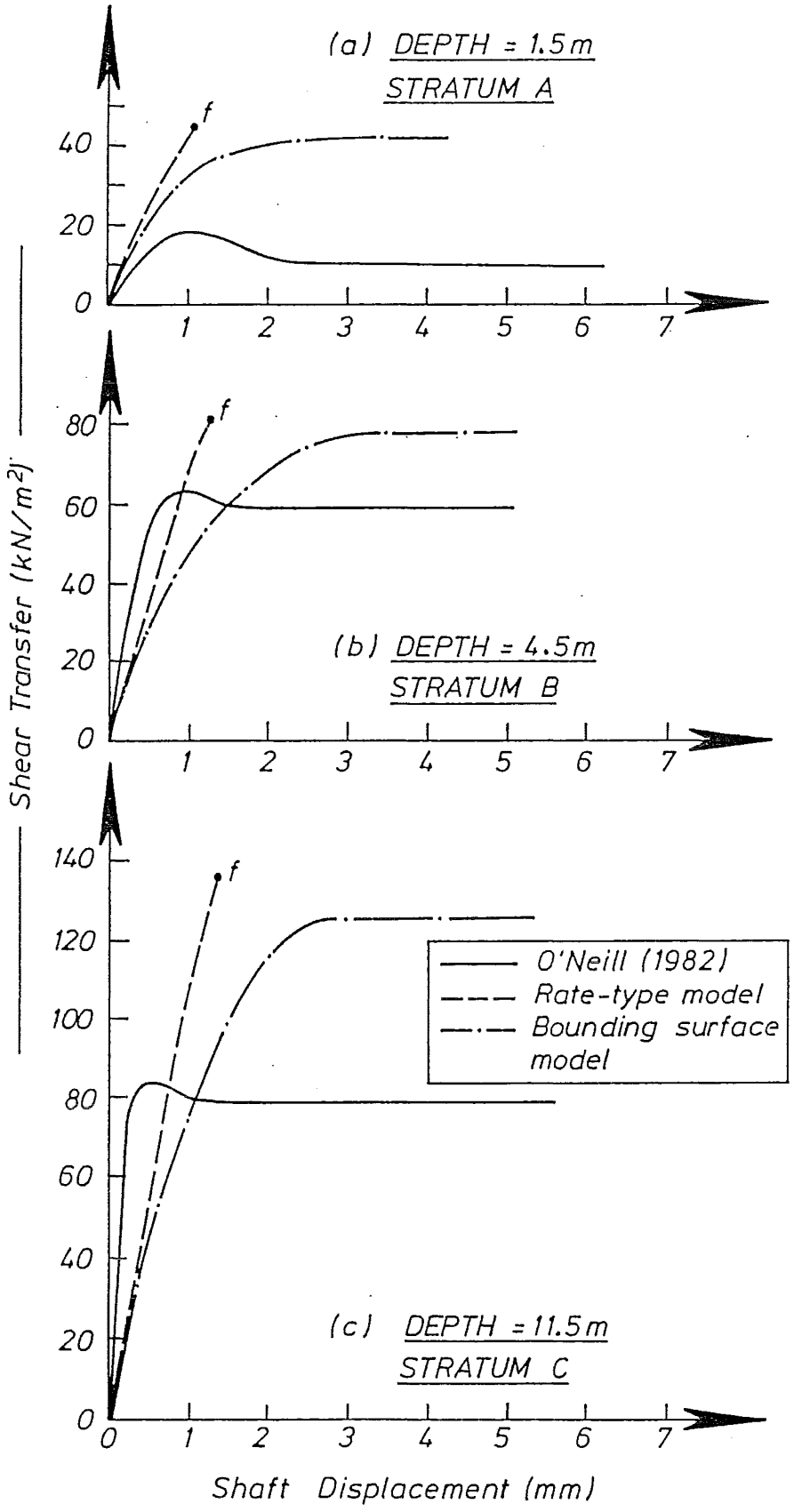

Figure 5.15 Predicted and measured shear transfer and pile shaft displacement relationship at depths (a) 1.5m (b) 4.5m and (c) 11.5m, Houston test site.

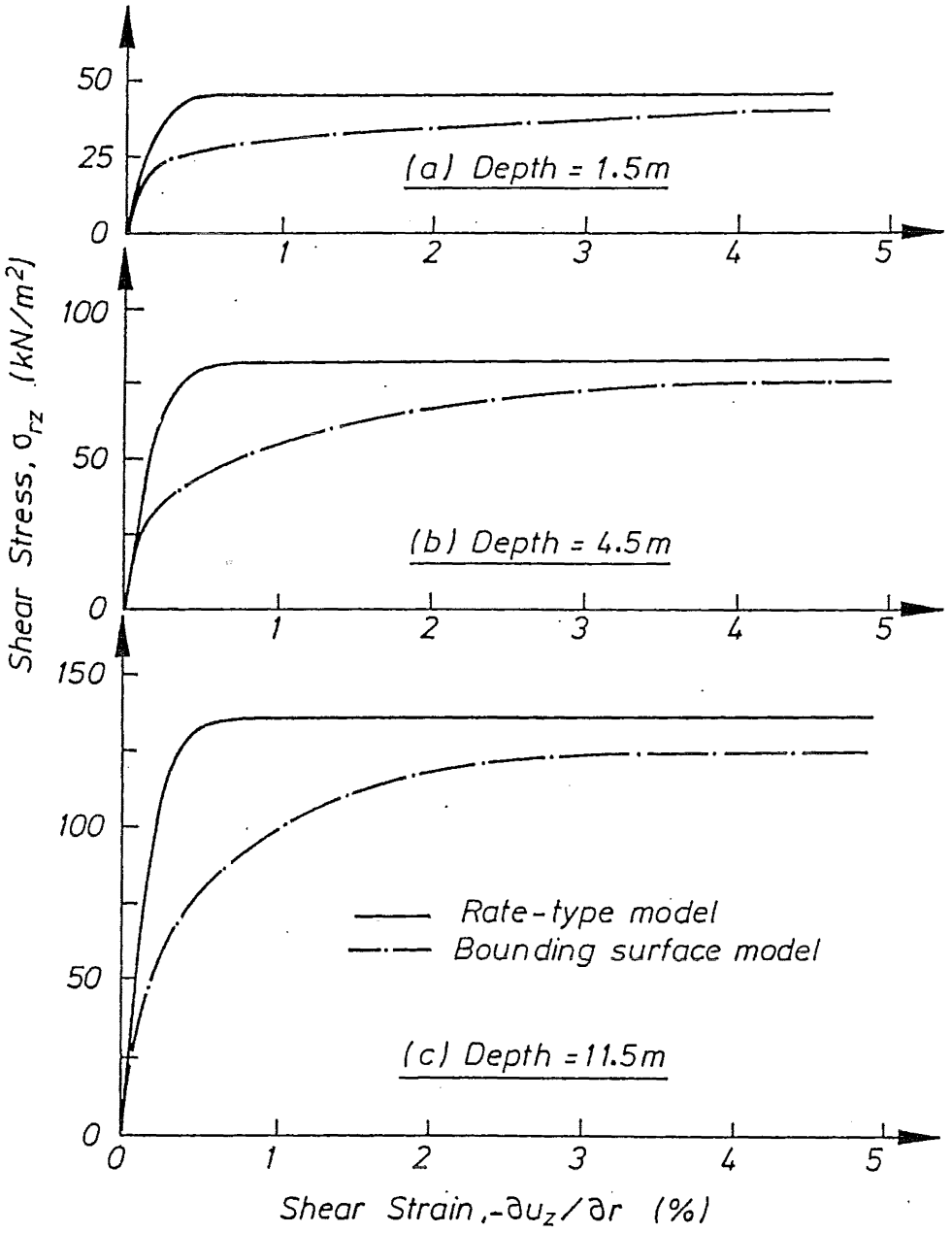

Figure 5.16 Shear stress and strain responses of Bounding surface model and rate-type model for soils at depths (a) 1.5m (b) 4.5m and (c) 11.5m, Houston test site.

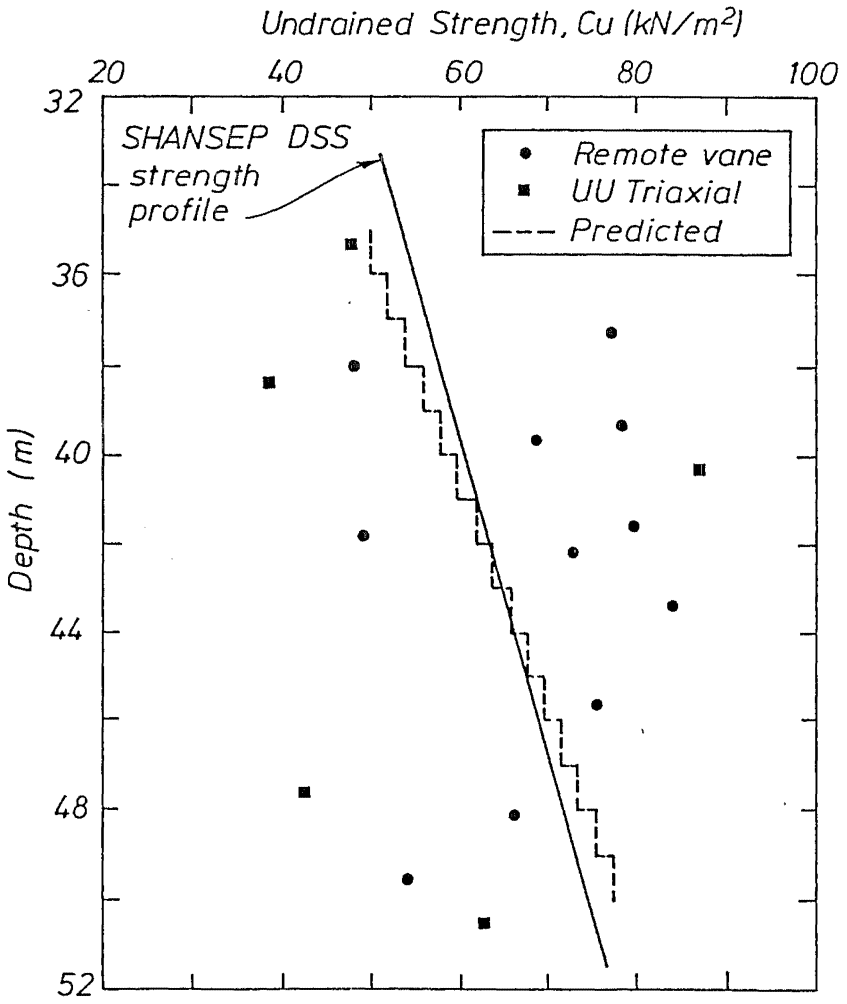

Figure 5.17 Predicted and measured undrained shear strength, Empire test site.

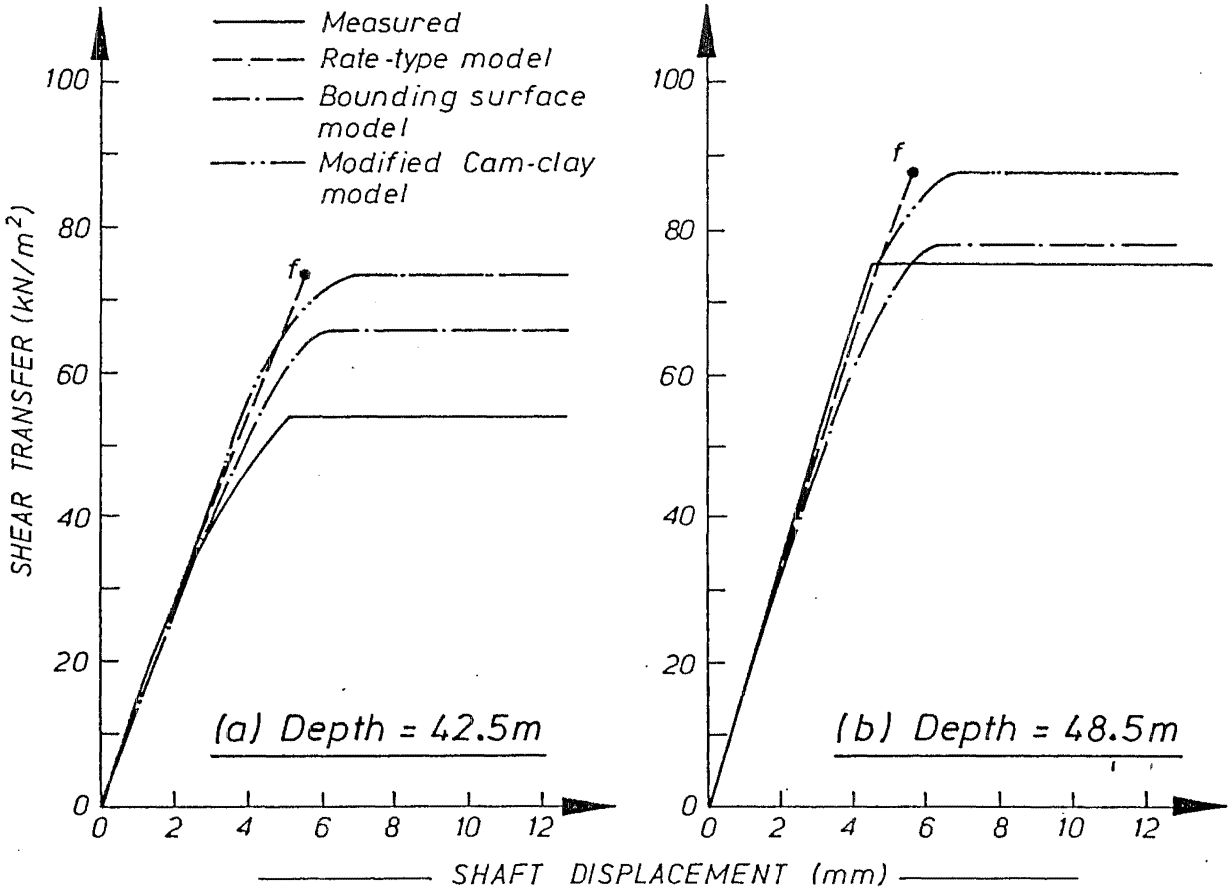

Figure 5.18 Predicted and measured shear transfer and pile shaft displacement relationship at depths (a) 42.5m and (b) 48.5m, Empire test site.

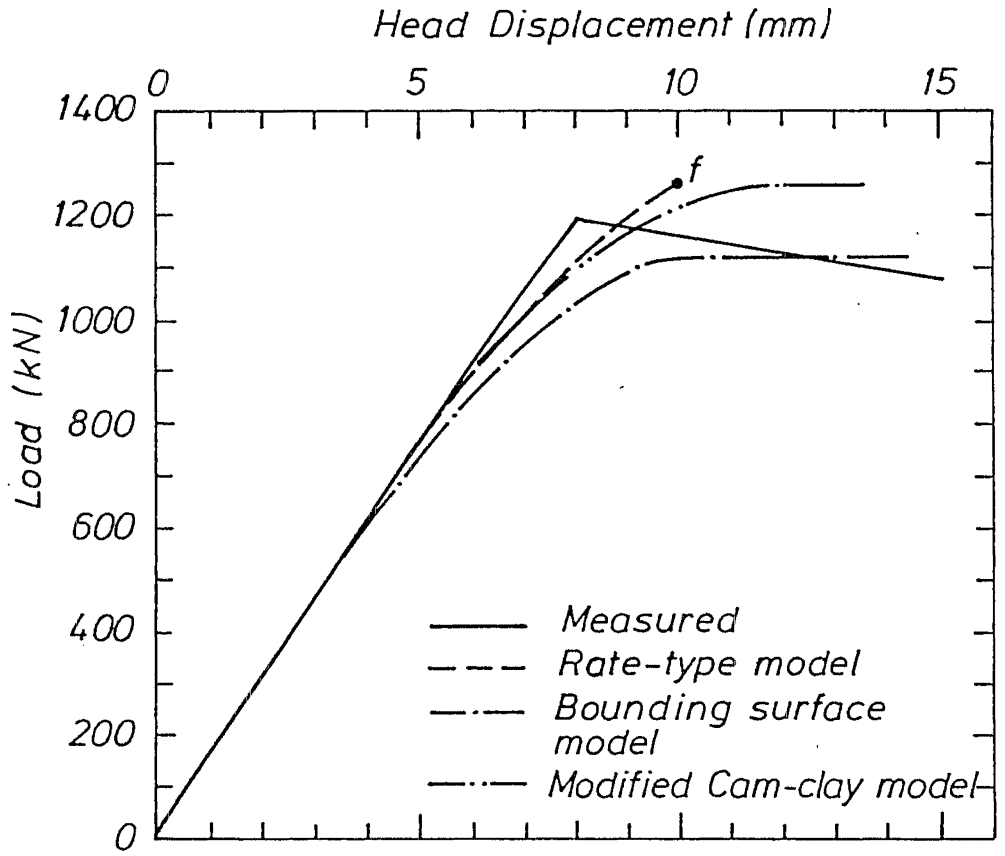

Figure 5.19 Predicted and measured pile load and displacement responses, Empire test site.

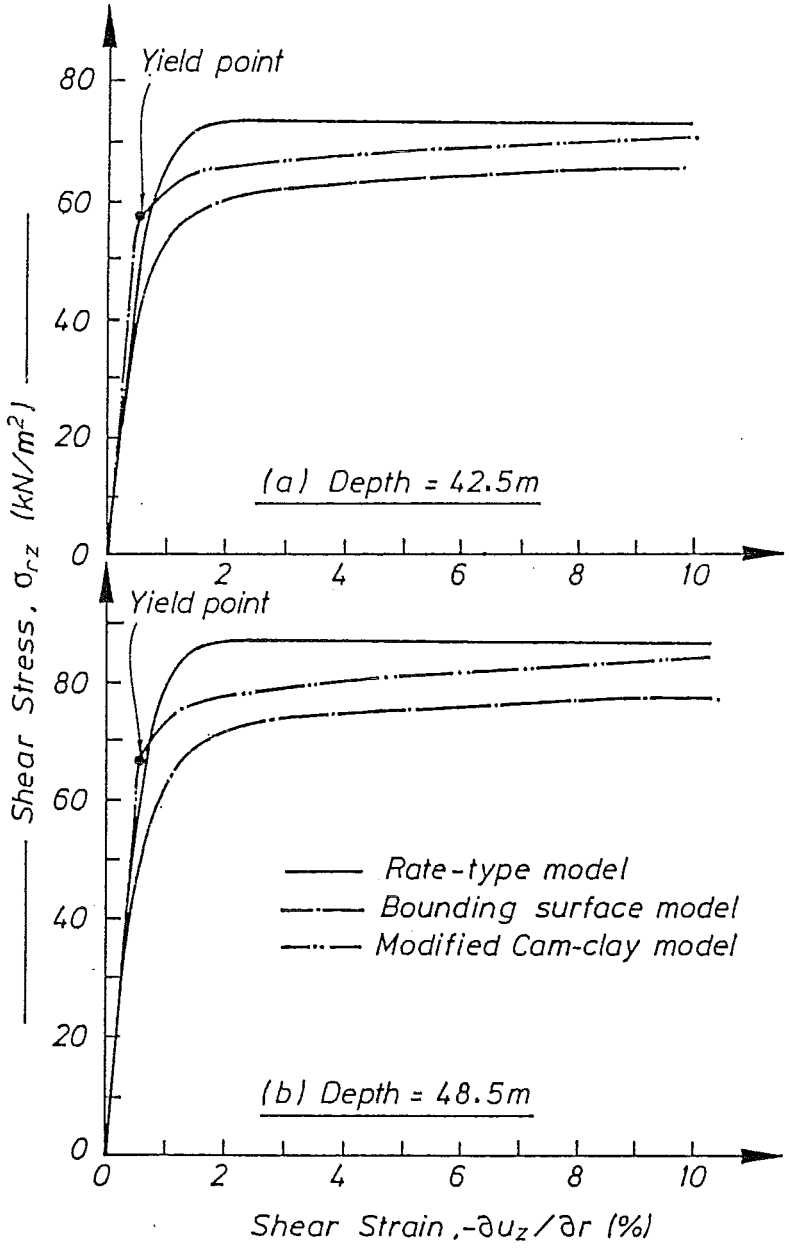

Figure 5.20 Shear stress and strain responses of Bounding surface, rate-type and modified Cam-clay models for soils at depths (a) 42.5m and (b) 48.5m Empire test site.

CHAPTER SIX

CONCLUSSION

This work may be separated into three parts. The first part mainly involves the evaluation existing soil models under undrained conditions. The second part of the work is to evaluate the currently used methods for representation of the pile installation process. The third part of the work involves comparing the soil models in particular application to the axially loaded pile problem.

In chapter two, three soil models, the modified Cam-clay, the bounding surface and the rate-type model, have been reviewed briefly. All these soils models employ the concepts of critical state theory .The modified Cam-clay model and the bounding surface model are developed based on plasticity theory, the rate-type model is founded upon hypoelasticity theory. In our work, no attempt has been made to modify these three soil models but, instead, particular interest is paid to comparing their modelling features. All three soil models are compared in triaxial and simple shear under undrained and monotonic loading conditions.

The modified Cam-clay model and the rate-type model are closely related by the similarity of their yield surfaces. In our comparisons, the rate-type model provided better predictions than did the modified Cam-clay model. The modified Cam-clay model is relatively restricted for predictions of normally consolidated to lightly overconsolidated clay, but the rate-type model does not exhibit this limitation. For the special case where only monotonic loading and undrained conditions are concerned, the choice of the rate-type model rather than the modified Cam-clay model to represent overconsolidated clay is more appropriate. Another advantage of using the rate-type model for undrained conditions is that only three soil parameters, G, Cus and N_c are required and all these can be easily evaluated from standard soil test results.

In some boundary value problems, even monotonic application of structural loading may involve unloading in some parts of the soil mass. However, theoretically, the rate-type model is valid for monotonic loading or undrained cyclic loading conditions only. The formulation of the loading equation of the rate-type model is well founded, therefore, future development will require further investigation of the formulation for the unloading equation so that violation of the condition of continuity does not exist. Furthermore, the feature of the rate-type model which defines the loading-unloading condition based on the sign of the stress power or work rate has been criticized by Mroz (1980) because it may not be applicable for some materials such as metals. Therefore, further work with the rate-type model is required to compare soil test results under various stress and strain conditions in order to evaluate the validity of using the stress power to differentiate loading or unloading conditions.

The bounding surface model developed by Dafalias applies bounding surface plasticity theory to clays. The yield surface previously defined in classical plasticity theory, such as the yield surface of the modified Cam-clay model, becomes a bounding surface in this model. For stress state inside the bounding surface, (i.e., a overconsolidated clays), the model may predict plastic deformation. This is achieved by relating the plastic modulii $\bar{H}$ and H by the distance δ. The radial mapping rule, which determines the distance δ, adopted in this model can be considered as a special form, another choice of mapping rule may be possible. The new ideas employed by the bounding surface model make it possible to predict soil test results for normally consolidated to heavily overconsolidated clays successfully. However, this model requires 11 model parameters which needs extensive soil test results to be determined.

Among the modified Cam-clay model, the bounding surface model and the rate-type model, particularly in their application to undrained deformation problems, the rate-type model appears to be most efficient, especially when insufficient soil test results exist to evaluate the model parameters for the more complicated soil models.

In chapter three, solutions for both the cylindrical cavity expansion approach and the simple pile method have been studied. Both method may be employed to investigate stress and pore pressure changes in soils due to pile installation. The advantage of these two methods is that they do not require complex numerical techniques and solution methods. The newly introduced simple pile method initially appeared to have advantages over the cylindrical cavity expansion approach because it may include the pile tip effect due to pile advancements. Baligh (1984) considered that, for deep penetration in soft clay at high confining pressure, the strain field around the pile tip is less affected by shearing response of the medium. As a result of this consideration, Baligh approached the problem by assuming that the strain field in a soft clay due to pile installation can be approximated by an ideal fluid.

In our analysis, we have used the rate-type model to represent the soil. We found that the simple pile method results in unrealistic pile-soil interaction. The surface shear traction is acting downward along the simple pile and eventually results in tensile stress in the pile at some distance above the pile tip. Furthermore, as the soil rigidity decreases, the magnitude of the downward shear traction increases. For very soft clay, the downward shear traction may be as high as 60% of the Cus value. This is contrary to the basic consideration of this method. In addition to this, from our results, the stress distribution around the tip is directly affected by the components of the rate of deformation. As a result of these findings, the effective stress distribution especially close to the pile shaft may be less than reliable. Therefore accurate determination of the strain field of the soil around the pile is important and further development of the pile installation problem incorporating realistic pile-soil interaction is necessary.

Comparisons between the solutions of the cylindrical cavity expansion approach and the simple pile method indicates that some similarity of stress distributions outside the critical state region may be expected,(i.e., where soils are mainly elastic), but stress distributions inside the

critical state region are quite different. Inside the critical state region, especially within a few pile radii of the shaft, the stress distribution predicted from both methods are suspect. Firstly, the pile tip effects have not been captured in the cylindrical cavity expansion approach. Secondly, the unrealistic shear distribution results from the simple pile method will directly influence the stress distributions of components S_{rr}, $S_{\theta\theta}$ and S_{zz} in this region.

Comparisons between the predicted excess pore pressure distributions obtained from both methods also show dissimilarity inside the critical state region. The excess pore pressures evaluated from the simple pile method are based on selecting an integration path where the equilibrium equation is less dependent upon the shear component, S_{rz}. The results are also compared with field measurement from full size pile test results. The simple pile method was found to provide better agreement with test results than does the cylindrical cavity expansion approach.

The simple pile method may be useful to approximate the excess pore pressure for the deep penetration problem. However, since this method may not reasonably predict the effective stress especially in regions close to the pile, the use of these results to develop the effective stress pile capacity model may not be successful except until a more realistic pile soil interaction has been developed.

In chapter four, we approached the axially loaded pile problem by using an idealized one-dimensional pile model. We considered that the soil is "undisturbed" by pile installation and that soil displacement caused by pile loading occurs vertically only. The formulation and solution method for this pile model has been discussed. An analytic solution for shear transfer and pile shaft displacement were obtained from the rate-type model. Numerical solutions were required for the modified Cam-clay and bounding surface model.

In chapter five, the pile models were used to predict actual measurements of pile test results. All three soil models have been used to represent the soils and compared in this way.

Three well documented pile test results available from engineering literature have been used. The test soil at the Empire test site is lightly overconsolidated while the test soils in both Hendon and Houston test sites are heavily overconsolidated. The rate-type model and the bounding surface model have been used to represent lightly to heavily overconsolidated soils, while the modified Cam-clay model has only been used to represent the lightly overconsolidated soils at the Empire test site.

In this comparisons the rate-type model and the bounding surface model represent extremes of sophistication. The bounding surface model is quite complex and offers an wide range of possible responses, while the rate-type model is particularly simple but encompasses a far more limited response range. These facts are clearly reflected by the number of parameters required for each model: eleven for the bounding surface model versus two for the particular application of rate-type model in this problem. The modified Cam-clay model is less complex than the bounding surface model, but is more restricted to represent lightly overconsolidated clays.

The select value of the elastic shear modulus appeared to be an important factor affecting the predictions of shear transfer, load diffusion and pile load-displacement response of our one-dimensional pile model. Generally , reliable estimation of the change in soil shear modulus before and after pile installation is difficult, (i.e., especially as the measured value of shear modulus generally depends on the type of shear test and testing device such as pressuremeter, plate bearing test or triaxial test, etc), therefore assumption of a constant shear modulus distribution in the radial direction may remain a useful approximation. Further, this approximation may be appropriate for the soil at a greater depth around a jacked pile as we have found that the pile model gives good agreement between predicted and measured soil displacements at Hendon test site.

From both pile test results in heavily overconsolidated soil, it has been found that Randolph's equation overestimates the actual size of the radius of influence measured from test results. This leads to overestimation of soil displacements from about one pile radius outside the pile shaft. But it has been pointed out that reasonable shear transfer and pile shaft displacement relationships may be possible using Randolph's equation.

The one-dimensional pile model which has been used here may oversimplify the actual three dimensional soil-pile system. We have not considered the limiting skin friction problem. Nevertheless, surprisingly good agreement between theoretical predictions of load diffusion, shear transfer, pile load-displacement response and actual measured data is found for all test piles at working loads.

Finally, for the class of problems considered here, all soil models appear to give roughly equally good predictions. This is only slightly surprising in light of the relatively simple deformation field which has been used, nevertheless, it emphasizes the point that use of more complex modelling methods is not always justified.

REFERENCE

(1) Acar Y.B. & Tumay, M.T., (1986) "Strain field around cones in steady penetration," J. Geot. Eng. Vol. 112, pp. 207-213.

(2) Airey D.W. & Wood D.M (1987) "An evaluation of direct simple shear tests on clay" Geotechnique 37 No. 1, pp. 25-35.

(3) American Petroleum Institute (1981), API Recommended practice for Planning, Designing, and Constructing Fixed Offshore Platforms, API, Production Division, 211 North Ervay, Suite 1700, Dalbs Texas 75201.

(4) Anderson K.H. (1976) "Behaviour of clay subjected to undrained cyclic loading," Proc. lst Int. Conf. on Behaviour of offshore structure, Norwegian Institute of Technology, pp. 392-403.

(5) Atkison J.H. & Bransby P.l. (1978) The mechanic of soils; an introduction to critical state soil mechanics. McGraw Hill.

(6) Aurora, R.P., Peterson, E.H. & O'Neill, M.W. (1980) "Model study of load transfer in slender pile," J.Geot. Eng'g. Div., ASCE, Vol. 106, No.GT8, pp. 941-945.

(7) Azzouz, A.S. & Lutz, D.G., (1986) "Shaft behaviour of a model pile in plastic empire clays,", J. Geot. Eng. Div. ASCE, Vol.112, No.4, pp. 389-406.

(8) Bakholdin B.V. & Bolshakov N.M., (1973) "Investigation of the state of stress of clays during pile driving; Soil Mech. and Found. Eng. 10, pp. 300-305.

(9) Baligh, M.M.,(1984) "The simple-pile approach to pile installation in clays," in Analysis and Design of Pile Foundations, Symp. ASCE, Geot. Eng'g Div., San Fancisco, California, ed. J.R. Meyer, pp. 310-330.

(10) Baligh M.M ,(1985) "Strain path method," J. Geot. Eng. Div., ASCE, Vol.111, No. 9, pp. 1108-1135.

(11) Baligh, M.M.,(1986a) "Undrained deep penetration, I: shear stresses," Geotechnique 36, No. 4, pp. 471-485.

(12) Baligh, M.M.,(1986b) "Undrained deep penetration, II: pore pressures stresses," Geotechnique 36, No. 4, pp. 487-501.

(13) Banerjee, P.K. & Stipho, A.S., (1978) "Associated and non-associated constitutive relations for undrained behaviour of isotropic soft clays," Int. J. Num Anal. Methods of Geomech, Vol.2, pp. 35-56.

(14) Banerjee P.K. & Stipho A.s./ (1979) "An elastoplastic Model for heavily overconsolidated clays," Int. J. Num. Anal. Method Geomech. Vol.3, pp. 97-103

(15) BCP Committee (1971) "Field tests on piles in sand," Soil & Foundation Vol.11, No. 2, pp. 29-49

(16) Bishop (1964) "The measurement of soil properties in the triaxial test, William Clowes & sons, London

(17) Burden R.L., Faires, J.D. & Reynolds, A.C., (1981) "Numerical Analysis" Prindle Weber & Schnidt, Boston, Massachusetts.

(18) Burland, J.B., (1973) "Shaft friction of piles in clay" Ground Engineering, Vol. 3, No. 3, pp. 30-42.

(19) Butterfield R. & Banerjee, P.K., (1970) "The effect of pore water pressures on the ultimate bearing capacity of driven piles," Proc. 2nd South-East Asian Conf. on Soil Eng'g, Singapore, pp. 385-394.

(20) Carter, J.P., Booker, J.R.& Wroth, C.P.,(1982) "A critical state soil model for cyclic loading," in Soil Mech.- Transient and Cyclic Loads, Ed. G.N. Pande and O.C. Zienkiewicz, John Wiley & Sons, pp. 219-252.

(21) Casagranda, A., 1936 "Characteristics of Cohesionless soils affecting the stability of slopes and Earth fills." J. Boston Soc. Civil Eng., pp. 257-276

(22) Cheung K.C (1985) " Axially loaded piles," M.E thesis, University of Canterbury.

(23) Cooke, R.W., Price, G. & Tarr, K., (1973) " Strains and displacements around friction piles," Proc. 8th Int. Conf. Soil. Mech. Found. Eng'g, Moscow 2, No.1, pp.53-60.

(24) Cooke, R.W., Price, G. & Tarr, K., (1979) "Jacked piles in London clay : a study of load transfer and settlement under working conditions " Geotechnique 29, No. 2, pp. 113-147.

(25) Cox, W.R., Kraft, L.M. & Verner, E.A., (1979), "Axial load tests on 14-inch pipe piles in clay," The 11th Annual offshore technology Conference, Houston, Texas., April 30-May 3, pp. 1147-1158.

(26) Coyle, H.G., & Reese, L.C.,(1966) "Load transfer for axially loaded piles in clay," J.S.M.F.D., ASCE, Vol. 92, SM2, pp. 1-26.

(27) Coyle, H.M., & Sulaiman, I.H.,(1967) "Skin friction for steel piles in sand," J.S.M.F.D., ASCE, Vol. 93, SM6, pp. 261-278.

(28) Dafalias Y.F. & Popov, E.P., (1975) "A model of nonlinearly hardening materials for complex loading" Acta Mechanica 21, Springer-Verlag, pp. 173-192

(29) Dafalias Y.F.& Popov E.P., (1976) "Plastic internal variables formalism of cyclic plasticity," J. Appl. Mechanics. Vol. 98 No. 4, pp. 641-650

(30) Dafalias Y.F. & Herrmann L.R., (1980) "A generalized bounding surface constitutive model for clays," in Symposium on limit Equilibrium, plasticity and generalized stress strain applications in Geotechnical Engineering. ed. Yong R.N., and Selig E.T. Hollywood, Florida October 27-31, 1980

(31) Dafalias, Y.F. & Herrmann, L.R., (1982) "Bounding surface formulation of soil plasticity" in Soil Mechanics-Transient and Cyclic Loads, Edited by Pande G.N and Zienkiewicz O.C John Wiley & Son Ltd. pp. 253-282.

(32) Davis R. O. & Mullenger G., (1978) "A rate-type constitutive model for soil with a critical state "Int. J. Num. Anal. Methods Geomech., Vol. 2, pp. 255-282

(33) Davis R.O. & Mullenger G., (1979) "A simple rate-type constitutive representation for granular media," in numerical methods in Geomechanics, Aachen. Ed. W. Wittke, Balkema, Rotterdam, Vol.1, pp. 415-421.

(34) Davis, R. O., Scott, R.F. & Mullenger, G. (1984) "Rapid expansion of a cylindrical cavity in a rate-type soil," Int. J. Num. Anal.. Method, Geomech., Vol.8, pp. 125-140.

(35) Davis R.O. & Mullenger G., (1984) " Some simple boundary value problems for dilatant soil in undrained conditions," in Mechanics of Eng'g Material, ed. C.S. Desai & R.H Gallagher, John Wiley & Sons ltd. pp. 197-210.

(36) Desai, C.S. & Siriwardane H.J., 1984 Constitutive Laws for Engineering Materials, with Emphasis on Geologic Materials, Prentice-Hall, Inc. Englewood Cliffs, New Jersey.

(37)Desai, C.S., (1978) "Effects of driving and subsequent consolidation on behaviour of driven piles," . Int. J. Num. Anal. Methods Geomech, No. 2, pp. 283-301

(38) Desai, C.S., Somasundaram, S. & Frantziskanis G., (1984) "A hierarchical approach for constitutive modelling of Geologic material, Int. J. Num. Anal. Methods. in Geomech.

(39) DiMaggio, F.L. & Sandler, I.S.,(1971) "Material model for granular soils," J. Eng. Mech. Div., ASCE, Vol. 97, No. . Em3, pp. 935-950.

(40) Drucker, D.C, Gibson, R.E. & Henkel, D.J., (1957) "Soil mechanics and work hardening theories of plasticity," Trans. ASCE 122, pp. 338-346.

(41) Dyvik, R., Berre, T., Locasse, S. & Roadim, B.(1987) "Comparison of truly undrained and constant volume direct simple shear tests," Geotechnique 37, No. 1, pp. 3-10

(42) Eeleken van, H. A. M. & Potts D.M (1978) "The behaviour of Drammen clay under cyclic loading," Geotechnique 28 pp. 173-196.

(43) Eeleken van, H.A.M.(1980) " Isotropic yield surfaces in three dimensions for use in soil mechanics," Int. Num. Anal. Method. Geomech. Vol. 4. pp. 89-101.

(44) Eskinazi S (1962), "Principles of fluid mechanics" Allyn and Bacon, Inc., Boston

(45) Focht, J.A. & Kraft, L.M.,(1981) " Prediction of capacity of long piles in clay," Sym. Geot. Aspects of Coastal and Offshore Structures, Bangkok, 14-18 Dec., pp. 95-113.

(46) Gilbert, G.D., (1954) "Shear strength properties of weald clay." Ph.D Thesis, London.

(47) Green A.E. (1956) "Hypoelasticity and plasticity," Proc. Roy. Soc. London. Vol.234., pp. 46-59

(48) Gudehus, G. & Kolymbas, D.,(1979) "A constitutive law of the rate type for soils," Proc. 3rd. Int. conf. Num. Methods Geomech., Aachen, ed. Wittke W., pp. 319-330.

(49) Hashiguchi K. (1980) "Constitutive equations of elastoplastic materials with elastic-plastic transition", J. Appl. Mech., Vol. 47, pp. 266-272.

(50) Henkel D.J., (1956) "The effect of overconsolidation on the behaviour of clays during shear" Geotechnique No. 6, pp. 139-150.

(51) Henkel, D.J., (1960) "The shear strength of saturated remoulded clays," Proc. ASCE. Spec. Conf. on shear strength of Cohesive soils," Banlder, pp. 533-554.

(52) Heydinger, A.G., & O'Neill, M.W.,(1986) "Analysis of axial pile-soil interaction in clay," Int. J. Num. Anal. Methods Geomech., Vol. 10, pp. 367-381.

(53) Iwan, W.D. (1967) " On a class of models for the yielding behaviour of continuous and composite systems," J. Appl. Mech. Vol. 34, pp. 612-617.

(54) Kirby, R.C. & Wroth, C.P., (1977) "Application of critical state soil mechanics to the prediction of Axial Capacity for Driven piles in clays," 9th Annual Offshore Technology Conf., pp. 483-494

(55) Kirby R.C., Esrig M.L. & Murphy B.S (1983) "General effective stress method for piles in clay, Part I-Theory "in Conf. Geot. Pract. Offshore Eng'g ASCE, ed. Wright S.g, University of Texas at Austin. pp. 457-498.

(56) Koizumi Y. & Ito K., (1965) "Field tests with regard to pile driving and bearing capacity of pile foundation," Soils and Foundations, 7, (3), pp. 130-53.

(57) Kraft, L.M., Cox,W.R. & Verner, E.A., (1981) "Pile load tests: cyclic loads and varying load rates," J. Geot. Eng. Div. ASCE, Vol.107,No.GT1, pp. 1-19.

(58) Kraft, L.M., Ray, R.P. & Kakaaki, T.,(1981) "Theoretical t-z-curves," J. Geot. Eng'g Div., ASCE, Vol. 107, No. GT11, pp. 1543-1562.

(59) Kraft L.M. & Ray, R.P., Kagawa., (1981) "Theoretical t-z curves," J. Geot. Eng. Div., ASCE, Vol. 107, No. GT11, pp. 1543-1561

(60) Kraft L.M. (1982) "Effective stress capacity model for piles in clays" J. Geot. Eng'g. Div. ASCE, Vol. 108, No. GT11, pp. 1387-1404.

(61) Krieg, R.D.,(1975) "A practical two-surface plasticity theory," J. Appl. Mech., Vol. 42, pp. 641-646.

(62) Ladanyi, B. (1972) "In-situ determination of undrained stress-strain behaviour of sensitive clays with pressuremeter," Canadian Geotechnical Journal, Vol.9, pp. 313-319.

(63) Ladd, C.C. & Foott, R.C. (1974) " New design procedure for stability of soft clays," J. Geot. Eng'g Div., ASCE, Vol. 100, NO. GT7, pp 763-786.

(64) Lambe T.W. (1967) "The stress path method" J. Soil Mech. and Found., ASCE, Vol. 93, SM6, pp. 309-331.

(65) Lambe T.W. & Marr W.A. (1979) "Stress path method: Second edition", J. Geot. Eng'g Div., ASCE, Vol. 105 No. GT6, pp. 727-738

(66) Levadoux, J. N. & Baligh M.M.,(1980) "Pore pressure during cone penetration," Research Report R80-15, Order No. 666, Department of Civil Engineering, MIT.

(67) Lo K.Y. & Stermac A.G., (1965) "Induced pore water pressure during pile driving operation," Proc. 6th Int. Conf. soil, Mech. Found. Eng'g., Montreal, 2, pp. 285-289.

(68) Marsland, A. & Randolph, M.F., (1977) "Comparisons of results from pressuremeter tests and large in situ plate tests in London clay" Geotechnique 27, No.2, pp. 217-243.

(69) Mattes, N.S. & Poulos, H.G.,(1969) "Settlement of single compressible piles," J.S.M.F.D., ASCE, Vol.95, SM1, pp. 627-641.

(70) Mayne P.W. (1980) " Cam-clay predictions of undrained strength," J . Geot. Eng'g Div., ASCE, Vol. 106 , No. GT11, pp. 1179-1200.

(71) Meyerhof, G.G. (1976) "Bearing capacity and settlement of pile foundation" J. Geot. Eng'g Div Vol. 102 No. GT3, pp. 197-227.

(72) Mitachi, T. & Kitago, S., (1979) "The influence of stress history and stress system on the stress-strain-strength properties of saturated clay," Soils and Foundations, Vol. 19 No. 2, pp. 45-61.

(73) Mitachi, T. &Kitago, S., (1980) "The undrained triaxial and plane strain behaviour of saturated remould clay," Soils and Foundations, Vol.20, No. 1, pp. 13-28.

(74) Mroz, Z., (1967) "On the description of anisotropic workhardening," J. Mech. and Phys. Solid., London, Vol. 15, pp. 163-175.

(75) Mroz, Z., Norris, V.A. & Zienkiewicz, O.C.,(1978) "An anisotropic hardening model for soils and its application to cyclic loading," Int. J. Num. Anal. Methods Geomech. Vol. 2, pp. 203-221.

(76) Mroz, Z., Norris, V.A. & Zienkiewicz, O.C., (1979) "Application of an anisotropic hardening model in the analysis of elastic-plastic deformation of soils," Geotechnique 29 No. 1, pp. 1-34.

(77) Mroz Z. (1980) "On hypoelasticity and plasticity approaches to constitutive modelling of inelastic behaviour of soils" Int. J. Num. Anal Methods Geomech., Vol.4, pp. 45-55

(78) Mroz Z., Norris, V.A. & Zienkiewicz O.C. (1981) "An anisotropic, critical state model for soils subject to cyclic loading," Geotechnique 31. No. 4, pp. 451-469.

(79) Mullenger, G., Scott, R.F. & Davis P. O., (1984) "Rapid shearing in a rate-type soil surrounding a cylindrical cavity," Int, J. Num. Anal. Method Geomech., Vol. 8, pp. 141-155.

(80) Nakase, A. & Kamei, T., (1986) "Influence of strain rate on undrained shear characteristics of Ko-consolidated cohesive soil", soils and foundations Vol.26, No. 1, pp. 85-95.

(81) Nayak G.C. & Zienkiewicz, O.C. (1972) "Elasto-plastic stress analysis a generalization for various constitutive relations including strain softening," Int. J. Num Method in Eng. Vol. 5, pp. 113-135.

(82) Nystrom, G.A.,(1984) "Finite-strain axial analysis of piles in clay," Proc. Symp. Geot. Eng'g Div., ASCE, San Francisco, ed. J.R., Meyer, pp. 1-20.

(83) O'Neill, M.W., Hawkins, R.A. & Audibert, J.M.E., (1982a) "Installation of pile group in overconsolidated clay," J. Geot. Eng'g Div., ASCE, Vol. 108, No. GT11, pp. 1369-1385.

(84) O'Neill, M.W., Hawkins, R.A. & Mahar, L.J., (1982b) "Load transfer mechanisms in piles and pile groups," J. Geot. Eng'g Div., ASCE, Vol. 108, No. GT12, pp. 1605-1623.

(85) O'Neill, M.W., (1983) "Side load transfer in driven and drilled piles," J. Geot Eng. Div. ASCE, Vol.109, No. 10, pp. 1259-1266.

(86) Ottaviani, M. & Marchetti, S.,(1979) "Observed and predicted test pile behaviour," Int. J. Num. Anal. Methods Geomech., Vol. 3, pp. 131-143.

(87) Palmer A.C (1972) "Undrained plane-strain Expansion of a cylindrical cavity in clay a simple interpretation of the pressuremeter test." Geotechnique Vol.22, No. 3, pp. 451-457.

(88) Parry, R.H.G. (1960) "Triaxial compression and extension tests on remoulded saturated clay," Geotechnique, Vol. 10, No.4, pp. 166-180.

(89) Parry, R.H.G. & Nadarajah, V., (1973) "Observations on laboratory prepared, lightly over-consolidated specimens of Kaolin," Geotechnique, Vol.24, No. 3, pp. 345-358.

(90) Parry, R.H.G. (1977) "A study of skin friction on piles in stiff clay," Ground Eng'g Vol. 10, No. 8, pp. 33-37.

(91) Potts D.M. & Martins, J.P., (1982) "The shaft resistance of axially loaded piles in clay " Geotechnique 32, No. 4, pp. 369-386

(92) Potts, D.M. & Gens, A.,(1984) " The effect of plastic potential in boundary value problem involving plane strain deformation," Int. Num. Anal. Method. Geomech., Vol. 8, pp. 259- 286.

(93) Poulos, H.G. & Davis, E.H.,(1968) "The settlement behaviours of single axially-loaded incompressible piles and piers," Geotechnique 18, pp. 351-371.

(94) Poulos, H.G.,(1979) "Settlement of single piles in non-homogeneous soil," J. Geot. Eng'g Div., ASCE, Vol. 105, GT5, pp. 627-641.

(95) Prevost J.H. & Hoeg K. (1975) "Soil mechanics and plasticity analysis of strain softening," Geotechnique 25, No. 2, pp. 279-297

(96) Prevost, J.H.,(1977) "Mathematical modeling of monotonic and cyclic undrained clay behaviour," Int. J. Num. Anal. Geomech., Vol. 1, pp. 195-216.

(97) Prevost, J.H.,(1978) "Anisotropic undrained stress-strain behaviour of Clays," J. Geot. Eng'g. Div., ASCE, Vol. 104, No. GT8, Aug, pp. 1075-1090.

(98) Randolph, M.F. & Wroth C.P. (1977) " A fundament approach to predicting the deformation of vertically loaded piles," University of Cambridge CUED/D - Soils/TR38.

(99) Randolph, M.F., Carter, J.P. & Wroth C.P., (1978a) "Driven piles in clay: (I) Installation, Modelled as the expansion of a cylindrical cavity," University of Cambridge CUED/D - Soils/TR53.

(100) Randolph, M.F., Carter, J.P. & Wroth C.P., (1978b) "Driven piles in clay :(II) Consolidation after driving" University of Cambridge CUED/D - Soils/TR54.

(101) Randolph M.F., Steenfelt, J.S. & Wroth C.P., (1979) "The effect of pile type on design parameters for driven piles," in Design parameters in Geotechnical engineering, British Geot. Soc. London 1979.

(102) Randolph M.F. & Wroth, C.P., (1981) "Application of the failure state in undrained simple shear to the shaft capacity of driven piles." Geotechnique 31 No. 1, pp. 143-157.

(103) Randolph M.F. & Worth C.P., (1982) " Recent developments in understanding the axial capacity of piles in clay" Ground Engineering Vol.15 No. 7, pp. 17-32.

(104) Reese, l.c., Hudson, B.S. & Vijayvergija, B.S., (1969) "An investigation of the interaction between bored piles and soil," Proc. 7th Int. Conf. S.M. & F.E., Vol. 2, pp. 211-215.

(105) Romano M., (1974) "A continuum theory for granular media with a critical state" Arch-Mech., Vol. 26, pp. 1011-1028

(106) Roscoe, K.H., Schofield, A. & Wroth, C.P., (1958) "On the yielding of Soils," Geotechnique, Vol.8 pp. 22-53

(107) Roscoe K.H., Schofield, A. & Thurairajah, A., (1963) "Yielding of clays in state wetter than critical," Geotechnique, No. 3, pp. 211-240

(108) Roscoe, K.H. & Burland, J.B., (1968) "On generalized stress-strain behaviour of wet clay", in Engineering Plasticity, ed. J Heyman and F.A. Leckie, Cambridge Univ. Press, Cambridge, pp. 535-609.

(109) Roy, M., Rlanchet, R., Tavenas, F. & Rochelbe, P.L. (1981) "Behaviour of a sensitive clay during pile driving" Canadian Geot. Jour. Vol.18, pp. 67-85.

(110) Salvadori, M.G. & Baran, M.L., (1964) "Numerical Methods in Engineering " Prentice-Hall, Englewood Cliffs, N.J.

(111) Schofield, A.N. & Wroth, C.P. (1968) " Critical state soil mechanics" McGraw-Hill Book Co., London.

(112) Seed, H.B., & Reese, L.C.,(1957) "The action of soft clay along friction piles," Trans. ASCE, Vol. 122, pp. 731-754.

(113) Tavenas, F. & Leroueil. S., (1977) "Effects of stresses on time on yielding of clays," Proc. Int. Conf. Soil. Mech. and Found. Eng'g, Tokyo, pp. 319-326

(114) Taylor, D.W., (1948) "Fundamentals of soil Mechanics.," John Wiley & Sons, New York.

(115) Tokuoka T., (1971) "Yield Conditions and flow rules derived from hypo-elasticity" Arch. Rat. Mech. Anal. No. 42, pp. 239-252.

(116) Tomlinson M.J., (1971) "Some effects of pile driving on Skin friction," in Behaviour of piles, ICE., London, pp. 107-114.

(117) Truesdell, C. & Noll. W. (1965) "The non-linear field theories of mechanics, " in Fluggs, (ed.) Handbuch der physik, III/3, Berlin, Springer-Verlag.

(118) Truesdell, C.,(1955) "Hypoelasticity," J. Ration. Mech. Anal., Vol. 4, pp. 83-133.

(119) Tumay, M.T., Acar, Y.B., Cekirge M.H. & Ramesh, N.,(1985) "Flow field around cones in steady penetration," J. Geot. Eng'g Div. , ASCE, Vol. 111, No. 2, pp. 193-204.

(120) Vesic A.S. (1972) "Expansion of cavities in infinite soil mass", J. Soil, Mech. Found. Div. ASCE, Vol.98 SM3, pp. 265-290

(121) Vesic A.S., (1977) Design of pile foundation, Synthesis of Highway practical, No. 42, Transportation Research Board, Washington.

(122) Vijayvergiya, V.N. & Focht, J.A., (1972) "A New Nay to predict capacity of piles in clay" Offshore Technology conference, Houston TX. Vol.2, pp. 865-874.

(123) Windle, D. & Wroth, C.P., (1977) "In situ measurement of the properties of stiff clays" Proc. 9th. Int. Conf. S.M. & F.E., pp. 347-352.

(124) Wroth, C.P., (1971) "Some aspects of the elastic behaviour of over-consolidated clay," Stress Strain Behaviour of soils, Proc. Roscoe Memorial Symposium, Cambridge, Ed. R.H.G.Parry, Foulis, pp. 347-361.

(125) Wroth C.P., Carter, J.P. & Randolph, M.F., (1978) "Stress changes around a pile driven into cohesive soil," University of Cambridge CUED/D - Soils/TR55

(126) Wu, T.H., Loh, A.K. & Malvern, L.E., (1963) "Study of failure envelopes of soils," Proc., ASCE, Vol.89, SM1, pp. 145-181

(127) Zienkiewicz, O.C., (1977) "The finite element method," 3rd ed., London, McGraw-Hill.

(128) Zytynski. M., Randoplh, M.F. & Wroth C.P. (1978) " On modelling the unloading- reloading behaviour of soil," Int. Num. Anal. Method. Geomech. Vol. 2, pp 87-94.

APPENDIX A

FORMULATIONS FOR BOUNDING SURFACE MODEL

(i) Distance factor α

The relationship between $\bar{\sigma}_{ij}$ and σ_{ij} is given by

$$\bar{\sigma}_{ij} = \alpha(\sigma_{ij}, \varepsilon^{p}_{kk}) \, \sigma_{ij} \qquad \text{Eq.(2.24)}$$

Substituting Eq. 2.24 into 2.23, we may arrive at the following expression

$$F = F (\alpha \, \sigma_{ij} \, , J_0(\varepsilon^{p}_{kk})) = 0 \qquad (A.1)$$

Using Eq. 2.24, we find that the stress invariants corresponding to the image stress are related to J_1, J_2 and J_3 by

$$\begin{aligned} \bar{J}_1 &= \alpha \; J_1 \\ \bar{J}_2 &= \alpha^2 \, J_2 \\ \bar{J}_3 &= \alpha^3 \, J_3 \end{aligned} \qquad (A.2)$$

When σ_{ij} lies on the elliptic bounding surface, α can be evaluated from Eqs. 2.24, A.1, and A.2. It is given by

$$\alpha = \frac{-E + \sqrt{E^2 - 4 D C}}{2 D} \qquad (A.3)$$

where

$$\begin{aligned} C &= \frac{2 - R}{R} J_0^2 \\ D &= J_1^2 + \left(\frac{R - 1}{N} \right)^2 J_2 \\ E &= - \frac{2 J_0 J_1}{R} \end{aligned} \qquad (A.4)$$

In contrast, when σ_{ij} lies on the hyperbolic bounding surface , α is also given by Eq. A.3, replacing E, C and D as follows

$$\begin{aligned} C &= - \frac{2 J_0^2}{R} \frac{A_C}{N_C} \\ D &= J_1^2 - \left(\frac{\sqrt{J_2}}{N} \right)^2 \\ E &= 2 J_0 \left(\frac{1}{R} + \frac{A_C}{N_C} \right) \frac{\sqrt{J_2}}{N} - \frac{2 J_0 J_1}{R} \end{aligned} \qquad (A.5)$$

(ii) Normal Vector n_{ij}

The normal vector to the bounding surface is given by

$$n_{ij} = \frac{1}{g} \frac{\partial F}{\partial \bar{\sigma}_{ij}} \tag{A.6}$$

where

$$g = \left[\frac{\partial F}{\partial \bar{\sigma}_{ij}} \frac{\partial F}{\partial \bar{\sigma}_{ij}} \right]^{1/2} \tag{A.7}$$

The term $\partial F / \partial \bar{\sigma}_{ij}$ has the form

$$\frac{\partial F}{\partial \bar{\sigma}_{ij}} = \frac{\partial F}{\partial \bar{J}_1} \frac{d\bar{J}_1}{d\bar{\sigma}_{ij}} + \frac{\partial F}{\partial \sqrt{\bar{J}_2}} \frac{d\sqrt{\bar{J}_2}}{d\bar{\sigma}_{ij}} + \frac{\partial F}{\partial \bar{N}} \frac{\partial N}{\partial \omega} \frac{d\omega}{d\bar{\sigma}_{ij}} \tag{A.8}$$

Using Eq. 2.27, Eq. A.8 can be expressed as

$$\frac{\partial F}{\partial \bar{\sigma}_{ij}} = \frac{\partial F}{\partial \bar{J}_1} \delta_{ij} + \frac{\partial F}{\partial \sqrt{\bar{J}_2}} \frac{\bar{\sigma}^*_{ij}}{\sqrt{\bar{J}_2}} + \frac{\partial F}{\partial N} \Pi \left(\frac{\bar{\sigma}^*_{ik} \bar{\sigma}^*_{kj}}{\sqrt{\bar{J}_2}} - \frac{\sqrt{\bar{J}_2}}{3} \delta_{ij} - \frac{1}{\sqrt{6}} \sin(3\omega)\, \bar{\sigma}^*_{ij} \right) \tag{A.9}$$

where

$$\Pi = \frac{3\sqrt{6}\, N\, (1-n)}{(1 + n - (1 - n) \sin 3\omega)\, \bar{J}_2} \tag{A.10}$$

Substituting Eqs. A.9 and A. 10 into A.7, we have

$$g^2 = 3 \left(\frac{\partial F}{\partial \bar{J}_1} \right)^2 + \left(\frac{\partial F}{\partial \sqrt{\bar{J}_2}} \right)^2 + \left(\frac{\partial F}{\partial N} \right)^2 \frac{\bar{J}_2 \Pi^2}{6} [\, 1 - \sin^2(3\omega)\,] \tag{A.11}$$

The normal vector is obtained form Eqs. A. 9, and A. 11 when the form of the bounding surface is known. The unit normal vector to the elliptic bounding surface is obtained from Eq. 2.29 and A.6. It is given by

$$n_{ij} = \frac{1}{g} \left[Q\, \delta_{ij} + V \left(\bar{\sigma}^*_{ij} + W \left(\frac{\bar{\sigma}^*_{ik} \bar{\sigma}^*_{kj}}{\sqrt{\bar{J}_2}} - \frac{\sqrt{\bar{J}_2}}{3} \delta_{ij} - \frac{1}{\sqrt{6}} \sin(3\omega)\, \bar{\sigma}^*_{ij} \right) \right) \right] \tag{A.12}$$

and

$$g^2 = 3\, Q^2 + V^2 J_2 \left(1 + \frac{W^2}{6} [\, 1 - \sin^2(3\omega)\,] \right) \tag{A.13}$$

where

$$\begin{aligned} Q &= 2 \left(\bar{J}_1 - \frac{J_0}{R} \right) \\ V &= 2 \left(\frac{R - 1}{N} \right)^2 \\ W &= \frac{3\sqrt{6}\, (n - 1)}{[\, 1 + n - (1 - n) \sin 3\omega\,]} \end{aligned} \tag{A.14}$$

Similarly, the unit vector to the hyperbolic surface is obtained form Eq. 2.30, A.12 and A.13 by replacing V in Eq. A.14 as follows

$$V = \left[2 J_0 \left(\frac{1}{R} + \frac{A_c}{N_c} \right) \frac{1}{N} - \frac{2 \sqrt{\bar{J}_2}}{N^2} \right] \frac{1}{\sqrt{\bar{J}_2}} \tag{A.15}$$

(iii) Plastic Modulus of the Bounding Surface

The plastic modulus of the bounding surface is given by Eq. 2.10. However, it can be rewritten as

$$\bar{H} = - \frac{\partial F}{\partial J_0} \frac{dJ_0}{d\varepsilon^p_{kk}} \frac{n_{jj}}{g} \tag{A.16}$$

Using Eq. 2.20 in A. 16, we have

$$\bar{H} = - \frac{\partial F}{\partial J_0} \left(\frac{1 + e_i}{\lambda - \kappa} \right) J_0 \frac{n_{jj}}{g} \tag{A.17}$$

when σ_{ij} lies on the elliptic bounding surface, H is obtained form Eq. 2.29 and A.17. It has the form

$$\bar{H} = \frac{6}{R} \left[\bar{J}_1 - (2 - R) J_0 \right] J_0 \left(\frac{1 + e_i}{\lambda - \kappa} \right) \frac{Q}{g^2} \tag{A.18}$$

Finally , for σ_{ij} lies on the hyperbolic bounding surface, Eq. 2.30, H is given by

$$\bar{H} = \frac{6}{R} \left[\bar{J}_1 - R \left(\frac{1}{R} + \frac{A_c}{N_c} \right) \frac{\sqrt{\bar{J}_2}}{N} + 2 \frac{A_c}{N_c} J_0 \right] J_0 \left(\frac{1 + e_i}{\lambda - \kappa} \right) \frac{Q}{g^2} \tag{A.19}$$

APPENDIX B

FORMULATIONS OF THE RATE-TYPE MODEL:

Undrained Triaxial and Simple Shear Conditions

(i) Triaxial Conditions

Following Davis and Mullenger(1984), the effective stress σ_{ij} is non-dimensionalized by the following expression.

$$S_{ij} = \frac{\sigma_{ij} - p_c \delta_{ij}}{\sqrt{2}\,\bar{M}} \qquad (B.1)$$

Using Eq. B.1 in Eqs. 2.44 and 2.47, the loading equation becomes

$$\overset{\circ}{S}_{ij} = \beta \left[D_{ij} - 2 S_{ij} (S_{mn} D_{mn}) \right] \qquad (B.2)$$

and the unloading equation is expressed by

$$\overset{\circ}{S}_{ij} = \beta D_{ij} \qquad (B.3)$$

Here, $S_{mn}D_{mn}$ is the stress power. Loading or unloading occurs when $S_{mn}D_{mn}$ is $\geq$ or < 0, respectively.

For undrained triaxial conditions the deformation field is given by

$$[D_{ij}] = \begin{bmatrix} \dot{\xi} & 0 & 0 \\ 0 & -\dot{\xi}/2 & 0 \\ 0 & 0 & -\dot{\xi}/2 \end{bmatrix} \qquad (B.4)$$

where ξ represents the natural compressive axial strain.The effective stress field is given by

$$[S_{ij}] = \begin{bmatrix} S_a & 0 & 0 \\ 0 & S_r & 0 \\ 0 & 0 & S_r \end{bmatrix} \qquad (B.5)$$

where subscripts a and r represent the axial and radial directions in the soil, respectively.

During loading, when $S_{ij} D_{ij} \geq 0$, we obtain the following expressions from Eqs. B. 2, B.4 and B. 5.

$$\begin{aligned} \dot{S}_a &= \beta \left[\; 1 \; - 2 S_a (S_a - S_r) \right] \dot{\xi} \\ \dot{S}_r &= \beta \left[-1/2 - 2 S_r (S_a - S_r) \right] \dot{\xi} \end{aligned} \qquad (B.6)$$

We assume that ξ_i denotes the initial strain, and the initial pressure P_i and deviatoric stress Q_i are given by

$$\begin{aligned} P_i &= \frac{1}{3} (S_{ai} + 2 S_{ri}) \\ Q_i &= S_{ai} - S_{ri} \end{aligned} \qquad (B.7)$$

where S_{ai} and S_{ri} represent the initial stresses in axial and radial direction respectively. The effective stress in the soil may be obtained by integrating Eqs. B. 6.

$$S_a = P_i \cosh (C1) \operatorname{sech} (\sqrt{3}\, \beta\, \xi + C2) + \frac{1}{\sqrt{3}} \tanh (\sqrt{3}\, \beta\, \xi + C2)$$
$$S_r = P_i \cosh (C1) \operatorname{sech} (\sqrt{3}\, \beta\, \xi + C2) - \frac{1}{2\sqrt{3}} \tanh (\sqrt{3}\, \beta\, \xi + C2) \qquad (B. 8)$$

where

$$C1 = \tanh^{-1} \left(\frac{2}{\sqrt{3}} Q_i \right)$$
$$C2 = C1 - \sqrt{3}\, \beta\, \xi_i \qquad (B.9)$$

However when Sij Dij < 0, unloading occurs. Using Eqs. B. 4 and B. 5 into B. 3, we have

$$S_a = \beta\, \xi + (S_{ai} - \beta\, \xi_i)$$
$$S_r = -\beta\, \xi/2 + (S_{ri} + \beta\, \xi_i/ 2) \qquad (B.10)$$

Finally, the pore pressure can be evaluated from the equilibrium considerations and the effective stress field.

(ii) Simple Shear

In a simple shear deformation problem, we assume that the deformation of a soil element is described by the following expressions.

$$x = X - \Pi\, Z$$
$$y = Y$$
$$z = Z \qquad (B.11)$$

where X, Y and Z are the initial coordinate of a soil element in the reference configuration at time t = 0. Here, $\Pi = \Pi (t)$ is a function of time which describes the position of the soil element, x, y and z, after deformation for time $t \neq 0$. When the deformation is small, Π is approximately equal to the engineering shear strain γ_{xz} which produces positive shear stress as illustrated in Fig. 2.27. Using Eq. B.11, we find that the components of the rate of deformation and spin tensor are given by

$$[D_{ij}] = \begin{bmatrix} 0 & 0 & \frac{1}{2}\dot{\Pi} \\ 0 & 0 & 0 \\ \frac{1}{2}\dot{\Pi} & 0 & 0 \end{bmatrix} \qquad (B.12)$$

and

$$[W_{ij}] = \begin{bmatrix} 0 & 0 & \frac{1}{2}\dot{\Pi} \\ 0 & 0 & 0 \\ -\frac{1}{2}\dot{\Pi} & 0 & 0 \end{bmatrix} \qquad (B.13)$$

where

$$\dot{\Pi} = -\frac{\partial \dot{x}}{\partial z}$$

If we assume that the non-zero effective stress tesor has the form

$$[\,S_{ij}\,] = \begin{bmatrix} S_{xx} & 0 & S_{xz} \\ 0 & S_{yy} & 0 \\ S_{xz} & 0 & S_{zz} \end{bmatrix} \tag{B.14}$$

then, using Eq.B.12 to B.14 in Eq. B.2, we have the following four equations.

$$\begin{aligned} \dot{S}_{xx} &= (-2\beta S_{xx} + 1)\, S_{xz}\, \dot{\Pi} \\ \dot{S}_{yy} &= (-2\beta S_{yy})\, S_{xz}\, \dot{\Pi} \\ \dot{S}_{zz} &= (-2\beta S_{zz} - 1)\, S_{xz}\, \dot{\Pi} \\ \dot{S}_{xz} &= (-2\beta S_{xz}^2 + \frac{\beta^2 - 1 + \Psi}{2\beta})\, \dot{\Pi} \end{aligned} \tag{B.15}$$

where Ψ is given by

$$\Psi = 1 - \beta\,(S_{xx} - S_{zz}) \tag{B.16}$$

If we consider that S_{xxi}, S_{yyi} and S_{zzi} are the initial stress state of the soil element in the X, Y and Z directions, then, when time t= 0, Eq. B.16 has the following form.

$$\Psi_i = 1 - \beta\,(S_{xxi} - S_{zzi}) \tag{B.17}$$

Integrating Eqs. B.15, we obtained the following analytic expressions.

$$\begin{aligned} S_{xx} &= (S_{xxi} - \frac{1}{2\beta})\,\Sigma + \frac{1}{2\beta} \\ S_{yy} &= S_{yyi}\,\Sigma \\ S_{zz} &= (S_{zzi} + \frac{1}{2\beta})\,\Sigma - \frac{1}{2\beta} \\ S_{xz} &= \frac{1}{2\beta}\sqrt{(1-\Sigma)[(\beta^2 - 1) + (\beta^2 - 1 + 2\Psi_i)\,\Sigma]} \end{aligned} \tag{B.18}$$

where

$$\Sigma = \frac{\Psi}{\Psi_i} \tag{B.19}$$

or

$$\Sigma = \frac{2(\beta^2 - 1)\,\varpi}{(\varpi - \Psi_i)^2 + (\beta^2 - 1)(\beta^2 - 1 + 2\Psi_i)} \tag{B.20}$$

in which ϖ is given by

$$\varpi = (\beta^2 - 1 + \Psi_i)\, e^{(\beta^2 - 1)^{1/2}\,\Pi} \tag{B.21}$$

The solution method arriving Eq. B.18 and B.19 may be found from Mullenger et al.(1984).

APPENDIX C

APPROXIMATION FOR THE RATIO OF κ TO λ

Summarized below is a list of 87 data for clays available from Mayne (1980). Column (i) is the clay type, column (ii) and (iii) are measured effective angles of friction and the ratio of κ to λ, respectively. In some cases when the ratio of κ to λ is not available or only either κ or λ is available for the clay, it may be possible to use Eq. 2.55 to obtain the approximate values of ratio of κ to λ. Using the angle of friction given in column (i) and Eq. 2.55, the resulting value of ratio of κ to λ is summarized in column (iv) while the resulting error expressed in percentage is shown in column (v) for comparison. From these results, we note that Eq. 2.55 successfully predicted 54 data with less than 25% error. Therefore, use of Eq. 2.55 to obtain approximate values of the κ/λ ratio may be appropriate for most clays.

	(i)	(ii) angle of friction ϕ^o	(iii) measured $(1 - \kappa/\lambda)$	(iv) approximation $(1 - \kappa/\lambda)$	(v) error %
1	Agnew	25.0	0.49	0.66	-33.6
2	Alaskan Gulf	34.5	0.70	0.93	-33.4
3	Amuay	29.9	0.60	0.80	-33.7
4	Atchafalaya	21.0	0.77	0.54	29.7
5	Backswamp	22.2	0.64	0.58	10.1 #
6	Bangalore Kaolinite	25.5	0.33	0.67	-105.6
7	Bangalore Montmorillonite	12.5	0.17	0.31	-87.4
8	Bangkok	25.4	0.73	0.67	8.2 #
9	Bath Kaolinite	24.5	0.43	0.64	-48.9
10	Bentler	22.7	0.59	0.59	-8.5 #
11	Boston Blue	26.8	0.75	0.71	5.9 #
12	Bradwell	20.0	0.38	0.51	-36.9
13	Buckshot Clay	26.7	0.68	0.70	-3.0 #
14	Calcium Illite	24.2	0.59	0.63	-7.3 #
15 16	Calcium Montmorillonite	12.5	0.19	0.31	-61.1
17	Calcutta	30.2	0.54	0.81	-48.1

18	Concord Blue	24.8	0.68	0.65	4.4 #
19	Connecticut Varved	20.9	0.72	0.54	25.2
20	Drammen Clay	28.0	0.88	0.74	15.2 #
21	Drammen Clay	30.7	0.78	0.82	-5.0 #
22	Drammen Clay	25.1	0.88	0.66	25.0 #
23	East Atchafalaya	18.8	0.52	0.48	6.7 #
24	East Atchafalaya	21.5	0.49	0.56	-14.1 #
25	East Atchafalaya	21.7	0.60	0.56	6.1 #
26	Ghana	20.8	0.29	0.54	-85.2
27	Grundite	32.3	0.41	0.87	-109.9
28	Hackensack Varved	19.0	0.76	0.49	35.9
29	Halloysite	34.3	0.84	0.93	-10.8 #
30	Hokkaido Clay	34.0	0.79	0.92	-16.6 #
31	Hokkaido Silt A	35.1	0.77	0.95	-24.0 #
32	Hokkaido Silt B	34.9	0.80	0.94	-18.6 #
33	Hokkaido Silt B	35.1	0.85	0.95	-11.5 #
34	Illite	24.60	0.49	0.64	-31.3
35	Japanese	33.7	0.73	0.91	-24.9 #
36	Kanpur Clay	29.0	0.66	0.77	-16.5 #
37	Kaolin	22.00	0.32	0.57	-78.9
38	Kaolin	23.5	0.39	0.61	-58.0
39	Kaolinite	29.2	0.13	0.78	-497.5
40	Kars Leda	28.3	1.00	0.75	24.8 #
41	Kawasaki	35.9	0.84	0.97	15.4 #
42	Keuper Marl	25.9	0.76	0.68	10.1 #
43	Khor-al-Zubair	27.3	0.68	0.72	-5.5 #
44	Kinnegar	27.0	0.86	0.71	16.8 #
45	Lagunillas	26.5	0.59	0.70	-18.7 #
46	Lansisalmi	19.5	0.36	0.50	-37.6
47	Lilla Edet	24.3	0.37	0.64	-71.0
48	Liskeard	26.1	0.85	0.69	18.8 #
49	Little Belt	21.0	0.45	0.54	-19.5 #
50	London Clay	18.4	0.38	0.47	-22.5 #
51	Long Island coastal	22.8	0.48	0.59	-23.1 #
52	Massachusetts	30.5	0.22	0.81	-265.3
53	Milazzo	23.0	0.63	0.60	4.9 #
54	Modndal	27.0	0.72	0.71	1.0 #
55	New England	32.0	0.72	0.86	-20.0 #
56	New Providence	30.5	0.72	0.81	-13.1 #

57	Newfield	30.5	0.51	0.81	-61.3
58	Ohio Silt	32.9	0.71	0.88	-24.7 #
59	Oslo	27.0	0.62	0.71	-15.4 #
60	Ottawa Estuarine	35.3	0.83	0.95	-15.3 #
61	Plastic Holocene	32.9	0.71	0.88	-23.9 #
62	Portland	32.00	0.77	0.86	-11.9 #
63	Portsmouth	21.0	0.71	0.54	23.5 #
64	Range De Fleuve	28.6	0.92	0.76	17.5 #
65	Rann of Kutch	26.0	0.45	0.68	-50.8
66	Regina	20.0	0.56	0.51	7.4 #
67	Saint Alban	27.0	0.97	0.71	26.6
68 69	San Francisco Bay Mud	35.2	0.57	0.95	-67.5
70	Sault Ste Marie	28.9	0.74	0.77	-3.4 #
71	Scott	33.4	0.92	0.90	2.5 #
72	Seattle	28.8	0.52	0.77	-48.6
73	Shellhaven	23.0	0.78	0.60	23.1 #
74	Simple Clay	23.1	0.55	0.60	-9.4 #
75	Sodium Illite	20.7	0.37	0.53	-44.8
76	Soft Bangkok	20.0	0.65	0.51	21.2 #
77	Spestone Kaolin	17.2	0.74	0.44	40.9
78	Spestone Kaolin	22.6	0.70	0.59	16.5 #
79	Terra Roxa	29.2	0.87	0.78	10.9 #
80	Texcoco	34.0	0.73	0.92	-26.4
81	Tjipanundjang	35.0	0.47	0.95	-101.6
82	Toledo	20.0	0.62	0.51	16.8 #
83	Vicksburg	25.9	0.73	0.68	6.5 #
84	Vienna	25.8	0.67	0.68	-1.2 #
85	Virgina coastal	28.5	0.48	0.76	-57.0
86	Weald	22.0	0.53	0.57	-7.5 #
87	Weirton	19.0	0.50	0.49	2.22 #
# error less than 25%					

APPENDIX D

EVALUATION OF EFFECTIVE STRESSES FOR THE SIMPLE PILE METHOD

The effective stresses around the simple pile may be obtained from the rate-type model by directly carrying out the integrations along each stream line in a cylindrical coordinate system. But we have found that the following method significantly reduced the computation time.

We introduce a new coordinate system ($\hat{X}_1, \hat{X}_2, \hat{X}_3$), as shown in Fig. D.1, which is related to the cylindrical coordinate by a clockwise rigid rotation of the r, z plane. Any seconcd order tensor functions in the original cylindrical coordinates may be related to new coordinate system by the following orthogonal transformation.

$$\hat{H}_{ij} = R_{im}\, H_{mn}\, R^{T}_{nj} \tag{D.1}$$

or

$$H_{ij} = R^{T}_{im}\, \hat{H}_{mn}\, R_{nj} \tag{D.2}$$

where H_{ij} and $\hat{H}_{ij}$ represent the components of a tensor function in the cylindrical coordinates and in the new coordinates, respectively, and, R_{ij} is the transformation tensor given by

$$[\, R_{ij} \,] = \begin{bmatrix} \cos\varphi & 0 & -\sin\varphi \\ 0 & 1 & 0 \\ \sin\varphi & 0 & \cos\varphi \end{bmatrix} \tag{D.3}$$

If we assume that the soil particle along the stream line is always located on the X_3 axis, then the new coordinate frame has an angular velocity which is defined by

$$\varphi = -\frac{V_z \sin\varphi}{\rho} \tag{D.4}$$

Using Eq. 3.10 and 3.22 in Eq. D.1, the components of the the stress tensor and that of rate of deformation tensor in the new coordinate frame may be denoted by $\hat{S}_{ij}$ and $\hat{D}_{ij}$, respectively. They have the following form

$$[\, \hat{S}_{ij} \,] = \begin{bmatrix} \hat{S}_{11} & 0 & \hat{S}_{13} \\ 0 & \hat{S}_{22} & 0 \\ \hat{S}_{13} & 0 & \hat{S}_{33} \end{bmatrix} \tag{D.5}$$

and

$$[\, \hat{D}_{ij} \,] = \begin{bmatrix} \hat{D}_{11} & 0 & 0 \\ 0 & \hat{D}_{22} & 0 \\ 0 & 0 & \hat{D}_{33} \end{bmatrix} \tag{D.6}$$

where $\hat{D}_{11} = -2\hat{D}_{22} = -2\hat{D}_{33} = 2\,(a^2 V_z / 4\rho^3)$. Using Eq.D.2, D.5 and D.6 in the Eq.3.13, we arrive at

$$\frac{d\hat{S}_{11}}{d\varphi} = \beta \left[-2\,\hat{S}_{11}\,(2\,\hat{S}_{33} - \hat{S}_{22} - \hat{S}_{11}) - 1 \right] \Lambda - 2\,\hat{S}_{13}$$

$$\frac{d\hat{S}_{22}}{d\varphi} = \beta \left[-2\,\hat{S}_{22}\,(2\,\hat{S}_{33} - S_{22} - \hat{S}_{11}) - 1 \right] \Lambda$$

$$\frac{d\hat{S}_{33}}{d\varphi} = \beta \left[-2\,\hat{S}_{33}\,(2\,\hat{S}_{33} - \hat{S}_{22} - \hat{S}_{11}) + 2 \right] \Lambda + 2\,\hat{S}_{13} \qquad \text{(D.7)}$$

$$\frac{d\hat{S}_{13}}{d\varphi} = \beta \left[-2\,\hat{S}_{13}\,(2\,\hat{S}_{33} - \hat{S}_{22} - \hat{S}_{11}) \right] \Lambda + (\hat{S}_{11} - \hat{S}_{22})$$

where

$$\Lambda = -\frac{1}{4} \sin\varphi \left[\frac{a_0^2}{a^2} + \frac{1}{2}\,(1 + \cos\varphi) \right]^{-1} \qquad \text{(D.8)}$$

Numerical solution of Eq.D.7 is well behaved throughout the soil mass except for $a_0 \leq 0.05a$. To evaluate the effective stress along the pile surface, it is necessary to integrate Eq.D.7 by changing the independent variable φ into time, t, together with Eqs. 3.6 and 3.7 by assuming a constant value for the uniform flow velocity V_z. Finally, the resulting effective stress, S_{ij}, may be obtained from $\hat{S}_{ij}$ using Eq.D.2.

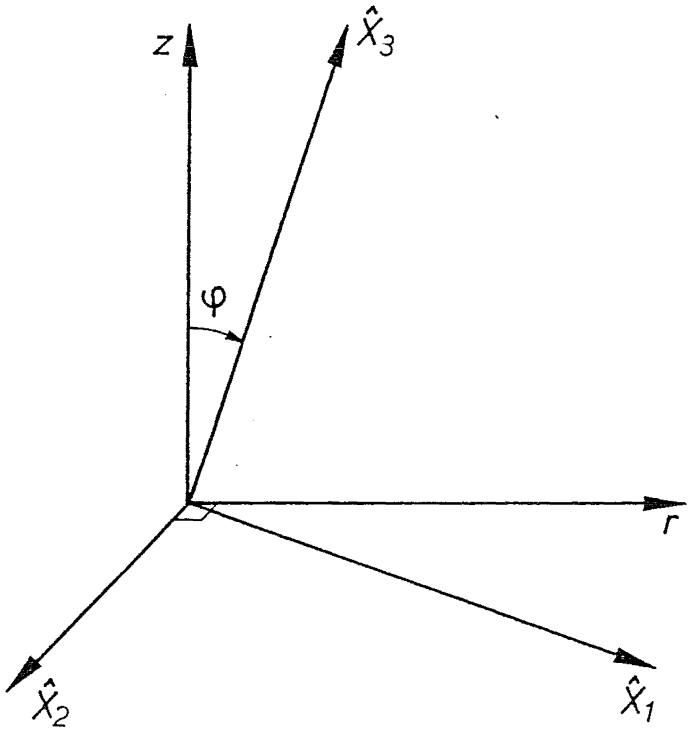

Figure D.1 Rotation of a coordinate system in r-z plane.

Classn:

BEHAVIOUR OF AXIALLY LOADED PILES

K. C. Cheung

Abstract: It is an analytic investigation, using modern constitutive models for soils. Both pile installation effects and load-displacements response are investigated. It is found that the simple pile method is inadequate to represent pile installation effects and results in unrealistic pile-soil interaction. Good agreement between the one-dimensional pile model and field test results is found.

Department of Civil Engineering, University of Canterbury,
Doctor of Philosophy Thesis, 1988